Autophagy in Epidermis

Olufolake A. E. Akinduro

BARTS AND THE LONDON SCHOOL OF MEDICINE & DENTISTRY

QUEEN MARY UNIVERSITY OF LONDON

A thesis submitted in fulfilment of the requirements of the Degree of Doctor in Philosophy

University of London

2013

Supervisor: Professor Carolyn Byrne

Co-Supervisors: Professor Catherine Harwood, Dr. Daniele Bergamaschi

Abstract

Organ-transplant recipients (OTRs) on a new class of immunosuppressants, rapamycin and its analogues, have reduced cutaneous Squamous Cell Carcinomas (cSCCs). Rapamycin, an mTORC1 inhibitor, is also a known autophagy inducer in experimental models. Autophagy, which literally means self-eating, is a cell survival mechanism but can also lead to cell death. Therefore, the main hypothesis behind this work is that rapamycin prevents epidermal tumourigenesis by either affecting epidermal mTOR regulation of autophagy and/or selectively affecting epidermal AKT isoform activity.

Epidermal keratinocytes move from the proliferating basal layer upwards to the granular layers where they terminally differentiate, forming a layer of flattened, anucleate cells or squames of the cornified layer which provides an essential environmental barrier. However, epidermal terminal differentiation, a specialised form of cell death involving organelle degradation, is poorly understood.

The work presented in this thesis shows that analysis of the autophagy marker expression profile during foetal epidermal development, indicates autophagy is constitutively active in the terminally differentiating granular layer of epidermis. Therefore, I hypothesize that autophagy is a mechanism of organelle degradation during terminal differentiation of granular layer keratinocytes.

In monolayer keratinocytes, activation of terminal differentiation is accompanied by autophagic degradation of nuclear material, nucleophagy. This suggests that constitutive autophagy is a pro-death mechanism required for terminal differentiation. In cultured keratinocytes and in epidermal cultures, rapamycin-mediated mTORC1 inhibition strongly increases AKT1 activity as well as up-regulates constitutive granular layer autophagy promoting terminal differentiation.

Therefore, autophagy is an important fundamental process in keratinocytes which may be the mechanism by which terminally differentiating keratinocytes of the

epidermal granular layer degrade their organelles required for barrier formation. This may have implications for the treatment of patients with barrier defects like psoriasis. In immunosuppressed OTRs, rapamycin may promote epidermal autophagy and AKT1 activity adding to its anti-tumourigenic properties.

Table of contents

List of Figures

List of Tables

List of Appendices

Abbreviations

3-MA	3-Methyl adenine
ABCA12	ATP-binding cassette transporter A12
Aks	Actinic keratosis
AMPK	Adenosine monophosphate-activated protein kinase
APS	Ammonium persulphate
ATG	Autophagy-related gene
ATP	Adenosine triphosphate
BAD	Bcl-2-associated death promoter
BCC	Basal Cell Carcinoma
Bcl-2	B-cell lymphoma 2
BCN1	Beclin1
BSA	Bovine serum albumin
CatD	CathepsinD
DAPI	4', 6-diamidino-2-phenylindole
DFCP1	Double-FVYE-containing protein 1
DMEM	Dulbecco's Modified Eagle Medium
DMSO	Dimethyl sulphoxide
DNA	Deoxyribonucleic acid
DTT	Dithiothreitol
EDTA	Ethylenediaminetetraacetic acid
EGTA	Ethylene glycol tetraacetic acid
EGF	Epidermal growth factor
ER	Endoplasmic reticulum
FCS	Foetal Calf Serum
FKBP12	FK-06 binding protein 12
H	Hour
H & E staining	Hematoxylin and Eosin staining
HCQ	Hydroxychloroquine
HKGS	Human Keratinocyte Growth Serum

HPV	Human Papilloma Virus
HPV8-CER	Human Papilloma Virus 8 Common Early Region
HSC	Haematopoietic Stem Cell
IHC	Immunohistochemistry
IR	Insulin receptor
IRS-1	Insulin Receptor Substrate-1
K1	Keratin 1
K6	Keratin6
K10	Keratin 10
K14	Keratin 14
KLK7	Kallikrein7
LB	Lamellar body
LC3	Microtubule-associated protein 1 light chain 3 alpha
Min	minutes
mTOR	mammalian target of rapamycin
mTORC1	mammalian target of rapamycin complex 1
mTORC2	mammalian target of rapamycin complex 2
nHEKs	neonatal Human Epidermal Keratinocytes
NMSC	Non-melanoma skin cancer
OTR	Organ Transplant Recipient
p53	Protein 53
p62	Sequestosome1
PAS	Pre-autophagosomal structure
PBS	Phosphate Buffered Saline
pPD	pPolyphenylenediamine
PDK1	Phosphatidylinositide-dependent kinase 1
PI3K	Phosphatidylinositol 3-kinase
PIP3	phosphatidylinositol-(3,4,5)triphosphate
PIPES	piperazine-N,N′-bis(2-ethanesulfonic acid)
REKs	Rat Epidermal Keratinocytes
RNA	Ribonucleic acid
ROS	Reactive oxygen Species

RT	Room Temperature
S6K	Ribosomal S6 kinase
SCC	Squamous Cell Carcinoma
cSCC	Cutaneous Squamous Cell Carcinoma
SDS	Sodium dodecylsulphate
TBS	Tris Buffered Saline
TLR	Toll-Like Receptor
TSC	Tuberous sclerosis complex
Ub	Ubiquitin
ULK1	Unc-51 like kinase 1 (*C. elegans*)
UV	Ultravolet
VMP1	Vacuole membrane protein 1
Vps	Vacuolar protein sorting
W.B.	Western Blotting
WIPI	WD-repeat protein interacting with phosphoinositides

Acknowledgements

First I would like to thank my supervisor Professor Carolyn Byrne for all her support and guidance throughout my PhD. I also thank Professor Mike Philpott for his support and invaluable advice especially towards the end of my project. I would like to give a big thanks to my family, my parents and my brothers, Seyi and Ola, for their constant support and enthusiasm. Finally I would like to thank my husband, Dele, for his encouragement, love and for believing in me all through my PhD.

Declaration

I declare that the work presented in this thesis is my own.

Chapter 1

Introduction

Introduction

1.1 The epidermis

1.1.1 Structure and function of the epidermis

The skin is the largest organ of the body and is made up of three layers, the epidermis (the epithelieum), the dermis (connective tissue) and the hypodermis (adipose tissue). The epidermis is the outermost layer of the skin which protects the organism from its environment and also acts as a permeability barrier by preventing loss of internal fluids and influx of external substances and microbes, maintaining internal homeostasis. The epidermis also plays a role in the organism's immune response (reviewed in Jain and Weninger 2013).

As a multilayered structure, the epidermis is mainly comprised of keratinocytes, but it also contains melanocytes, Langerhans cells and Merkel cells. The epidermis is continuously renewed by keratinocytes of the basal layer which divide and differentiate to form cells of the spinous, granular and cornified layers (Fig. 1.1). The proliferating basal layer is a heterogeneous population comprising of epidermal stem cells (~10%), which have the ability to regenerate the epidermis, and transit-amplifying cells (60%), which have a limited self-renewal capacity and undergo differentiation after a few cycles (Watt 1998).

Keratinocytes of the basal layer proliferate and differentiate upwards forming keratinocytes of the spinous layer, which also differentiate and activate their terminal differentiation pathways to form the granular layer (Fig. 1.1). In the

granular layer, keratinocytes begin to lose their organelles, express structural proteins characteristic for epidermal terminal differentiation, leading to the flattening, collapse and the eventual death of the cells. These flattened and dead cells, corneocytes, form the cornified layer (Fig. 1.1). Corneocytes are rich in proteins and are embedded in a lipid matrix, giving the epidermis its water-retention and, chemical and mechanical protection properties, ensuring the epidermal barrier function. Keratinocyte proliferation, differentiation and terminal differentiation, a form of cell death, therefore occur sequentially (Blank 1953; reviewed in Candi *et al.* 2005; Proksch *et al.* 2008).

Different stages of keratinocyte differentiation are characterised by the expression of certain intermediate filament proteins, the keratins. Keratins help maintain the cell structure and play a major role in ensuring the mechanical resistance of the epidermis. The main structural proteins in proliferating basal keratinocytes are keratins comprising keratin14 (K14) and keratin 5 (K5) (Fig. 1.1). In supra-basal cells, the calcium concentration increases resulting in activation of the differentiation pathway which is accompanied by expression of markers for early differentiation and eventually terminal differentiation (Fig. 1.1). During early differentiation in the spinous layer, K14 and K5 expressed by proliferating basal keratinocytes are replaced by Keratin1 (K1) and Keratin10 (K10) (Fuchs and Cleveland 1998; Porter and Lane 2003; Strelkov *et al.* 2003).

In the granular layer, terminally differentiating keratinocytes undergo a specialised non-apoptotic form of cell death whereby the nuclei and organelles are degraded and corneocytes are formed. In humans, foetal granular layer formation occurs between 22 and 25 weeks, whereas it is developed between E15.5 and E18.5 in mice (Hardman *et al.* 1998; Hardman *et al.* 1999).

Although terminally differentiating keratinocytes lose their organelles, they are still metabolically active. In the granular layer, terminal differentiation is characterised by the synthesis of structural proteins like filaggrin, involucrin, loricrin and small

proline-rich proteins (Fig. 1.1; Steven and Steinert 1994; reviewed in Candi *et al.* 2005; commenatry in Elias 2012).

Initially, the filaggrin pre-cursor, pro-filaggrin, is synthesized. Electron microscopy analysis shows that pro-filaggrin forms keratohyalin granules (F-granules) in the granular layer. Profilaggrin is then processed to filaggrin which binds to keratin bundles leading to the collapse and flattening of granular layer keratinocytes (Steven *et al.* 1990; Manabe *et al.* 1991). Filaggrin also plays an important role in maintaining epidermal homeostasis. In the cornified layers, filaggrin is degraded to urocanic acid which is a component of the natural moisturizing factor ensuring hydration of the epidermis and protection from UV irradiation (Rawlings *et al.* 1994; Rawlings and Harding 2004).

Another terminal differentiation marker, loricrin is also present as L-granules in granular layer keratinocytes (Steven *et al.* 1990; Manabe *et al.* 1991). However, unlike filaggrin, loricrin is not assocated with keratohyalin bundles but is present as cytoplasmic and nuclear aggregates (Manabe *et al.* 1991; Ishida-Yamamoto *et al.* 1996).

There is a calcium gradient in epidermis with the lowest concentration in the basal keratinocytes (Fig. 1.1). The calcium concentration gradually increases through the spinous layers and peaks in the granular layer before it drastically declines in the cornified layer (Fig. 1.1; Menon *et al.* 1985; Elias *et al.* 2002b). Calcium is present both in the intracellular as well as in the intercellular space of the epidermis (Menon *et al.* 1985). Calcium regulates *in vitro* and *in vivo* keratinocyte differentiation and lamellar body (LB) formation and secretion (Yuspa *et al.* 1989; Menon *et al.* 1994; Lee *et al.* 1998; Elias *et al.* 2002b).

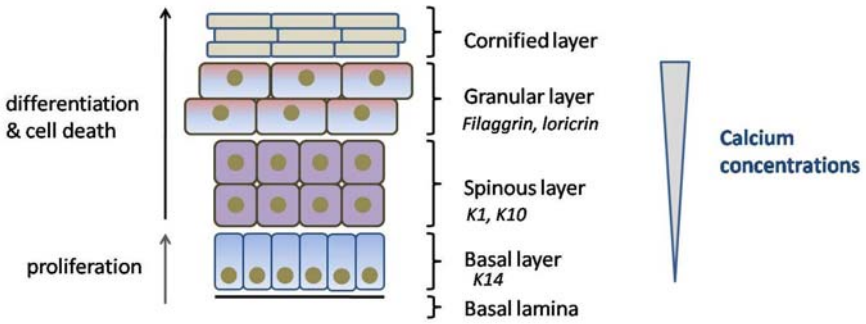

Figure 1.1: A scheme of the epidermis

The epidermis is comprised of the proliferating basal layer which proliferates and differentiates upwards to form the cells of the spinous layer. These cells further differentiate to form granular layer keratinocytes which undergo terminal differentiation, a specialised form of cell death. Keratinocytes of the granular layer lose their organelles, taking on a flattened morphology and further differentiate forming the cornified layer.

In the basal layer, intra- and inter-cellular calcium levels are very low. This increases gradually moving upwards from the basal layer to the granular layer, where calcium concentrations peak. In the cornified layer, calcium levels drop drastically which is also a signal for LBs to secret their cargo into the intercellular space.

The synthesis of LBs starts in the supra-basal layers and they are enriched in the granular layers where they accumulate in the uppermost granular layer cells. In response to certain signals, like calcium levels, LBs secrete their contents into the interra-cellular space between granular and cornified layers (Lee *et al.* 1998). This layer of LB secretions prevents epidermal fluid efflux or influx from the environment, providing barrier properties of the skin (Elias and Brown 1978; reviewed in Landmann 1988).The LB secretions surround each corneocyte as it is being formed, leading to the brick and mortar structure of the *stratum corneum*, where the corneocytes are the "bricks" and LB secretions represent the "mortar" (reviewed by Menon *et al.* 2012).

Proteomics characterization of LBs shows that LBs contain over 980 components (Raymond *et al.* 2008). LBs contain proteases like CathepsinD (CatD) and Kallikrein7 (KLK7) which have previously been implicated in the desquamation process (Sondell *et al.* 1995; Ishida-Yamamoto *et al.* 2004). LBs are generally believed to be related to lysosomes. This is supported by the fact that LBs also contain lysosomal luminal proteins like CatD and lysosomal membrane proteins like LAMP1 and LAMP2 (Raymond *et al.* 2008).

The Rab proteins and Rab-related proteins, which are important for vesicular trafficking,, are also present in LBs (van Weeren *et al.* 2004; Ishida-Yamamoto *et al.* 2007; Tolmachova *et al.* 2007; Raymond *et al.* 2008). Rab-GTP proteins link vesicle membranes to trafficking complexes which bind to specific effectors characteristic for certain membrane compartments (Pfeffer 2001). Proteins required for vacuolar protein sorting (Vps), like Vps20 and Vps35 were also discovered in the LBs suggesting a role for the sorting of LB cargo (Raymond *et al.* 2008).

Other important components of LBs are antimicrobial peptides (Oren *et al.* 2003) which are required for epidermal immunity. Therefore, LBs provide the epidermal permeability barrier as well as its anti-microbial properties.

1.1.2 The epidermal response to UV exposure

One of the greatest hazards the epidermis is constantly exposed to is UV irradiation. UV exposure leads to inflammation, sunburn, erythema, early aging and skin cancers (Weedon *et al.* 1979). There are three solar UV wavelengths, UVA (320-400nm), UVB (290-320nm) and UVC (<290nm). UVA exposure leads to increased reactive oxygen species (ROS) and this causes oxidative modifications of DNA leading to DNA strand breaks, whereas UVB directly damages DNA forming cyclobutane pyrimidine dimers and 6-4 photoproducts. In addition to directly causing DNA damage, UVB also increases ROS leading to oxidation of DNA, proteins and lipids and activates certain signalling pathways (Bickers and Athar 2006). Low levels of DNA damage lead to cell cycle arrest and induction of nuclear excision repair mechanisms (Ichihashi *et al.* 2003). However, excessive DNA damage leads to apoptosis and the formation of sunburn cells in the epidermis. Sunburn cells have pyknotic nuclei and an eosinophilic cytoplasm.

The epidermis protects itself from UV with enzymatic and non-enzmatic antioxidants. One of the pathways activated by high ROS levels is the Keap1-Nrf-2 pathway (Fig. 1.2), which regulates the expression of ROS-detoxifying enzymes and anti-oxidants like glutathione (Itoh *et al.* 1997). Under normal conditions, Nrf2 is bound to Keap1 and retained in the cytoplasm where Nrf2 is ubiquitinated and degraded via the proteasome (Fig. 1.2; McMahon *et al.* 2003). Oxidative stress induces the release of Nrf2 from Keap1 and Nrf2 translocation into the nucleus where it acts as a transcription factor activating expression of detoxifying enzymes and antioxidant proteins (Itoh *et al.* 1999; Wakabayashi *et al.* 2003). The expression of the protein p62, or Sequestome 1 (SQSTM1), is also induced by nuclear Nrf2 in response to high ROS levels. In the cytosol, p62 binds damaged and ubiquitinated proteins and aggregates, targeting them for degradation via autophagy (see section 1.2). Ubiquitinated cargo bound to p62 is transported to the autophagosomal membrane where p62 binds to the Microtubule-associated protein 1 light chain 3

(LC3) (see section 1.2). LC3 is an autophagy protein which is essential for the autophagy process and is associated with the autophagosome membrane (see section 1.2). p62 acts as an adapter between ubiquinated cargo and LC3 within the autophagosome membrane (Pankiv *et al.* 2007). The proteosome degrades ubiquitinated short-lived and dysfunctional proteins, whereas autophagy degrades ubiquitinated, p62-bound dysfunctional and long-lived proteins as well as organelles (see section 1.2.7).

However, p62 has also been shown to bind to Keap1, displacing Nrf2 and allowing Nrf2 translocation into the nucleus (Fig. 1.2). This feedback-loop between p62 and Nrf2 ensures constantly elevated levels of p62 in response to high ROS (Fig. 1.2; Jain *et al.* 2010; Komatsu *et al.* 2010). Therefore, there is a link between the epidermal UV response, the regulation of Nrf2, and p62-mediated proteosome degradation and p62-mediated autophagy.

UV-induced DNA mutations can lead to activation of oncogenes and repression of tumour-suppressors which can cause skin cancers (Eberle *et al.* 2007). One of the protective mechanisms of the epidermis against this is the induction of apoptosis and the formation of sunburn cells. Therefore, a deregulation in the UV-induced ROS-detoxifying and pro-apoptotic pathways, can contribute to the formation of skin cancers.

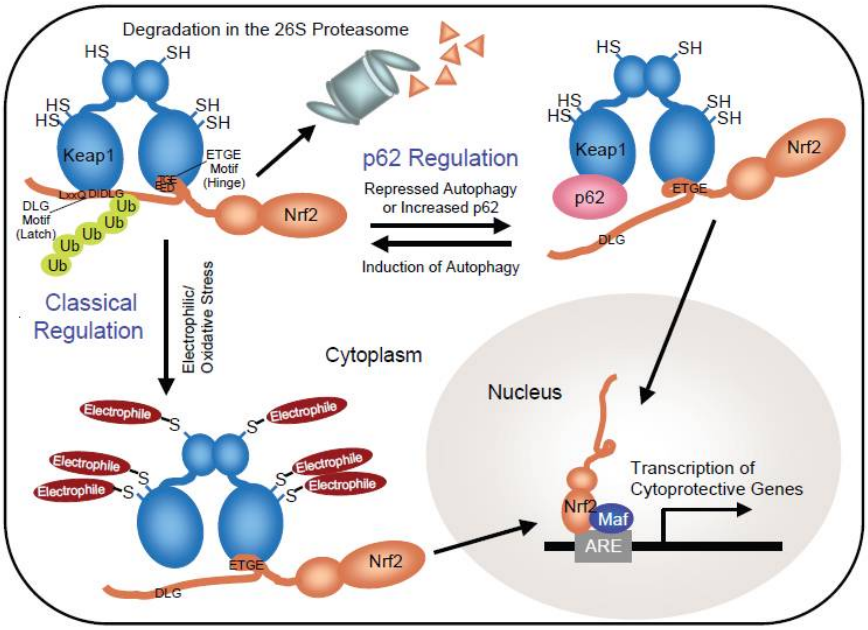

Figure 1.2: p62 regulation of the Nrf2-Keap1 pathway

(Komatsu *et al.* 2010)

Under normal, unstressed conditions, Nrf2 is bound to Keap1 in the cytoplasm, this leads to the ubiquitination of Nrf2 and its degradation in the proteasome. Oxidative stress changes the conformation of Keap1 and this releases Nrf2 from Keap1. Nrf2 then translocates to the nucleus where it activates the transcription of antioxidant genes as well as p62. p62 is then transported into the cytoplasm where it can bind damaged and ubiquitinated proteins targeting them for selective autophagic degradation. Autophagic degradation of p62 bound cargo also reduces the amount of p62 within the cell.

p62 can also bind to Keap1 preventing it from binding Nfr2, which allows Nrf2 to further increase transcription of antioxidant enzymes and also p62. This feedback loop between p62 and the Nrf2-Keap1 pathway allows a continuous increase in p62 levels in response to oxidative stress. Autophagic degradation of p62 is used to control p62 levels within the cell. (Komatsu *et al.* 2010)

1.1.3 Psoriasis vulgaris, a cutaneous barrier defect disease

Psoriasis vulgaris is a skin barrier defect which affects 2% of the world population. The main cause of psoriasis is still unknown but genetics, immunity and environmental factors influence disease incidence and progression. Pathologically, psoriasis is characterised by epidermal hyperproliferation, abnormal keratinocyte terminal differentiation, infiltration of activated neutrophils and T lymphocytes into the dermis and epidermis, and increased vascularisation (reviewed in Raychaudhuri 2012). Psoriasis is also linked to arthritis, diabetes mellitus and heart attacks (Gelfand *et al.* 2006; Scarpa *et al.* 2006).

Compared to normal skin, psoriasis is also characterised by a higher proportion of proliferating keratinocytes. In healthy keratinocytes, γ-Interferon (IFN-γ) inhibits cell growth and induces keratinocyte differentiation by phosphorylating and activating STAT-1α. However, IFN-γ fails to activate STAT-1 in psoriatic keratinocytes, leading to hyperproliferation. Reduced NFκB activity in psoriatic keratinocytes also contributes to hyperproliferation (Jackson *et al.* 1999; Camisa 2000). Psoriatic keratinocytes produce high amounts of TNFα, IL-6 and IL-8 which stimulate inflammation and also, hyperproliferation (reviewed in Griffiths and Barker 2007; reviewed in Raychaudhuri 2012).

In psoriatic skin, the epidermal granular layer is reduced or absent and hyperkeratosis (thickening of the epidermis) and parakeratosis (retention of the nuclei in terminally differentiating keratinocytes of the granular layer) develop. This causes cracks and breaks in the barrier because of defective corneocyte-corneocyte connections and their inability to secrete lipids into the extracelllular space (reviewed in Griffiths and Barker 2007). Also, early epidermal differentiation markers like K1 and K10 are strongly expressed all through the epidermis, whereas markers of terminal differentiation like filaggrin and loricrin are completely abolished. This suggests deregulated psoriatic keratinocyte differentiation. K6 and K16, which are absent in healthy epidermis and are only expressed under stress

conditions in body epidermis, are strongly expressed in psoriatic lesions. Published data suggests that the high keratinocyte turn-over and limited life-span of psoriatic keratinocytes leads to their pre-mature cell death before terminal differentiation can occur (Iizuka *et al.* 2004). Therefore in psoriasis, keratinocyte terminal differentiation and the immune response of the skin are deregulated. Also, the vasculature in psoriatic lesions is dilated and irregular (Smith and Barker 1995).

1.1.4 Cutaneous Squamous Cell Carcinoma

Non-Melanoma Skin Cancer (NMSC) is the most frequent cancer in the world and its rate of incidence is increasing 3-8% per year (Diepgen and Mahler 2002; Ramos *et al.* 2004). Although the NMSC, Basal Cell Carcinoma (BCC) has a higher incidence than Cutaneous Squamous Cell Carcinomas (cSCCs), the mortality rate of cSCCs is much higher due to metatstasis (Alam and Ratner 2001).

cSCCs commonly develop from Actinic Keratoses (AKs), which are precancerous epidermal lesions. The main risk factor contributing to AKs and cSCC formation is UV exposure (Leiter and Garbe 2008). AKs are characterised by enlarged, irregular and hyperchromatic nuclei as well as dysplastic epidermis with abnormal keratinocyte proliferation and disrupted differentiation. This leads to thickening of the *stratum corneum* and parakeratosis. However, in AKs, abnormal keratinocytes are still confined to the epidermis (Fig. 1.3). Progression to cSCCs is accompanied by invasion of the dermis by these atypical keratinocytes (Fig. 1.3). Metastatic cSCCs show invasion of these abnormal keratinocytes not only in the dermis but also in other tissues and organs without any connection to the epidermis (Fig. 1.3) (reviewed in Ratushny *et al.* 2012).

Transformed epidermal stem cells, and not the transient amplifying cells, from the hair follicle bulge and the basal layer give rise to cSCCs (reviewed in Ratushny *et al.* 2012). The main risk factor for the formation of cSCCs is UV exposure which results

in UV-induced p53 inactivation, in addition to widespread DNA damage and ROS formation.

p53, a well characterised tumour-suppressor, is deregulated in most cSCCs. Mutations in p53 are thought to be initiating events required for cSCC formation leading to uncontrolled keratinocyte proliferation and activation of anti-apoptotic mechanisms (Campbell *et al.* 1993; Ortonne 2002). p53 mutant cells are prone to genome instability and acquisition of other mutations required for cSCC progression (Brash *et al.* 1991; Ortonne 2002). Other risk factors for cSCC formation and progression are Human Papilloma Virus (HPV) infection and immuno-suppression.

Figure 1.3: Clinical and histological comparison of normal skin, AKs, cSCC and metastatic SCC (Ratushny *et al.* 2012)

Healthy epidermis is characterised by a well-defined basal layer and normal stratification with the spinous, granular and cornified layers above. Histologically, AKs has abnormal keratinocytes and irregular stratification, a thickened cornified layer which is parakeratotic. This can progress to cSCCs where dysplastic keratinocytes are no more confined to the epidermis but also invade the dermis and neighbouring tissues. In metastatic SCCs, the abnormal keratinocytes are also found in other non-epidermal tissues and organs. (Ratushny *et al.* 2012)

1.1.5 The Human Papilloma Virus and Cutaneous Squamous Cell Carcinoma

Recent publications propose that beta-HPV (β-HPV) is an additional risk factor for cSCC formation in epidermodysplasia verruciformis (EV) as well as in immunosuppressed patients. HPV may allow the survival and proliferation of UV-induced DNA-damaged cells leading to cancers (Storey and Simmonds 2009).

HPVs are small non-enveloped double-stranded circular DNA viruses which cause hyperproliferative skin conditions. HPVs enter the epidermis via lesions where they replicate in keratinocytes since they require keratinocyte differentiation to complete their cell cycle (Egawa 2003; Doorbar 2005). The HPV proteins E6 and E7 directly bind to the tumour suppressors p53 and the retinoblastoma protein, deregulating the cell cycle and prevent apoptosis leading to immortalisation of HPV-infected keratinocytes (reviewed in Aldabagh *et al.* 2013). There are different types of HPVs: the α-HPVs are mainly mucosal, and some variants pose a high risk for cancers like cervical cancer. β-HPVs are mainly cutaneous and have been associated with cSCCs (Harwood *et al.* 2004; Neale *et al.* 2013). However, their exact role is still unclear.

Most people have cutaneous β-HPV infections with no consequences to their health (Antonsson *et al.* 2003; Harwood *et al.* 2004). However, β-HPVs are often found in warts and SCCs of both immunosuppressed and immunocompetent patients. Recent published data shows that the β-HPV5 and β-HPV8 E6 proteins bind to p300 targeting it for degradation (Muench *et al.* 2010). p300 is a transcriptional co-activator for many pathways including p53. Also, β-HPV E6 proteins may lead to degradation of the pro-apoptotic protein Bak, which is a key player in UV-induced apoptosis. Since UV exposure und β-HPV infections have been associated with cSCCs, it is believed that HPV-mediated degradation of Bak may prevent cell death of UV-transformed cells promoting their survival and proliferation leading to cSCC formation (Underbrink *et al.* 2008; reviewed in McLaughlin-Drubin *et al.* 2012).

However, a very recent study shows that there is no link between HPVs and cSCCs and other viruses may also play an important role in cSCC initiation, but not progression (Arron *et al.* 2011; commentary in Schiller and Buck 2011). These differing conclusions may be due to contaminations or the use of different viral genome detection methods.

1.1.6 Immuno-suppression in Organ-Transplant Recipients and Cutaneous Squamous Cell Carcinoma

Immuno-suppressed organ-transplant patients (OTRs) are at a high risk of developing cSCCs. Immunosuppressive drugs are required to prevent allograft rejection but they also makes OTRs more susceptible to multiple side effects including development of cSCCs. OTRs have a 60-100-fold higher incidence of cSCCs compared to the healthy population (Berg and Otley 2002; Hofbauer *et al.* 2010). It is thought that the reason for this is not only due to reduced immunosurveillance but also because of an impaired DNA-damage repair system, which allows mutations to accumulate, promoting cancer (Leblanc *et al.* 2011).

UVA cannot directly induce DNA damage, but it increases cellular ROS levels which can in turn cause DNA damage. One of the immunosuppressant drugs commonly used, azathioprine, increases the effects of UVA-induced ROS on DNA damage (O'Donovan *et al.* 2005). Other immunosuppressant drugs, the calcineurin inhibitors like tacrolimus and cyclosporine, directly promote tumour formation as a side effect (Hojo *et al.* 1999; Wu *et al.* 2010).

However, patients on a new class of immunosuppressants, sirolimus, also known as rapamycin and its analogues, show reduced incidence and progression of cSCCs (Wulff *et al.* 2008; McQuillan *et al.* 2009; Salgo *et al.* 2010). These effects of rapamycin may be due to its anti-proliferative and anti-angiogenic effects (Guba *et*

al. 2002; Koehl *et al.* 2004; Geissler 2008), however the exact mechanism resulting in reduced SCCs remains unknown. Rapamycin also has side effects which include ulcers, oedema, acne, thrombocytopenia, leukopenia, hyperlipidemia and delayed wound healing (Leblanc *et al.* 2011), which reduce its popularity as an immunosuppressant.

Rapamycin, produced by the bacteria *Steptomyces hygroscopicus,* was initially isolated from the soil of the island Rapa Nui, also known as Easter Island. Although it has anti-fungal properties, it is mainly used as an immunosuppressant. Rapamycin is a member of the newer class of immunosuppressants, the inhibitors of the mammalian target of rapamycin (mTOR) (Sehgal 2003).

Formatted: Font: Italic

Inhibition of mTOR activity by rapamycin is due to the formation of a drug-receptor complex, by rapamycin binding to the FK binding protein complex (FKBP-12), blocking mTOR complex 1 (mTORC1) activity. Immunosuppression with rapamycin occurs via rapamycin-induced mTORC1 inhibition preventing p70S6 kinase activity which regulates mRNA translation required for lymphocyte proliferation, differentiation and activation (Sehgal 2003; Leblanc *et al.* 2011).

1.1.7 The AKT/mTOR pathway in epidermis

AKT (or protein kinase B) is a serine/threonine kinase localised mainly in the cytoplasm. AKT is activated by growth factors as well as insulin. Deregulation of AKT is associated with diabetes and cancers (reviewed in Sale and Sale 2008), including skin cancers (Segrelles *et al.* 2002; O'Shaughnessy *et al.* 2007b). There are three AKT isoforms, AKT1, AKT2 and AKT3 (Manning and Cantley 2007). AKT1 is ubiquitously expressed in most cells and tissues, whereas high AKT2 levels are associated with

insulin target tissues like fat cells, liver and muscle. AKT3 is mainly expressed in the brain (Hodgkinson *et al.* 2002; Yang *et al.* 2003). In adult epidermis, the predominant AKT isoform is AKT1 which regulates keratinocyte differentiation (Calautti *et al.* 2005; Thrash *et al.* 2006; O'Shaughnessy *et al.* 2007). AKT2 is strongly expressed in foetal epidermis and is associated with less differentiated keratinocytes (O'Shaughnessy *et al.* 2007).

Knockout mouse studies show that both AKT1-null and AKT2-null mice lack epidermal defects (Cho *et al.* 2001; Cho *et al.* 2001b), whereas AKT1 and AKT2 double-knockout mice have severe epidermal defects and die neonatally (Peng *et al.* 2003). This suggests redundancy between AKT1 and AKT2 in epidermis. In cSCCs, increasing tumour grade is associated with higher expression and activation of AKT2 coinciding with a down-regulation in AKT1 expression and phosphorylation (O'Shaughnessy *et al.* 2007b).

Under nutrient-rich conditions, growth factors and insulin are abundant and bind to receptors at the plasma membrane (Fig. 1.4). This activates the class I phosphatidylinositol 3-kinase (PI3K), which produces phosphatidylinositol-(3,4,5)triphosphate (PIP3) recruiting AKT to the plasma membrane (Fig. 1.4; Andjelkovic *et al.* 1997; Frech *et al.* 1997). At the plasma membrane AKT is phosphorylated at T308 by the phosphoinositide-dependent kinase 1 (PDK1) (Alessi *et al.* 1997), enabling phosphorylation of AKT at a second site, S473, by mTOR complex 2 (mTORC2) (Sarbassov *et al.* 2005; Fig. 1.4). This leads to full activation of AKT and its translocation to the cytoplasm or nucleus where it activates down-stream targets. AKT phosphorylates and inactivates the tuberous sclerosis complex (the TSC1-TSC2 complex) as well as the proline-rich AKT substrate 40kDa (PRAS40) leading to mTORC1 activation (Fig. 1.4; Inoki *et al.* 2002; Kovacina *et al.* 2003; Vander Haar *et al.* 2007).

Down-stream of mTORC1 are 4E-binding protein 1 (4E-BP1) and ribosomal S6 kinases (S6Ks) which regulate mRNA translation and protein synthesis. Other

mTORC1 down-stream processes are lipid synthesis, inflammation, glycolysis and autophagy (reviewed in Johnson *et al.* 2013). However, there is a second rapamycin-insensitive mTOR complex, mTORC2, which has different activators and different down-stream targets including AKT (Fig. 1.4).

The mTORC1 inhibitor, rapamycin, inhibits mTORC1 kinase activity. However, in many cells, there is a negative feedback loop between mTORC1 and the Insulin Receptor Substrate 1 (IRS-1) leading to increased AKT phosphorylation when mTORC1 is inhibited (Fig. 1.4; Harrington *et al.* 2004; Shah *et al.* 2004; Um *et al.* 2004). In epidermis, this negative feedback loop is also active with AKT1 responding to rapamycin-induced mTORC1 inhibition (see section 4.1; Sully *et al.* 2012). Therefore, rapamycin treatment increases epidermal AKT1 phosphorylation and activity, which is associated with keratinocyte differentiation, promoting the anti-proliferative and pro-differentiation effects of AKT1. This may be another mechanism by which rapamycin can reduce SCC tumour incidence and progression.

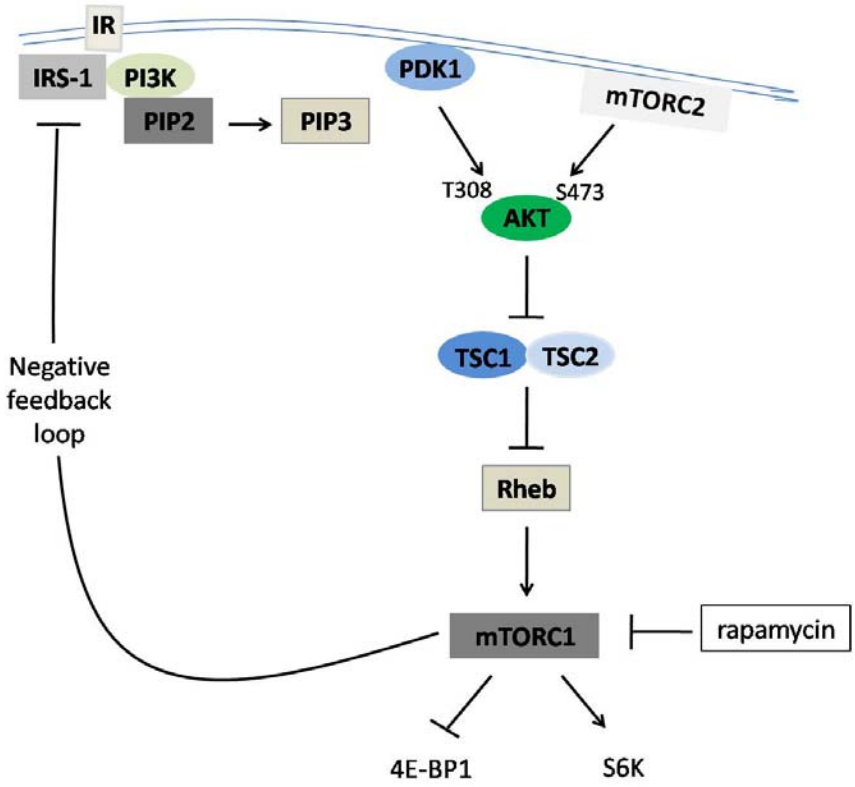

Figure 1.4: The AKT/mTOR pathway

Under nutrient-rich conditions, Insulin binds to the insulin receptor, IR, at the plasma membrane. This activates IRS-1 and the class I PI3kinase, PI3K, which produces PIP3 and recruits AKT. AKT is phosphorylated at T308 by PDK1 and at S473 by mTORC2 leading to its full activation. Active AKT then phoshorylates the TSC1-TSC2 complex, inactivating it and leading to Rheb-mediated activation of mTORC1 and its down-stream targets.

There is also a negative feedback loop between mTORC1 and IRS-1. Active mTORC1 inhibits IRS-1 preventing further activation of AKT. However, inhibition of mTORC1 with rapamycin, for example, also inhibits this negative feedback loop leading to the accumulation of phosphorylated and activated AKT.

1.2 Autophagy

Autophagy literally means self-eating, and is generally used to describe cellular processes leading to the degradation of cytoplasmic components within lysosomes (Levine and Klionsky 2004; Shintani and Klionsky 2004; Mizushima 2007). There are three types of autophagic pathways which differ based on their interaction with the lysosome. Macroautophagy (referred to as autophagy) is a conserved catabolic process characterised by formation of intracellular membrane structures which degrade and recycle cytosolic proteins and organelles, providing building blocks for new protein and organelle synthesis (Arstila and Trump 1968; reviewed in Mizushima 2007). Therefore, autophagy is important for cell growth and maintenance of homeostasis

There are also different types of specialised autophagy targeting different organelles like mitophagy (mitochondria), xenophagy (microbes), pexophagy (peroxisomes) and nucleophagy (nuclei) (Klionsky *et al.* 2007; Cecconi and Levine 2008; Levine and Kroemer 2008; Park *et al.* 2009; Mizushima and Levine 2010; McGee *et al.* 2011).

The second form of autophagy is chaperone-mediated autophagy which involves the targeted degradation of proteins recognized by the molecular chaperone Hsp70, and their translocation across the lysosomal membrane (Cuervo *et al.* 1995; reviewed in Arias and Cuervo 2011). This pathway does not degrade lipids or organelles.

The third form of autophagy is microautophagy, which is the random engulfing of parts of the cytosol by the lysosomal membrane. However, this form of autophagy has not been well characterised (Ahlberg *et al.* 1982; reviewed in Mizushima *et al.* 2011).

1.2.1 mTORC1 and its regulation of autophagy

mTORC1 is the main nutrient, energy, oxygen and stress sensor in the cell. Growth factors and insulin signals are transmitted to mTORC1 via AKT (Fig. 1.4), whereas the cellular energy status, amino acid levels and intracellular calcium concentrations are transmitted to mTORC1 via 5' AMP-activated protein kinase (AMPK) (Fig. 1.5). Under nutrient rich conditions, catabolic processes like autophagy which is down-stream of mTORC1, are inhibited. mTORC1 blocks the autophagy process by negatively regulating the ULK1 complex which initiates autophagy (section 1.2.2).

Under starvation conditions, AMPK inhibits anabolic processes, such as protein synthesis, growth and proliferation, and promotes catabolic processes, such as autophagy (Fig. 1.5). Low glucose levels lead to increased AMP/ATP ratios activating AMPK (Fig. 1.5) which blocks mTORC1 activity indirectly via TSC2 and also directly by phosphorylating raptor. Low oxygen levels also activate AMPK leading to a down-regulation in mTORC1 activity (Fig. 1.5; Salt *et al.* 1998; reviewed in Hardie *et al.* 2012).

mTORC1 is also sensitive to amino acid levels (Fig. 1.5). Amino acids are essential for mTORC1 activity. Insulin and growth factor stimulation alone, in the absence of amino acids, are not able to activate mTORC1 signalling. However, the exact mechanism by which this occurs is still unclear (Hara *et al.* 1998; Wang *et al.* 1998; Sancak *et al.* 2008; reviewed in Jewell and Guan 2013).

Increased calcium levels activate the Calcium/Calmodulin Activated Kinase, CaMKKβ which also influences AMPK signalling and its down-stream effects on mTORC1 (Fig. 1.5). Both intracellular and extracellular calcium levels influence autophagy, however, there is still some controversy regarding the exact role of calcium and autophagy (Hawley *et al.* 2005; reviewed in Decuypere *et al.* 2011).

Sphingolipids are major components of biological membranes. The sphingolipids, ceramide and sphingosine 1-phosphate have been shown to induce autophagy,

however, they do so via different mechanisms. Ceramide inhibits mTORC1 activity (Fig. 1.5) and also increases the levels of the autophagy protein Beclin1, (BECN1), which is essential for the autophagy process (see section 1.2.2). However, sphingosine 1-phosphate only further increases autophagy levels under starvation conditions (Daido *et al.* 2004; Scarlatti *et al.* 2004; Lavieu *et al.* 2006; Lavieu *et al.* 2007).

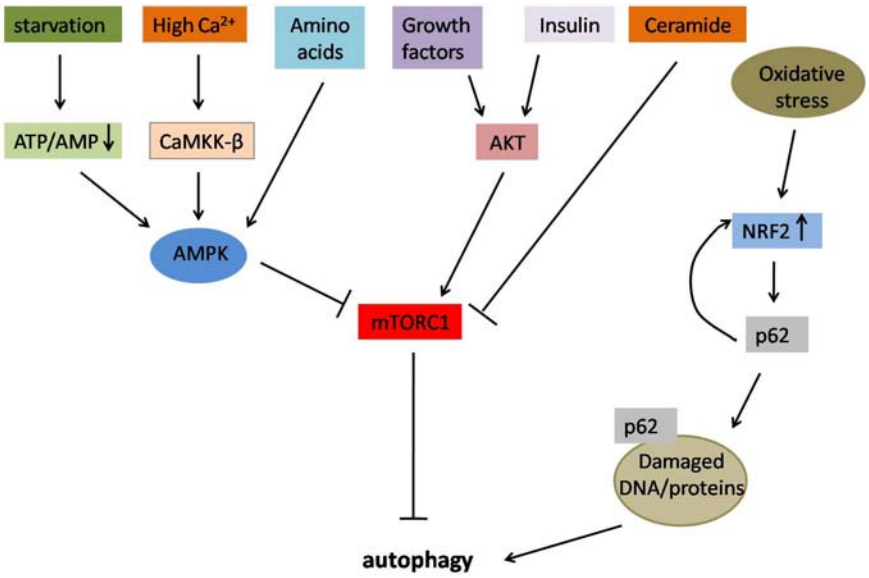

Figure 1.5: mTORC1 and its regulation of autophagy

AKT and AMPK transfer the nutrient and stress status of the cell to mTORC1 which regulates anabolic and catabolic processes. Starvation, calcium levels and low amino acid levels activate AMPK leading to its inhibition of mTORC1 and activation of catabolic processes like autophagy.

AKT is activated by growth factors and insulin which leads to activation of mTORC1 and inhibition of autophagy. Ceramides also influence mTORC1 activity and can act as autophagy inducers by blocking mTORC1 activity. Oxidative stress also leads to increased Nrf2 gene transcription of antioxidants and p62. p62 can further increase Nrf2 activity thereby, increasing p62 levels. High p62 levels also increase autophagy.

1.2.2 The autophagy process

Autophagy can be divided into different steps; the initiation of isolation-membrane formation; the elongation and closure of the double membrane forming autophagosomes; maturation by autophagosome and autolysosome fusion (autolysosomes); and their degradation (Fig. 1.6). Autophagosome formation can be increased rapidly by starvation, then fusing with lysosomes leading to its degradation. The autophagosome half-life can be as short as 10-25 min (Hailey *et al.* 2010).

For autophagosome formation, an isolation membrane is formed and elongated (Fig. 1.6). The main source of the isolation membrane is the ER (Axe *et al.* 2008; Hayashi-Nishino *et al.* 2009; reviewed in Mizushima and Komatsu 2011). However, other organelles such as the mitochondria, the plasma membrane and the ~~g~~*G*olgi can also provide the double-membrane required for autophagosome formation (Hailey *et al.* 2010; Ravikumar *et al.* 2010; Yen *et al.* 2010; Moreau *et al.* 2011; Takahashi *et al.* 2011; Moreau *et al.* 2012; Yamamoto *et al.* 2012; Takahashi *et al.* 2013).

Autophagy is regulated by autophagy-related (ATG) genes which were initially identified in yeast~~s~~ (Tsukada and Ohsumi 1993). The characterisation of these ATG genes in yeasts led to the discovery of the pre-autophagosomal structure (PAS). The PAS is a single punctate structure in close proximity to the yeast vacuole membrane. The PAS, where most ATG ~~genes~~ proteins colocalise, initiates the formation of the autophagic membrane. A recent study suggests that a similar structure is present in mammalian cells close to the ER (reviewed in Mizushima *et al.* 2011).

mTORC1 is the main autophagy regulator in yeasts and in mammals (Blommaart *et al.* 1995; Noda and Ohsumi 1998; Ravikumar *et al.* 2004). Under nutrient-rich conditions, active mTORC1 activates anabolic process such as protein synthesis and inhibits catabolic processes such as autophagy. Therefore, mTOR inhibitors such as rapamycin are widely used as autophagy inducers.

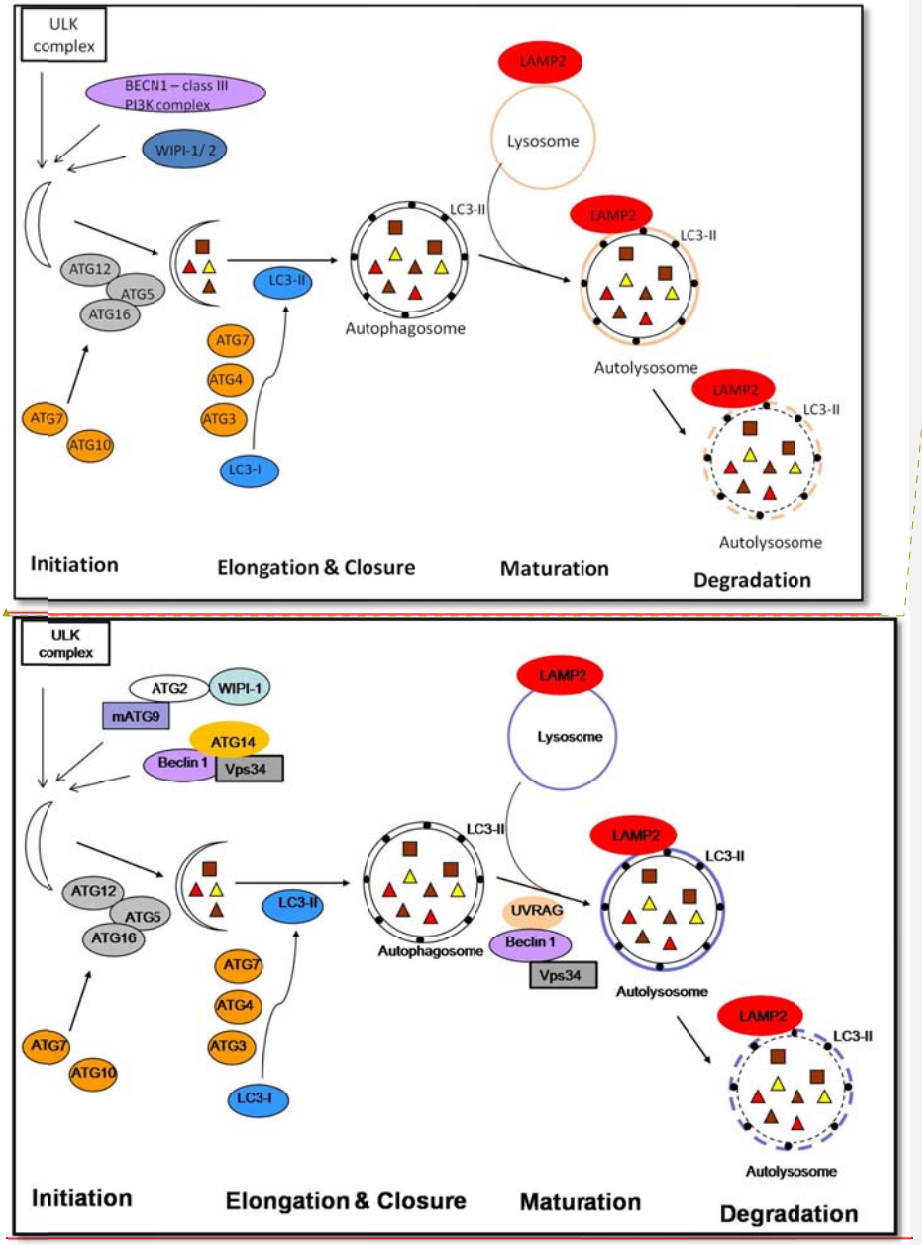

Figure 1.6: A simplified scheme of the autophagy pathway

Formatted: Font: 12 pt, Italic

For the initiation step, the ULK complex, the BECN1-class III PI3kinase complex and the WIPI ~~complex~~ proteins enable isolation membrane formation. For the elongation of the isolation membrane, the ATG5-ATG12-ATG16L complex is localised to the isolation membrane, where it modifies cytoplasmic LC3 to LC3II. LC3II is incorporated in the double membrane and allows its closure, forming the autophagosome. The autophagosome then fuses with lysosomes, forming the autolysosome~~, and this is regulated by Rab7 and the BECN1-Vps34-UVRAG complex~~. This leads to the degradation of the autolysosome and its cargo.

The ULK1 complex

One of the autophagy complexes required for isolation membrane formation is the Atg1/Unc-51-like kinase (ULK) complex which comprises of ULK1/2, mATG13, FIP200 and ATG101 (Fig. 1.7a; Mizushima and Levine 2010). There are two ULK isoforms, ULK1 and ULK2 (Ganley *et al.* 2009; Jung *et al.* 2009), of which ULK1 is the main isoform involved in the autophagy pathway (Chan *et al.* 2007). The ULK1-mATG13-FIP200-ATG101 is constitutively formed in mammalian cells and is thought to be the initial step in the autophagy process (Fig. 1.7a; Itakura and Mizushima 2010; Mizushima *et al.* 2011). This complex is phosphorylated and inactivated by mTORC1 under nutrient-rich conditions, preventing it from participating in the autophagy process ~~and activating it~~ (Fig. 1.7a; Ganley *et al.* 2009; Jung *et al.* 2009).

The class III PI3kinase complex

Phosphatidylinositol 3-phosphate (PI3P) is present in autophagosome membranes and is required for autophagosome formation (Obara *et al.* 2008). Vacuolar protein sorting protein 34~~43~~ (Vps34 in yeasts and class III PI3K, hVps34 in mammals) produces PI3P for autophagy. In mammals, hVps34 forms a class III PI3kinase complex consisting of ATG14L, BECN1 and p150 (Itakura *et al.* 2008; Matsunaga *et al.* 2009), which is also required for isolation-membrane formation (Fig. 1.7b). There are other hVps34 complexes which have other roles, like the UVRAG-hVps34-BECN1 complex which is important for autophagosome-lysosome fusion and endosomal trafficking (Fig. 1.7b; Liang *et al.* 2008). Another hVps34 complex, Rubicon-UVRAG-hVps34-BECN1 inhibits the autophagic process (Fig. 1.7b; Matsunaga *et al.* 2009). Also, binding of BECN1 to Bcl-2 prevents BECN1 from participating in the autophagic process (Pattingre *et al.* 2005). Therefore, the regulation of the pro-autophagy class III PI3kinase activity and the PI3P levels determines autophagy initiation (reviewed in Mizushima *et al.* 2011).

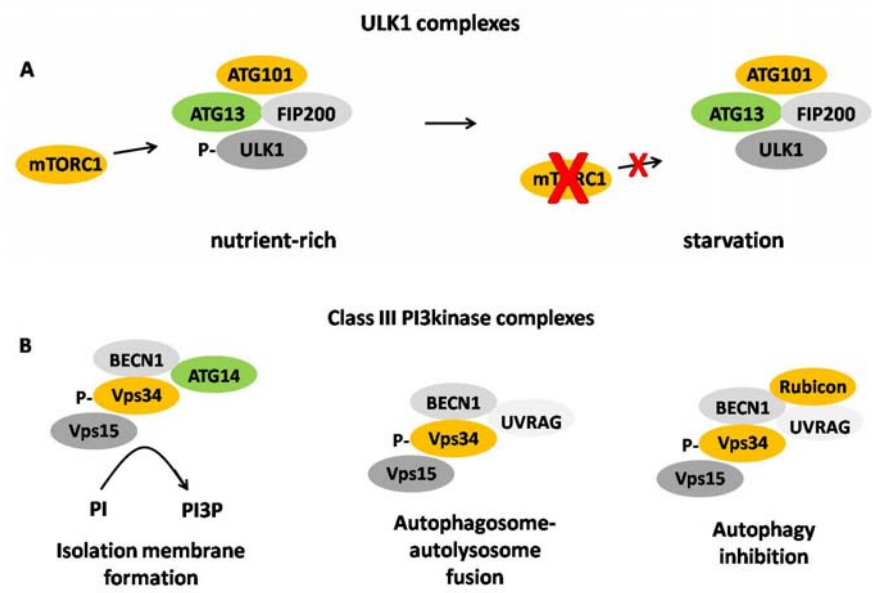

Figure 1.7: The ULK1 complex and the class III PI3kinase complexes

(adapted from Ichimura and Komatsu 2011)

(a) Under nutrient rich conditions and mTORC1 activation, the ULK1 complex comprised of ATG101, ATG13, FIP200 and ULK1 is phosphorylated and inactivated by mTORC1. However, under starvation conditions and mTORC1 inactivation, ULK1 is activated and can participate in the autophagy pathway.

(b) The class III PI3kinase complex which induces isolation membrane formation is comprised of BECN1, ATG14, Vps15 and Vps34. This complex produces PI3P which is required for isolation membrane formation. There are two other Vps34 complexes with different functions. The BECN1- Vps15- Vp33- UVRAG complex is important during autophagosome to lysosome fusion for the maturation of autophagic vesicles. The third complex comprised of BECN1, Vps15, Vps34, UVRAG and Rubicon has autophagy inhibitory effects.

(adapted from Ichimura and Komatsu 2011)

ATG14L and DFCP1

The ULK1 complex activity stimulates localisation of the autophagy protein, ATG14L to the ER. ATG14L is also present on the forming isolation membrane as well as the autophagosome. At the ER, ATG14L recruits the class III PI3kinase complex which produces PI3P (Fig. 1.8). In nutrient-rich conditions, the Double-FYVE-containing protein 1 (DFCP1) ubiquitously localises to the ER and the Golgi membranes, however, under starvation, DFCP1 binds to PI3P in specific spots on the ER, where it colocalises with ATG14L and the class III PI3kinase complex ((Axe, 2008 #390)Fig. 1.8). These DFCP1 concentrated spots on the ER are sites of isolation membrane formation and expansion, the omegasome (Matsunaga *et al.* 2009; Itakura and Mizushima 2010; Matsunaga *et al.* 2010; Mizushima *et al.* 2011).

Comment [MSOffice1]: Check formatting

Field Code Changed

ATG9

Atg9, the only transmembrane autophagy protein, was initially discovered in yeasts as a component of small vesicles which cycle between the PAS and other cytosolic membranes and, is essential for isolation membrane formation (Reggiori *et al.* 2005; Mari *et al.* 2010). Under nutrient-rich conditions in mammals, mATG9 is synthesized in the ER and localises to the Golgi, the trans-Golgi network and to endosomes. Under starvation conditions, mATG9 positive vesicles shuttle between these organelles and the LC3 positive isolation membrane, which is regulated by ULK1 and the class III PI3kinase complex (Fig. 1.8; Young *et al.* 2006). The exact function of ATG9 is still unclear, but there are two hypotheses: the first one is that ATG9 vesicles may supply certain factors or lipids, and also remove unwanted components, required for formation and elongation of the isolation membrane. Another possibility is that the ATG9 containing vesicles may not have any specific function, but transient interaction of ATG9 with the isolation membrane may be required for autophagosome formation (Mizushima *et al.* 2011; Rubinsztein *et al.* 2012).

VMP1

Another protein required for mammalian autophagosome formation is the Vacuole Membrane Protein 1 (VMP1), which interacts with BECN1 in the class III PI3kinase complex (Fig. 1.8; Ropolo *et al.* 2007; Itakura and Mizushima 2010). VMP1 is associated with the ER and the Golgi, and also transiently with the forming isolation membrane (Fig. 1.8; Itakura and Mizushima 2010; Mizushima *et al.* 2011). However, the exact role of VMP1 is still unclear.

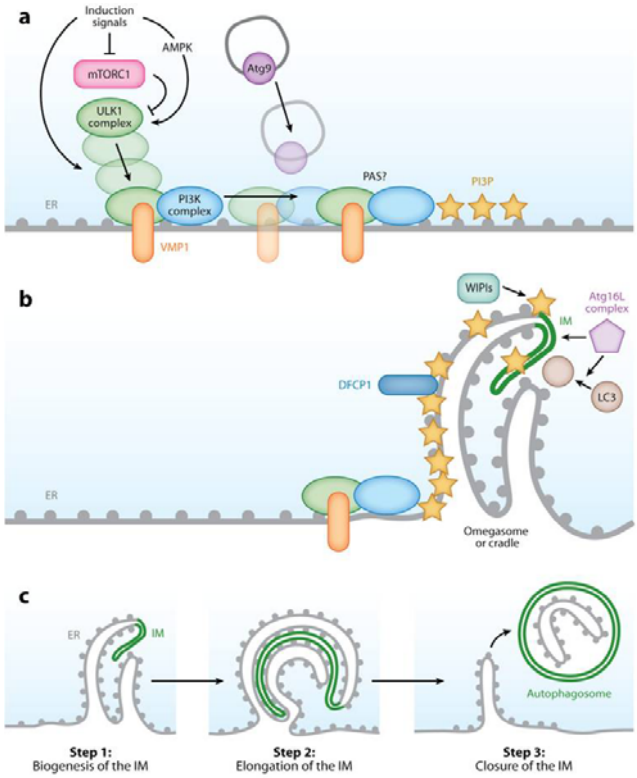

Figure 1.8: A model of autophagosome formation on the ER

(Mizushima *et al.* 2011)

(a) Inhibition of mTORC1 activates ULK1 which translocates to the ER. The class III PI3kinase also translocates to the ER where it interacts with the ULK complex and possibly with VMP1 and ATG9 at the mammalian equivalent of the PAS. The PI3kinase produces PI3P.

(b) The ER membrane is deformed, forming a cradle or the omegasome where the isolation membrane is formed. The PI3P effectors DFCP1 and the WIPI complex are recruited. The ATG5-ATG12-ATG16L complex also binds to the forming isolation membrane and modifies LC3 for its incorporation in the isolation membrane.

(c) The isolation membrane expands within the omegasome and is released upon closure and formation of the autophagosome.

(Mizushima *et al.* 2011)

The WIPI1/2 complex

Other PI3P-interacting proteins are the mammalian Atg18 homologues, the WD-repeat protein interacting with phosphoinositides (WIPI) 1-4 (Proikas-Cezanne *et al.* 2004; Polson *et al.* 2010). WIPI2 is commonly expressed in most cell lines, whereas WIPI1 is not widely expressed (Polson *et al.* 2010). In human cells, the WIPI proteins ~~WIPI1 and WIPI2 form a complex with mATG9~~interact weakly with ~~ and~~ ATG2 in contrast to yeasts where ATG2 and WIPI form a complex. This suggests the WIPI proteins may have other functions in humans ~~((~~Behrends, 2010 #189)Fig. 1.8). The WIPI1/2 complexes have been shown to localise to the same compartment ~~on the ER like ATG14L, and another autophagy protein ATG16L1, the ULK complex and DFCP1 at the omegasome~~like LC3 where they bind PIP3 at the omegasome (Proikas-Cezanne *et al.* 2004; Fig. 1.8; Itakura and Mizushima 2010; Polson *et al.* 2010; Tooze *et al.* 2010; Gaugel *et al.* 2012).

Comment [MSOffice2]: Check formatting

The ATG5-ATG12 conjugate

For the elongation and closure of the isolation membrane, two ubiquitin conjugation systems play a role; the ATG5-ATG12 and the LC3-PE conjugates (Fig. 1.9). Right after synthesis, ATG12 is modified by an E1 enzyme (ATG7) and E2 enzyme (ATG10) activating ATG12 enabling it to bind to ATG5 and form the ATG5-ATG12 conjugate (Fig. 1.9; Mizushima *et al.* 1998; Ichimura *et al.* 2000). ATG5-ATG12 interacts with ATG16L constitutively forming the ATG5-ATG12-ATG16L complex independent of nutrient conditions (Fig. 1.9). Upon autophagy induction, the ATG5-ATG12-ATG16L complex binds to the outer surface of isolation-membrane contributing to its elongation and closure, before dissociating from the membrane (Mizushima *et al.* 2001). The ATG5-ATG12-ATG16L complex is required for LC3 cleavage and lipidation to LC3-PE (LC3 II) (Fig. 1.9).

LC3 (ATG8)

The yeast Atg8 has three mammalian homologues, LC3, GABARAP and GATE-16. The C-terminus of the LC3 precursor is ~~modified~~ cleaved and lipidated by a cysteine protease ATG4, an E1 enzyme ATG7 and an E2 enzyme ATG3 in the cytosol before binding to phosphatidylethanolamine (PE), to form LC3II which is incorporated in the autophagic double-membrane (Fig. 1.9; Ichimura *et al.* 2000; Kabeya *et al.* 2000; Kabeya *et al.* 2004). The processing of LC3 to LC3II is catalysed by ATG16L from the ATG5-ATG12-ATG16L complex at the isolation membrane (Fig. 1.9; Fujita *et al.* 2008). LC3II is incorporated in the outer and inner membrane of the autophagosome (Fig. 1.6; Fig. 1.9). Outermembrane LC3II is also a substrate for ATG4, which ~~modifies LC3II and~~ releases it from the outermembrane of the autophagosome via deconjugation to be recycled (Fig. 1.9; Kirisako *et al.* 2000; Tanida *et al.* 2004). *In vitro* studies have shown that LC3II is required for elongation of the isolation membrane and membrane tethering (Nakatogawa *et al.* 2007).

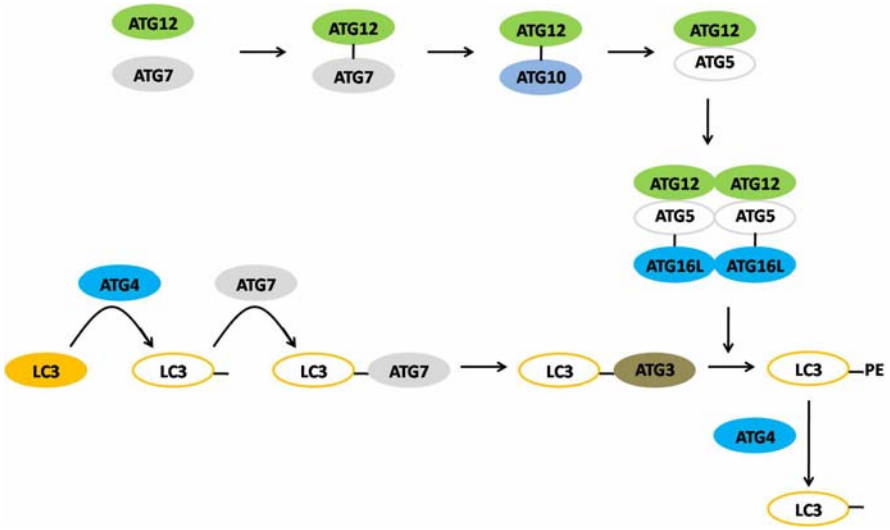

Figure 1.9: Formation of the ATG5-ATG12-ATG16L complex and processing of LC3

(adapted from Ichimura and Komatsu 2011)

In the autophagy process, there are two ubiquitin conjugation systems, the ATG5-ATG12 and the LC3-PE conjugates. ATG12 is modified by ATG7 and ATG10, an E1 and an E2 enzyme respectively, which allows ATG12 to bind to ATG5, forming the ATG12-ATG5 conjugate. This then binds to ATG16L and forms the ATG5-ATG12-ATG16L complex constitutively irrespective of the cellular nutrient status.

The ATG5-ATG12-ATG16L complex is required for LC3 processing. LC3 is found freely in the cytoplasm and is modified and cleaved by a protease, ATG4, an E1 enzyme ATG7 and an E2 enzyme ATG3 which allows it to bind to phosphatidylethanolamine (PE), forming LC3-PE or LC3II which is incorporated in both the inner and outer membranes of the autophagosome. LC3II is required for isolation membrane closure. However, the protease ATG4 recycles LC3 by freeing it from the outer membrane for formation of new membranes.

(adapted from Ichimura and Komatsu 2011)

p62

Autophagy can either be an unselective process of bulk degradation of long-lived proteins and organelles, or it can be selective degradation of certain cargo. During the selective autophagy process, adaptor proteins like p62/SQSTM1 (sequestosome1), bind to ubiquitinated cargo targeting these to the forming autophagosome where p62 also binds to LC3 leading to the eventual engulfment of the cargo by the autophagosome, followed by its degradation (Fig. 1.6; Pankiv *et al.* 2007; Kirkin *et al.* 2009). p62 also plays an important role in the epidermal response to UV exposure and high intracellular ROS levels (see section 1.1.2; Pankiv *et al.* 2010). Therefore, p62 plays an important role in the selective autophagic degradation of ubiquiniated cargo compared to the non-selective, p62-independent autophagy. Autophagy also plays a role in regulating p62 levels which is degraded during selective autophagy. Therefore, monitoring the turn-over rate of p62 can be used as a read-out for selective autophagic flux.

Maturation of autophagosomes

For the maturation of autophagosomes, they have to fuse with lysosomes which are localised in the perinuclear regions (Fig. 1.6). Autophagosomes move along microtubules to the peri-nuclear regions (Ravikumar *et al.* 2005). Autophagosome-lysosome fusion is regulated by Rab7 and the UVRAG-Vps34-Beclin1 complex to form the autolysosome (Fig. 1.6; Fig. 1.7; Gutierrez *et al.* 2004; Ganley *et al.* 2011). The lysosomal transmembrane protein LAMP2 is also required for autophagosome-lysosome fusion (Fig. 1.7; Tanaka *et al.* 2000). Lysosomal enzymes degrade contents of the autolysosome as well as its inner LC3 positive membrane (Nakamura *et al.* 1997; Tanida *et al.* 2008). The degradation products are then reused for signalling and metabolic pathways. Therefore, LC3 is used as a marker for autophagosomes since changes in LC3II levels indicate the turn-over rate of autophagosomes by

fusion with lysosomes leading to their degradation (Kabeya *et al.* 2000; Rubinsztein *et al.* 2009; Klionsky *et al.* 2012).

1.2.3 Autophagy as a cell survival and as a cell death mechanism

Autophagy is a fundamental cellular process required to balance cell metabolism and cell growth with environmental stress. Based on its roles, autophagy can broadly be classified under basal autophagy and induced autophagy. In most cells, basal autophagy is quite low and is required for intra-cellular clearance and maintenance of cell homeostasis. Induced autophagy occurs at much higher levels and is in response to stress conditions like prolonged starvation where non-essential proteins and organelles are degraded to provide energy and nutrients ensuring cell survival (Mizushima 2005). Blocking autophagy under such conditions sensitizes cells to starvation-induced apoptotic cell death (Boya *et al.* 2005).

However, induction of autophagy can also lead to cell death. Type I cell death, apoptosis, is characterised by cytoplasm and chromatin condensation, DNA and cell fragmentation which are degraded by phagocytosis. Another type of cell death which occurs via autophagy, type II cell death, is characterised by accumulation of autophagic vesicles and degradation of cellular organelles and DNA via autophagy. The two types of cell death do not only show morphological differences, but the mechanism of degradation of cellular components differs. In type I cell death, lysosomal enzymes are supplied by phagocytes whereas in type II cell death, lysosomal enzymes are from the dying cells' lysosomes.

There is a lot of controversy regarding the type II cell death mechanism. Some studies suggest that autophagy accompanies cell death, which means that inhibiting autophagy would only change cell morphology but not cell fate. Other reports suggest that cell death is due to autophagy which implies that inhibition of

autophagy would ensure cell survival (Shintani and Klionsky 2004; reviewed in Debnath *et al.* 2005; Gonzalez-Polo *et al.* 2005).

1.2.4 Autophagy and "stemness"

Embryonic stem cells are pluripotent stem cells in the embryo which can undergo self-renewal and differentiation into all the different tissues. During embryogenesis, autophagy is induced by fertilisation of the oocytes where it provides building blocks for protein synthesis in the pre-implantation development of the embryo (Tsukamoto *et al.* 2008; Tsukamoto *et al.* 2008). Therefore, in embryonic stem cells, autophagy is required for development and differentiation.

In hematopoietic stem cells (HSCs), published data suggests that autophagy is required for HSC quiescence, self-renewal and differentiation into the different haematopoietic lineages. Inhibition of autophagy reduces HSC self-renewal capacities and during HSC differentiation, impaired autophagy increases differentiation into the myeloid lineage. The progress from quiescence to self-renewal and differentiation is accompanied by increased mTOR signalling and the fine regulation of autophagy levels (reviewed in Guan *et al.* 2013).

There is one report suggesting that dermal and epidermal stem cell populations also have high levels of autophagy which is believed to preserve their stemness. As these skin stem cells differentiate into immature dermal fibroblasts and immature keratinocytes, autophagy levels are down-regulated (Salemi *et al.* 2012).

However, in neuronal stem cells, the opposite is true with increased autophagy promoting neurone differentiation (Vazquez *et al.* 2012; reviewed in Guan *et al.* 2013). Therefore, autophagy plays different roles in stem cells, depending on their origin and, proliferation or differentiation stage.

1.2.5 Autophagy during development and differentiation

Stress-induced autophagy leads to differentiation in yeast, soil amoeba and worms (Tsukada & Ohsumi, 1993; Otto et al, 2004; Melendez et al, 2003).

During the neonatal starvation period, autophagy ensures survival right after birth. A massive increase in autophagy was observed in tissues like heart and diaphragm to compensate for the sudden high-energy requirements at birth. Also, autophagy was up-regulated in lung and skin which are tissues initially in amniotic fluid and at birth, suddenly exposed to air. It is suggested that adapting to this change in environment requires autophagy (Kuma *et al.* 2004).

In mammals, erythrocytes are specialised cells which transport haemoglobin required for gas exchange in the blood lungs and peripheral tissues. Erythrocytes develop from reticulocytes which lose their organelles and undergo membrane-remodelling as well as changes in volume. Recent studies show that autophagy interacts with the endosomal pathway for organelle degradation and maturation of reticulocytes to functional erythrocytes (Fader *et al.* 2008; Nishida *et al.* 2009; Bodemann *et al.* 2011; Griffiths *et al.* 2012).

Melanocytes are melanin-producing cells found mainly in the basal layer of the epidermis, but they are also present in the lens, the middle ear, bones and heart. Mature melanosomes which are lysosome-related organelles, are produced in melanocytes and are then transferred to neighbouring keratinocytes leading to the skin colour (Van Den Bossche *et al.* 2006; Tobin 2008)(Byers, 2006). Published data shows that in melanocytes, melanin synthesis in the melanosome is regulated by autophagy proteins (Ganesan *et al.* 2008; Ho *et al.* 2011). Within keratinocytes, the fine tuning of autophagic degradation of melanosomes determines the skin colour ~~(Murase et al, 2013)~~(Murase *et al.* 2013). Deregulated autophagic degradation of melanosomes contributes to human skin diseases due to disorders in melanosome biogenesis like vitiligo and the Hermansky-Pudlak Syndrome (Boissy *et al.* 1983; Smith *et al.* 2005).

Formatted: Font color: Red

Monolayer keratinocyte cultures are capable of autophagy (Wang and Levine 2011) and culture stress induced by unsuitable culture media increases expression of LC3 and ATG5-ATG12 which is proposed to lead to early keratinocyte differentiation (Aymard *et al.* 2011). However, this report from Aymard *et al.* is based on experiments in immortalized monolayer keratinocytes under inappropriate culture conditions, which may not give much insight into the *in vivo* situation. These results suggest stress-induced autophagy can induce early keratinocyte differentiation *in vitro*.

1.2.6 Autophagy and aging

Dietary restriction and dwarfism has been shown to extend life span in rodents, which may be due to reduced mTORC1 activity and increased autophagy (reviewed in Masoro 2009; Wang and Miller 2012). In fruit flies, rapamycin-mediated TOR inhibition extends lifespan via its down-stream effects on autophagy and S6K (Bjedov *et al.* 2010). However, in mice, rapamycin-induced mTORC1 inhibition not only extends their lifespan but also, reduced signs of aging in tissues (Harrison *et al.* 2009; Wilkinson *et al.* 2012). Therefore, mTORC1 inhibition due to starvation or rapamycin treatment, increases autophagy and may be responsible for delaying aging in flies and rodents.

1.2.7 Autophagy, the Ubiquitin Proteasomal System and Reactive Oxygen Species

At physiological levels, ROS functions as a signalling molecule. However, high intracellular ROS activates the Nrf2-Keap1 pathway which regulates the balance between oxidant and anti-oxidant responses in the cell (section 1.1.2). p62 is involved in a feedback loop ensuring Keap1 cannot bind to Nrf2 leading to a further increase in gene expression of anti-oxidants and p62 (see section 1.1.2; Jain *et al.* 2010; Komatsu *et al.* 2010). Abnormally high levels of ROS lead to oxidative damage of nuclear and mitochondrial DNA, proteins and lipids, which are then ubiquitinated and recognised by p62 which targets these for degradation via autophagy.

The p62 protein has a C-terminal ubiquitin-associated domain (UBA), which binds to both mono- and poly-ubiquitin, however it has a preference for mono-ubiquitin and Lys^{48}- or Lys^{63}-linked poly-ubiquitin chains (reviewed in Johansen and Lamark 2011). Therefore, ubiquitin is a signal allowing p62 recognition and binding to substrates targeting them for autophagy. The cellular ubiquitination system specifies whether a protein will be degradaed via the proteasome or autophagy. Proteins with ubiquitin branches on Lys^{48} are targeted to the proteasome, whereas single ubiquitin and polyubiquitin chains branched on other Lys residues are targeted for autophagy (reviewed in Johansen and Lamark 2011; Shaid *et al.* 2013). Some ubiquitinated proteins can be degraded by both the proteasome and autophagy. p62 has also been shown to target ubiquitinated organelles for autophagic degradation (Kim *et al.* 2008).

Inhibition of the UPS (Ubiquitin Proteosomal System) increases autophagy which is then the only mechanism for degradation of ubiquitinated proteins. However, inhibition of autophagy does not increase UPS-mediated degradation, but leads to the accumulation of p62 positive aggregates and formation of inclusion bodies (reviewed in Wang and Qin 2013). Accumulation of damaged proteins, lipids and organelles in autophagy incompetent tissues can further increase ROS levels and induce DNA damage response signalling leading to abnormal cell division and

genome instability and, tumour formation (Mathew *et al.* 2009). Therefore, defective autophagy can lead to the formation of tumours.

1.2.8 Autophagy, immunity and inflammation

Both the innate and the adaptive immune responses are also influenced by autophagy. Autophagy plays an important role in the early development of B and T cells as well as in the efficient functioning of mature B and T cells (Crotzer and Blum 2009; English *et al.* 2009; Pua *et al.* 2009; Conway *et al.* 2013).

Recent studies show that autophagy ~~is the main mechanism regulating~~ regulates~~macrophage~~ the secretion of cytokines and chemokines by macrophages and dendritic cells, ~~enabling macrophage-mediated control of~~which regulates cell recruitment and immune responses (Saitoh *et al.* 2008; Harris *et al.* 2011; Shi *et al.* 2012). Deregulation in cytokine secretion via autophagy has been implicated in a number of inflammatory diseases like Crohns disease, rheumatoid arthritis and systemic lupus erythematosus, where treatment with mTOR inhibitors reduces disease severity (reviewed in Jones *et al.* 2013).

Also, autophagy is directly involved in the elimination of intracellular pathogens like bacteria, fungi and viruses (Nakagawa *et al.* 2004; Harris *et al.* 2009; Lapaquette *et al.* 2010; Nicola *et al.* 2012).

In the epidermal barrier defect condition, psoriasis, it is thought that the high levels of cytosolic p62 in lesional psoriatic keratinocytes activates Toll-Like Receptor-induced inflammatory responses via Nf-κB signalling, thereby contributing to keratinocyte hyperproliferation and epidermal inflammation (Boya *et al.* 2005; Miller 2008; Di Cesare *et al.* 2009; Lee *et al.* 2011).

1.2.9 Autophagy and tumourigenesis

In healthy cells, autophagy may have a tumour suppressive function but in established tumours, it is required for cancer cell survival. Monoallelic loss of BECN1 in mice shows partially impaired autophagy which leads to age-related formation of various tumours (Qu *et al.* 2003; Yue *et al.* 2003). In humans, monoallelic loss of the BECN1 locus has been associated with ovarian cancers, breast cancers and prostate cancers (White 2012). However, there are no reports of homozygous loss of BECN1 in tumours and BECN1-/- mice die around E7.5 showing severe signs of impaired embryonic development (Yue *et al.* 2003). Therefore, reduced autophagy may increase the risk of tumour formation.

Autophagic degradation of ubiquitinated mitochondria is called mitophagy. Damaged mitochondria can be a source of high ROS levels leading to increased cellular stress. Mitophagy (autophagic degradation of mitochondria) reduces the number of mitochondria as well as reduces ROS levels by degrading damaged mitochondria. However, defects in mitophagy lead to increased ROS levels which activate the Nrf2-Keap1 pathway, increasing expression of antioxidants and p62. In cells with defective autophagy, there are high levels of p62, as well as accumulation of ubiquitinated cargo bound to p62 which can form protein aggregates. The UPS cannot degrade ubiquitinated protein aggregates. Therefore these accumulate and can lead to genome instability and acquisition of DNA mutations leading to tissue damage. This also causes inflammation which has been shown to contribute to liver cancers (Sakurai *et al.* 2008). Monoallelic loss of BECN1 also increases inflammation in the liver (Mathew *et al.* 2009). Therefore, defective autophagy leads to high ROS levels and accumulation of p62 aggregates as well increased inflammation, contributing to tumour formation.

Moreover, autophagy has also been linked with increased tumour growth. It has been shown that in advanced tumours, cancer cells require autophagy to compensate for the reduced nutrient availability and especially to tolerate the

hypoxic conditions within certain tumour regions. Also, autophagy assists cancer cells in surviving chemotherapy by degrading toxic and damaged organelles and proteins (Degenhardt *et al.* 2006). Inhibition of autophagy in such tumours has been shown to induce tumour cell death (Karantza-Wadsworth *et al.* 2007; Mathew *et al.* 2007; Mathew *et al.* 2009; White 2012).

Therefore, it is generally accepted that autophagy inhibition leads to accumulation and proliferation of abnormal cells, inducing tumourigenesis. Later, autophagy is up-regulated in the more advanced tumour stages ensuring survival (Chen *et al.* 2010; Mathew and White 2011).

There are also more than 20 on-going phase I and phase II clinical trials for the use of autophagy inhibitors in cancer therapy with the first generation autophagy inhibitor, hydroxychloroquine (HCQ) (Amaravadi *et al.* 2011). HCQ is a lysosomotropic and anti-malarial drug, which potently inhibits the late stages of autophagy by preventing degradation of autolysosomes (Klionsky *et al.* 2012). However, HCQ also has other unknown effects which may influence its anti-cancer properties (White and DiPaola 2009; Maycotte *et al.* 2012). Tumour cells which have adapted to the high stress conditions within established tumours require autophagy for their survival and this also renders them resistant to most anti-cancer treatments. However, autophagy inhibition in combination with anticancer treatments has been shown to increase the susceptibility of such resistant tumour cells to drug-induced cell death (White 2012).

1.3 Aims of this thesis

Organ-transplant recipients (OTRs) on a new class of immunosuppressants, rapamycin and its analogues, have a reduced incidence and progression of cSCCs (Wulff *et al.* 2008; McQuillan *et al.* 2009; Salgo *et al.* 2010), which may be due to rapamycin's anti-proliferative and anti-angiogenic effects (Guba *et al.* 2002; Koehl *et al.* 2004; Geissler 2008). However, rapamycin is also a known autophagy inducer in *in vitro* and *in vivo* experimental models. Therefore, the main hypothesis behind this work is that rapamycin prevents epidermal tumourigenesis by either affecting epidermal mTOR regulation of autophagy and/or selectively affecting epidermal AKT isoform activity.

- Initial experiments testing this hypothesis will determine whether autophagy markers and autophagic vesicles are present in adult epidermis and, if there is a link between development of the epidermis in the mouse foetus and the epidermal autophagy marker expression profile.

- Epidermal AKT isoforms regulate epidermal development and keratinocyte differentiation (O'Shaughnessy *et al.* 2007b; Sully *et al.* 2012). The AKT/mTORC1 pathway is also a known regulator of the autophagy process (Noda and Ohsumi 1998; Ravikumar *et al.* 2004). Therefore, the effects of rapamycin on epidermal AKT isoform activity as well as on epidermal autophagy will be investigated.

- The epidermis is the barrier which protects the organism from external insults (reviewed in Jain and Weninger 2013). To determine whether epidermal autophagy contributes to the epidermal barrier properties, the autophagy marker expression pattern in the epidermal ~~disease due to a~~barrier defect disease ~~defective barrier~~, psoriasis, will be analysed. This may have future implications for the treatment of such epidermal diseases. One of the main hazards and stress conditions the epidermis is constantly

exposed to is UV irradiation. Therefore, the effects of UV exposure on autophagy marker expression in the epidermis will be analysed. In an experimental setting, epidermal cultures are also constantly exposed to another kind of stress, culture shock or stress. The effects of culture stress on the autophagy marker expression profile in epidermal explant cultures will also be investigated. This may have implications for the interpretation of data. Autophagy is known to have different roles in cancer formation and cancer progression (Mathew and White 2011). Therefore, the levels of the autophagosome marker, LC3, will be analysed in non-rapamycin treated SCCs from immuno-compromised patients compared to immuno-competent patients. Results from these experiments would show whether the immune status of patients affects autophagy levels in skin cancers and this may have future therapeutic implications.

Chapter 2

Materials and Methods

Materials and Methods

Chemicals, reagents and solutions were purchased from Sigma (Missouri, USA), VWR (Leicestershire, UK), DAKO (Glostrup, Denmark), Invitrogen Ltd (Paisley, UK), BD (New Jersey, USA), Nunc (Roskilde, Denmark), Serotec (Kidlington, UK), Biosera (Boussens, France), Enzo (New York, USA), Dharmacon (Leicestershire, UK), Qiagen (Duesseldorf, Germany), Bio-Rad (California, USA), GE Healthcare (Buckinghamshire, UK).

2.1 Cell and Tissue Culture Methods

All cell culture was performed according to standard tissue culture techniques under aseptic conditions in laminar flow hoods. All sterile and disposable tissue culture plates, flasks, pipettes and falcons were purchased from BD and Nunc. All cells were grown at 37°C in a humidified chamber with 5% CO_2/95% atmospheric air. Epidermal explants and organotypics were cultured at 37°C in a humidified chamber with 10% CO_2/90% atmospheric air.

2.1.1 Cultivation Media

DMEM Culture Media	Dulbecco's Modified Eagle Medium (DMEM) (*Gibco*) with Glutamax, high Glucose (4500 mg/l) and Sodium pyruvate (110 mg/l), supplemented with 10% Foetal Calf Serum (FCS) (*South American Origin, Biosera*) and 0.5U/ml Pen/Strep (*Gibco*)
Medium 154	Calcium-free basal medium (*Gibco*) with 0.2 mM Calcium chloride, supplemented with 1% Human Keratinocyte Growth Supplement (HKGS) (*Gibco*) comprised of Epidermal Growth Factor (EGF), Transferrin, Insulin, Bovine Pituitary Extract and Hydrocortisone. For keratinocyte differentiation, the Calcium chloride concentration was increased to 1.2 mM (*Sigma*)
RM$^+$ media	DMEM/F12 (*Gibco*) supplemented with 10^{-10} M Cholera Toxin (*Sigma*), 10 ng/ml Epidermal Growth Factor (mouse) (*Serotec*), 0.4 ug/ml Hydrocortisone (*Sigma*), 5 ug/ml Insulin (*Sigma*), 5 ug/ml Transferrin (*Sigma*), 2 x 10^{-11} M 3', 3', 5' – Triiodo-L-thyronine sodium salt (*Sigma*)
Freezing Media	Cultivation media with 10% Dimethyl sulphoxide (DMSO) (*Sigma*)
Trypsin-EDTA (1x) (0.05%)	(*Gibco*)
Opti-MEM	(*Gibco*)
Phosphate Buffered Saline (PBS) (1x)	PBS tablets (*Invitrogen*) dissolved in water and sterilized.

Rat Collagen, **Type I**	Rat Tail Collagen (*B.D.*) working solution of 50 ug/ml in sterile 0.01 M Hydrogen chloride (*Sigma*).
Foetal Explant Media	William's E medium (*Gibco*) supplemented with 2 mM glutamine (*Sigma*), 10 ug/ml insulin (*Sigma*), 10 ng/ml hydrocortisone (*Sigma*), 0.5 U/ml Pen/Strep (*Gibco*)

2.1.2 Rat Epidermal Keratinocytes

Rat Epidermal Keratinocytes (REKs) are immortalised rat keratinocytes (Baden and Kubilus 1983). REKs were cultured in DMEM culture medium (10% FCS) which was changed every 2 days. At 70% confluency, the cells were trypsinized and split 1:5 and expanded or plated for experiments. REKs were used for cell monolayer and organotypic experiments.

2.1.3 3T3 Fibroblasts

The immortalised mouse fibroblast cell line, 3T3 fibroblasts (from Claire Hall, Cancer Research UK), were grown in DMEM culture medium. On reaching confluency, the cells were split 1:5 and expanded until enough cells were obtained for organotypic cultures.

2.1.4 Neonatal Human Epidermal Keratinocytes

Neonatal Human Epidermal Keratinocytes (nHEKs) (*Invitrogen*) are from a single donor less than 14 days of age. For my experiments, nHEKs from 6 different donors were analysed to rule out any artefacts due to donors' genetic background.

The purchased nHEKs were expanded according to the manufacturer's protocol to produce lab stocks. Flasks were first coated with collagen (5 µg/cm^2 surface, 1h, RT). Excess collagen was aspirated and the flasks were washed 3x with PBS to remove traces of Hydrogen chloride.

nHEKs were plated at 1.25 x 10^4 viable cells per T25 flask and grown in 154 medium up to 70% confluency. Stocks of ~ 2 x 10^5 cells per vial were frozen down (10% DMSO in 154 Medium, 0.2 mM Calcium chloride) and stored in liquid nitrogen.

nHEKs required for experiments were expanded up to passage 3 (split 1:4) in Medium 154. However, where more differentiated keratinocytes were required, the Calcium chloride concentration was increased to 1.2 mM for 48h. nHEKs were used for cell monolayer experiments.

2.1.5 SCC cell lines

The SCC cell lines listed below were isolated by C. Proby from dysplastic and malignant skin from one renal transplant patient. Isolated tumour cells from immunosuppressted transplant patients have been observed to have an extended lifespan *in vitro* (Purdie *et al.* 1993). Characterisation of the Met cell lines by C. Proby shows that the SCC cell lines have a keratin phenotype which is similar to the tumour of origin, and the PM cell lines isolated from dysplastic skin have a nearly normal keratin expression profile. The original tumours as well as early tumour cell line passages are positive for different HPV types, but the immortalised cell lines were HPV negative (Proby *et al.* 2000).

The cSCC cell lines were cultured in RM^+ culture media, and at 70% confluency they were split (1:4) and expanded or plated for monolayer experiments.

Table 2.1: SCC cell lines derived from tumours of a single patient, the tumour origin and the tumourigenicity of the cell lines in mice.

Cell line	Patient details	Tumourigenicity in mice
PM1	Dysplastic forehead skin	No
PM2	Dysplastic forehead skin	No
PM3	Dysplastic forehead skin	No
PM4	Dysplastic forehead skin	No
Met1	Modified differentiated primary SSC, back of left hand	50%
Met2	Recurrence of above	70%
Met4	Metastasis to left axilliary lymph node	100% in 50 days

2.1.6 Rapamycin treatment of monolayer cells

To analyse the effect of rapamycin (*Enzo*) on the AKT/mTORC1 pathway and on autophagy in monolayer cell cultures, the cells were treated with rapamycin/DMSO at a final concentration of 10 nM rapamycin and 0.1% DMSO for 2-4h. To determine protein expression levels and expression patterns, cells were lysed for Western blotting or fixed for immunohistochemistry analysis.

2.1.7 Hydroxychloroquine treatment of monolayer cells

Hydroxychloroquine (HCQ) (*Sigma*) is an antimalarial drug which also has lysosomotropic properties and neutralises the pH within lysosomal and endosomal vesicles preventing their degradation (Klionsky *et al.* 2008; Klionsky *et al.* 2012). HCQ is routinely used in cell culture experiments to block autophagy, leading to the accumulation of autolysosomes, for the assessment of completion of the autophagy process and also for the analysis of the autophagic flux.

Monolayer cells were treated with 200 uM hydrochloroquine for 2h (dissolved in sterile water and added to the culture media). Where cells were treated with both rapamycin and chloroquine, rapamycin treatment was done for 4h, and half way through the incubation time, chloroquine was added for the last 2h of treatment. Longer incubations with chloroquine were toxic for the cells.

2.1.8 Bafilomycin A1 treatment of monolayer cells

Bafilomycin A1 (BafA1) (Sigma) is a vacuolar ATPase inhibitor. Vacuolar ATPases hydrolyse ATP creating a proton gradient across membranes of lysosomal and endosomal vesicles enabling their acidification. BafA1 prevents vesicle acidification, increasing its pH and also blocks autophagosome – lysosome fusion (Bowman *et al.* 1988; Klionsky *et al.* 2008; Klionsky *et al.* 2012). Therefore, BafA1 is routinely used to block the autophagy pathway leading to accumulation of autophagic vesicles.

Monolayer keratinocytes were treated with 100 nM BafA1/DMSO, for 4h before harvesting. Where a combined treatment of rapamycin and BafA1 was required, both BafA1 and rapamycin were added to the culture media and cells were incubated with the drugs for 4h.

2.1.9 3-Methyl adenine treatment of monolayer cells

3-MA (*Sigma*) is a PI3kinase inhibitor which is commonly used as an autophagy inhibitor (Seglen and Gordon 1982; Klionsky *et al.* 2012). However, 3-MA targets both the class I and the class III PI3kinases, and its preference for one class of PI3kinases depends on the culture conditions, and possibly also on the cell type (Wu *et al.* 2010).

Therefore, I performed initial experiments to determine which class of PI3kinases 3-MA would target in my cells under the given cultre conditions. 3-MA was prepared according to the manufacturer's instructions, by dissolving in boiling water at 0.5 M stock concentration and immediately diluted in medium at concentrations up to 20 mM. Cells were treated with 3-MA for up to 24h before harvesting for Western blotting.

2.1.10 Transfection of cell monolayer cultures with siRNA

siRNA transfections were perfomed in primary keratinocytes to determine whether autophagy is required for organelle degradation during terminal differentiation. A knockdown of key autophagy proteins was done using siRNAs against ULK1 and WIPI1 (*Dharmacon*). As a control, a pool of non-targeting siRNAs was used (*Dharmacon*). The non-targeting siRNAs are against firefly luciferase mRNA and there are no reports suggesting off target effects of this siRNA, according to the manufacturer. To determine whether the transfection was successful, a siGLO LaminA/C control was also used (*Dharmacon*). SiGLO LaminA/C prevents expression of the human proteins LaminA and LaminC which are highly expressed in most cells. An siRNA-mediated knockdown of LaminA and LaminC has not had any negative effects on the tested cells according to the manufacturer. The siGLO fluorophore is also expressed in the nucleus of transfected cells where it is highly expressed allowing judgement of the transfection efficiency.

SiGENOME SMARTpool siRNAs were shipped as dried pellets, therefore, they were diluted in 1x siRNA buffer (*Dharmacon*) to a stock concentration of 20 uM. The transfection reagent HiPerfect (*Qiagen*) was used because experience in my department had shown that the efficiency of siRNA transfections of primary keratinocytes is higher with HiPerfect than with the more commonly used DharmaFECT (*Dharmacon*). Also, HiPerfect is less toxic for primary keratinocytes than DharmaFECT.

The day before the transfection was planned, primary keratinocytes of Passage 2 were plated on collagen-coated 6-wells plates at a density of 2 x 10^5/6 well, in 2 ml M154 medium without Pen/Strep. The next day, the transfection was perfomed.

Primary keratinocytes were transfected with an end-concentration of 50 nM siRNA.

For one 6 well and per siRNA,

Tube 1: 5 ul (20 uM siRNA stock) + 195 ul M154 medium (0.2 mM Calcium chloride, without HKGS and Pen/Strep) = 200 ul in total

Tube 2: 12 ul HiPerfect + 188 uL M154 medium (0.2 mM Calcium chloride, without HKGS and Pen/Strep) = 200 ul in total

The contents of each tube were mixed carefully and both tubes were incubated for 5 min at RT.

The contents of Tube 1 were added to Tube 2 (= 400 ul in total), mixed carefully and incubated at room temperature for 20 min.

M154 medium (1.6 ml; 0.2 mM Calcium chloride, with HKGS, without Pen/Strep) was added to the transfection mix to give a total volume of 2ml/6well. The medium on the cells to be transfected was aspirated and replaced with the transfection medium. 12h later, the transfection medium was aspirated and replaced with fresh 154 Medium (0.2 mM, with HKGS, without Pen/Strep). 72h after the transfection, the cells were harvested for cell lysates or for immunocytometry (see section 2.4).

The cells transfected with the non-targeting siRNA were the negative control for the experiment and the cells transfected with siGLO Lamin A/C were an early indication for an effective transfection. siGLO can be detected 24h after tranfection and its intensity peaks at 48h.

2.1.11 Transfections of cell monolayer cultures with plasmid DNA

To determine which AKT isoform responds to rapamycin treatment with increased phosphorylation, due to rapamycin-mediated inhibition of the negative feedback loop between mTORC1 and IRS-1 (section 1.1.7), REKs were transfected with pcDNA™3.1 (vector control; *Invitrogen*), HA-tagged AKT1 (*Addgene*) and HA-tagged AKT2 (*Addgene*) constructs (Table 2.3; Appendix 17). Both AKT constructs contain an shRNA specific for either the AKT1 or the AKT2 isoform, with an HA-tag (Table 2.3; Appendix 17). The HA-tag is suitable for immunoprecipitation of the HA-tagged protein, allowing separation of the over-expressed AKT isoforms from the endogenous AKT proteins.

Table 2.2: HA-tagged AKT constructs and the vector control construct and their sources

Construct name abbreviation	Construct full name	Construct source
HA-AKT1	Addgene plasmid 9021: 1477 pcDNA3 flag HA AKT1	William J Sellers, Dana-Farber Cancer Institute, Boston, MA, USA
HA-AKT2	Addgene plasmid 16000: pcDNA3 Hygro HA AKT2	Morris J Birnbaum, University of Pennsylvania, PA, USA
pcDNA™3.1	pcDNA3.1	Invitrogen

REKs were transfected with the AKT constructs using Lipofectamine™2000 (*Invitrogen*), according to the manufacturer's protocol. Lipofectamine is a lipid based transfection reagent which forms liposomes in an aqueous environment trapping the negatively charged DNA to be transfected within. The surface of the

liposomes is positively charged allowing the liposomes to fuse with the negatively charged plasma membrane transferring the DNA into the cells. The transfected DNA needs to be transported into the nucleus for transcription.

Another experiment was performed to confirm the initial results on the effects of rapamycin on the AKT isoforms. A knockdown of the AKT1 isoform was performed using two different shRNA sequences as well as a scrambled shRNA (Table 2.3). The two shAKT1 and the scrambled shRNA constructs were purchased from SABiosciences, Qiagen.

Table 2.3: shAKT1 sequences and the scrambled shRNA control and their source

Construct name abbreviation	**shRNA sequence**	**Construct source**
shAKT1, A1	GCACCGCTTCTTTGCCAACAT	SABiosciences, Qiagen
shAKT1, A3	GAGGCCCAACACCTTCATCAT	SABiosciences, Qiagen
Scrambled shRNA	Undisclosed	SABiosciences, Qiagen

For the transfection of REKs with HA-AKT1 or shAKT1 constructs, REKs were plated the day before to give an optimal cell density with 40-50% confluency at the time of transfection, which corresponds to ~0.5 x 10^5 cells per 6 well.

For one 6 well and per construct,

Tube 1: 2 ug DNA + 250 ul Opti-MEM

Tube 2: 10 ul Lipofectamine™2000 + 250 ul Opti-MEM

Each tube (~250 ul) was mixed carefully and incubated for 5min at RT. The contents of Tube 1 was added to Tube 2 (~250 ul), mixed carefully and incubated for 30min at RT. 1.5ml of DMEM medium (without Pen/Strep) was added to the transfection

mix (total of ~2ml) and mixed carefully. The medium on the cells to be transfected was aspirated and replaced with the transfection media.

8h after the transfection, the transfection media was aspirated and replaced with fresh DMEM medium (without Pen/Strep). The cells were treated 72h after the transfection and harvested. Previously, a time-course was performed to determine the optimal harvesting time-point for maximum HA-AKT over-expression and maximum AKT knockdown which was found to be 72h after transfection.

2.1.12 Foetal Explant Cultures

The epidermis from E15.5 wild-type CD1 mouse embryos was isolated and cultured for 3 days before harvesting. Mouse embryos were removed from the uterus in their individual amniotic sacks. Using a dissecting microscope, the skin was pulled off the trunk of the embryos and spread out on filter paper, dermis side down. These were grown on metal grids at the air-liquid interface of Foetal Explant Media (section 2.1.1). The culture media was changed daily until harvesting after 72h in culture.

For experiments analysing the effects of mTORC1 inhibition, the foetal explants were also treated basally with vehicle, 1 uM and 5 uM rapamycin/DMSO, and 2.5 uM Torin1/DMSO in Foetal Explant Media for 72h, before harvesting. The drug concentrations used are the minimum drug concentration required to effectively inhibit mTORC1 activity. These were previously established in the lab by K. Sully, and thereafter used routinely. However, effective drug treatment was always assessed in the samples by determining the residual epidermal mTORC1 activity on its downstream target, S6 phosphorylation.

Before harvesting, explants were halved. One half was fixed in Bouin's solution (*Sigma*) and the other was wrapped in aluminium foil, shock frozen in liquid nitrogen and stored at -80°C until protein lysates were prepared (see section 2.4).

2.1.13 Adult Ear Explant Cultures

For adult ear explant cultures, the ears from 3 month old adult CD1 and C57B/6 mice were harvested. The ears were washed 3x in DMEM culture media with 1% antimycotics and 1% antibiotics (*Sigma)* and then rinsed 3x in DMEM culture media. The dorsal ear epidermis was carefully pulled off the ear cartilage (the ear cartilage with the ventral ear epidermis discarded) using a dissecting microscope and placed on sterile filter paper. The ear explants were cultured at the air-liquid interface of DMEM culture media for 48h. The culture media was changed daily. Before harvesting, the ear explants were halved. One half was fixed in Bouin's solution (*Sigma*) and the other was wrapped in aluminium foil, shock frozen in liquid nitrogen and stored at -80°C until protein lysates were prepared (see section 2.4).

2.1.14 REK-Organotypics

REKs were used in 3D-cultures to mimic keratinocyte differentiation due to their ability to form a barrier (Marjukka Suhonen *et al.* 2003). Human De-Epidermalised Dermis (DED) (*Euro Skin Bank; www.eurotissuebank.nl*), is cadaver skin preserved in glycerol which eliminates most bacteria, viruses and kills all cells. DEDs are used as a dermal matrix on which the keratinocytes can grow, differentiate and stratify. The DED was first washed in warm PBS to free the skin from glycerol in which it is stored. The DED was then incubated in 1% antimycotics/ 1% antibiotics/PBS for 10-15 days at 37°C, to free the dermis from the epidermis, which was scraped off before use.

The DED was cut into squares of 2 cm x 2 cm. With the help of cloning rings (diameter ~ 1 cm), 10^6 3T3 fibroblasts were plated per ring on the dermal side of the DEDs. As a control for confluency, an equal number of fibroblasts were plated in a cloning ring placed in an empty dish sealed with sterile Vaseline.

The fibroblasts were allowed to proliferate and migrate into the DEDs providing growth factors for the keratinocyte organotypic cultures. After 2 days, or when the confluency control plated on a dish showed that the fibroblasts were 100% confluent, the DEDs with fibroblasts were turned dermal and fibroblast side down, and the cloning rings replaced on the epidermis side. 10^5 REKs per ring were plated on the epidermis side of the DEDs, in DMEM culture media. Another confluency control was made for the REKs.

When the control reached confluency, which was after 3-4 days, the DEDs were lifted onto metal grids and cultured at the air-liquid interface of the DMEM culture media for 12 days. The organotypics were treated for 3 days with vehicle or rapamycin before harvesting. Basal rapamycin treatment was carried out by growing organotypics in DMEM culture media supplemented with vehicle, 1 uM or 5 uM rapamycin. Before harvesting, the organotypic cultures were halved and fixed in Bouin's solution.

2.2 Antibodies used for Immunohistochemistry and for Western blotting

Table 2.4: List of primary antibodies used for immunohistochemistry and Western blot analysis

Antigen	Species	Clonality	Application and dilution	Manufacturer
ABCA12	rabbit	polyclonal	IF (1:200)	gift from Prof. D. Kelsell
β-Actin	mouse	monoclonal	WB (1:2000)	Sigma
AKT	rabbit	polyclonal	WB (1:1000)	Cell Signaling
AKT1	mouse	monoclonal	WB (1:3000)	Cell Signaling
phospho-AKT (S473)	rabbit	polyclonal	WB (1:500), IF (1:10)	Cell Signaling
ATG5	rabbit	monoclonal	IF (1:200)	Sigma
BECN1	rabbit	monoclonal	WB (1:1000)	Epigenomics
BECN1	rabbit	polyclonal	IF (1:500)	Cell Signaling
CatD	mouse	monoclonal	IF (1:200)	Abcam
Filaggrin	rabbit	polyclonal	WB (1:1000), IF (1:400)	Zymed
Filaggrin	mouse	monoclonal	IC (1:80), IF (1:400)	Biomeda
HP1α	rabbit	polyclonal	IC (1:200)	Cell Signaling
Aceylated Histone H3 (Lys 14)	rabbit	polyclonal	IC (1:200)	Upstate
KLK7	goat	polyclonal	IF (1:200)	Santa Cruz
K1 (human)	rabbit	polyclonal	WB (1:1000), IF (1:400)	Covance
K1 (mouse)	rabbit	polyclonal	IF (1:400)	Covance
K6	rabbit	polyclonal	IF (1:500)	Covance
K14	rabbit	polyclonal	WB (1:2000), IF (1:1000)	Covance
LMNA	rabbit	polyclonal	IC (1:200)	Abcam
LAMP2	mouse	monoclonal	IC (1:400)	Abcam
LC3	rabbit	polyclonal	WB (1:500), IF (1:50), IC (1:200)	Cell Signaling

Table continued on next page

Table 2.4 (continued): List of primary antibodies used for immunohistochemistry and Western blot analysis

Antigen	Species	Clonality	Application and dilution	Manufacturer
Loricrin	rabbit	polyclonal	IF (1:500)	Covance
mTOR	rabbit	polyclonal	WB (1:1000)	Cell Signaling
phospho-mTOR (S2448)	rabbit	polyclonal	WB (1:1000), IF (1:100)	Cell Signaling
phospho-mTOR (S2481)	rabbit	polyclonal	WB (1:1000), IF (1:50)	Abcam
p62 (D-3)	mouse	monoclonal	IC (1:80)	Santa Cruz
S6	rabbit	monoclonal	WB (1:1000)	Cell Signaling
phospho-S6	rabbit	polyclonal	WB (1:1000), IF (1:250)	Cell Signaling
ULK1	rabbit	polyclonal	IF (1:50), IC (1:200)	Santa Cruz
WIPI1	rabbit	polyclonal	WB (1:1000), IF (1:50), IC (1:200)	Sigma
WIPI2	rabbit	polyclonal	WB (1:1000), IF (1:50), IC (1:200)	Sigma

Table 2.5: List of secondary antibodies used for immunohistochemistry and Western blot analysis

Isotype	Fluorescent Link	Application	Manufacturer
Goat anti-rabbit	-	W.B. (1:5000)	Jackson ImmunoResearch Labs.
Goat anti-mouse	-	W.B. (1:5000)	Jackson ImmunoResearch Labs.
Goat anti-rabbit	Alexa fluor 488	IHC (1:800)	Invitrogen
Goat anti-mouse	Alexa fluor 566	IHC (1:800)	Invitrogen
Rabbit anti-goat	Alexa fluor 566	IHC (1:800)	Invitrogen

2.3 Immunofluorescence histochemistry and immunofluorescence cytometry

Formatted: Left

Immunofluorecence histochemistry (tissue) and immunofluorescence cytometry (cells) is used to identify the expression pattern and the localisation of proteins of interest in paraffin-embedded tissue samples and in cell monolayer cultures.

All staining was documented using the Nikon Eclipse E600 microscope with a mercury fluorescence light source (*Nikon*). The Spot Advanced (version 4) software was used for image acquisition. For Z-stack images, a confocal microscope was used, the Carl Zeiss Laser Scanning Microscope LSM 510 META (*Carl Zeiss Ltd., Hertfordshire, UK*). Editing of images was done using Photoshop and the ImageJ software.

Already fixed and embedded (Bouin's) adult human facelift skin was kindly provided by Dr. W. Harrison (Institute of Cell and Molecular Science, London, UK), sections of psoriatic archive material were a kind gift from Dr. R. Hannen (Institute of Cell and Molecular Science, London, UK) and Prof. Dr. C. Harwood (Institute of Cell and Molecular Science, London, UK), sections of cSCCs were kindly provided by Prof. Dr. C. Harwood (Institute of Cell and Molecular Science, London, UK), the CD1 mouse embryos and the CD1 and C57B/6 adult mouse tissue were obtained from the Queen Mary Mouse facility (Queen Mary University of London, London, UK), CD1 newborn mouse dorsal skin for electron microscopy analysis was a kind gift from Dr. K. Braun (Institute of Cell and Molecular Science, London, UK), sections of UV irradiated FvB and HPV8 transgenic adult mouse epidermis were kind gifts from Dr. B. Akgül (Institute of Virology, University of Cologne, Cologne, Germany) .

2.3.1 Immunohistochemistry solutions

Peroxidase Block	0.3 % H_2O_2 (*Sigma*) in H_2O
Citric Buffer	10 mM Citric Acid (*Sigma*) (pH6.0), 0.05% Tween (*Sigma*)
Blocking Buffer	5% goat serum (*Vector Labs*), 1% Bovine Serum Albumine (BSA) (*Sigma*) in PBS (*Invitrogen*); for primary antibodies raised in goat, blocking buffer was 1% BSA
PBS-Tween	PBS (*Invitrogen*), 0.05% Tween (*Sigma*)
pPolyphenylene-diamine (pPD-Antifade)	5 mg pPD (*Sigma*), 0.5ml 100 mM Tris (*Sigma*) (pH 8.5), 4.5 ml Glycerol (*Sigma*). Mixed for 30 min, RT.
Permeabilisation Buffer	0.01% Saponin (*Sigma*), 80 mM PIPES (*Sigma*) (pH 6.8), 5 mM EGTA (*Sigma*) (100 mM Stock in 1M NaOH), 1 mM $MgCl_2$ (*Sigma*)

2.3.2 Paraffin-embedding of tissue

Tissue was first fixed in Bouin's solution (*Sigma;* gentle shaking, 2h, RT), washed 3 times (70% ethanol, gentle shaking, 1h, RT) and left in fresh 70% ethanol over night. The tissue was dehydrated using the Tissue TEK VIP (*Sakura Finetek USA Inc., California, USA*) and embedded in paraffin the next day. Sections of 3-4 microns where cut onto Superfrost®Plus microscope slides (*Gerhart Menzel Glasbearbeitungswerk GmbH & Co. KG, Braunschweig, Germany*), using the Leica RM2535 microtome (*Leica Biosystems, Nussloch, Germany*).

2.3.3 Hematoxylin and Eosin (H & E) staining

Hematoxylin and Eosin (H&E) staining was performed to examine tissue morphology. The hematoxylin stain is incorporated in the nuclei, staining them dark blue, and eosin gives the cytoplasm a pinkish tint.

Paraffin-embedded sections were freed from wax by short incubations in xylene and then hydrated in an alcohol series with increasing water content listed below. Subsequently, the nuclei were stained by first dipping in Ehrlich's Hematoxylin for 30s – 2 min, washing off excess hematoxylin in flowing water and differentiating in 1% acid alcohol. Slides were washed once again in flowing water and examined under the microscope for staining.

The cytoplasm was stained in eosin for 3 - 5 min, followed by a brief wash in flowing water. This was followed by dehydration of the sections in an alcohol-xylene series (see below) and mounted with Depex (*VWR*).

Hydration of paraffin-embedded tissue sections:

100 % Xylene	5 min
100 % Xylene	3 min
100 % Ethanol	3 min
100% Ethanol	3 min
90 % Ethanol	3 min
70 % Ethanol	3 min
H_2O	3 min

Dehydration of tissue sections before mounting with Depex:

H_2O	3 min
70 % Ethanol	2 min
90 % Ethanol	2 min
100 % Ethanol	2 min
100 % Ethanol	2 min
100 % Xylene	2 min
100 % Xylene	2 min

2.3.4 Immunofluorescence histochemistry staining of tissue sections

After hydration of paraffin-embedded tissue in a xylene-alcohol series (section 2.4.3), antigen-retrieval was done in Citric Buffer (section 2.4.1) and left to cool down to room temperature. The cooled samples were washed once (PBS, 5min). The sections on the microscopy slides were outlined with a DAKO pen (*DAKO*) which ensures that buffers and antibody are retained within the marked region and do not spread over the whole slide, since very small volumes of antibodies are being used and the whole tissue section should preferably be covered by buffer or diluted antibodies. This was followed by blocking in Blocking Buffer (section 2.4.3; 1h, RT) in a humidity chamber and then incubating with primary antibody, diluted in Blocking Buffer (Table 2.4 for antibody dilutions) and incubated over night at 4°C in a humidity chamber. The next day, excess primary antibody was removed with 3 washes (PBS-Tween, 5min) and incubated with the appropriate fluorophore-coupled secondary antibody, against the antigen of the primary antibody (1:800 in Blocking Buffer, 1.5h, RT). This was followed by 3 washes (PBS-Tween, 5min) and the staining of the nuclei with 4', 6-diamidino-2-phenylindole (DAPI) (1:1000 in PBS,

5 min, RT). Excess DAPI was removed with one wash in PBS (5min, RT). Coverslips were mounted on the slides with the sections using pPD-Antifade (section 2.4.1) to preserve the immunofluorescence staining.

2.3.5 Immunofluorescence cytochemistry staining of cell monolayers

Keratinocytes were grown on autoclaved, collagen-coated coverslips (section 2.1.4) in 24 well plates and harvested at 70% confluency. The cells were washed twice (cold PBS) to remove traces of medium. Permeabilisation of cells in Permeabilisation Buffer (section 2.4.1; 2 min, RT) followed. The cells were then fixed in cold methanol:acetone (1:1) (2 min, RT) and washed 3 times (PBS-Tween, 2 min). The fixed cells were first incubated in Blocking Buffer (1h, RT) in the 24 well plates. Before incubating with the primary antibody, the coverslips were transferred to microscopy slides, cell side up, and the coverslip edges were outlined with a DAKO pen (*DAKO*) to ensure buffers stay on the coverslips and do not spread over the whole microscopy slide. The cells were incubated in primary antibody, diluted in Blocking Buffer (Table 2.4 for antibody dilutions), over night at 4°C in a humidity chamber. The next day, excess primary antibody was removed with 3 washed in PBS-Tween (2min) before incubating with the appropriate fluorophore-coupled secondary antibody (1:800 in Blocking Buffer, 1.5h, RT). The excess secondary antibody was removed with 3 washes in PBS-Tween (2 min) and then the nuclei were stained with DAPI (1:1000 in PBS, 5 min, RT). This was followed by one wash in PBS (2min, RT). The cells on the coverslips were mounted on microscopy slides using pPD-Antifade (section 2.4.1) with the cell side down, between coverslip and slide.

2.4 Transmission Electron Microscopy analysis

Transmission Electron Microscopy (TEM) was performed to analyse the keratinocyte morphology more closely and determine whether autophagic vesicles are present in the different epidermal layers.

2.4.1 Transmission Electron Microscopy solutions

Phosphate Buffer (0.1M)	3.1 g Sodium phosphate monobasic monohydrate (*Sigma*), 10.9 g Sodium phosphate dibasic (pH 7.4) (*Sigma*), in 1l (kindly provided by the Pathology Core Facility of Queen Mary University of London).
TEM fixative	4% Glutaraldehyde (*Sigma*) in phosphate buffer

2.4.2 Transmission Electron Microscopy

3 day old dorsal mouse skin from CD1 mice was harvested and cut into strips of 1 mm width. The strips were then fixed in TEM fixative (1h, RT, gentle shaking) and then stored at 4°C until processing and embedding in LR White. LR White is a low toxicity resin which improves the stability of the sections under the electron beam compared to the acrylic resins. The processing, embedding, cutting and imaging of the TEM sections were performed by the Pathology Core Facility of Queen Mary University of London.

2.5 Western Blotting

Western blotting is used to detect and estimate the expression levels of proteins of interest in a cell lysate. The proteins in the cell lysate are denatured and then separated according to their size with a sodium dodecyl sulphate polyacryl amide gel electrophoresis. The proteins are then transferred from the gel to a nitrocellulose membrane using the electrophoretic mobility of the proteins. The membrane is incubated in primary and secondary antibodies and the protein of interest is detected via chemiluminiscent labelling.

2.5.1 Western Blotting solutions

Tris Buffered Saline (TBS) 10x	1.5 M Sodium chloride (*Sigma*), 0.1 M tris (hydroxymethyl) aminomethane (Tris) (*Sigma*), pH 8.0 with HCl (*Sigma*)
Tween - Tris Buffered Saline (TTBS) 1x	1x TBS, 0.05% Tween (*Sigma*)
Running Buffer 10x	2 M Glycine (*Sigma*), 250 mM Tris (*Sigma*), 10 % sodium dodecyl sulphate (SDS) (*Sigma*)
Transfer Buffer 10x	2 M Glycine (*Sigma*), 250 mM Tris (*Sigma*)
Stripping Buffer 1x	62.5 mM Tris (*Sigma*) (pH 6.8), 2% SDS (*Sigma*), 100 mM β-Mercaptoethanol (*Sigma*)
RIPA lysis Buffer	150 mM Sodium chloride (*Sigma*), 1.0% Igepal (*VWR*), 0.5% Sodium deoxychalate (*Sigma*), 0.1% SDS (*Sigma*), 50 mM Tris (*Sigma*) (pH8.0), 100 uM Sodium pervanadate (*Sigma*), 1 mM Phenylmethanesulfonyl fluoride (*Sigma*), 1 mM Sodium fluoride, Protease tablets (*Roche*) 1 per 50 ml Stored at -20°C

Sample Buffer (Stock)	180 mM Tris (*Sigma*) (pH6.8), 6% SDS (*Sigma*), 28% Glycerol (*Sigma*), 0.001% Bromphenol Blue (*Sigma*)
Sample Buffer (S.B.) 3x	S.B.: 1 M Dithiothreitol (*Sigma*) (DTT) = 3:1
Epidermal Separation Buffer	5 mM Ethylenediaminetetraacetic acid (*Sigma*) (EDTA) in PBS (*Invitrogen*), 0.1 mM PMSF (*Sigma*)
Epidermal Lysis Buffer	10 mM Tris (*Sigma*) in PBS (*Invitrogen*), ~~0.1 (pH 7.5),~~ 5% SDS (*Sigma*), 20% β-Mercaptoethanol (*Sigma*), 0.001% Bromphenol blue (*Sigma*)
Coomassie blue Stain	0.2% Coomassie blue (*Sigma*), 20% Methanol (*Sigma*), 0.5% Acetic acid (*Sigma*)
Coomassie blue Destain	30% Methanol (*Sigma*)

2.5.2 Protein extraction from monolayer cells

Before lysis, monolayer cells were washed 2x (cold PBS). The cell monolayer was incubated in RIPA buffer (5 min, on ice) and later scraped off the culture dish. Lysed cells were centrifuged (13 000 rpm, 10 min, 4°C) and the pellet of cell debris discarded. The protein concentration was determined using a Pierce BCA Protein Assay Kit (*Thermo Scientific, ~~Massachusettes~~Massachusetts, USA*). To prevent degradation of very small proteins, like LC3, due to freeze-thaw cycles, lysates were immediately prepared for protein separation and blotting (lysate: S.B. (2:1), 100°C, 5 min) before storage at -80°C. Protein lysates were thawed a maximum of 3 times.

2.5.3 Protein extraction from explants

Explants for protein analysis were stored at -80°C (sections 2.1.12 and 2.1.13). The frozen explant tissue was incubated in ice cold Epidermal Separation Buffer (section 2.5.1; 3 min, on ice). Using a dissecting microscope, the explants were first peeled off the filter paper and then the dermis was carefully pulled off the epidermis. The epidermis was incubated in Epidermal Lysis Buffer (see section 2.5.1; 10 - 15 min, on ice) and then boiled (100°C, 10 min), vortexing a few times to ensure efficient epidermal lysis.

Protein concentration analysis using a BCA assay was not possible because the Epidermal Lysis Buffer contains DTT, which would falsify results. Therefore, the explant protein concentration was estimated with an SDS-gel (see section 2.5.5) and Coomassie blue staining (see section 2.5.5; 1h, gentle shaking). Protein bands were made visible by destaining the gel in Destain Solution (see section 2.5.5; over night, RT, gentle shaking). Based on the intensity of the bands, the protein concentration was estimated.

2.5.4 Immunoprecipitation

Immunoprecipitation (IP) is a method used to purify a specific protein or groups of proteins from lysates by using an antibody, specific for a target protein which is bound to a solid material. IPs were perfomed on protein lysates from REKs transfected with HA-tagged AKT1 and HA-tagged AKT2 to separate these proteins from the endogenous AKT proteins and analyse the phosphorylation status of the pulled-down proteins. As a control, lysates from REKs expressing the empty vector, pCDNA3.1 were used (section 2.1.11).

First, the protein concentration in the whole cell lysates from the transfected REK cell lines was determined using a Pierce BCA Protein Assay Kit (*Thermo Scientific, ~~Massachusetts~~Massachusetts, USA*). For the IP, a monoclonal HA-agarose

conjugate (Clone HA-7; *Sigma*) was used. This is a mouse monoclonal antibody against HA which has been immobilised on agarose beads. The IP was performed according to the manufacturer's instructions.

All steps were performed on ice and in a 4°C centrifuge. Per IP, 40 ul of monoclonal HA-agarose conjugates was washed 5 times with 1 ml of RIPA buffer (12 000g, 30s) and the supernatant discarded. 200 ug of fresh RIPA cell lysate was then added to the cleared resin, brought to a final volume of 300 ul with RIPA buffer and incubated on an orbital shaker for 2h at 4°C. This was followed by 5 washes of the resin in 1 ml RIPA buffer (12 000g, 30s) and the supernatant discarded. Finally, the beads were incubated with 30 ul 3x Sample buffer (section 2.5.1) and denatured (100°C, 5 min). The immuno-precipitated and denatured protein was separated from the agarose beads by centrifugation (12 000g, 1 min) and the supernatant transferred to a fresh tube. The samples were then loaded on an SDS poly-acrylamide gel and analysed by Western blotting (section 2.5.5).

2.5.5 SDS poly-acrylamide gel and Western blotting

A 12.5% resolving gel was used when analyzing small proteins (12-25 kDa), whereas an 8% gel was used for proteins larger than 30 kDa.

Table 2.6: Components of the SDS polyacrylamide resolving Gel

	8% (>30 kDa)	**12.5% (<30 kDa)**
30% Acrylamide	2 ml	3.1 ml
1.5M Tris/HCl (pH 8.8)	3 ml	3 ml
10% SDS	76 µl	76 µl
H_2O	2.43 ml	1.3 ml
10% APS	36 µl	36 µl
TEMED	5 µl	5 µl

Table 2.7: Components of the SDS polyacrylamide stacking Gel

	4%
30% Acrylamide	660 µl
1.5M Tris/HCl (pH 8.8)	630 µl
10% SDS	50 µl
H_2O	3.6 ml
10% APS	25 µl
TEMED	5 µl

The Kaleidoscope Pre-stained Protein Standard (*Bio-Rad*) was used as a size indicator. Separation of proteins in the lysates according to their size was performed by loading the same amount of protein of each denatured sample lysate (section 2.5.2 and 2.5.3) on the SDS poly-acrylamide gel, as well as the protein standard for reference purposes. The SDS gel electrophoresis was performed using running buffer (section 2.5.1) and the Mini-PROTEAN®Tetra Cell system from Bio-Rad.

After separation on the SDS-gel, protein bands were transferred to a 45 micron Hybond-C™ extra, nitrocellulose membrane (*GE Healthcare*) with transfer buffer (section 2.5.1) and using the Mini-Transblot®Cell from Bio-Rad at 100V, 1.5h, 4°C. After the transfer, the blotting membrane was incubated in 5% milk/TTBS (1h, RT) to block the unreacted sites on the membrane reducing unspecific binding of antibodies.

Membranes were incubated in a primary antibody (in 5% BSA/TTBS, 2h, RT, OR overnight, 4°C; Table 2.4 for antibody dilutions) specific for the protein of interest. The excess primary antibody was removed with 4 washes (TTBS, 5 min) before incubating in a horseradish peroxidase-conjugated secondary antibody (1:800 in 5% milk/TTBS, 1h, RT). After another 4 washes (TTBS, 5 min), the secondary antibody-bound to protein on the membrane was made visible by using ECL plus (*GE*

Healthcare, Buckinghamshire, UK) which emits a chemiluminescent signal. This is captured in a dark room on Hyperfilm (*GE Healthcare, Buckinghamshire, UK*) and the film is developed using a Hyperprocessor automatic Autoradiography Film Processor (*GE Healthcare, Buckinghamshire, UK*).

For analysis of multiple proteins, with the same or similar size on one membrane, the already bound primary antibody was removed by incubating the membrane in stripping buffer (section 2.5.1; shaking, 10 - 15 min, 50°C). The stripped membrane was blocked (5% milk/TTBS, 1h) before incubating with the next primary antibody.

Chapter 3

RESULTS

Analysis of Autophagy in Epidermis

Analysis of Autophagy in Epidermis

Introduction

Autophagy is a process by which intracellular organelles and proteins are degraded. It plays an important role during starvation, aging, immune response, cell growth as well as in cancer (reviewed in Deretic 2008).

Formatted: Font color: Auto

Recent publications suggest that autophagy is important in keratinocyte biology. Cultured psoriatic keratinocytes respond to drug treatment by induction of autophagy (Wang and Levine 2011). During early differentiation, the keratinocyte cell line, HaCaT has been shown to express higher levels of the autophagosome marker, LC3 and also more LC3 aggregates, pointing to increased autophagosome formation and an up-regulation in autophagy (Aymard *et al.* 2011). In cancers, increased autophagy rescues SCC cell lines from cell death induced by chemotherapy (Claerhout *et al.* 2010).

However, it must be noted that all published data on autophagy in keratinocytes are based on *in vitro* monolayer cultures. Different autophagy proteins are crucial for the different stages of the autophagic process. So, for my PhD project, the autophagy proteins ULK1, WIPI1, BECN1, ATG5-ATG12 and LC3, which have different functions in the autophagy pathway, are used as markers for autophagy. For the initiation of double-membrane formation~~, three complexes are required. ULK1 is required for~~ the ULK protein-kinase complex~~, WIPI1 is important in the mATG9-ATG2-WIPI1 complex~~ and the class III PI(3) kinase complex of which BECN1 is a key component are required. The elongation of the double-membrane is catalysed by the ATG5-ATG12 complex. Cytoplasmic LC3I is cleaved and lipidated to LC3II which is incorporated into the double-membrane and this is required for

Comment [MSOffice3]: review

membrane closure and autophagosome formation. For completion of the autophagic process and degradation of autophagic vesicles, LC3II positive autophagosomes fuse with lysosomes to form LC3II/LAMP2 double-positive autolysosomes (see section 1.2.2).

The aim of this chapter is to establish whether autophagy markers are present in epidermis. For this, the expression pattern of autophagy markers was determined in adult mouse and adult human skin using a panel of commercially available antibodies against ULK1, WIPI1, BECN1, ATG5-ATG12 and LC3. Also, autophagy marker expression during foetal terminal differentiation and skin barrier acquisition was investigated to determine whether the autophagic pathway is important during terminal differentiation, as the terminal differentiation stages are temporally separated during foetal development. Monolayer keratinocytes were used as an *in vitro* model to mimic the differentiation stages in epidermis and to further analyse the observations made in tissue samples. In these monolayer keratinocyte cultures, the expression profile of markers of epidermal differentiation was first determined, and this was followed by analysis of autophagy markers expression. The morphology of monolayer keratinocyte populations at different stages of differentiation reveals striking differences which appear to be due to autophagy in the differentiated cells. Autophagy in differentiated monolayer keratinocytes is further characterised and its role in keratinocyte differentiation is examined.

Results

3.1 Expression of autophagy markers in adult epidermis

In order to investigate whether autophagy markers are expressed in normal adult epidermis, samples of mouse and human skin were used. Initially, normal adult mouse and adult human epidermis were characterised by using a panel of antibodies against proteins specific for the different layers within the epidermis. I determined the protein expression pattern of keratin14 (K14), which is a marker of proliferating keratinocytes, keratin1 (K1), a marker of early differentiation characteristic for supra-basal layer keratinocytes and filaggrin and loricrin which are normally expressed in keratinocytes of the terminally differentiating granular layer (Fig. 1.1). Terminal differentiation occurs just before the cells undergo cornification and cell death, and turn off expression of supra-basal K1.

Immunofluorescence analysis of these epidermal differentiation markers in both adult mouse and adult human epidermis shows that K14, which is a marker of proliferating keratinocytes is expressed in the basal and para-basal cells of the epidermis samples (Fig. 3.1). K1 which is characteristic for early differentiating keratinocytes is expressed in the supra-basal layers of adult mouse and adult human epidermis (Fig. 3.1). The terminal differentiation marker loricrin is present in the granular layers of the samples of adult epidermis analysed (Fig. 3.1). Filaggrin which is another marker of epidermal terminal differentiation is also expressed in the granular layers of the adult epidermis (Fig. 3.1). These results show that the samples of adult mouse and human epidermis I used have a normal expression of epidermal differentiation markers and are suitable for further analysis of autophagy protein expression in adult epidermis.

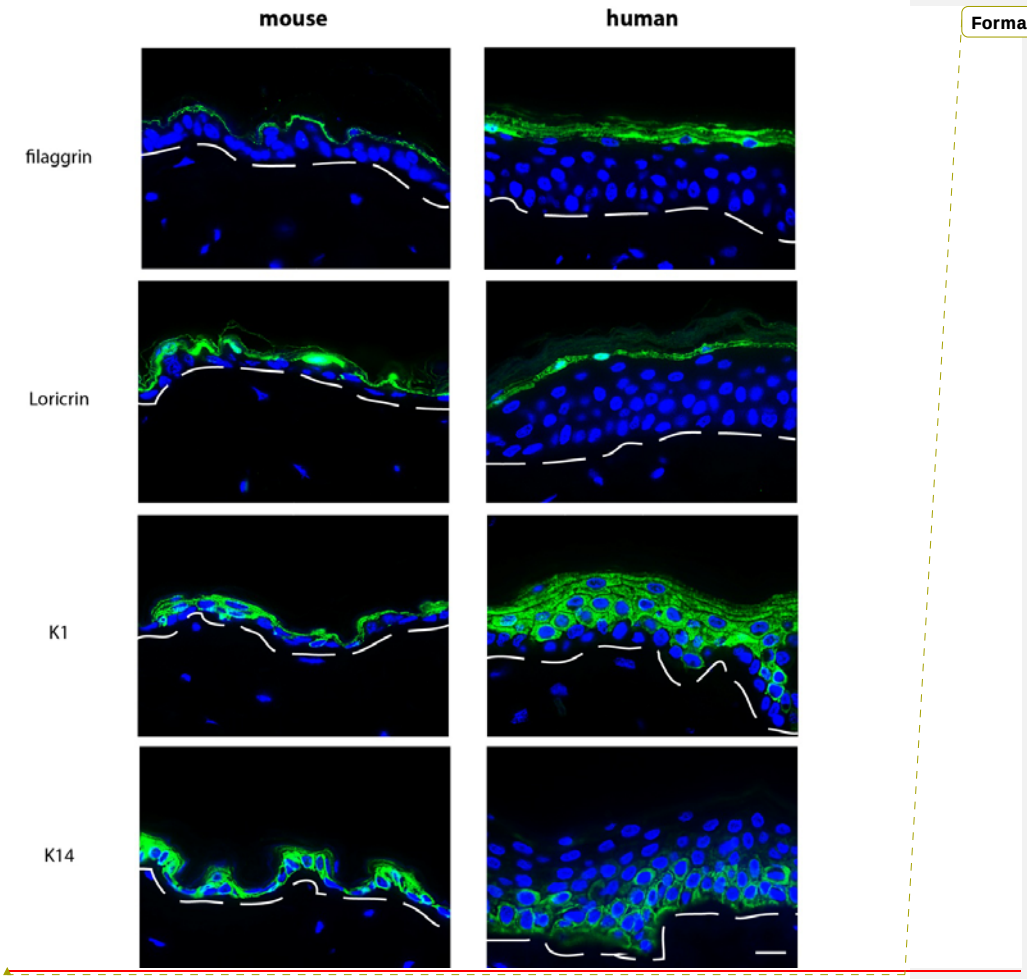

Formatted: Font: 12 pt

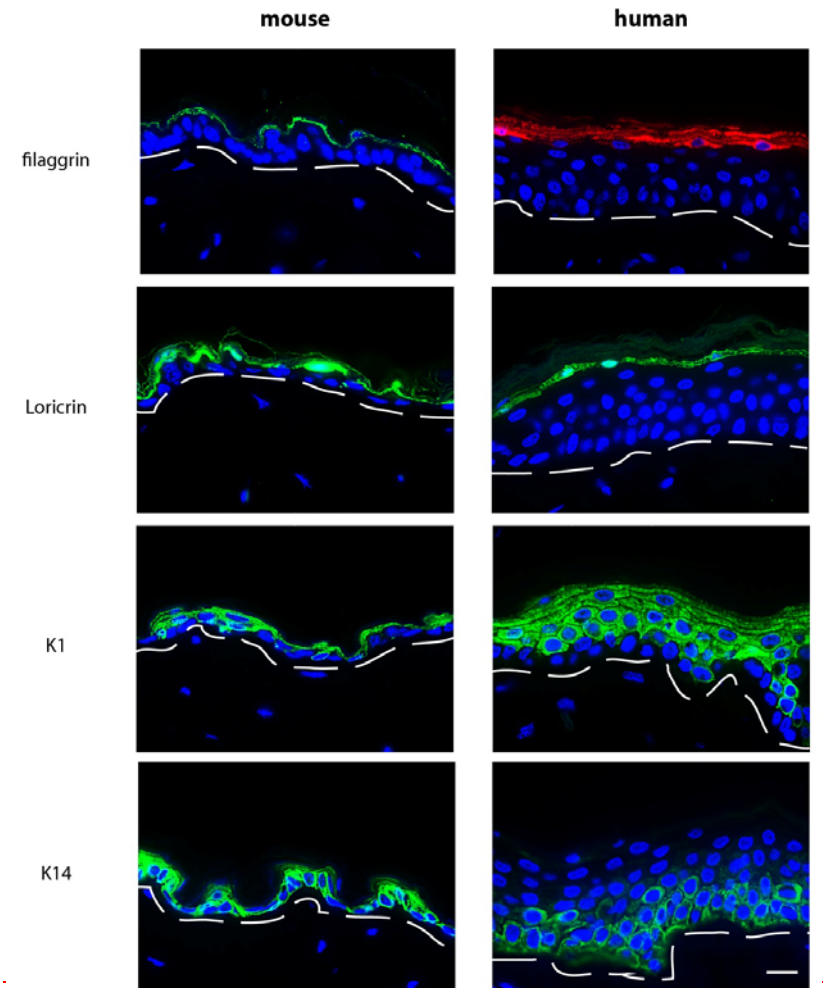

Figure 3.1: Expression of epidermal differentiation markers in adult mouse and human epidermis.

The terminal differentiation markers filaggrin and loricrin are expressed in the granular layers of both adult mouse and human epidermis. K1, a marker of early differentiation, is present in the supra-basal layers. K14, a marker of undifferentiated keratinocytes, is expressed in the basal and para-basal layers.

This figure is representative of n=3 biopsies of normal human facelift skin and n=2 samples of both dorsal and ventral adult mouse skin.

Bar = 20um. Dotted line = basement membrane.

The expression profile of autophagy markers was then established in the same adult mouse and human skin samples using immunofluorescence analysis. To date, commercially available antibodies against LC3, the autophagosome marker, recognise unlipidated LC3 (LC3I) as well as the membrane-bound form (LC3II). So immunofluorescence analysis of LC3 would detect all forms of LC3. However, it has been published that membrane-bound LC3II appears as LC3 positive aggregates or puncta (Kabeya *et al.* 2000; Klionsky *et al.* 2012) and this is also widely accepted as one of the indications for the presence of autophagosomes. I show that with immunofluorescence analysis, LC3 is expressed in all layers of adult epidermis with the highest expression levels in the granular layer, where it occurs as large aggregates suggesting the presence of autophagosomes (Fig. 3.2).

ULK1 is a downstream target of mTORC1 and a component of the ULK protein-kinase complex required for the autophagy initiation stage where the double-membrane is formed (Chan *et al.* 2007; Hara *et al.* 2008; Chan and Tooze 2009; Ganley *et al.* 2009; see section 1.2.2). In adult epidermis, immunofluorescence analysis shows that ULK1 is expressed in the supra-basal layers, however with higher intensity and ULK1 puncta formation in the granular layer (Fig. 3.2).

For double-membrane formation during autophagy, a second complex comprised of mATG9, ATG2 and WIPI1/2 is required. This WIPI1 complex localises to the first initiation complex, the ULK protein-kinase complex, for double-membrane formation (Tooze *et al.* 2010; Codogno *et al.* 2012; Gaugel *et al.* 2012; see section 1.2.2). In some cells types, WIPI1 can localise to autophagic vesicles colocalising with LC3 and showing a punctate expression pattern (Proikas-Cezanne *et al.* 2007). I observe that WIPI1 is mainly expressed as large aggregates in the granular and cornified layers of adult epidermis (Fig. 3.2) suggesting high levels of autophagic activity may occur in the upper epidermal layers.

The autophagy protein BECN1 can promote or repress the autophagic pathway depending on its binding partners (section 1.2.2). BECN1 participates in two

autophagy-promoting class III PI3kinase complexes and one autophagy-repressing class III PI3kinase complex (Fig. 1.7b). The pro-autophagy complexes are components of a third autophagy initiation complex required for isolation membrane formation (Matsunaga *et al.* 2009). Therefore, BECN1 is essential for autophagy. However, analysis of BECN1 expression alone is not a read-out for active autophagy since it does not shed light on its binding-partners and BECN1 activity. In Figure 3.2, analysis of BECN1 expression in adult epidermis shows that BECN1 is strongly expressed in the basal and para-basal layers. However, in the granular layer where other autophagy markers are strongly expressed (LC3, ULK1 and WIPI1), there are a few BECN1 positive aggregates (Fig. 3.2).

During the autophagy process, the fresh isolation membrane is elongated and enlarged until it closes forming the autophagosome. For this elongation process, the ATG5-ATG12 complex interacts with the double-membrane and is bound transiently until membrane closure, when it is set free again (section 1.2.2; Mizushima *et al.* 2001). Right after synthesis of ATG5, it is immediately modified and binds to ATG12 constitutively (Fig. 1.9; Codogno and Meijer 2006). However, it has also been shown that under some pro-apoptotic conditions, in the absence of autophagy and in some cell types, ATG5 is cleaved and does not form a complex (Codogno and Meijer 2006; Yousefi *et al.* 2006; Shi *et al.* 2013). With immunofluorescence analysis, I show that in adult epidermis the ATG5-ATG12 complex is strongly expressed in the basal layer, but it is also present at lower levels in the granular layer (Fig. 3.2). This expression pattern is very similar to that observed with BECN1.

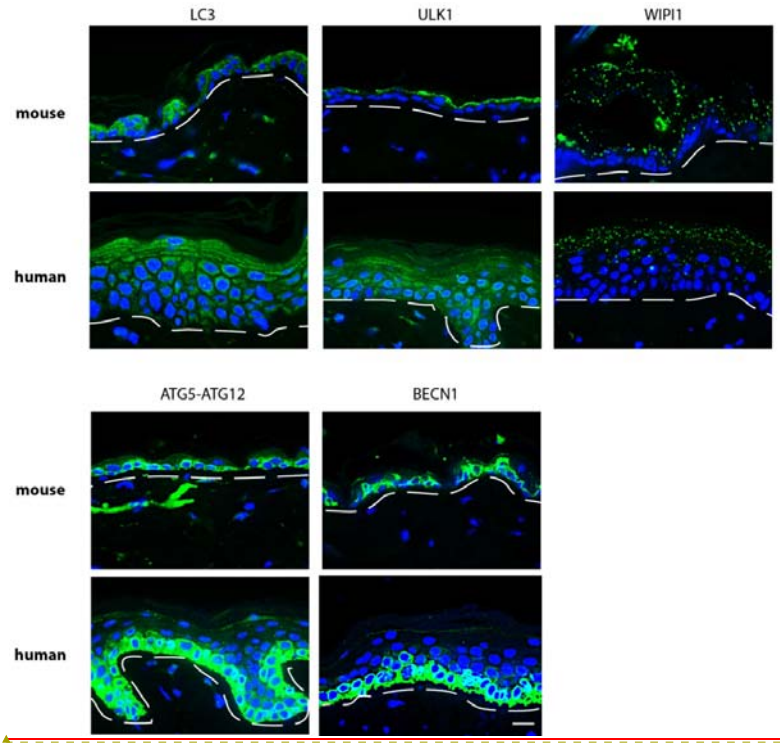

Figure 3.2: Expression of autophagy markers in adult mouse and human epidermis.

In adult mouse and human skin, the autophagosome marker LC3 is expressed in all layers of epidermis with the strongest expression in the granular layer where it is present as aggregates. ULK1, required for the initiation stages of autophagy, is expressed in all epidermal layers with the highest intensity in the granular layer. WIPI1, which also participates in double-membrane formation, is mainly present as aggregates in the granular layers. ATG5-ATG12 required for elongation of the isolation membrane is highly expressed in the basal layer but is also present at lower levels in the granular layers. BECN1, which has different functions in autophagy, one of which is in the initiation process, is mainly present in the basal layer with a few puncta in the granular layers. *This figure is representative of n=3 biopsies of normal human facelift skin and n=2 samples of both dorsal and ventral adult mouse skin. Bar = 20um. Dotted line = basement membrane.*

Formatted: Font: Calibri, 12 pt

Formatted: Space After: 0 pt

~~**Figure 3.2: Expression of autophagy markers in adult mouse and human epidermis.**~~

~~In adult mouse and human skin, the autophagosome marker LC3 is expressed in all layers of epidermis with the strongest expression in the granular layer where it is present as aggregates. ULK1, required for the initiation stages of autophagy, is expressed in all epidermal layers with the highest intensity in the granular layer. WIPI1, which also participates in double-membrane formation, is mainly present as aggregates in the granular layers. ATG5-ATG12 required for elongation of the isolation membrane is highly expressed in the basal layer but is also present at lower levels in the granular layers. BECN1, which has different functions in autophagy, one of which is in the initiation process, is mainly present in the basal layer with a few puncta in the granular layers. *This figure is representative of n=3 biopsies of normal human facelift skin and n=2 samples of both dorsal and ventral adult mouse skin. Bar = 20um. Dotted line = basement membrane.*~~In summary, the mouse and human skin samples, used to determine the autophagy marker expression profile, show normal epidermal differentiation (Fig. 3.1). The autophagy markers LC3, ULK1, WIPI1, BECN1 and ATG5-ATG12 are present in adult epidermis (Fig. 3.2). An unexpected finding was that the autophagosome marker LC3 is strongly expressed in the granular layer of adult epidermis and it is also present as aggregates indicating autophagic vesicles. Also ULK1 and WIPI1 show a strong granular layer expression pattern in epidermis (Fig. 3.2). The proteins BECN1 and ATG5-ATG12 are highly expressed in the basal layer however, they are also present in the granular layer at lower levels. Since autophagy proteins required for the autophagic process are all present in the granular layer, these results suggest that autophagy may occur in the upper layers of epidermis. Also, LC3 aggregates in the granular layer indicate the presence of autophagosomes. However, the strong expression of BECN1 and ATG5-ATG12 in the basal layers may have other functions (addressed in chapter 5).

3.2 Expression of autophagy markers during barrier acquisition in foetal epidermis

The presence of autophagy markers and especially LC3 aggregates in the granular layer of adult epidermis (Fig. 3.2) indicates that autophagy may be important for epidermal terminal differentiation which occurs in the granular layer. Therefore, the expression pattern of autophagy markers was analyzed in mouse foetal epidermis during the period of granular layer formation and barrier acquisition. During foetal development, there is temporal separation of the terminal differentiation and barrier formation steps. Therefore, developmental expression studies both reinforce adult studies plus inform about stages of terminal differentiation requiring autophagy.

During development, the formation of the epidermal barrier correlates with formation of the cornified layer. In mouse foetal development, the epidermal barrier is formed between E15.5 and E18.5 (Hardman *et al.* 1998). Therefore, the autophagy marker expression profile in epidermis of mouse embryos over this period in development was analysed. Initially, I needed to determine the exact time-point for granular layer formation in the samples of mouse foetal epidermis used. The expression pattern of epidermal differentiation markers was established with immunofluorescence analysis.

The expression of the terminal differentiation marker filaggrin, which is characteristic for keratinocytes of the granular layer, was analysed in foetal epidermis over the period from E15.5 to E18.5 to determine exactly when the granular layer is formed in these samples. At E15.5 there is no filaggrin-expressing granular layer (Fig. 3.3) indicating the absence of terminally differentiating keratinocytes. However, at E16.5, there are low levels of filaggrin in the upper layers of foetal epidermis (Fig. 3.3) indicating activation of terminal differentiation in the upper layers. These results are compatible with published data showing that the

first signs of granular layer formation occur at E16.5 during mouse foetal development (Hardman *et al.* 1998)

Filaggrin expression is increased in the granular layers at E17.5 and E18.5 (Fig. 3.3) indicating the presence of an intact granular layer. These observations of filaggrin expression patterns suggest that in the samples of foetal epidermis analysed, terminal differentiation and granular layer formation is activated at E16.5.

The expression pattern of another terminal differentiation marker Loricrin, was analysed in these samples of foetal epidermis. Loricrin is very strongly expressed in the upper epidermal layers including the upper supra-basal layers at E15.5 and E16.5 (Fig. 3.3). When compared to the expression of loricrin in adult epidermis where it is confined to the granular layer (Fig. 3.1), E15.5, and E16.5 show a very unusual expression pattern of loricrin (Fig. 3.3). This expression pattern of loricrin during foetal development at E15.5 and E16.5 may be as a result of the still immature and not yet fully functional terminal differentiation process at these early time points. However, at E17.5 and E18.5 when the granular layer is formed loricrin is present only in the upper layers of the epidermis, similar to adult skin (Fig. 3.1), which corresponds to the filaggrin-positive granular layers (Fig. 3.3).

The marker for early keratinocyte differentiation, K1, which is expressed in the supra-basal layers of normal adult epidermis (Fig. 3.1), is present in the supra-basal layers of mouse foetal epidermis from E15.5 to E18.5 (Fig. 3.3). These results show that early epidermal differentiation has probably occurred before E15.5 in the supra-basal layer.

In the normal adult epidermis, proliferating basal layer keratinocytes express K14 (Fig. 3.1). In mouse foetal epidermis over the period of barrier formation, the K14 expressing basal layer is present at E15.5 to E18.5 (Fig. 3.3) indicating that the proliferating keratinocytes are confined to the basal layer like in normal adult epidermis.

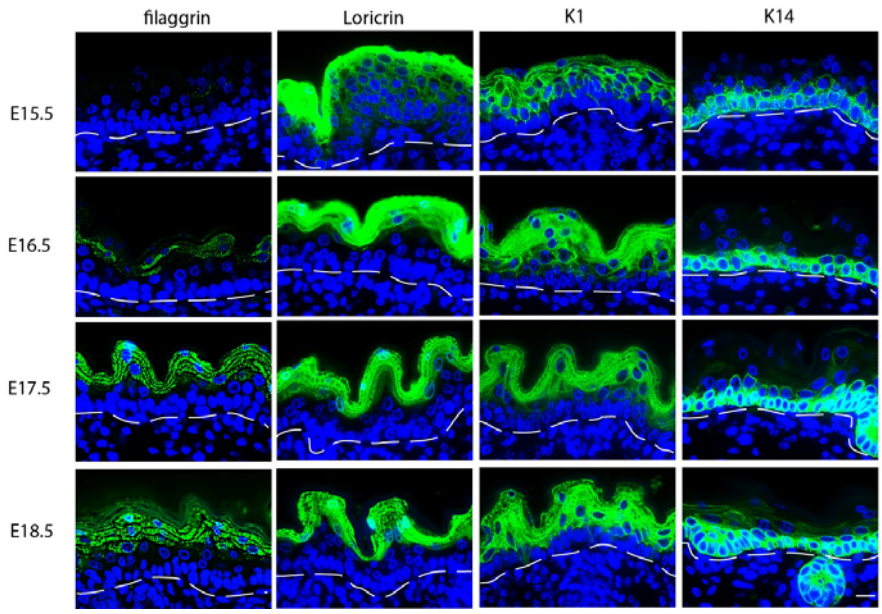

Figure 3.3: Expression of epidermal differentiation markers during mouse foetal barrier acquisition.

Expression of the terminal differentiation marker filaggrin is induced at low levels at E16.5. Filaggrin is present at higher levels in the upper layers of E17.5 and is maintained at similar levels at E18.5. Another granular layer marker, loricrin is strongly expressed in the supra-basal layers of E15.5 and E16.5. This unusual expression pattern changes to the granular layer at E17.5 and E18.5 where it is also expressed in adult epidermis. The early marker of differentiation, K1, which is usually expressed in the spinous layer of epidermis, is present in the supra-basal layers of E15.5 to E18.5. K14 which is a marker of proliferating keratinocytes is expressed in the basal layer of epidermis from E15.5 to E18.5.

This figure is representative of n=2 samples of mouse foetuses from 2 different litters.

Bar =20um. Dotted line = basement membrane.

In the foetal mouse samples used, I established that granular layer formation is initiated E16.5 corresponding to already published data (Hardman *et al.* 1998). At E15.5 before granular layer formation, the epidermis is comprised of the proliferating basal layer and keratinocytes of the spinous layer (Fig. 3.3). Therefore, to determine whether autophagy may be important during barrier acquisition, the expression pattern of autophagy markers was analysed in mouse foetal epidermis from E15.5 to E18.5.

At E15.5, low levels of LC3, ULK1, WIPI1 and ATG5-ATG12 can be detected in the upper layers of the epidermis (Fig. 3.4). At E16.5, corresponding to the initiation of granular layer formation in foetal skin (Fig. 3.3; (Hardman, 1998 #206), there is a high induction of LC3 and ULK1 expression in the uppermost layers, corresponding to the early granular layers (Fig. 3.4). The levels of WIPI1 and granular ATG5-ATG12 are also further increased in the upper layers at E16.5 (Fig. 3.4). This is also accompanied by switching-on of BECN1 expression in the basal and upper layers at this time-point (Fig. 3.4). This autophagy marker expression pattern is maintained until birth and remains in adult skin (Fig. 3.2). In summary, I observe that autophagy marker expression is highly up-regulated at E16.5 which corresponds to the time-point when the granular layer is formed and barrier acquisition occurs in foetal epidermis.

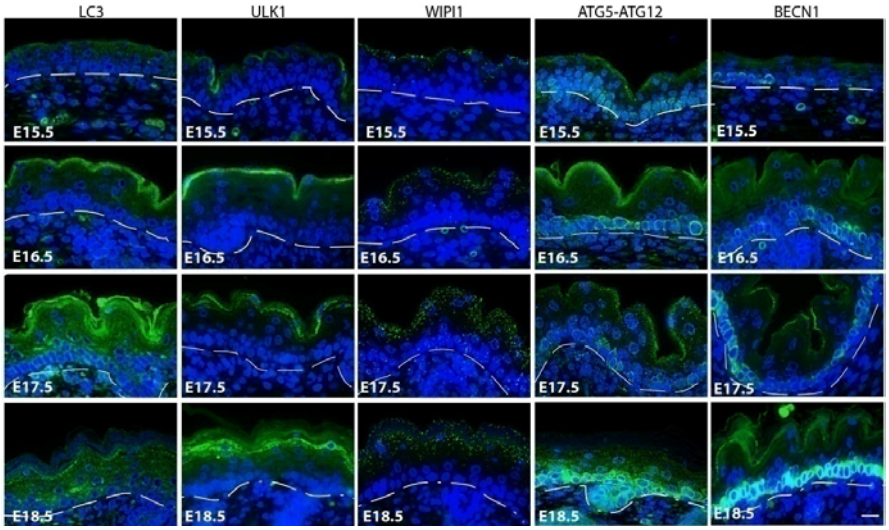

Figure 3.4: Expression of autophagy markers during barrier acquisition in mouse foetal epidermis.

At E15.5 there are low levels of LC3, ULK1, WIPI1 and ATG5-ATG12 in the upper layers of the epidermis. At E16.5, when the first attempts at barrier formation occur, there is an increase in the expression of LC3 and ULK1 in the upper layers and also, a moderate increase in WIPI1 and ATG5-ATG12 in the granular layers. Basal and granular BECN1 expression is also activated at E16.5. This pattern of autophagy marker expression is maintained at E17.5 and E18.5.

This figure is representative of n=2 samples of mouse foetuses from 2 different litters.

Bar = 20um. Dotted line = basement membrane.

In conclusion, I show that autophagy markers are present in the granular layer of adult epidermis. Also, LC3, the autophagosome marker, is present at its highest concentrations in the granular layer of adult epidermis where it appears to form LC3 aggregates suggesting formation of autophagosomes. During granular layer formation in mouse foetal development, autophagy marker expression is highly up-regulated at E16.5, the time-point when the granular layer is formed.

These results indicate that autophagy may play an important role in the granular layer where keratinocytes undergo terminal differentiation, a specialised form of cell death. Based on these findings, I hypothesize that autophagy plays an important role in the granular layer where organelles are degraded and keratinocytes undergo terminal differentiation.

3.3 Characterisation of epidermal granular layer LC3 aggregates

In sections 3.1 and 3.2, I have shown by immunofluorescence analysis that LC3 is strongly expressed in the granular layer of epidermis where it appears to be present as aggregates. Also, formation of the granular layer during mouse foetal development is accompanied by a high induction of autophagy marker expression. These results indicate that autophagy may play an important role in barrier formation.

It has been published that some cellular processes may use the autophagic machinery for non-autophagic processes leading to the formation of LC3 positive vesicles which do not participate in classical autophagy. In some cells, bacteria and yeasts are engulfed in LC3 positive single-membrane phagosomes and degraded (Sanjuan *et al.* 2007; Sanjuan *et al.* 2009). Also, in some macrophages, phagosomes containing apoptotic cells are LC3 positive (Florey *et al.* 2011; Martinez *et al.* 2011). Other LC3 positive single-membrane structures containing engulfed live cells have been discovered within a host cancer cells (Florey *et al.* 2011). Different viruses can hijack the autophagic machinery, inducing formation of LC3 positive double-membrane vesicles which are used for virus replication (English *et al.* 2009; Reggiori *et al.* 2010). Therefore, I need to determine whether granular layer LC3 aggregates colocalise with markers for other known organelles of the granular layer.

I have shown that filaggrin is present in the granular layer of epidermis (Fig. 3.1). Published data analysing epidermal terminal differentiation by electron microscopy shows that the filaggrin precursor, pro-filaggrin, is accumulated in granular layer keratinocytes as aggregates, termed F-granules (Steven *et al.* 1990). Since epidermal terminal differentiation is a complicated process and is not well understood, it is possible that the autophagic machinery may be used for filaggrin processing in the upper layers of epidermis and may interact with the F-granules. Therefore, using immunofluorescence analysis, I wanted to determine whether granular layer filaggrin colocalises with LC3 positive puncta.

Double immunofluorescence staining for filaggrin (red) and LC3 (green) expression in adult human epidermis shows that filaggrin is expressed in the uppermost epidermal granular layers (Fig. 3.5). LC3 is also present as aggregates in the granular layer (Fig. 3.2; Fig. 3.5). However, filaggrin (red) and LC3 (green) expression are spatially separated with the filaggrin positive layer above the LC3 expressing granular layer (Fig. 3.5). There are some regions where filaggrin (red) and LC3 (green) expression overlap and they appear to colocalise, but the size and shape of the granules differ suggesting they are different granules (purple arrow, Fig. 3.5). Therefore, it is concluded that LC3 aggregates are not filaggrin granules.

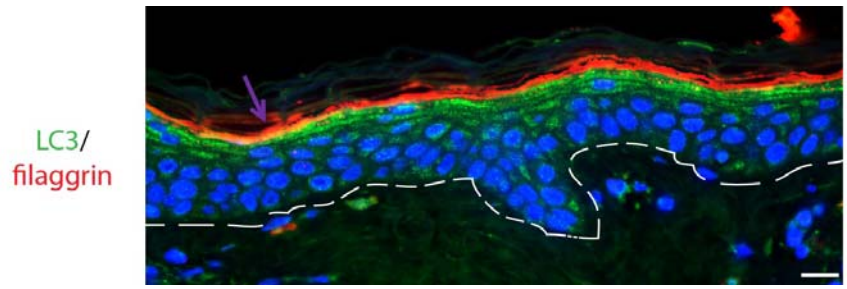

Figure 3.5: Localisation of LC3 aggregates and filaggrin granules in adult human epidermis.

LC3 (green) and filaggrin (red) are both strongly expressed in the granular layers of adult epidermis. However, filaggrin is expressed in the uppermost granular layers above the LC3 expressing layers, but sometimes the LC3 and filaggrin expressing layers do overlap. Where LC3 and filaggrin appear to and colocalise (purple arrow), the size and shape of the aggregates are different indicating they are different granules.

This figure is representative of n=3 biopsies of normal human facelift skin.

Bar = 20um. Dotted line = basement membrane. Purple arrow = regions of colocalisation.

The upper epidermal layers are regions of high lipid synthesis. Lipids among other compounds are processed within the lamellar body network which is more concentrated in the upper epidermal layers (Elias and Brown 1978; Landmann 1988; Lee *et al.* 1998; Elias 2012). Lamellar bodies are thought to originate from the Golgi, which has also been shown to give rise to autophagic membranes in some cells. Also, both lamellar bodies and autolysosomes~~phagic vesicles~~ contain lysosomal enzymes (Locke and Sykes 1975; Raymond *et al.* 2008; Nishida *et al.* 2009; Yen *et al.* 2010). Therefore, the next question I asked is whether granular layer LC3 aggregates are lamellar bodies or are part of the lamellar body machinery. I used immunofluorescence microscopy to determine if the LC3 aggregates present in the upper layers of epidermis are distinct from known lamellar body markers.

Cathepsin D (CatD) is an aspartic protease which is highly expressed in granular keratinocytes, where it is a component of the lamellar body cargo (Ishida-Yamamoto *et al.* 2004). Therefore, antibodies against LC3 and CatD were used to localise autophagosomes and lamellar bodies in adult human skin.

Double immunofluorescence staining with antibodies against CatD (red) and LC3 (green) shows that both proteins are present in different layers of epidermis with CatD in the uppermost granular layer above the LC3 positive layer (Fig. 3.6). However, there are a few LC3-CatD double-positive regions in the basal and granular layers (purple arrow, Fig. 3.6). CatD is also a lysosomal protease. Therefore, the observed colocalization may be due to fused autophagosomes and CatD containing lysosomes, since autophagosomes fuse with lysosomes during the maturation step, for the degradation of autophagic cargo. However, in epidermis there are few regions of LC3 and CatD colocalisation. Therefore, it is concluded that epidermal LC3 aggregates in the granular layer are not part of the lamellar body machinery.

LC3/ CatD

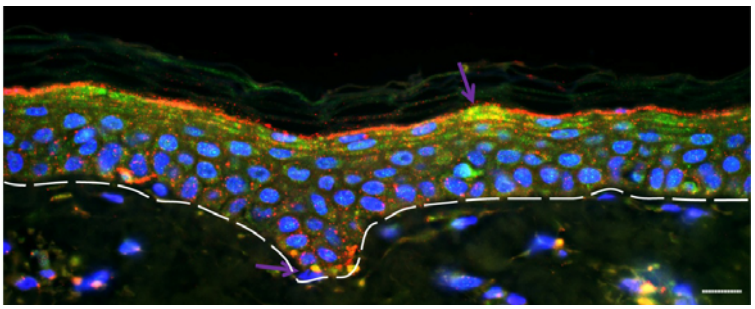

Figure 3.6: Localisation of LC3 aggregates and CatD positive lamellar bodies in adult human epidermis.

Both LC3 (green) and CatD (red) are expressed in all layers of the epidermis with the strongest expression in the granular layers. However, LC3 and CatD granules sometimes colocalise (purple arrows). Regions of LC3 and CatD colocalisation in the basal layer and the upper layers (purple arrows) could be due to CatD also being present in lysosomes, and autophagosomes fuse with lysosomes during the autophagy maturation stage. However, LC3 and CatD expression rarely colocalise in epidermis.

This figure is representative of n=3 biopsies of normal human facelift skin.

Bar = 20um. Dotted line = basement membrane. Purple arrow = regions of colocalisation.

In this section, I have shown that granular layer LC3 aggregates do not colocalise with markers for filaggrin granules or lamellar bodies, which are both organelles characteristic of granular layer keratinocytes and may have a common origin with autophagic vesicles. These data supports the initial hypothesis that autophagy plays an important role in the granular layer where organelles are degraded and keratinocytes undergo terminal differentiation.

Next, I wanted to determine whether double-membrane vesicles are present in the epidermis. Transmission electron microscopy (TEM) is routinely used to confirm the presence of double-membrane vesicles in cell cultures and in tissues (Yla-Anttila *et al.* 2009; Klionsky *et al.* 2012). However to date, publications on the structure and the components of the epidermis with TEM analysis do not show epidermal double-membrane vesicles. A reason for this may be that most of the TEM on the epidermis was carried out in the 1970s and 1980s when the focus was on other epidermal organelles. Also, the method of tissue fixation and embedding material of the samples plays a very important role in maintaining membrane morphology.

Therefore, I decided to perform TEM analysis of 3 day old mouse epidermis. Mouse epidermis was used since it was more easily available than adult human epidermis. Also, 3 day old mouse skin was used because newborn mouse epidermis resembles adult epidermis more closely with more epidermal layers compared to adult mouse epidermis which is very thin. I decided to use 3-day old mouse skin and not newborn skin because the skin, as well as other organs, has been shown to have high levels of autophagy right after birth to compensate for the short neonatal period of starvation, and it may also be a stress response to the new external conditions the neonate is exposed to (Kuma *et al.* 2004).

TEM analysis of 3-day old mouse epidermis shows that double-membrane vesicles are present in the lower layers as well as in the granular layers of the epidermis (Fig.

3.7). These double-membrane vesicles contain autophagic cargo confirming that they are autophagic vesicles (Fig. 3.7). However, autophagic vesicles of granular layer keratinocytes are oval-shaped whereas basal and para-basal double-membrane vesicles are more rounded (Fig. 3.7). This different morphology may be due to the flattened shape of granular layer keratinocytes. Also, granular autophagic vesicles have a width of about 200 nm whereas the spherical basal and para-basal vesicles have a cross-section of 400-500 nm (Fig. 3.7).

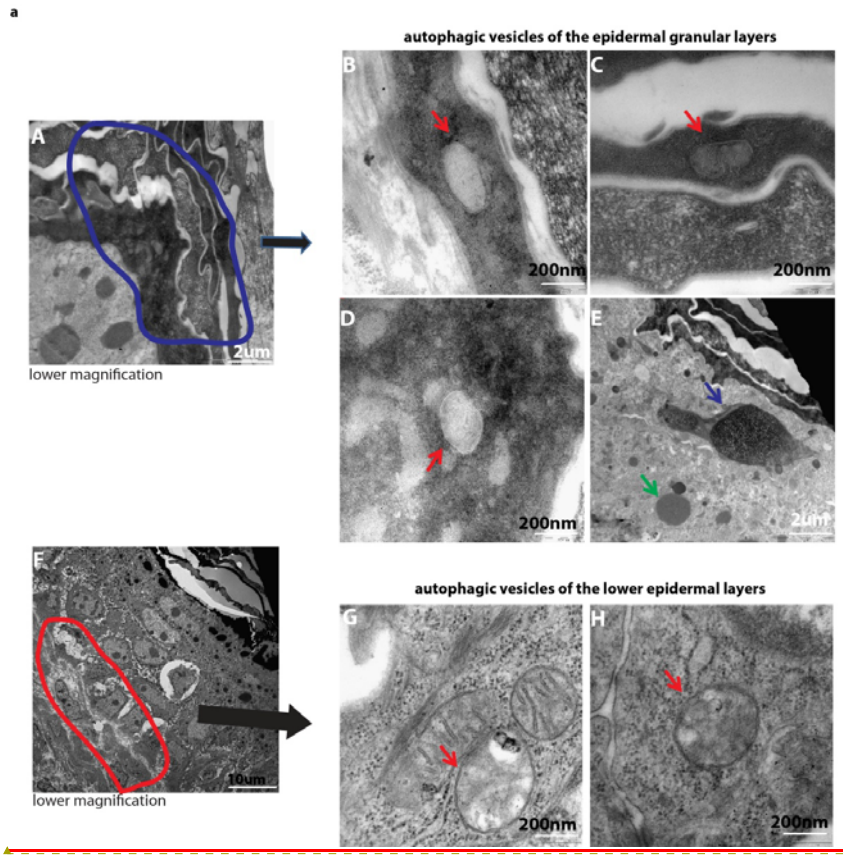

Figure 3.7: Transmission Electron Microscopy for autophagic vesicles in epidermis

(a) 3-day old mouse epidermis was analysed with Transmission Electron Microscopy (TEM) for the presence of autophagic vesicles in all layers of the epidermis. **A)** Low magnification TEM image shows granular and cornified layers, and the uppermost supra-basal layer. Blue selection shows granular layers selected for closer analysis. **B-D)** Red arrows indicate double-membrane vesicles in granular layer keratinocytes. **E)** Green arrow indicates a rounded protein aggregate, probably an L-granule and the blue arrow indicates an irregularly shaped large protein aggregate, probably an F-granule. **F)** Low magnification TEM image shows lower epidermal layers. Red selection shows region selected for more detailed analysis. **G-H)** Red arrows indicate double-membrane vesicles in basal layer keratinocytes.

Figure 3.7 continued on the next page.

Formatted: Font: 12 pt, Bold

Formatted: Font: Bold

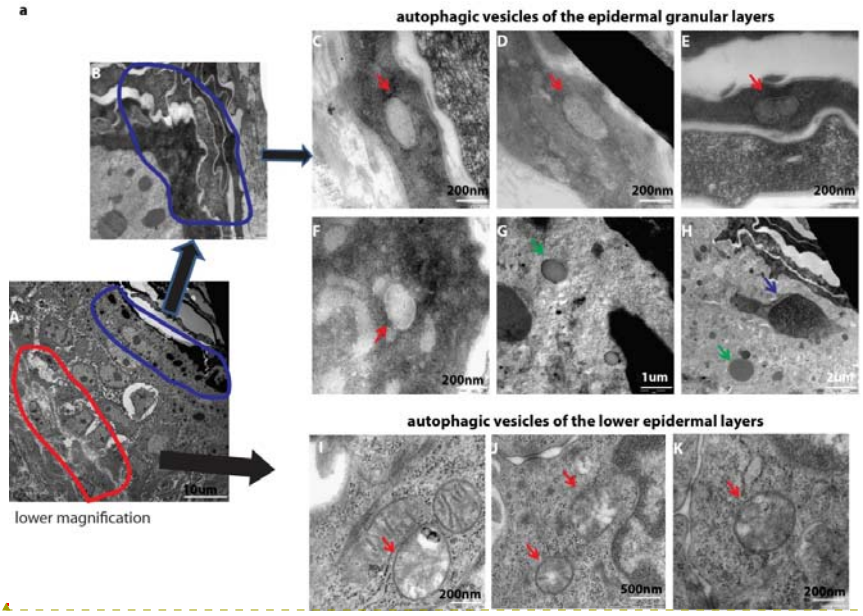

Figure 3.7: Transmission Electron Microscopy for autophagic vesicles in epidermis

(a) 3 day old mouse epidermis was analysed with Transmission Electron Microscopy (TEM) for the presence of autophagic vesicles in all layers of the epidermis. **A)** Low magnification image shows a TEM image of all layers of the epidermis. Blue and red selections show regions selected for more detailed analysis. **B)** Higher magnification of the upper epidermal layers shows granular and cornified layers, and the uppermost supra basal layer. Blue selection shows granular layers selected for closer analysis. **C-F)** Red arrows indicate double membrane vesicles in granular layer keratinocytes. **G-H)** Green arrows indicate rounded protein aggregates, probably L-granules and blue arrow indicates an irregularly shaped large protein aggregate probably an F-granule. **I-K)** Red arrows indicate double membrane vesicles in basal layer keratinocytes.

Figure 3.7 continued on the next page.

This figure is representative of n=2 samples of 3 day old mouse epidermis. White bars = scale of each image. Purple and red elliptical selections represent regions selected for closer TEM analysis. Black arrows indicate selected regions and the higher magnification images of these regions. Small red arrows indicate double membrane vesicles. Green arrows indicate round protein aggregates of granular layer keratinocytes. Blue arrows indicate irregular shaped protein aggregates of granular layer keratinocytes.

Formatted: Font: 12 pt, Bold

b

Enlargements of epidermal autophagic vesicles

double-membrane vesicles of the granular layer

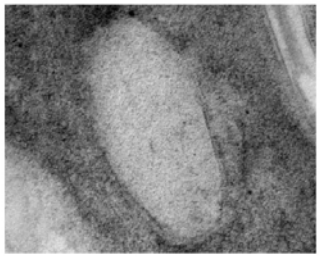

double-membrane vesicles of the basal and para-basal layers

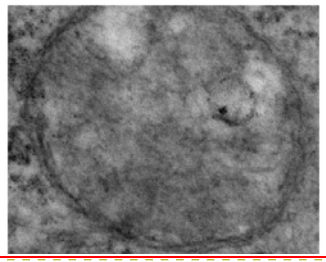

Formatted: Font: 12 pt, Font color: Text 1

Formatted: Space After: 24 pt

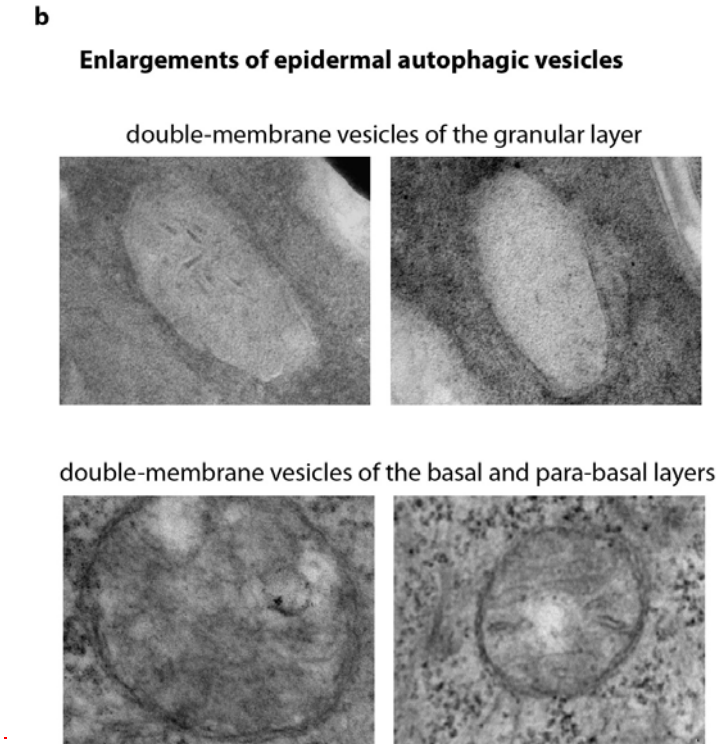

Figure 3.7 continued.

Figure 3.7: Transmission Electron Microscopy for autophagic vesicles in epidermis

(b) Enlargements of autophagic vesicles of the granular layer~~s~~ and of the basal and para-basal layers show~~s~~ the autophagic vesicle double-membrane and cytoplasmic cargo within the vesicles.

This figure is representative of n=2 samples of 3 day old mouse epidermis. White bars = scale of each image. ~~Purple~~ Blue and red elliptical selections represent regions selected for closer TEM analysis. Black arrows indicate selected regions and the higher magnification images of these regions. Small red arrows indicate double-membrane vesicles. Green arrows indicate round protein aggregates of granular layer keratinocytes. Blue arrows indicate irregular shaped protein aggregates of granular layer keratinocytes.

~~*This figure is representative of n=2 samples of 3 day old mouse epidermis.*~~

Therefore, TEM analysis shows that double-membrane vesicles which contain sequestered cytoplasmic material are present in epidermis, strongly suggesting the presence of autophagosomes. Granular layer autophagic vesicles differ from autophagic vesicles of the lower epidermal layers in their size, shape and engulfed cargo. To date, all publications on autophagy in keratinocytes are based on monolayer culture models. With TEM analysis, I show that autophagic vesicles are present in the epidermis *in vivo*. However, immuno-EM for LC3 would confirm that these epidermal double-membrane vesicles are also LC3 postitive. But this is work in progress and due to time-constraints cannot be carried out and included in this report.

Therefore, as a next step I analysed keratinocyte autophagy in more detail in cultured terminally differentiating cells compared to proliferating undifferentiated keratinocytes. An established model of monolayer primary human keratinocyte cultures was used (Yuspa *et al.* 1989).

3.4 Characterisation of autophagy in keratinocyte monolayer cultures

In the previous sections I have shown that LC3 aggregates as well as other autophagy markers are present in the upper layers of adult epidermis where terminal differentiation occurs (Fig. 3.2). Also LC3, ULK1, WIPI1 and ATG5-ATG12 are highly up-regulated in foetal epidermis when barrier formation is initiated (Fig. 3.4). These LC3 aggregates are different from other known organelles in the granular layer such as filaggrin granules and lamellar bodies (section 3.3). Therefore, I hypothesize that autophagy is the mechanism by which granular layer keratinocytes degrade their organelles and undergo terminal differentiation.

To test this hypothesis, primary human keratinocytes were used as a culture model to mimic the differentiation stages in epidermis. The upper layers of the epidermis have higher intracellular calcium levels than the proliferating basal layer and this is thought to regulate keratinocyte differentiation (Fig. 1.1; Menon *et al.* 1985; Yuspa *et al.* 1989; Elias *et al.* 2002). In the field of skin research, it is well established that *in vitro,* keratinocytes are stimulated to differentiate by increasing the calcium content of the media (Yuspa *et al.* 1989).

Initially I carried out experiments to determine whether the keratinocytes in my culture model would respond to calcium-induced differentiation. Primary human neonatal foreskin keratinocytes (*Invitrogen*) were used as my monolayer culture model. After stimulating differentiation by increasing the calcium content of the media, protein lysates from undifferentiated and differentiated cell populations were analysed for expression of keratinocyte differentiation markers by Western blotting. Cells cultured in high calcium media are labelled as differentiated whereas, keratinocytes grown in the low calcium, proliferation media are labelled as undifferentiated (Fig. 3.8).

To determine whether high calcium media could induce keratinocyte terminal differentiation, the expression of the terminal differentiation marker filaggrin was analysed. Western blotting shows that unprocessed filaggrin, pro-filaggrin, is present in both differentiated and undifferentiated keratinocytes (Fig. 3.8). However, processed shorter-chain filaggrin is associated with differentiated keratinocytes (Fig. 3.8). K1, a marker of early terminal differentiation, is also present in the differentiated population compared to the undifferentiated cells where it is not expressed (Fig. 3.8). K14, which is present in the proliferating basal keratinocytes of epidermis, is highly expressed in the undifferentiated monolayer keratinocytes and is reduced in the differentiated keratinocyte cultures (Fig. 3.8).

Therefore, Western blot analysis of monolayer keratinocyte cultures shows that the undifferentiated keratinocyte culture consists mainly of K14 expressing proliferating cells. However, the differentiated keratinocyte population is comprised of keratinocytes at different stages of differentiation. The differentiated keratinocyte cultures have K14 expressing proliferating keratinocytes, K1 positive differentiated cells representing keratinocytes of the supra-basal layers, and filaggrin positive terminally differentiating keratinocytes like in the granular layer of epidermis. Therefore, this monolayer culture model mimics the epidermis by providing two main populations - undifferentiated, proliferating keratinocytes and differentiated keratinocytes.

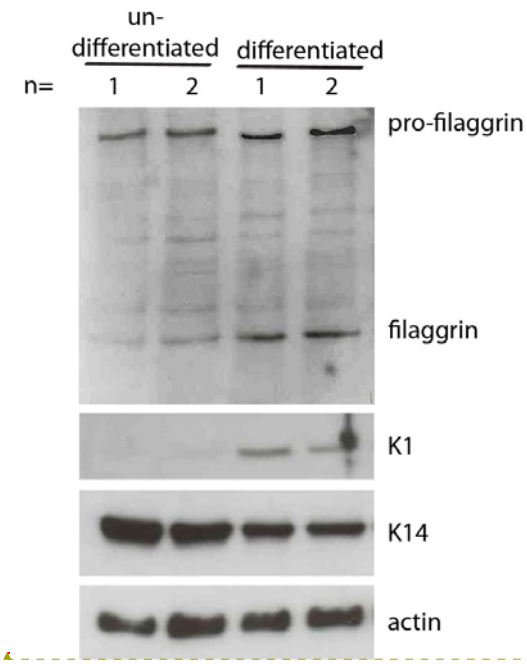

Formatted: Font: 12 pt, Font color: Red

~~**Figure 3.8: Expression of epidermal differentiation markers in undifferentiated and differentiated monolayer keratinocytes.**~~

~~Differentiation in primary human monolayer keratinocyte cultures is induced by culturing keratinocytes in media with high calcium content. Processed filaggrin, usually present in the granular layers of epidermis, is strongly expressed in differentiated keratinocytes, indicating activation of terminal differentiation. However the filaggrin precursor, pro-filaggrin, is present in both undifferentiated and differentiated keratinocytes. K1, a marker of early differentiation in keratinocytes of the spinous layer, is absent in undifferentiated cells but is expressed in the differentiated population. K14, a marker of the basal layer, is expressed in undifferentiated keratinocytes but is reduced in the differentiated population.~~

~~*This figure is representative of n=2 individual experiments (see Appendix 1).*~~

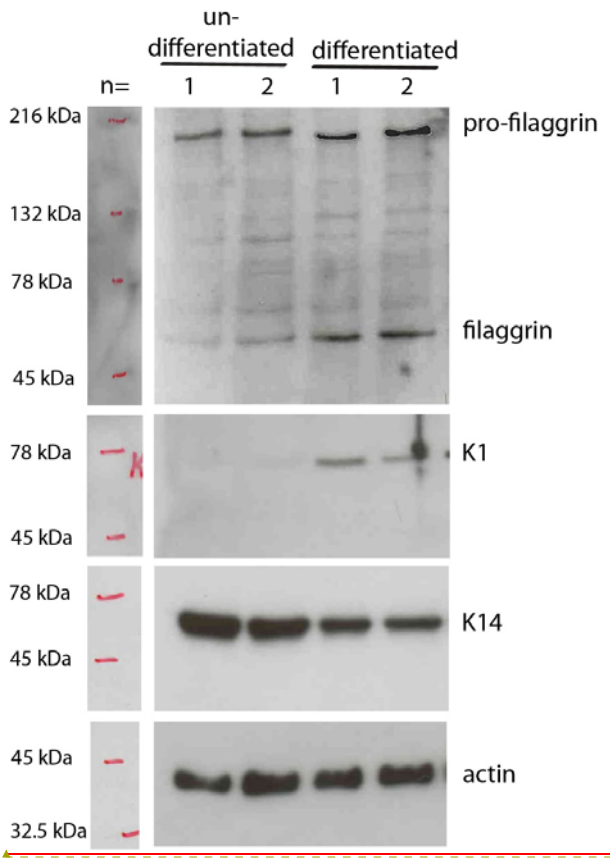

Figure 3.8: Expression of epidermal differentiation markers in undifferentiated and differentiated monolayer keratinocytes.

Differentiation in primary human monolayer keratinocyte cultures is induced by culturing keratinocytes in media with high calcium content. Processed filaggrin, usually present in the granular layers of epidermis, is strongly expressed in differentiated keratinocytes, indicating activation of terminal differentiation. However the filaggrin precursor, pro-filaggrin, is present in both undifferentiated and differentiated keratinocytes. K1, a marker of early differentiation in keratinocytes of the spinous layer, is absent in undifferentiated cells but is expressed in the differentiated population. K14, a marker of the basal layer, is expressed in undifferentiated keratinocytes but is reduced in the differentiated population.

This figure is representative of n=2 individual experiments (see Appendix 1).

Formatted: Font: 12 pt

Formatted: Space After: 0 pt, Line spacing: 1.5 lines

Formatted: Space After: 24 pt

The monolayer primary keratinocyte cultures I used maintain their undifferentiated proliferative state in low calcium media but they can activate their differentiation pathway when cultured in high calcium media. So this culture model provides two keratinocyte populations.

The next experiment I performed was to establish whether there is a difference between the autophagy marker expression profiles of basal proliferating keratinocytes and differentiated keratinocyte cultures. Western blotting of protein lysates from both undifferentiated and differentiated keratinocytes was used to establish the differences in expression levels of autophagy proteins.

Figure 3.9 shows the total levels of autophagy marker expression in cultured undifferentiated and differentiated keratinocytes. Western blot analysis shows very similar expression levels of autophagy proteins in both keratinocyte cultures (Fig. 3.9a). ULK1 appears to be up-regulated in the differentiated keratinocytes (Fig. 3.9a). This increased ULK1 expression in the differentiated cells could not be confirmed with repetitions of the experiment (Appendix 2) suggesting that there are small variations in autophagy protein expression levels with each experiment. Therefore, a higher experiment "n" number is required to rule out these variations.

Autophagy is a very dynamic process and quantification of the rate of LC3 turn-over from free cytoplasmic LC3I to membrane-bound LC3II (LC3II/LC3I) is routinely used by autophagy researchers as a read-out for autophagic flux (Karim *et al.* 2007; Klionsky *et al.* 2012). Another read-out for autophagy is the LC3II/actin ratio, which represents the amount of membrane-bound LC3 (LC3II) normalised to actin. High LC3II/actin levels indicate high autophagy levels (Rubinsztein *et al.* 2009; Klionsky *et al.* 2012). To determine whether there is a difference between autophagy levels in

undifferentiated and differentiated keratinocytes, I determined the rate of LC3 turn-over (LC3II/LC3I) and the amount of LC3II per cell (LC3II/actin) for both undifferentiated and differentiated keratinocytes (Fig. 3.9b).

The values for LC3II/LC3I show that there is a higher turn-over rate of LC3I to LC3II in undifferentiated keratinocytes compared to the differentiated cultures (Fig. 3.9b). Quantification of LC3II/actin shows that there is a higher amount of membrane-bound LC3 (LC3II) in the undifferentiated keratinocyte cultures compared to the differentiated population (Fig. 3.9c). This difference is also statistically significant.

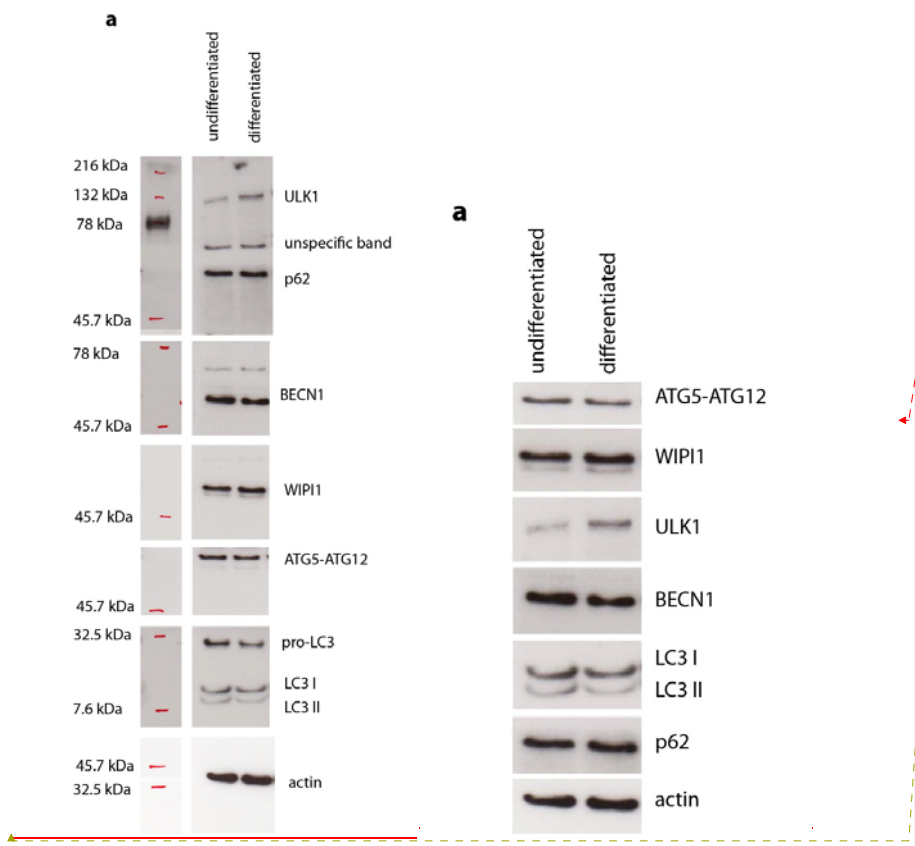

Figure 3.9: Comparison of autophagy marker expression in undifferentiated and differentiated keratinocyte monolayer cultures.

(a) Analysis of autophagy marker expression levels in undifferentiated and differentiated keratinocytes by Western blotting. One blot of n=3 experiments is shown here. There is no striking difference in autophagy marker expression levels between undifferentiated and differentiated keratinocytes. However, this Western blot shows higher ULK1 levels in the differentiated keratinocytes. This was not observed in the other repetitions of the experiment (see Appendix 2). With each experiment, there is some variation in autophagy marker expression levels in monolayer keratinocyte cultures, therefore, n=3 experiments were analysed (see Appendix 2).

Figure 3.9 continued on the next page.

Formatted: Font: 12 pt

Formatted: Space After: 24 pt

Formatted: Normal

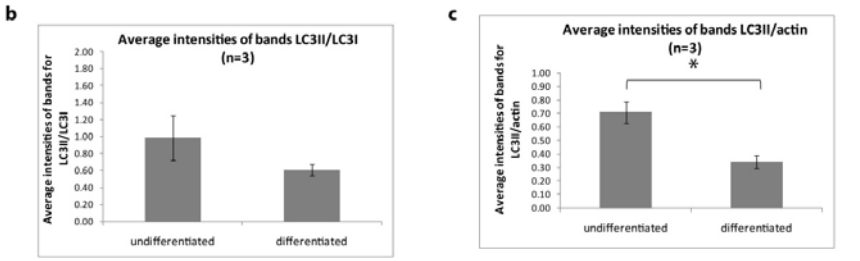

Two tailed paired t-test for average band intensities of LC3II/actin (n=3 experiments) undifferentiated and differentiated keratinocytes: P<0.05

Figure 3.9: Comparison of autophagy marker expression in undifferentiated and differentiated keratinocyte monolayer cultures.

Figure 3.9 continued.

(b) Quantification LC3 turn-over from LC3I to LC3II (LC3II/LC3I) showing average values for LC3II/LC3I band intensities for n=3 individual experiments. The level of LC3II/LC3I is reduced in the differentiated keratinocytes compared to the undifferentiated cells suggesting undifferentiated keratinocytes have a higher turn-over rate of LC3I to LC3II. However, this difference is not statistically significant.

(c) Quantification of total LC3II levels (LC3II/actin) showing average values for LC3II/actin band intensities for n=3 individual experiments. The level of LC3II/actin in undifferentiated keratinocyte monolayer cultures is higher than in and the differentiated keratinocyte population. This suggests that the total levels of membrane-bound LC3 are higher in undifferentiated keratinocytes compared to the differentiated cells. This difference is statistically significant, P<0.05.

Quantification of bands was done with ImageJ. This figure is representative of n=3 individual experiments (see Appendix 2).

Using Western blot analysis, I show that there is a statistically significant difference in total LC3II levels (LC3/actin ratios) in undifferentiated and differentiated keratinocytes. The undifferentiated keratinocyte population also has a higher turn-over of LC3I to LC3II (LC3II/LC3I ratios). These data suggest that undifferentatied keratinocytes have a higher rate of basal autophagy compared to the differentiated population. However, the levels of the other autophagy proteins analysed are similar in both keratinocyte populations. Since the differentiated keratinocyte population is a mix of keratinocytes at different stages of differentiation, a change in autophagy marker expression levels in one of the differentiation stages may not be detected by Western blotting. Therefore, the next step was to determine whether the cellular localisation of autophagy markers within undifferentiated and differentiated cells was altered. To investigate this, I cultured monolayer keratinocytes on coverslips and performed immunofluorescence staining for autophagy markers.

Initially, there did not appear to be any obvious difference in autophagy marker expression patterns between undifferentiated and differentiated keratinocytes (Fig. 3.10). The ATG5-ATG12 complex shows similar expression levels and expression patterns in both keratinocyte populations. However, WIPI1 appears to be slightly up-regulated in the differentiated cells (Fig. 3.10). On closer examination, immunofluorescence analysis shows accumulation of the proteins ULK1, LC3 and p62 in some peri-nuclear regions of some differentiated cells (Fig. 3.10, red arrows), although the total protein levels of ULK1 and p62 do not appear to change when compared to undifferentiated cells (Fig. 3.9). These “pockets” of peri-nuclear proteins ULK1, LC3 and p62 only appear to be present in some differentiated keratinocytes, and not in the undifferentiated cells.

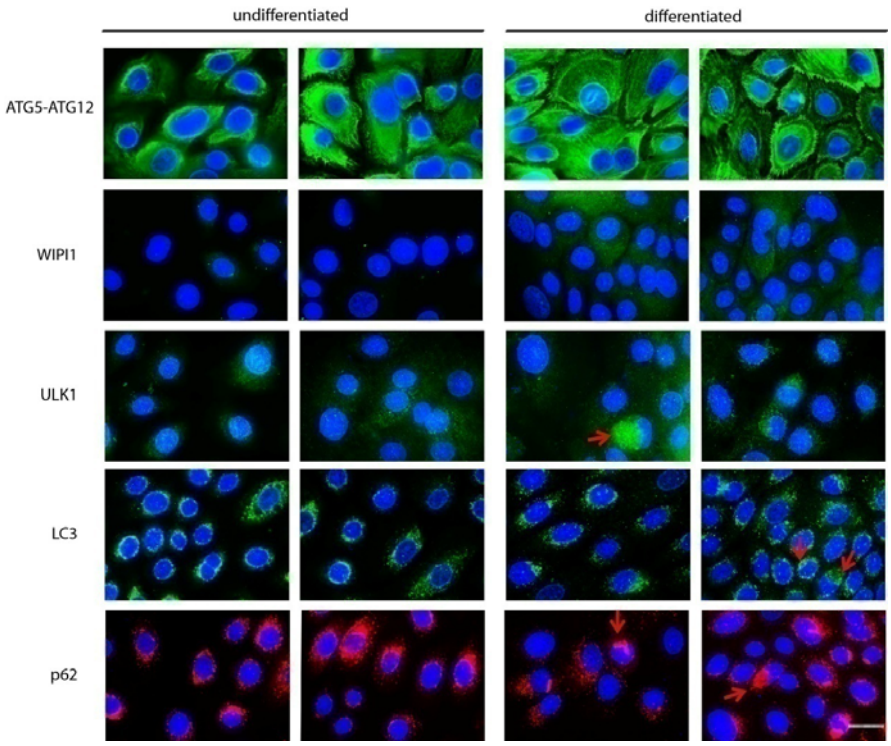

Figure 3.10: Cellular localisation of autophagy markers in undifferentiated and differentiated keratinocyte monolayer cultures.

Immunofluoresence staining for autophagy markers ATG5-ATG12, WIPI1, ULK1, LC3 and p62 show no difference in expression levels in undifferentiated and differentiated keratinocytes. WIPI1 expression appears to be slightly increased in the differentiated population. However, compared to the undifferentiated keratinocytes, the some of the differentiated keratinocytes show accumulation of ULK1, LC3 and p62 in ~~some~~ their peri-nuclear regions indicated by red arrows. ~~But overall expression levels of ULK1, LC3 and p62 appear to be equal in both keratinocyte populations.~~

This figure is representative of n=5 individual experiments.

Bar =20um. Red arrows = regions of peri-nuclear protein accumulation.

These results indicate that differentiated keratinocytes may have reduced levels of autophagy compared to undifferentiated keratinocyte monolayer cultures. However, the striking difference between both keratinocyte populations is the localisation of autophagy proteins within the cells. Therefore, I examined the cell morphology and cellular localisation of autophagy proteins in both cultured keratinocyte populations more closely.

3.5 Nucleophagy in differentiating keratinocytes

I have shown that there is no difference in autophagy marker expression levels between undifferentiated and differentiated keratinocyte populations (Fig. 3.9). However, in the differentiated keratinocytes, immunofluorescence analysis of autophagy proteins shows peri-nuclear localisation of pools of LC3, p62 und ULK1 (Fig. 3.10). To analyse this in more detail, the cell morphology of the two keratinocyte populations was examined.

First, the cell monolayers were stained with DAPI to determine whether there are any differences in the size or shape of the nuclei in the differentiated keratinocytes compared to the undifferentiated cells.

By analysing the DAPI stained nuclei of both keratinocyte populations, a marked difference was observed. The differentiated keratinocyte population was characterised by the presence of cells with irregular or misshaped nuclei (Fig. 3.11a), whereas, these misshaped nuclei are very rare in the undifferentiated cells (Fig. 3.11a, 3.11b). In the differentiated population, ~11% (30 of 280 cells) of the cells have misshaped nuclei compared to ~2% (5 of 280 cells) in the undifferentiated cell culture (Fig. 3.11b). This difference is also statistically significant (Fig. 3.11b). Therefore, it is concluded that inducing differentiation in monolayer keratinocytes is associated with a change in the shape of the nuclei.

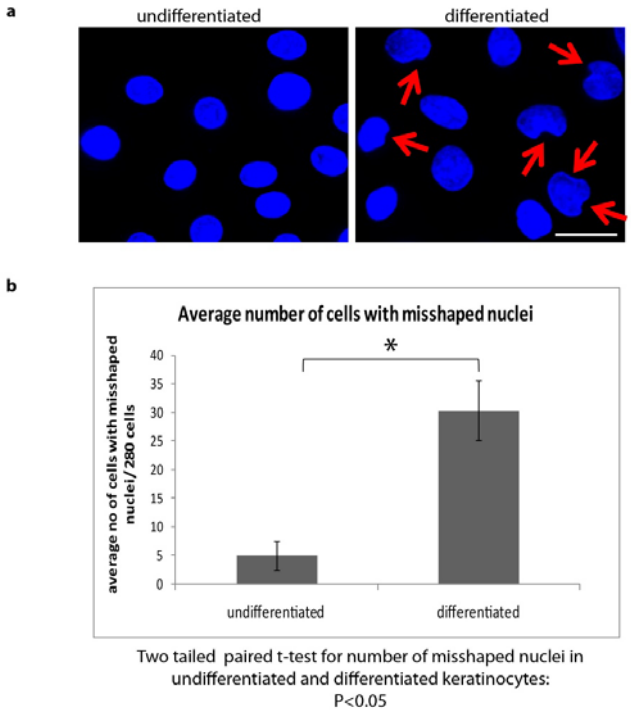

Figure 3.11: Changes in nucleus shape in differentiated keratinocytes compared to undifferentiated cells.

(a) Immunofluorescence analysis of DAPI-stained nuclei in undifferentiated and differentiated keratinocytes shows some cells have misshaped nuclei in the differentiated cell culture (red arrows).

(b) Graph shows the average number of cells with misshaped nuclei per total of 280 cells in both undifferentiated and differentiated keratinocyte cultures. There is a significantly higher number of misshaped nuclei in the differentiated keratinocyte population (30 of 280 cells) compared to the undifferentiated keratinocytes (5 of 280 cells).

This figure is representative of n=3 individual experiments. Total number of cells determined using ImageJ. Number of cells with misshaped nuclei counted manually. For statistical relevance, two tailed paired t-test, P<0.05 (see Appendix 3).

Bar = 20um. Red arrows = misshaped nuclei.

The next step was to determine why differentiation in culture is characterised by a change in the morphology of the nuclei. To determine whether an apoptotic cell death in differentiated cultures is a cause for the misshaped nuclei, I performed immunofluorescence analysis on the monolayer keratinocyte cultures with an antibody against cleaved Caspase-3 (cl. C-3). Cleavage and activation of C-3 occurs when apoptosis is induced and it is a classic marker for apoptosis (Christopher Potten). As a positive control for apoptosis, cells were treated with staurosporine. At low concentrations staurosporine is an ATP-competitive protein kinase inhibitor, whereas it induces apoptosis at higher concentrations (Gani and Engh 2010).

Field Code Changed

In figure 3.12, I show that staurosporine-treated undifferentiated and differentiated keratinocytes are cl. C-3 positive, indicating activation of the apoptotic pathway due to staurosporine treatment. However, the untreated undifferentiated and differentiated keratinocyte populations, including cells with misshaped nuclei, are negative for cleaved C-3 (Fig. 3.12). These results show that under normal culture conditions, both undifferentiated and differentiated keratinocytes are not apoptotic. Also, the cells with irregular shaped nuclei have not activated their apoptotic pathway, suggesting that another mechanism is responsible for the change in nuclei morphology.

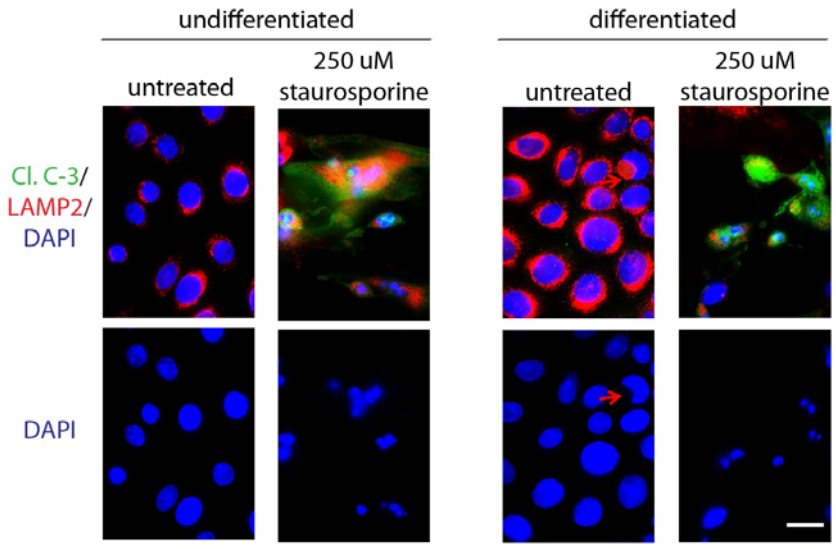

Figure 3.12: Expression of apoptosis marker, cleaved Caspase-3 (cl. C-3), in undifferentiated and differentiated keratinocyte monolayer cultures.

Immunofluorescence analysis shows the expression of cl. C-3 (green) and LAMP2 (red) in undifferentiated and differentiated keratinocytes. As a positive control for apoptosis, both undifferentiated and differentiated keratinocytes were treated with staurosporine to induce apoptotic cell death. Cl. C-3 (green), as well as LAMP2 (red) are expressed in the cytoplasm of the positive controls for apoptosis of both keratinocyte populations. However, untreated undifferentiated and differentiated keratinocytes do not express cl. C-3. Cells with misshaped nuclei (red arrows) are not positive for cl. C-3, whereas, missing parts of the nuclei are LAMP2 positive.

This figure is representative of n=2 individual experiments (see Appendix 4 for more images). Bar = 20um. Red arrows = misshaped nuclei.

In the previous section, I show that some cells within the differentiated keratinocyte population have strong peri-nuclear expression of ULK1, LC3 and p62 (Fig. 3.10). Closer analysis of these cells shows that ~11% of the differentiated keratinocyte population have irregular shaped nuclei (Fig. 3.11), and this is not due to an apoptotic cell death (Fig. 3.12). Therefore, I analysed the expression of the autophagosome marker LC3 in differentiated keratinocytes with misshaped nuclei more closely, and also compared them to the undifferentiated cell population. Using immunofluorescence analysis, keratinocyte monolayers were stained with an antibody against the autophagosome marker LC3 to show localisation of LC3 in cells with irregular shaped nuclei.

A more detailed examination of the keratinocyte cultures shows that the differentiated keratinocytes with misshaped nuclei have accumulation of LC3 aggregates where regions of the nuclei appear to have disappeared with the DAPI nuclear stain (Fig. 3.13). This unexpected observation suggests that the regions of missing nuclear material may be sites of high autophagic activity.

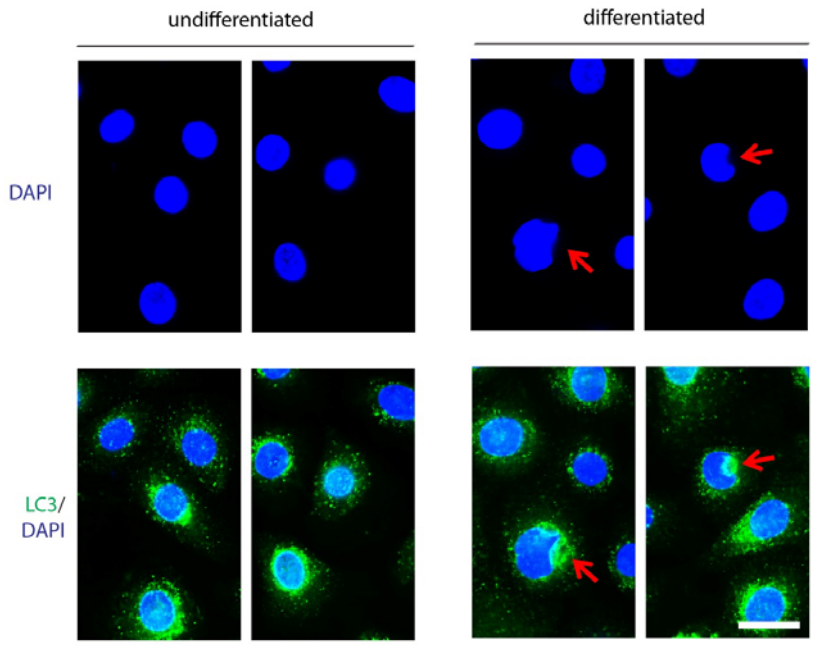

Figure 3.13: Localisation of autophagosome marker LC3, in differentiated keratinocytes with irregular shaped nuclei compared to the undifferentiated keratinocyte population.

DAPI staining of keratinocyte nuclei shows cells with misshaped nuclei in the differentiated population, whereas undifferentiated keratinocytes have regular nuclei. Immunofluorescence analysis of LC3 expression shows accumulation of LC3 in regions of missing nuclear material.

This figure is representative of n=5 individual experiments (see Appendix 5 for more images). Bar = 10um. Red arrows = regions of misshaped nuclei with peri-nuclear LC3 accumulation.

To determine if these LC3 aggregates in regions of missing nuclear material are really autophagosomes, a second marker was used. LAMP2 is a lysosomal membrane protein which labels lysosomes as well as autolysosomes, formed during the maturation step of the autophagic pathway where autophagosomes fuse with lysosomes (see section 1.2.2). Therefore, LC3/LAMP2 double-positive aggregates represent autolysosomes and the maturation step of the autophagic pathway, just before degradation of the autophagic vesicles.

To determine whether LC3 aggregates in the regions of missing nuclear material are also LAMP2 positive, immunofluorescence analysis of the keratinocyte monolayers, with two antibodies against LC3 and LAMP2, was done. Double staining for LC3 (green) and LAMP2 (red) shows that some of the LC3 aggregates in the undifferentiated keratinocytes are also LAMP2 positive (Fig. 3.14). However, in the differentiated cells, regions of missing nuclei are not only LC3 positive but also LAMP2 positive, suggesting the presence of autolysosomes and possibly also autophagic degradation of nuclear material (Fig. 3.14).

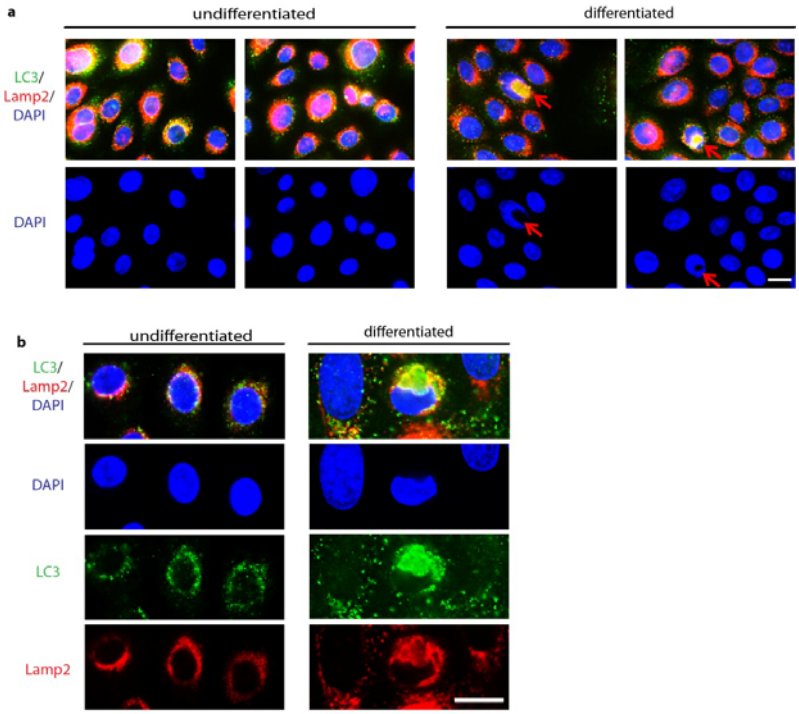

Figure 3.14: LC3 positive aggregates in regions of missing nuclear material of differentiated keratinocytes are also LAMP2 positive.

(a) The DAPI stain shows misshaped nuclei in the differentiated keratinocytes, whereas the undifferentiated cells have no misshaped nuclei. In the differentiated cultures, regions of missing nuclear material are positive for the autophagosome marker, LC3 (green), as well as the lysosome marker, LAMP2 (red). This suggests that LC3 aggregates have fused with lysosomes, representing autolysosomes, which degrade autophagic cargo.

(b) Enlarged images of undifferentiated keratinocytes, show that LC3 aggregates (green) are in the same regions as LAMP2 (red) puncta. However, it is unclear whether these LC3 and LAMP2 puncta are the same aggregates. In the regions of missing nuclear material of the differentiated keratinocytes, there is a large accumulation of LC3 aggregates and these are also LAMP2 positive suggesting nuclear degradation occurs via autophagy (nucleophagy).

This figure is representative of n=5 individual experiments. Bar = 10um. Small red arrows = regions of peri-nuclear protein accumulation.

Autophagic degradation of the whole nucleus or just parts of the nucleus have been reported by other groups to occur in yeasts, a bi-cellular organism *Tetrahymena thermophila, C. Elegans* and also in fibroblasts from a mouse model for nuclear envelopathies (Krick *et al.* 2008; Park *et al.* 2009; McGee *et al.* 2011; Liu and Yao 2012). I show that differentiation of keratinocytes in monolayer cultures is characterised by a set of cells with irregular shaped nuclei. These regions of missing nucleus~~i~~, shown with DAPI staining, are replaced by an accumulation of LC3/LAMP2 double-positive autolysosomes. This indicates that missing nuclear material in differentiated keratinocytes may be due to increased autophagy and autophagic degradation of the nucleus. Therefore, this form of autophagic nuclear degradation I observe in differentiated keratinocytes is termed nucleophagy.

To further characterise nucleophagy in differentiating keratinocytes, I analysed the localisation and expression pattern of a second autophagy marker, p62. p62 is a protein which recognises ubiquitinated autophagic cargo and binds to it. p62 can also bind to LC3 within the autophagosomal membrane, acting as an adaptor between LC3 and the autophagic cargo. So p62, which is commonly used as a read-out for targeted autophagic degradation of ubiquitinated cargo (Pankiv *et al.* 2007; Lamark *et al.* 2009; Johansen and Lamark 2011; Klionsky *et al.* 2012), was analysed in the keratinocyte monolayer cultures.

Immunofluorescence analysis of keratinocyte cultures was done using antibodies against LC3 and p62. The cellular localisation of LC3 and p62 would show whether LC3/LAMP2 nucleophagic vesicles are due to targeted autophagic degradation, or if nucleophagy is a random autophagic process in differentiated keratinocytes. With immunofluorescence staining for LC3 (green) and p62 (red), I show that most LC3 vesicles in undifferentiated keratinocytes are not p62 positive (Fig. 3.15). This indicates that basal autophagy in untreated proliferating keratinocytes is not targeted degradation of damaged proteins or organelles, but it is probably a random process supporting cell homeostasis. However, the nucleophagic regions in

the differentiated population, which have been shown to be positive for autolysome markers (Fig. 3.14), are also p62 positive (Fig. 3.15). This data suggests that nucleophagy in differentiating keratinocytes is regulated and targeted autophagic degradation of ubiquitinated cargo, which is most probably nuclear material.

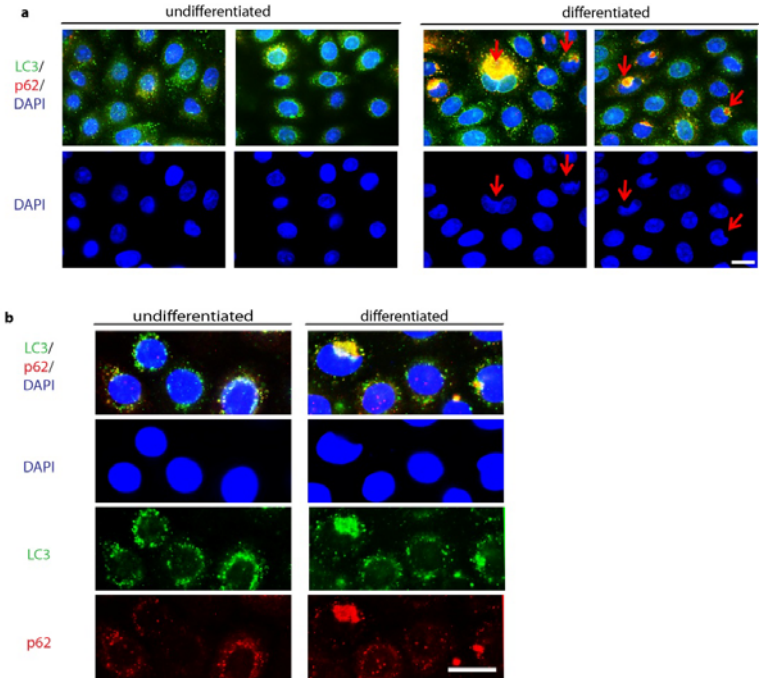

Figure 3.15: LC3 positive aggregates in regions of missing nuclear material of differentiated keratinocytes are also p62 positive.

(a) In both the undifferentiated and differentiated keratinocyte cultures, some LC3 (green) aggregates do colocalise with p62 (red). ~~cells, most LC3 aggregates (green) are not p62 positive (red). Also, there are very few p62 (red) positive aggregates in undifferentiated keratinocytes. T~~However, in the differentiated cultures, the DAPI stain shows keratinocytes with irregular nuclei and these~~in the differentiated population. In these cells with misshaped nuclei, the~~ nucleophagic regions which are LC3 positive (green) are also p62 positive (red). ~~This suggests that nucleophagy is targeted autophagic degradation of nuclear material.~~

(b) Enlargements of both undifferentiated and differentiated keratinocytes show more clearly that some cytoplasmic LC3 aggregates (green) are ~~not~~ p62 positive (red). However, the enlarged images of differentiated keratinocytes also show nucleophagic regions which are characterised by accumulation of LC3 vesicles (green) and these are also positive for the

marker of targeted autophagy, p62 (red). This suggests nucleophagy ~~is~~ may be targeted degradation of nuclear material.

This figure is representative of n=5 individual experiments. Bar = 10um. Small red arrows = regions of peri-nuclear protein accumulation.

In this section, I have shown that monolayer keratinocyte cultures represent different differentiation stages of epidermal keratinocytes. The undifferentiated keratinocytes are K14 positive, representing the proliferating basal layer. Whereas, the differentiated keratinocytes in culture express K14, K1, as well as cleaved filaggrin, indicating that a proportion of these cells have activated their terminal differentiation pathway. Therefore, the differentiated keratinocyte cultures are comprised of keratinocytes at different stages of differentiation.

Closer examination of keratinocyte cell morphology shows that the differentiated keratinocyte population is characterised by the presence of cells with misshaped nuclei (~11%), compared to the undifferentiated keratinocyte cultures where these cells are nearly absent (~2%). These regions of missing nuclear material are replaced by an accumulation of LC3/LAMP2/p62 positive autolysosomes. These results suggest that targeted autophagic degradation of nuclear material occurs in a proportion of differentiated keratinocytes. Therefore, I have termed this form of nuclear degradation, nucleophagy.

In summary, I have shown that keratinocyte differentiation *in vitro* is characterised by targeted autophagic degradation of the nuclei, nucleophagy.

3.6 Measuring autophagic flux in monolayer keratinocyte cultures

Autophagy is a very dynamic process and analysing autophagy proteins at one time point may not be representative of the true autophagic process. Autophagic flux can be analysed by measuring LC3 turn-over in the presence and in the absence of drugs which prevent degradation of autophagic vesicles by interfering with lysosomal function. This would give a true picture of how much autophagic cargo and autophagy proteins are processed over a certain period of time. Inhibitors like Ammonium chloride (NH_4Cl) and chloroquine increase lysosomal pH preventing function of lysosomal proteases (Fass *et al.* 2006; Klionsky *et al.* 2008; Xie *et al.* 2010). Other drugs routinely used like pepstatinA and E4Ad, block fusion of lysosomes with autophagosomes (Xie *et al.* 2010). The inhibitor Bafilomycin A1 (BafA1) has been shown to inhibit lysosomal protease function as well as prevent fusion of autophagosomes with autolysosomes (Klionsky *et al.* 2008). If cells treated with BafA1 show no increase in LC3II levels, this is an indication for defects in the late stages of autophagy (Rubinsztein *et al.* 2009). Therefore, to confirm that the autophagic pathway is completed and functional in the keratinocyte monolayer cultures, I compared BafA1-treated cells to untreated keratinocytes. Blocking the autophagy process with BafA1 would also allow measurement of autophagic flux (turn-over of LC3) in undifferentiated and differentiated keratinocytes.

With Western blotting I show that in both undifferentiated and differentiated keratinocytes, BafA1 treatment, which prevents degradation of autophagic vesicles, leads to accumulation of LC3II bands (Fig. 3.16a). This indicates that under normal culture conditions the autophagy process is completed in both keratinocyte populations. The LC3II/LC3I ratio is a read-out for autophagic flux and the turnover rate of LC3I to LC3II (Karim *et al.* 2007). The ratio of LC3II/actin is a measure of how much autophagy membrane-bound LC3 (LC3II) is present in the protein lysates. The LC3II/LC3I ratios and LC3II/actin ratios are higher in the BafA1 treated

undifferentiated and differentiated keratinocytes when compared to the untreated cells under normal culture conditions (Fig. 3.16b, c). These values indicate an accumulation of LC3II with BafA1 treatment, which blocks the last steps of the autophagy pathway, in both undifferentiated and differentiated keratinocytes. Therefore, in keratinocytes under normal culture conditions the autophagy process is completed since blocking the autophagy pathway with BafA1 leads to an accumulation of LC3II (Fig. 3.16). With these experiments, I also observed that ~~the~~ when autophagy is impaired, the LC3II/LC3I and LC3II/actin values are much higher for undifferentiated keratinocytes compared to differentiated keratinocytes (Fig. 3.16b, Fig. 3.16c). This indicates that undifferentiated keratinocytes may have a higher rate of autophagic flux compared to differentiated cells (Fig. 3.16b, Fig. 3.16c) supporting initial observations (Fig. 3.9). However, with Western blot analysis, quantification of p62 levels (p62/actin ratios) shows that blocking the autophagy pathway with BafA1 does not have a strong effect on p62 levels (Fig. 3.16d).

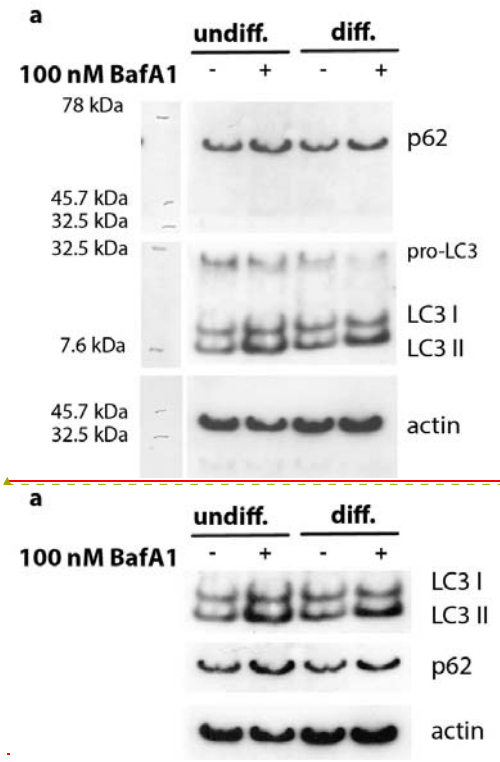

Formatted: Font: 12 pt, Font color: Text 1

Figure 3.16: Analysis of LC3 and p62 levels in undifferentiated and differentiated keratinocytes after BafA1 treatment.

(a) Western blotting of lysates from undifferentiated and differentiated keratinocytes treated with and without BafA1 shows accumulation of LC3II when autophagy is blocked with BafA1. This suggests that under normal culture conditions the autophagy process is completed and LC3II positive vesicles are degraded.

Figure 3.16 continued on the next page.

Western blot is representative of n =3 individual experiments (see Appendix 8).

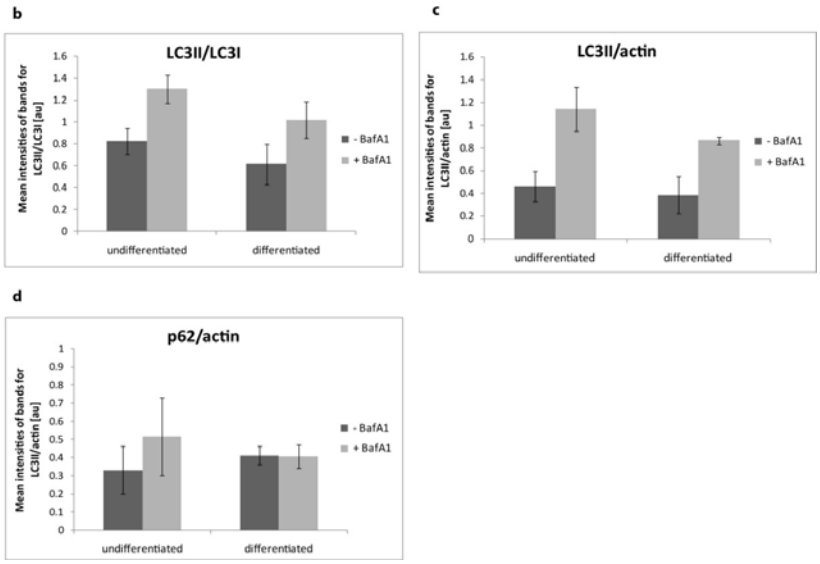

Figure 3.16: Analysis of LC3 and p62 levels in undifferentiated and differentiated keratinocytes after BafA1 treatment.

Figure 3.16 continued.

(b) Quantification of the intensities of LC3II protein bands normalised to LC3I (LC3II/LC3I), shows an increase in LC3II/LC3I ratios in both BafA1-treated undifferentiated and BafA1-treated differentiated keratinocytes compared to the untreated cultures. However, LC3II/LC3I levels are slightly higher ~~are lower~~ in the undifferentiated keratinocytes compared to the ~~-~~differentiated cells. However, this difference is not statistically significant.

(c) Quantification of the mean intensities of LC3II protein bands normalised to actin (LC3II/actin) shows increased LC3II/actin in both BafA1-treated undifferentiated and differentiated keratinocytes compared to untreated keratinocyte cultures. However, there is no significant difference between the LC3II/actin levels ~~are lower in~~ the BafA1-treated undifferentiated keratinocytes compared to the BafA1 treated differentiated cells.

(d) Quantification of mean intensities of p62 bands normalised to actin shows that there is a slight increase in p62 levels in BafA1-treated undifferentiated keratinocytes compared to the untreated undifferentiated cells. However, in the differentiated cultures, BafA1 has no effects on p62 levels. The difference in p62 levels between the undifferentiated and differentied populations is not statistically significant.

Quantification of n =3 individual experiments (see Appendix 8).

These results obtained with Western blotting were verified by immunofluorescence analysis with antibodies against LC3 and p62 in untreated and BafA1-treated undifferentiated and differentiated keratinocytes (Fig. 3.17). Quantification of LC3 and p62 expression was carried out by determining the intensities of protein expression per cell. With immunofluorescence analysis for LC3, I show increased LC3 intensity per cell in undifferentiated cells treated with BafA1 compared to untreated undifferentiated cells, suggesting accumulation of LC3 aggregates (Fig. 3.17b). In the differentiated keratinocytes, BafA1 treatment also leads to increased LC3 intensity per cell, indicating accumulation of LC3 aggregates when autophagy is blocked at the late stages (Fig. 3.17b). These data support results from Western blot analysis showing more membrane-bound LC3 (LC3II) after BafA1 treatment in both keratinocyte cultures (Fig. 3.16). Therefore, it is concluded that the autophagic pathway is functional in monolayer keratinocytes.

However, when comparing autophagy levels in the undifferentiated and differentiated keratinocytes, immunofluorescence analysis shows that blocking autophagy with BafA1 leads to a much higher increase in LC3 intensities per cell in the undifferentiated keratinocyte population (Fig. 3.17b). This confirms observations made by analysing total LC3 protein levels with Western blotting (Fig. 3.16c), where undifferentiated keratinocytes appear to have a higher rate of LC3 turn-over indicating a higher rate of autophagic flux. However, immunofluorescence analysis shows that the p62 levels are higher in the differentiated keratinocytes treated with BafA1 compared to untreated differentiated cells (Fig. 3.17c). This is not observed with Western blot analysis (Fig. 3.16d), where blocking autophagy has very little effects on p62 levels. Western blotting may not be as sensitive as immunofluorescence analysis where subtle changes occur.

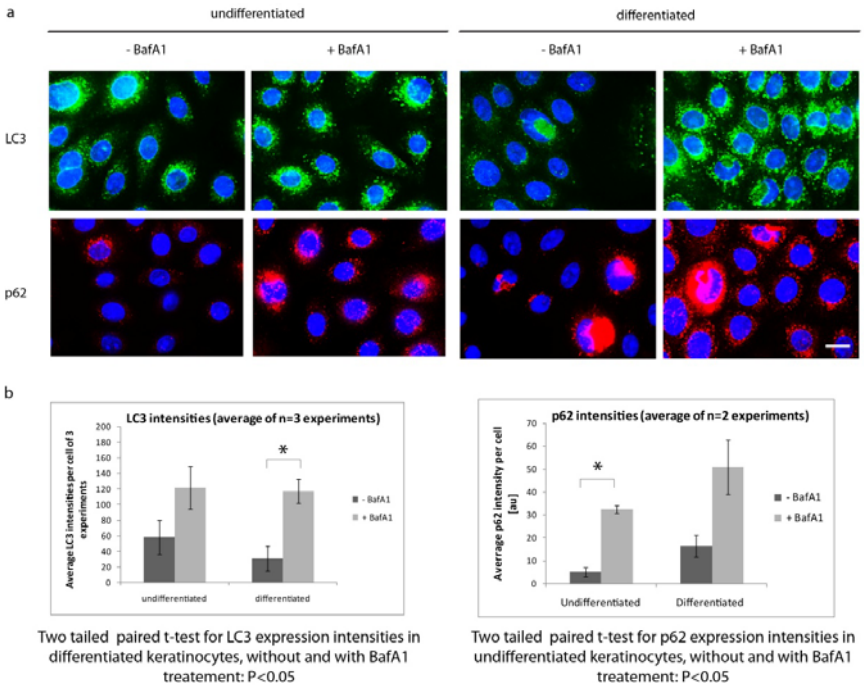

Two tailed paired t-test for LC3 expression intensities in differentiated keratinocytes, without and with BafA1 treatement: P<0.05

Two tailed paired t-test for p62 expression intensities in undifferentiated keratinocytes, without and with BafA1 treatement: P<0.05

Figure 3.17: Analysis of cellular protein expression patterns in undifferentiated and differentiated keratinocytes after BafA1 treatment.

(a) Immunofluorescence staining for LC3 (green) and p62 (red) in undifferentiated and differentiated keratinocytes treated with and without BafA1. In both keratinocyte populations, blocking autophagic flux with BafA1 leads to an increase in LC3 and p62 expression intensities.

(b) Quantification of LC3 fluorescence intensities per cell show an increase in LC3 intensities in BafA1-treated undifferentiated and differentiated keratinocytes compared to the untreated keratinocyte populations. This difference is also statistically significant in the differentiated keratinocyte cultures with $P<0.05$.

(c) Quantification of p62 intensities per cell show an increase in p62 levels in both BafA1-treated keratinocytes compared to untreated keratinocyte cultures. This difference is also statistically significant in the undifferentiated keratinocyte cultures with $P<0.05$.

Immunofluorescence images are representative of n=3 individual experiments. For quantification of intensities per cell, n=3 independent experiments were analysed (see Appendix 9). Bar = 10um.

In this section I have shown with Western blot and immunofluorescence analysis that treating keratinocyte monolayer cultures with BafA1 blocks autophagy and leads to accumulation of LC3 and p62 within the cells. This confirms that autophagy is functional and the autophagy process is completed in both undifferentiated and differentiated keratinocyte cultures under normal culture conditions.

Similar observations were also made when chloroquine, another inhibitor of the autophagy pathway, was used (see Appendix 6). However, chloroquine was only used in initial experiments because it may have additional effects on other cellular processes, which are still unclear, other than blocking autophagy (Maycotte *et al.* 2012).

The experiments performed in this section also show that autophagic flux is higher in undifferentiated keratinocytes compared to differentiated cells. Blocking autophagy with BafA1 or chloroquine leads to a greater accumulation of LC3, suggesting there is a higher turn-over of LC3, autophagic vesicles and autophagic cargo in undifferentiated keratinocyte monolayers.

Therefore, I conclude that in both undifferentiated and differentiated keratinocytes, the autophagy process, and most probably nucleophagy are functional. A direct measurement of autophagic flux in nucleophagic keratinocytes alone was not possible since this subset of the differentiated keratinocytes is not fully characterised and it is unclear on what basis to select the cells for. So the next step is to further characterise these nucleophagic keratinocytes in the differentiated cultures.

3.7 Characterisation of nucleophagy in differentiated keratinocytes

So far in this chapter, I have shown that differentiation in monolayer cultures is characterised by a the presence of some keratinocytes with irregular shaped nuclei. The regions of missing nuclear material are replaced by LC3/LAMP2 double-positive vesicles which are also p62 positive. This strongly suggests targeted autophagic degradation of the nuclei. Therefore, I hypothesize that nucleophagy is a mechanism by which terminally differentiating keratinocytes degrade their nuclei *in vitro*.

To test this hypothesis, I wanted to determine whether these autophagic vesicles in regions of missing nuclei actually do contain nuclear material. First, nucleophagic keratinocytes were analysed for expression of a histone interacting protein, Heterochromatin Protein 1α (HP1α) and also for the histone H3. HP1α is a member of the HP1 family of proteins which label heterochromatin, genetically inactive tightly packed DNA found at the periphery of the nucleus (Maison and Almouzni 2004).

Double immunofluorescence staining was carried out to determine the localisation of HP1α (green) and LAMP2 (red) in monolayer keratinocyte cultures. Analysis of the HP1α expression pattern alone shows that HP1α is mainly expressed in the nucleus of undifferentiated keratinocytes (Fig. 3.18). However, in the differentiated keratinocytes, HP1α is present in the nucleus, but also in the cytoplasm of some cells where it appears to form large peri-nuclear aggregates (Fig. 3.18). Double staining for HP1α (green) and LAMP2 (red) shows that the localisation of cytoplasmic HP1α overlaps with LAMP2 in differentiated keratinocytes (Fig. 3.18). Surprisingly, HP1α and LAMP2 colocalisation are in regions of missing nuclear material (Fig. 3.18). The functions of the HP1 proteins are to regulate heterochromatin formation and stability, gene expression as well as DNA repair and replication (Maison and Almouzni 2004; Quivy *et al.* 2008; Luijsterburg *et al.* 2009).

Therefore, to carry out these functions, the HP1 proteins are required to localise to the nucleus. However, the fact that HP1α is present in the nucleophagic regions suggests that nucleophagic vesicles contain nuclear material.

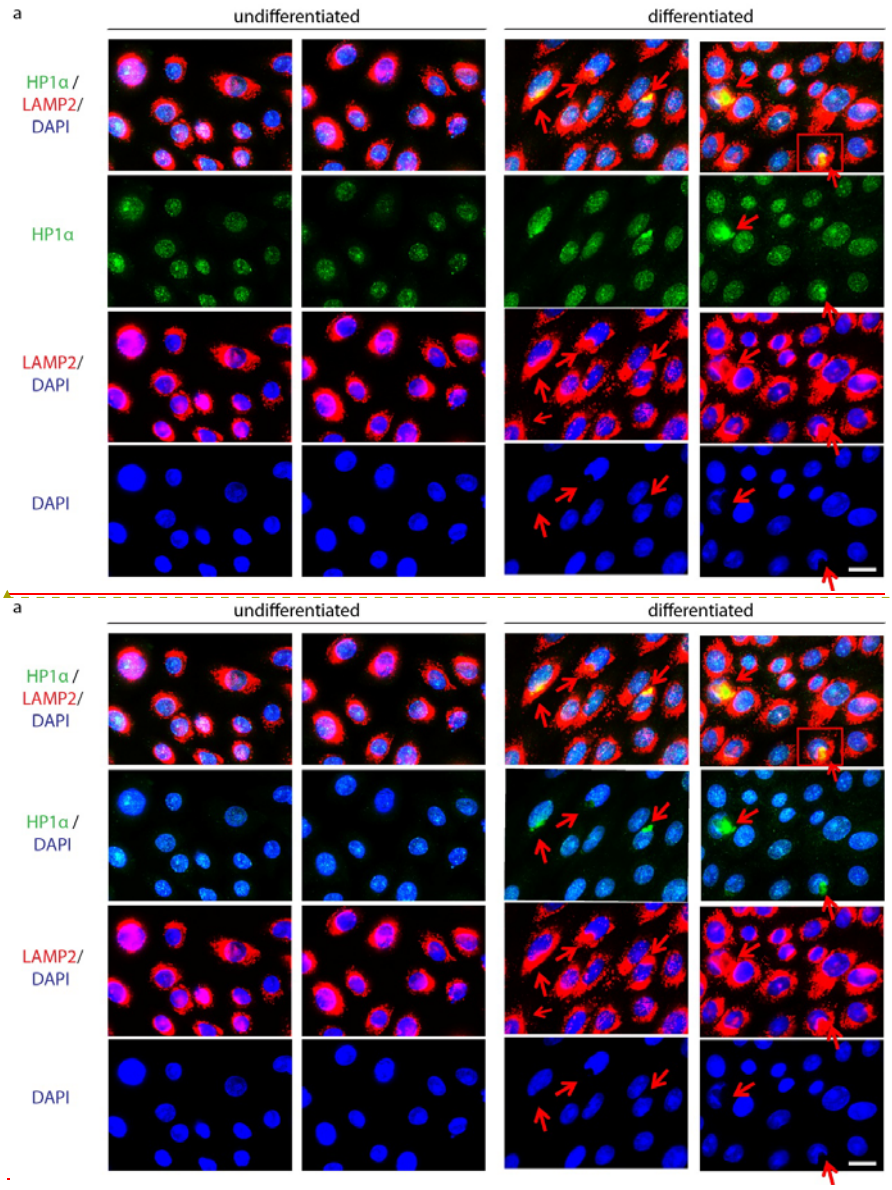

Figure 3.18: Expression of Heterochromatin Protein 1α (HP1α) and LAMP2 in keratinocyte monolayer cultures

(a) Double immunofluorescence staining for HP1α (green) and LAMP2 (red) in undifferentiated and differentiated keratinocytes shows that HP1α is mainly localised in the

Formatted: Font: 12 pt

nucleus of undifferentiated keratinocytes, while LAMP2 is cytoplasmic. In the differentiated keratinocytes, HP1α is also localised in the nucleus, however, some cells have cytoplasmic HP1α aggregates (red arrows). These regions of cytoplasmic HP1α overlap with LAMP2 expression. DAPI staining shows that these HP1α/LAMP2 double positive sites are in regions of missing nuclear material of differentiating keratinocytes.

Figure 3.18 continued on the next page.

Immunofluorescence images are representative of n=3 individual experiments. Bar = 10um. Small red arrows = regions of peri-nuclear protein accumulation. Red box = region selected for enlarged images.

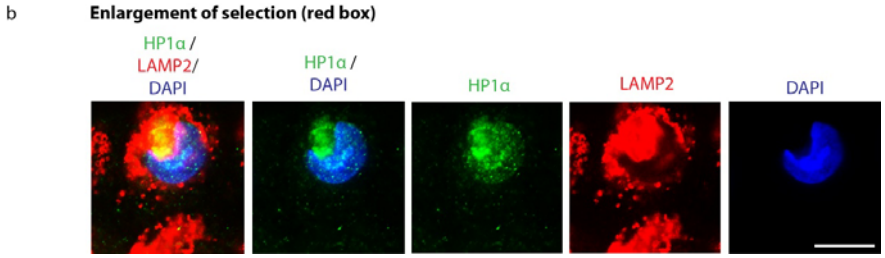

Figure 3.18: Expression of Heterochromatin Protein 1α (HP1α) and LAMP2 in keratinocyte monolayer cultures

Figure 3.18 continued.

(b) Enlarged images of a nucleophagic keratinocyte of the differentiated keratinocyte culture (red box in (a)) shows HP1α (green) is present in the nucleus as well as in the cytoplasmic region of missing nuclear material. HP1α colocalises with LAMP2 (red) in the nucleophagic region.

Immunofluorescence images are representative of n=3 individual experiments. Bar = 10um.

I show that LC3/LAMP2 positive nucleophagic regions of differentiated keratinocytes are also positive for HP1α, a nuclear protein suggesting that nucleophagic vesicle contain autophagic material.

To determine whether binding of the nuclear protein HP1α to nucleophagic vesicles is unspecific and a random process, I performed immunofluorescence analysis for the expression pattern of another nuclear protein, acetylated histone H3 (Lys14). Acetylation of histones is associated with transcriptional activation (Grunstein, 1997) and acetylation of histone H3 secifically at Lysin14 (Lys14) is required for transcriptional activation of target genes (Kasten, 2004). Immunofluorescence staining using an antibody against acetylated histone H3 (Lys14) shows that acetylated histone H3 (Lys14) is only present within the nuclei of both undifferentiated and differentiated keratinocytes (Fig. 3.19). Acetylated histone H3 (Lys14) is completely absent from nucleophagic regions (Fig. 3.19). Therefore, acetylated histone H3 (Lys14), which labels actively transcribed genes, is not present in nucleophagic regions and, the nuclear material within these regions differs from that within the still intact nucleus.

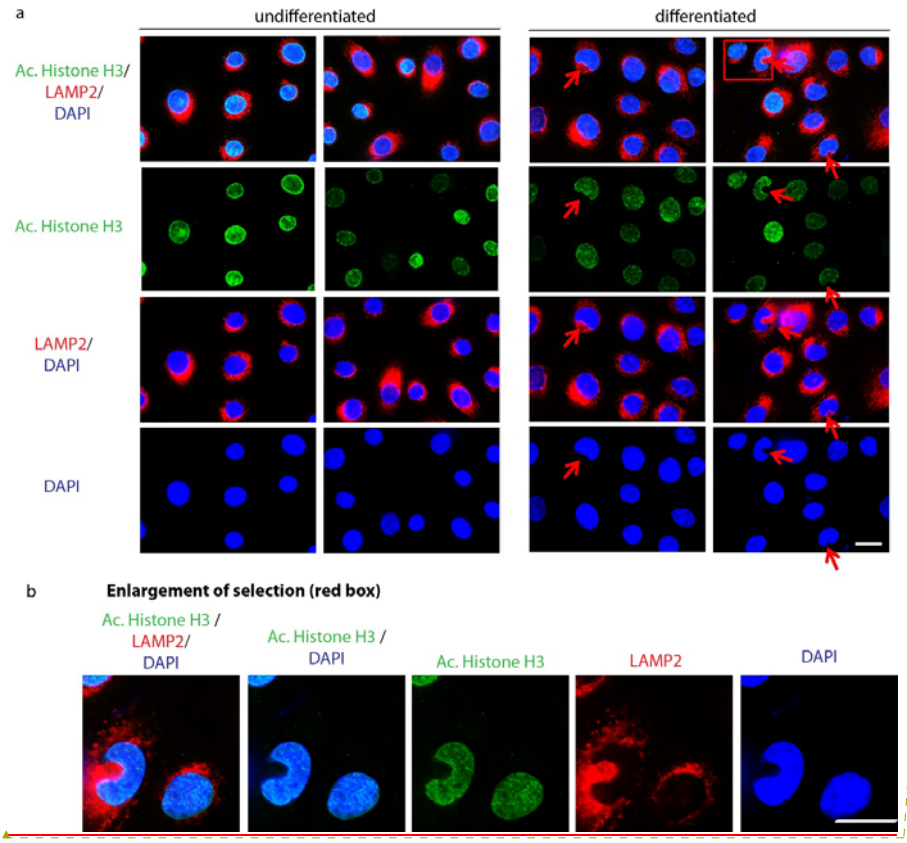

Figure 3.19: Expression of acetylated histone H3 (Lys14) and LAMP2 in keratinocyte monolayer cultures.

(a) Double immunofluorescence staining for acetylated histone H3 (Lys14) (green) and LAMP2 (red) in undifferentiated and differentiated keratinocytes shows that acetylated histone H3 (Lys14) is localised in the nucleus of both undifferentiated and differentiated keratinocytes, whereas LAMP2 is cytoplasmic. Nucleophagic regions of differentiated keratinocytes are not positive for acetylated histone H3.

(b) Enlargements show more clearly that acetylated histone H3 (Lys14) is present in only the intact nucleus and not in the nucelophagic regions or in the cytoplasm.

Immunofluorescence images are representative of n=3 individual experiments. Bar = 10um. Small red arrows = regions of peri-nuclear protein accumulation. Red box = region selected for enlarged images.

Formatted: Font: 12 pt

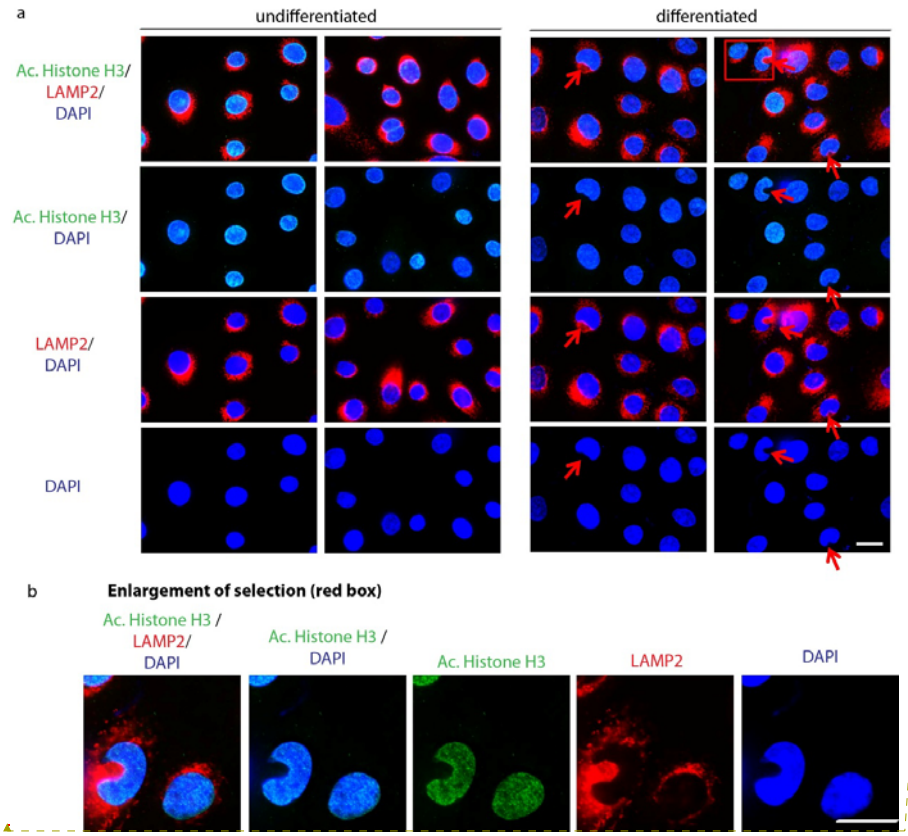

Formatted: Font: 12 pt

~~**Figure 3.19: Expression of acetylated histone H3 (Lys14) and LAMP2 in keratinocyte monolayer cultures.**~~

~~**(a)** Double immunofluorescence staining for acetylated histone H3 (Lys14) (green) and LAMP2 (red) in undifferentiated and differentiated keratinocytes shows that acetylated histone H3 (Lys14) is localised in the nucleus of both undifferentiated and differentiated keratinocytes, whereas LAMP2 is cytoplasmic. Nucleophagic regions of differentiated keratinocytes are not positive for acetylated histone H3.~~

~~**(b)** Enlargements show more clearly that acetylated histone H3 (Lys14) is present in only the intact nucleus and not in the nucelophagic regions or in the cytoplasm.~~

~~*Immunofluorescence images are representative of n=3 individual experiments. Bar = 10um. Small red arrows = regions of peri nuclear protein accumulation. Red box = region selected for enlarged images.*~~

In conclusion, actively transcribed chromatin is absent from nucleophagic regions suggesting the HP1α positive nuclear material in nucleophagic regions is transcriptionally inactive. In addition to this, these results suggest that the localisation of nuclear proteins, like HP1α, to the nucleophagic regions is a targeted process and the nuclear material within the nucleophagic regions differs from that within the still intact nucleus where gene transcription may still occur.

Therefore, in the differentiated keratinocytes with irregular nuclei, nucleophagic regions are HP1α positive but negative for acetylated histone H3 (Lys14). A reason for this may be that nucleophagy is a selective process and only certain regions of the nucleus which are no more required in terminally differentiating keratinocytes are initially degraded. The HP1 isoforms have also been shown to play a role in cellular processes other than regulating gene transcription. The HP1 isoforms are recruited to sites of DNA damage independently of DNA damage repair mechanisms (Luijsterburg *et al.* 2009). Therefore, HP1α may be present in the nucleophagic regions because the parts of the nucleus being degraded via autophagy may include DNA with hallmarks of DNA damage.

Next, I wanted to determine whether the HP1α positive nucleophagic vesicles are localised within the nucleus or outside the nucleus in the cytoplasm. If the nucleophagic vesicles are within the nucleus, then this would mean that the autophagic machinery would have to assemble in the nucleus, or the autophagic vesicles would have to be transported across the nuclear membrane. However, to date, autophagic vesicles have only been reported to be present in the cytosol where the autophagic machinery is known to assemble.

To check whether nucleophagic vesicles are within the nucleus or in the cytoplasm, I determined the expression pattern of the nuclear membrane protein LaminA (LMNA). Lamins are inner nuclear membrane proteins required for the maintenance of nuclear integrity (Hutchison 2002; Broers *et al.* 2006). Therefore, I performed

immunofluorescence analysis with double-staining for LMNA (green) and LAMP2 (red) in monolayer keratinocyte cultures.

Immunofluorescence analysis of LMNA shows that in both undifferentiated and differentiated keratinocytes, LMNA is expressed at the nuclear membrane (Fig. 3.20). In the nucleophagic keratinocytes, there is an accumulation of LMNA at the border between the still existing nucleus and the autophagic regions (Fig. 3.20). This clearly shows that the autophagic vesicles at the nucleophagic sites are outside the nucleus. But it also suggests that the nuclear membrane may play a role in nucleophagy. A reason for the increased LMNA expression at the border of the nucleus to the sites of nucleophagy may be due to an accumulation of over-expressed LMNA in these regions to compensate for a defective or leaky nuclear membrane. This LMNA expression pattern may also indicate that the nuclear membrane may act as a template and contribute to the autophagic membrane of the vesicles.

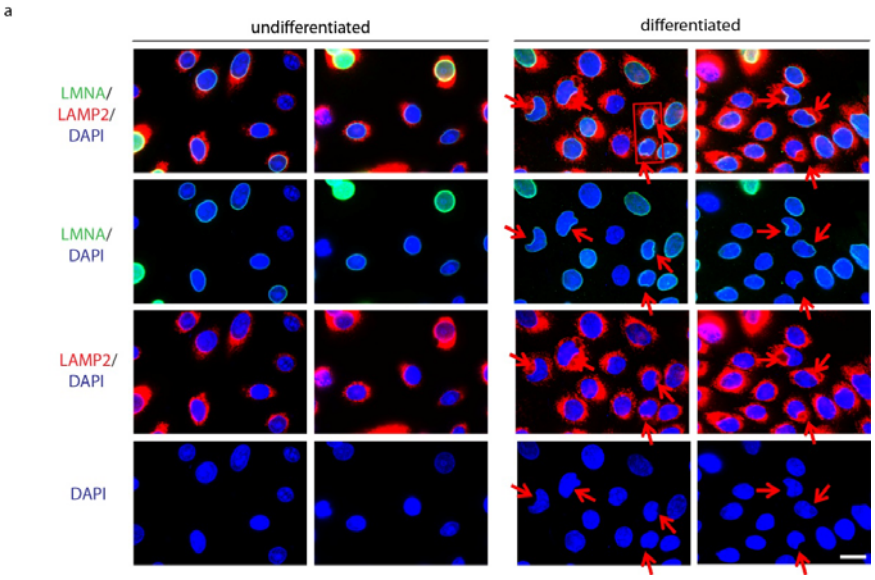

Figure 3.20: Expression of the nuclear membrane protein, LaminA (LMNA) and LAMP2 in keratinocyte monolayer cultures.

(a) LMNA (green) labels the nuclear membrane in both undifferentiated and differentiated keratinocytes. LMNA is excluded from LAMP2 (red) positive nucleophagic regions, with LMNA expressed in the nuclear membrane at the border between the still intact nucleus and the LAMP2 positive nucleophagic regions.

Figure 3.20 continued on the next page.

Immunofluorescence images are representative of n=3 individual experiments. Bar = 10um. Small red arrows = regions of peri-nuclear protein accumulation. Red box = region selected for enlarged images.

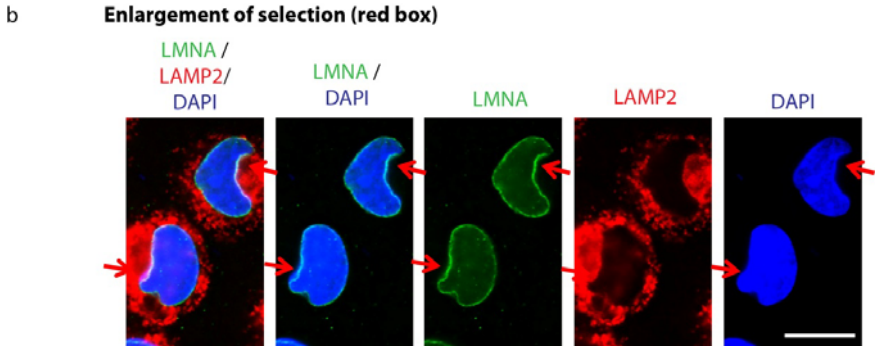

Figure 3.20: Expression of the nuclear membrane protein, LaminA (LMNA) and LAMP2 in keratinocyte monolayer cultures.

Figure 3.20 continued.

(b) The enlargements show that LMNA is more strongly expressed at the borders between nucleus and nucleophagic areas, indicating that the nuclear membrane is still present between nucleus and nucleophagic regions, and may also play a role in nucleophagy.

Immunofluorescence images are representative of n=3 individual experiments.

Small red arrows = regions LMNA accumulation. Bar = 10um.

With immunofluorescence analysis of LMNA expression, I show that nucleophagic vesicles are present in the cytosol (Fig. 3.20) however, they are positive for the nuclear protein HP1α (Fig. 3.18). What is unclear is whether nuclear material is transported out of the nucleus across the nuclear membrane to be degraded in nucleophagic vesicles, or whether nucleophagic vesicles in the cytosol engulf parts of the nucleus.

In this chapter, I have shown that nucleophagy in differentiating keratinocytes is targeted autophagic degradation of HP1α-positive nuclear material within autophagic vesicles in the cytosol. The HP1 proteins are important for heterochromatin formation, but they also localise to sites of DNA damage (Luijsterburg *et al.* 2009). Therefore, the next experiment I performed was to determine whether nucleophagy in differentiating keratinocytes is due to DNA double-strand breaks. Published data on a mouse model for laminopathies where nucleophagy in mammalian cells was initially observed shows that autophagy is a DNA damage response and leads to cell survival (Park *et al.* 2009).

To determine whether nucleophagy is required to degrade damaged DNA due to double-strand breaks, I analysed the expression pattern of γ-H2AX, a marker for DNA double-strand breaks in both undifferentiated and differentiated keratinocytes. γ-H2AX is the phosphorylated form of the core histone H2AX and phosphorylation occurs within minutes after DNA double-strand breaks (Rogakou *et al.* 1998; Rogakou *et al.* 1999).

Immunofluorescence staining with two antibodies against γ-H2AX (red) and LC3 (green) shows that these proteins do not colocalise in undifferentiated and differentiated keratinocytes (Fig. 3.21). Also, γ-H2AX is only present at low levels in the nucleus and is not present in LC3 positive regions of nuclear degradation suggesting nucleophagic vesicles do not contain damaged DNA with double-strand breaks (Fig. 3.21).

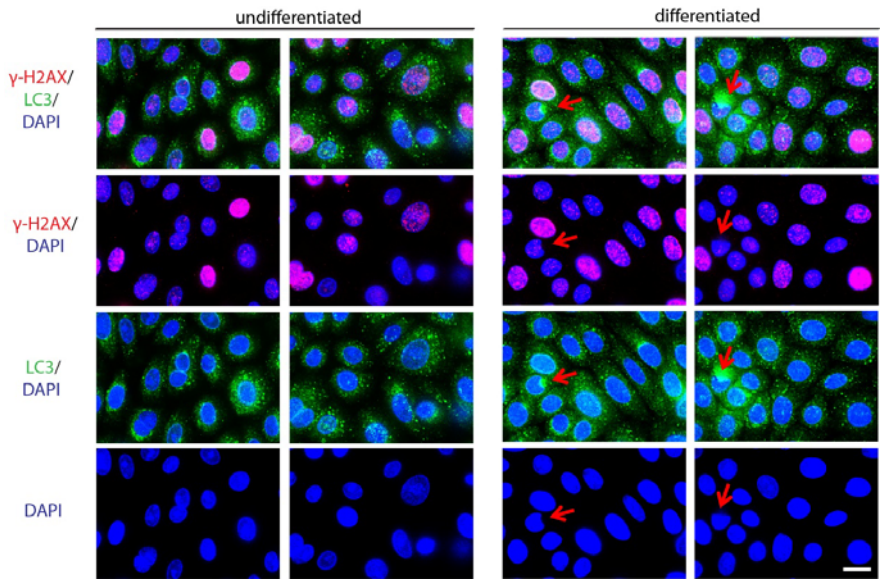

Figure 3.21: Expression of a marker for DNA double-strand breaks, γ-H2AX and LC3 in keratinocyte monolayer cultures.

γ-H2AX (red) is only expressed in the nuclei of both undifferentiated and differentiated keratinocytes. γ-H2AX (red) is absent from the LC3 positive (green) nucleophagic regions in the differentiating keratinocytes. This suggests that nucleophagic vesicles do not contain DNA with double-strand breaks.

Bar = 10um. Small red arrows = regions of nucleophagy.

In keratinocyte monolayer cultures, differentiation is characterised by the presence of some cells with irregular shaped nuclei. I have shown that autophagic vesicles are accumulated in the regions of missing nuclei and these vesicles contain HP1α positive nuclear material. However, other nuclear proteins like acetylated histone H3 are absent from sites of nucleophagy, suggesting that specific regions of the nucleus and specific proteins are targeted for autophagic degradation in nucleophagic cells. Also, immunofluorescene analysis of the nuclear membrane protein LMNA shows that the nucleophagic vesicles are outside the nucleus and in the cytosol. Nucleophagic vesicles do not contain DNA with double-strand breaks indicating that nucleophagy is not due to DNA damage.

These observations support my hypothesis that nucleophagy is a mechanism by which terminally differentiating keratinocytes degrade their nuclei *in vitro*. Therefore, I would like to determine whether autophagy is also used to degrade other organelles, like the ER and the Golgi, when the differentiation pathway is activated in keratinocyte monolayer cultures.

3.8 Autophagic degradation of other organelles in differentiating keratinocytes

I performed immunofluorescence analysis to find out if proteins specific to the ER and to the Golgi colocalise with LC3 positive autophagic vesicles. ~~The marker~~An antibody recognising the KDEL motif is used for analysis of the ER. KDEL is ~~an antibody which recognises the~~ an amino acid sequence~~s~~ of proteins which are retained within the ER (Pelham 1990). Immunofluorescence analysis of the KDEL motif expression shows ~~no~~ colocalisation of ~~the~~ ER proteins and LC3 aggregates in ~~both~~ the peri-nuclear regions of undifferentiated ~~and differentiated~~ keratinocytes (Fig. 3.22). However, in the differentiated keratinocyte cultures, ER proteins only sometimes colocalise with LC3 aggregates, but they appear to be completely excluded from the nucleophagic regions (Fig. 3.22). ~~Also, the ER appears to be excluded from the nucleophagic regions of the terminally differentiating keratinocytes (Fig. 3.22).~~ These results suggest that at this stage of differentiation in culture, the ER ~~is~~may not be degraded via autophagy in differentiated cells.

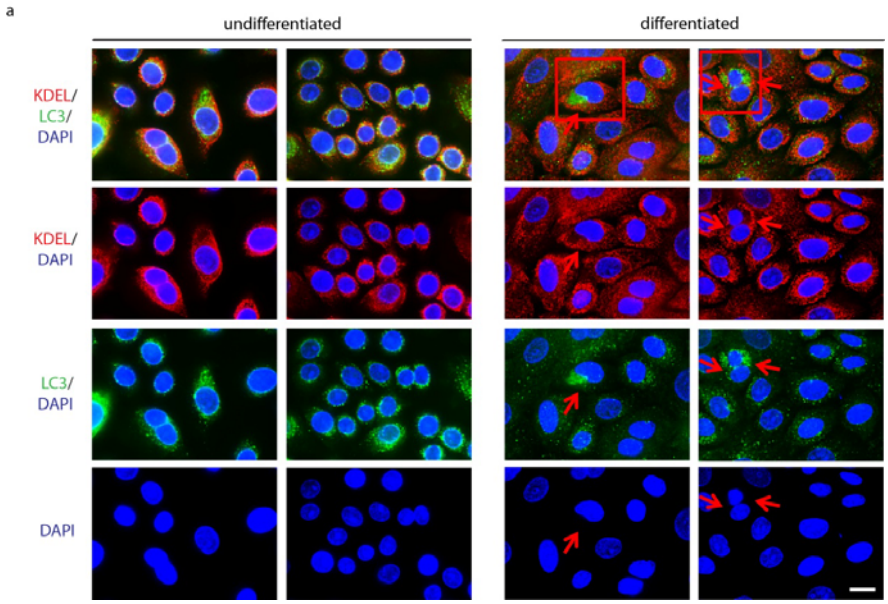

Figure 3.22: Expression of an ER marker, the KDEL motif and LC3 in keratinocyte monolayer cultures.

(a) Immunofluorescence staining for the ER marker (KDEL) (red) shows that KDEL is cytoplasmic in both undifferentiated and differentiated keratinocytes. ~~However,~~In the undifferentiated keratinocytes, LC3 (green) and the KDEL motif (red) ~~do not~~ colocalise in the peri-nuclear regions. However, in the differentiated keratinocytes, the KDEL motif (red) does not colocalsie with LC3 (green) and is completely excluded from the LC3 (green) positive nucleophagic regions. ~~both undifferentiated and differentiated keratinocyte populations, suggesting the ER is not degraded via autophagy under these culture conditions.~~

Figure 3.22 continued on the next page.

Immunofluorescence images are representative of n=2 individual experiments. Bar = 10um. Small red arrows = regions of peri-nuclear protein accumulation. Red box = region selected for enlarged images.

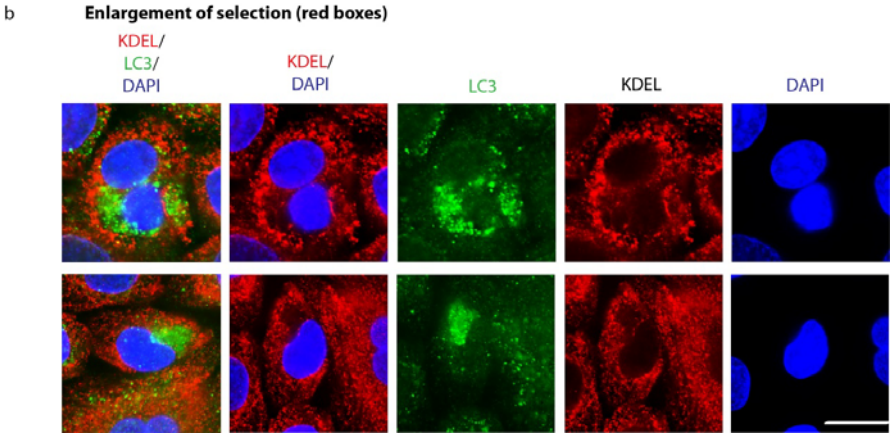

Figure 3.22 continued.

Figure 3.22: Expression of an ER marker, KDEL and LC3 in keratinocyte monolayer cultures.

(b) Enlargements of the nucleophagic regions of differentiated keratinocytes shows that the ~~ER~~ KDEL motif is excluded from LC3 positive nucleophagic vesicles.

Immunofluorescence images are representative of n=2 individual experiments. Bar = 10um. Small red arrows = regions of peri-nuclear protein accumulation. Red box = region selected for enlarged images.

I also performed double immunofluorescence staining for the Golgi protein GM130 and LC3 to find out if the Golgi colocalises with LC3 in keratinocyte monolayer cultures. GM130 is a peripheral cytoplasmic protein of the *cis-Golgi* matrix (Nakamura *et al.* 1995). With immunofluorescence analysis, I observe that GM130 sometimes, but not always, colocalises with LC3 in nucleophagic regions of differentiated keratinocytes (Fig. 3.23) indicating that the Golgi can also be degraded via autophagy during terminal differentiation.

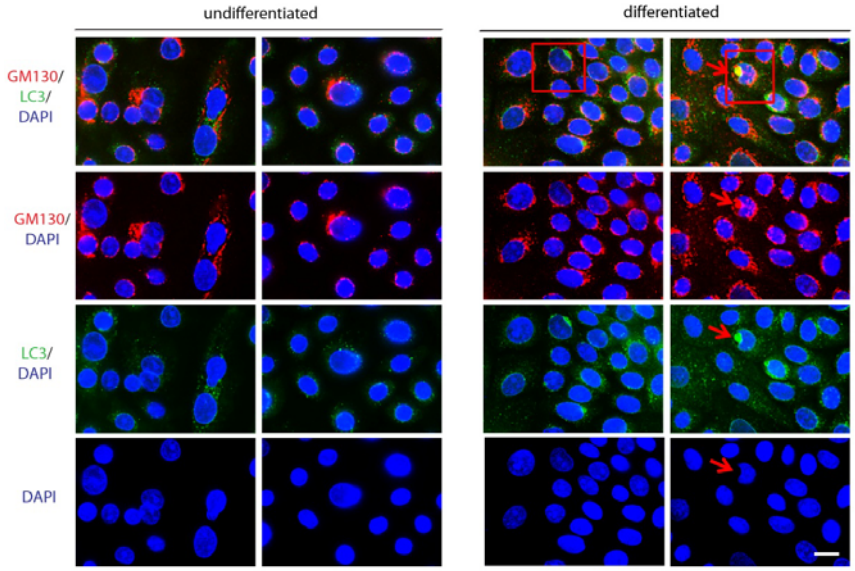

Figure 3.23: Expression of a Golgi marker, GM130 and LC3 in keratinocyte monolayer cultures.

(a) GM130 (red) is expressed in the cytoplasm of undifferentiated and differentiated keratinocytes. In undifferentiated cells, GM130 (red) and LC3 (green) ~~do not~~sometimes colocalise. However, ~~in~~ only very~~a~~ few differentiated cells, ~~GM130 and LC3 do~~ show colocalisation of GM130 and LC3 in nucleophagic regions. ~~indicat~~This indicates~~ing~~ that other organelles can also be degraded via autophagy during differentiation. But this does not occur as often as nucleophagy is observed in the differentiated cultures.

Figure 3.23 continued on the next page.

Immunofluorescence images are representative of n=2 individual experiments. Bar = 10um. Small red arrows = regions of peri-nuclear protein accumulation. Red box = region selected for enlarged images.

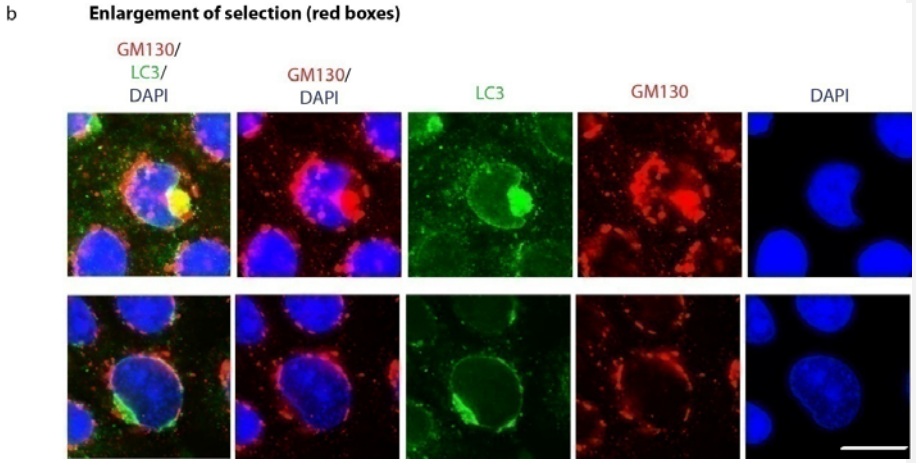

Figure 3.23 continued.

Figure 3.23: Expression of a Golgi marker, GM130 and LC3 in keratinocyte monolayer cultures.

(b) Enlargements of the rare nucleophagic regions where GM130 (red) and LC3 (green) colocalise, show that the LC3 aggregates appear to be the same aggregates which are GM130 positive. However, in most nucleophagic regions, LC3 and GM130 do not colocalise and enlargements show clearly that they are different aggregates.

Immunofluorescence images are representative of n=2 individual experiments. Bar = 10um.

With immunofluorescence analysis, I show that other organelles, apart from the nucleus, like the Golgi can also be degraded via autophagy when differentiation is activated in monolayer keratinocyte cultures. The differentiated keratinocyte culture is a mixed population of keratinocytes with different differentiation stages. Some cells may still be proliferating, while others express K1, a marker of early differentiation and others express filaggrin, a terminal differentiation marker (Fig. 3.8). At this stage of differentiation or very early terminal differentiation in culture, nucleophagy is probably the first form of autophagic degradation occurring and is probably also the most obvious form of autophagy to be detected *in vitro*.

Therefore, the next experiment I performed was to find out if autophagy is really required for the degradation of nuclei in differentiated keratinocyte cultures.

3.9 Autophagy inhibition in differentiating keratinocytes and its effects on nuclei degradation

In this chapter I have shown that activation of differentiation in monolayer cultures of primary keratinocytes is characterised by the presence of misshaped nuclei in some differentiated keratinocytes. Autophagy appears to be responsible for degrading the nuclei of these cells in the differentiated cultures. Therefore, I wanted to determine whether autophagy is essential for organelle degradation, especially degradation of nuclei, during differentiation *in vitro*.

3-MA is an inhibitor of the class III PI3kinase, Vps34 which is a key player in the autophagy pathway. 3-MA is routinely used in culture in block autophagy (reviewed in Klionsky *et al.* 2012). Therefore, to determine whether autophagy is required for degradation of nuclear material in differentiated cultured keratinocytes, I planned to use 3-MA to block autophagy when differentiation was induced. However, under some culture conditions and in some cells, 3-MA also inhibits the class I PI3kinase affecting the AKT/mTORC1 pathway (Wu *et al.* 2010; Klionsky *et al.* 2012). Since AKT/mTORC1 signalling is important for epidermal development and differentiation (Calautti *et al.* 2005; Thrash *et al.* 2006; O'Shaughnessy *et al.* 2007), any autophagy inhibitor I would use to determine the effects of autophagy during terminal differentiation must be specific for the autophagy pathway and not affect the AKT/mTORC1 pathway. Therefore, I tested the specificity of 3-MA on both class I and class III PI3kinases in the keratinocyte cell line, REKs.

Western blotting of REK lysates shows that 2 different 3-MA concentrations over a period of 4h, 24h and 48h has no effect on LC3 cleavage which occurs down-stream of the class III PI3kinase, Vps34 (Fig. 3.23). However, 3-MA inhibits phosphorylation of AKT and S6, which are down-stream of the class I PI3kinase (Fig. 3.23).

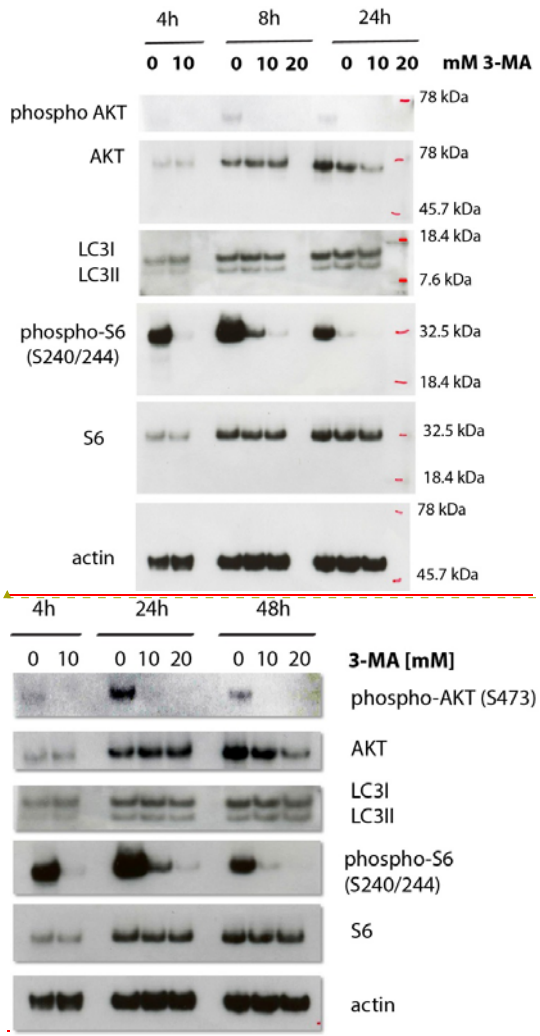

Figure 3.23: The effects of 3-MA on class I and class III PI3kinases in REKs.

Western blotting of lysates from REKs treated with 0-20mM 3-MA for 4h, 24h and 48h shows that all treatments with 3-MA down-regulate AKT phosphorylation as well as S6 phosphorylation. LC3 cleavage is unchanged by 3-MA treatment. These results show that 3-MA in cultured REKs down-regulates the class I PI3kinase, thereby reducing its downstream targets, phosphorylation of AKT and S6.

This Western blot is representative of n=2 experiments (see Appendix 11).

See Appendix 11 for effects of 3-MA in REKs at other concentrations.

Formatted: Font: 12 pt

Higher concentrations of 3-MA have no effect on LC3 cleaveage but still block phosphorylation of AKT and S6 (see Appendix 11). I conclude that in keratinocytes, 3-MA does not specifically inhibit the class III PI3kinase but affects the class I PI3kinase. Therefore, I had to use another approach to block autophagy during terminal differentiation.

To determine if autophagy is essential for organelle degradation, especially degradation of nuclei, during differentiation *in vitro*, a knockdown of key autophagy proteins was carried out using siRNAs against ULK1 and WIPI1. ULK1/2, ATG13 and FIP200 form an autophagy initiating complex which is directly regulated by mTORC1, transferring the nutrient status of the cell to the autophagic pathway (Jung *et al.* 2009). ULK1 was chosen as a target for a knockdown because ULK1 is present in both undifferentiated and differentiated keratinocyte cultures (Fig. 3.9 and Fig. 3.10) and it is predominantly expressed in the upper layers of adult mouse and human skin (Fig. 3.2), as well as in foetal epidermis (Fig. 3.4). So it is expected that a knockdown of ULK1 should mainly affect differentiating keratinocytes.

Another potential candidate for a knockdown experiment is WIPI1. WIPI1 is a human WD-repeat protein which interacts with phosphoinositides and has been shown to interact with autophagic structures under starvation conditions or mTORC1 inhibition. WIPI1 also colocalises with LC3 positive puncta (Proikas-Cezanne *et al.* 2004; Proikas-Cezanne *et al.* 2007; Polson *et al.* 2010). However, published data shows that in most tissues, the isoform WIPI2 is more abundantly expressed than WIPI1 (Polson *et al.* 2010). WIPI1 and WIPI2 are known to be components of the autophagy-initating complex however, their exact role has not yet been determined (Itakura and Mizushima 2010; Polson *et al.* 2010; Tooze *et al.* 2010; Gaugel *et al.* 2012; see section 1.2.2). Initially, the expression levels and expression patterns of WIPI1 and WIPI2 were analysed in cultured keratinocytes (Fig. 3.24a and b) as well as in epidermis (Fig. 3.24c).

Western blot analysis of WIPI1 and WIPI2 in protein lysates from monolayer keratinocyte cultures shows that both WIPI1 and WIPI2 isoforms are expressed at fairly equal levels in undifferentiated and differentiated keratinocyte cultures (Fig. 3.24a). However, immunofluoresence staining of monolayer keratinocytes suggests that in differentiated cells, there is more WIPI1 and WIPI2 compared to the undifferentiated keratinocytes (Fig. 3.24b). However, this was not observed with Western blotting (Fig. 3.24a).

In adult mouse and human epidermis, WIPI1 is mainly expressed as puncta in the upper layers (Fig. 3.24c). The other isoform, WIPI2 appears to be present in the cytoplasm as well as in the nucleus of keratinocytes of all layers of human epidermis. WIPI2 is also expressed strongly in the basement membrane (Fig. 3.24c). This nuclear expression pattern of WIPI2 has not been previously reported and this may suggest that WIPI2 has other functions in epidermis. Therefore, I decided that WIPI1, which is mainly expressed in the granular layers, would be a suitable target for a knockdown experiment to inhibit autophagy in the terminally differentiating keratinocytes.

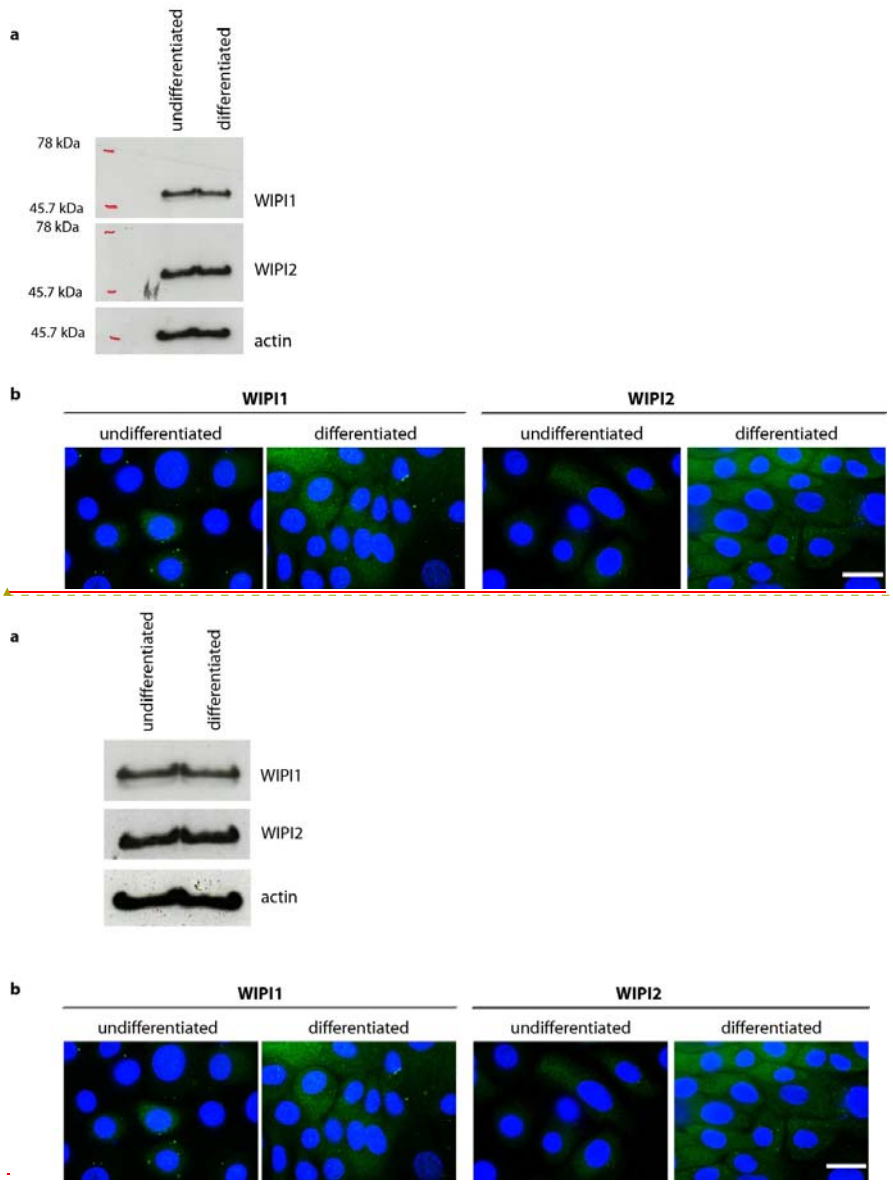

Figure 3.24: Expression of WIPI1 and WIPI2 isoforms in monolayer keratinocytes **(a)** Western blotting of lysates from undifferentiated and differentiated keratinocytes shows that both isoforms of WIPI1 and WIPI2 are strongly expressed in keratinocyte

Formatted: Font: 12 pt, Font color: Text 1

monolayer cultures. The expression levels of WIPI1 and WIPI2 appear to be fairly equal in both keratinocyte cultures.

(b) Immunofluorescence staining of WIPI1 and WPI2 in undifferentiated and differentiated keratinocytes confirms that both isoforms are expressed in both populations. However, the expression levels of both WIPI1 and WIPI2 appear to be lower in undifferentiated cells compared to the differentiated keratinocytes. This observation is not confirmed by Western blot analysis in (a).

Figure 3.24 continued on the next page.

The Western blot is representative of n=3 individual experiments and immunofluorescence images are representative of n=2 individual experiments. Bar = 10um.

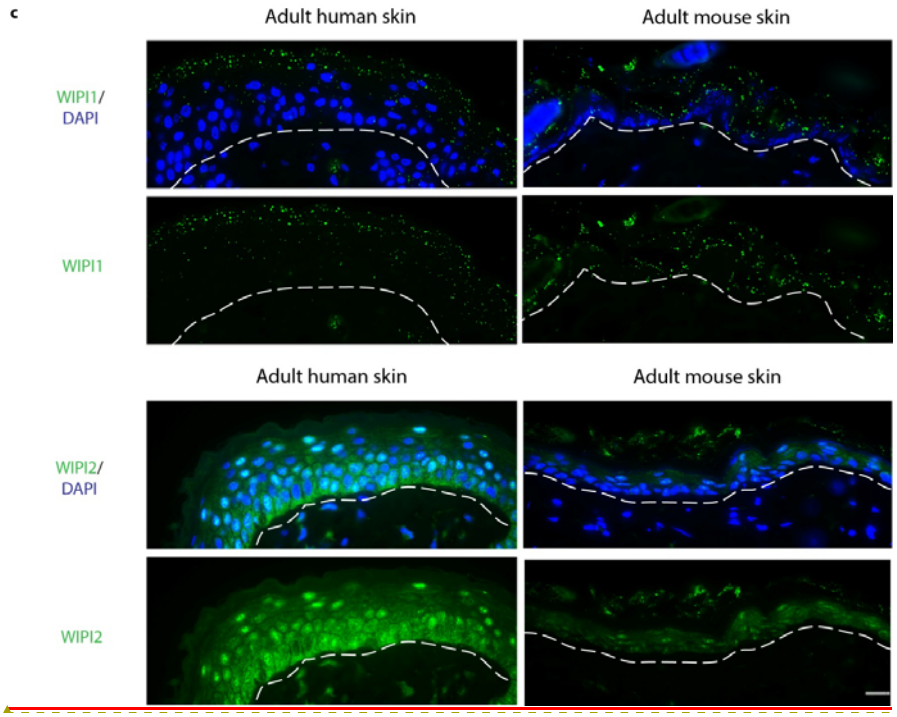

Formatted: Font: 12 pt, Bold

Figure 3.24 continued.

Figure 3.24: Expression of WIPI1 and WIPI2 isoforms in adult mouse and human epidermis

(c) Immunofluorescence analysis of WIPI1 and WIPI2 expression patterns in adult human and adult mouse epidermis show that WIPI1 is present as puncta in the upper layers of epidermis. However, staining for WIPI2 shows that it is localised in the cytoplasm as well as in the nucleus of all layers of epidermis.

Immunofluorescence images are representative of n=2 individual experiments. Bar = 20um.

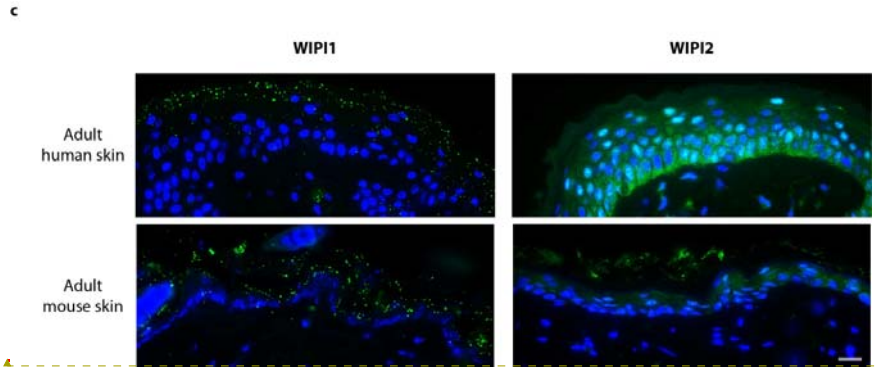

Formatted: Font: 12 pt, Bold

~~***Figure 3.24 continued.***~~

~~**Figure 3.24: Expression of WIPI1 and WIPI2 isoforms in adult mouse and human epidermis**~~

~~**(c)** Immunofluorescence analysis of WIPI1 and WIPI2 expression patterns in adult human and adult mouse epidermis show that WIPI1 is present as puncta in the upper layers of epidermis. However, staining for WIPI2 shows that it is localised in the cytoplasm as well as in the nucleus of all layers of epidermis.~~

~~*Immunofluorescence images are representative of n=2 individual experiments. Bar = 20um.*~~

In order to find out if autophagy is essential for degradation of nuclei, during differentiation *in vitro*, a knockdown of key autophagy proteins was carried out using siRNAs against ULK1 and WIPI1. Monolayer proliferating undifferentiated keratinocytes were transfected with the different siRNAs. 24h after transfection, differentiation was induced for a further 48h by increasing the calcium content of the media. Undifferentiated keratinocytes were cultured in medium with low calcium for the period before harvesting. The end-concentration of siRNAs used was 50nM. Titrations for lower contentrations (10nM and 25nM) showed that lower siRNA concentrations had no effects on nucleophagy.

Western blotting of protein lysates shows that 72h after siRNA transfection, both WIPI1 and ULK1 protein expression are still knocked down in undifferentiated and differentiated cells (Fig. 3.25a and c). In the WIPI1 knockdown cells, there is a ~~drastic~~ strong reduction in the number of nucleophagic cells in ~~the~~ keratinocytes grown under differentiation-inducing conditions. SiWIPI1 transfected and differentiated keratinocytes have hardly any nucleophagic cells (~2%) compared to the differentiated keratinocytes with non-targeting siRNA (~15%). This difference is also statistically significant ($p<0.05$) (Fig. 3.25b). Knockdown of ULK1 also reduces the number of nucleophagic keratinocytes in the differentiated population (~10%) (Fig. 3.25d). However, this reduction in nucleophagic cells with siULK1 is not as marked as with the WIPI1 knockdown.

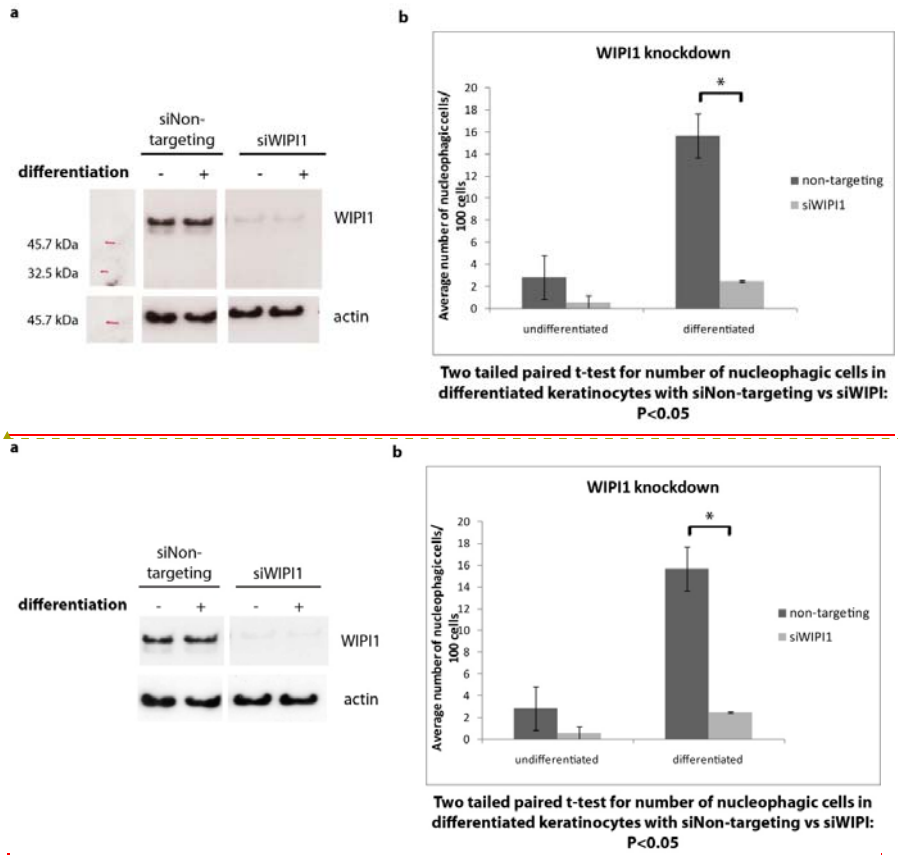

Figure 3.25: Inhibition of autophagy via siRNA knockdowns of ULK1 and WIPI1, and its effects on nucleophagy in differentiating keratinocytes.

(a) Western blotting of lysates from undifferentiated and differentiated keratinocytes transfected with non-targeting and with WIPI1 siRNA shows effective knockdown of WIPI1 in the siWIPI1 cells.

(b) Quantification of nucleophagic keratinocytes in both undifferentiated and differentiated cultures of cells transfected with non-targeting and with WIPI1 siRNA shows a drastic reduction in the proportion of nucleophagic cells in the differentiated WIPI1 knockdown keratinocytes compared to cells with non-targeting siRNA (~2% in siWIPI cells and ~18% in siNon-targeting cells). This difference is also statistically significant, two-tailed paired t-test, P<0.05.

Formatted: Font: 12 pt

Figure 3.25 continued on the next page.

Terminal differentiation induced by increasing calcium content of media 24h after siRNA transfection with 50nM siRNA. Cells harvested 48h after induction of differentiation (i.e. 72h after siRNA transfection).

For quantification, n=2 knockdown experiments analysed and number of nucleophagic cells counted per total number of 100 cells (see Appendix 10). Total number of cells determined with ImageJ and number of nucleophagic cells counted manually.

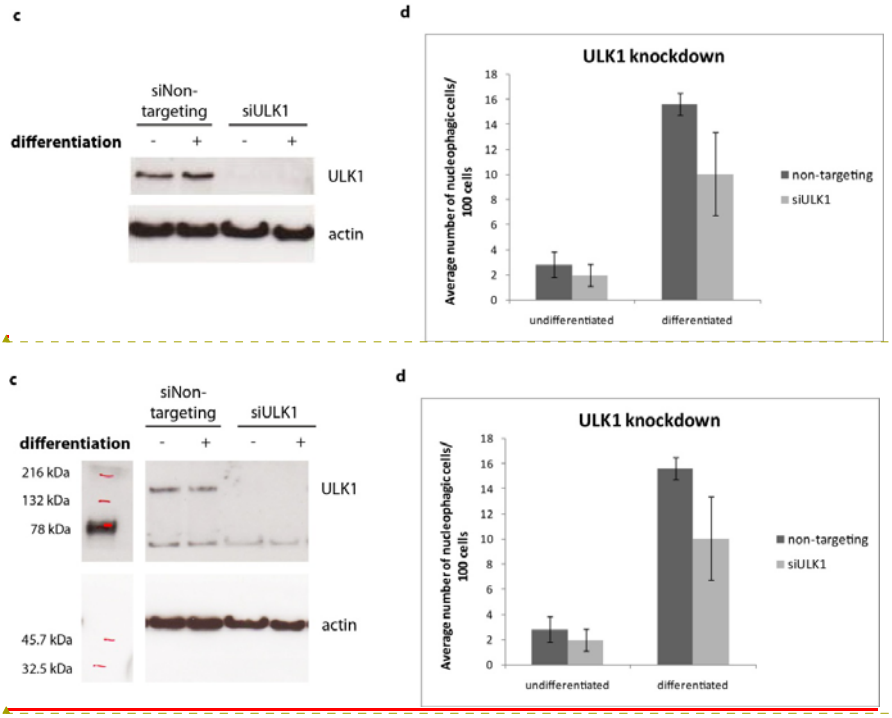

Figure 3.25: Inhibition of autophagy via siRNA knockdowns of ULK1 and WIPI1, and its effects on nucleophagy in differentiating keratinocytes.

Figure 3.25 continued.

(c) Western blotting of lysates from undifferentiated and differentiated keratinocytes transfected with non-targeting siRNA and siRNA against ULK1 shows that there is no ULK1 expression in siULK1 cells.

(d) Quantification of nucleophagic keratinocytes in both undifferentiated and differentiated cultures of cells transfected with non-targeting and with ULK1 siRNA shows there is also a reduction in the proportion of nucleophagic cells (~107% in siULK1 cells and ~168% in siNon-targeting cells) in the differentiated ULK1 knockdown cells compared to differentiated cells with non-targeting siRNA.

Terminal differentiation induced by increasing calcium content of media 24h after siRNA transfection with 50nM siRNA. Cells harvested 48h after induction of differentiation (i.e. 72h after siRNA transfection).

Formatted: Font: Bold

Formatted: Font: 12 pt, Bold

For quantification, n=2 knockdown experiments analysed and number of nucleophagic cells counted per total number of 100 cells (see Appendix 10). Total number of cells determined with ImageJ and number of nucleophagic cells counted manually.

Blocking autophagy via siRNA knockdowns of ULK1 and WIPI1 in keratinocyte monolayer cultures compared to cells with non-targeting siRNA, shows that there is a drastic reduction in the number of nucleophagic cells when differentiation is induced. Therefore, in the absence of functional autophagy *in vitro*, differentiating keratinocytes cannot degrade their nuclei. These data confirm that autophagy is the mechanism by which differentiating keratinocytes in culture degrade their nuclei.

So, with the next experiment I wanted to determine whether autophagy plays a role in terminal differentiation of keratinocytes. Terminal differentiation, a specialised form of keratinocyte cell death, occurs in granular layer keratinocytes where cells degrade their organelles. I hypothesize that autophagy is the mechanism by which terminally differentiating keratinocytes degrade their organelles in the granular layer. I have shown that blocking autophagy in keratinocyte cultures prevents autophagic degradation of the nuclei when differentiation is induced. Therefore, siRNA knockdown cultures were analysed for expression of markers of epidermal differentiation (Fig. 3.26).

In cells transfected with non-targeting siRNA, the early differentiation marker K1 is expressed at very low levels in the undifferentiated population, whereas, the differentiated siNon-targeting keratinocytes show strong K1 expression (Fig. 3.26). This confirms activation of early differentiation in the differentiated keratinocyte population, corresponding to keratinocytes of the supra-basal layers. The siULK1 and siWIPI1-transduced cells show a similar expression pattern for K1 with low levels of K1 in the undifferentiated keratinocytes and higher K1 in the differentiated cells (Fig. 3.26). These results show that blocking autophagy in monolayer keratinocyte cultures has no effect on the early differentiation of keratinocytes.

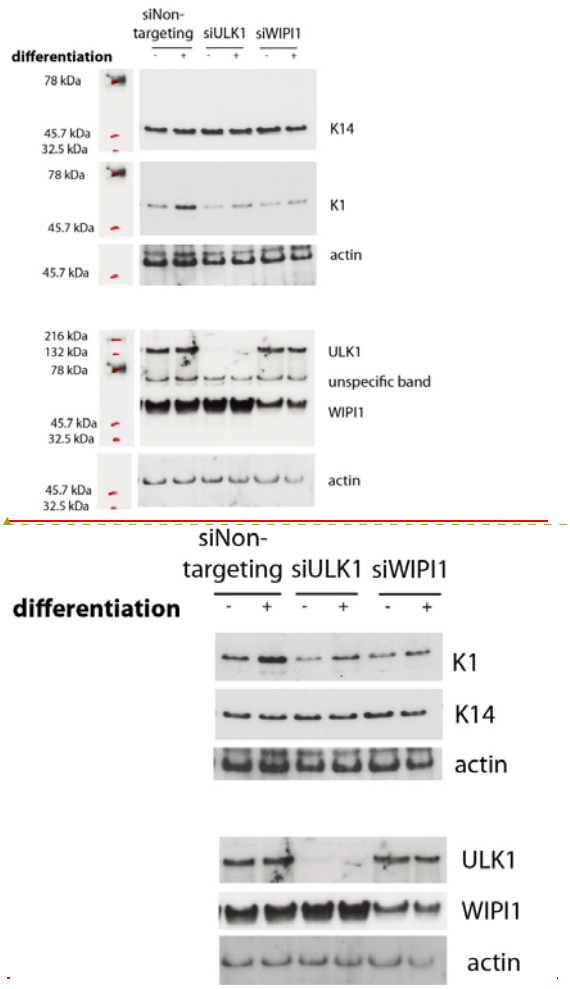

Figure 3.26: Expression of epidermal markers of differentiation in siULK1 and siWIPI1 keratinocytes.

The expression of differentiation markers K1 and K14 are analysed by Western blotting of lysates from undifferentiated and differentiated keratinocytes transfected with siRNAs against ULK1 and WIPI1. The Western blot shows markers of differentiation in the upper half and the lower panel showing expression of ULK1 and WIPI1. In the keratinocytes with non-targeting siRNA, K1 is expressed at lower levels in the undifferentiated keratinocytes compared to the differentiated keratinocytes. Both siULK1 and siWIPI1 cells express low

Formatted: Font: 12 pt, Font color: Red

levels of K1 in the undifferentiated keratinocytes. The differentiated keratinocytes of the ULK1 and WIPI1 knockdowns show increased K1 expression. K14 is expressed at equal levels in undifferentiated and differentiated keratinocytes with non-targeting siRNA. The undifferentiated and differentiated keratinocytes of both siULK1 and siWIPI1 knockdowns also express equal levels of K14. Therefore, the expression pattern of K1 and K14 in the siULK1 and siWIPI1 cells is very similar to the keratinocytes with the non-targeting siRNA.

For expression of K1 and K14 in other siULK1 and siWIPI knockdown experiments, see Appendix 10.

Terminal differentiation induced by increasing calcium content of media 24h after siRNA transfection with 50nM siRNA. Cells harvested 48h after induction of differentiation (i.e. 72h after siRNA transfection).

Formatted: Space After: 0 pt, Line spacing: 1.5 lines

In this section I have shown that a knockdown of ULK1 and WIPI1 in monolayer keratinocyte cultures drastically reduces the number of nucleophagic keratinocytes in the differentiated keratinocyte population compared to differentiated cells with non-targeting siRNA. Therefore, I conclude that autophagy is the mechanism by which differentiating keratinocytes degrade their nuclei *in vitro*.

However, blocking autophagy in the differentiated keratinocytes has no effects on the expression of K1 which is a marker for early differentiation in supra-basal keratinocytes. Also, the expression of K14, a marker for proliferating basal layer keratinocytes, is unaffected by a block in autophagy in both undifferentiated and differentiated keratinocytes (Fig. 3.26). These data show that blocking autophagy, via a knockdown of ULK1 and WIPI1 expression has no effect on proliferating undifferentiated and K1 positive, early differentiated keratinocytes.

In this chapter I show that autophagy is a mechanism of organelle degradation in differentiating monolayer keratinocytes. In epidermis, organelle degradation occurs in the granular layer where keratinocytes undergo terminal differentiation. Therefore, the nucleophagic keratinocytes I have characterised probably represents the keratinocytes which have been able to activate their terminal differentiation pathway in culture and also may express filaggrin. The expression levels of filaggrin could not be analysed in the ULK1 and WIPI1 knockdown cells due to the custom made filaggrin antibody used for my analysis not being available anymore. The commercially available anti-filaggrin antibodies either showed a preference for pro-filaggrin or for processed filaggrin. Further testing of anti-filaggrin antibodies was not possible due to the limited time I had left and would be an aim for future work.

However, I conclude that autophagy is the mechanism by which differentiating keratinocytes degrade their nuclei in culture.

Discussion

At the beginning of this chapter I set out to determine whether the autophagy process occurs in epidermis. In adult epidermis, I observe that LC3 aggregates are present in the granular layer where other proteins required for autophagy, like ULK1 and WIPI1, are strongly expressed. BECN1 and ATG5-ATG12 are also expressed in the granular layer but at very low levels (Fig 3.2). However, very low levels of autophagy proteins are enough to sustain autophagy (personal comm. N. Mizushima; Hosokawa *et al.* 2007). Therefore, these first results suggest that autophagy can occur in the granular layers of epidermis and they indicate that autophagy may be important in the granular layer. BECN1 and ATG5-ATG12 also show high basal and para-basal expression whereas LC3 aggregates are absent in these layers. A reason for this may be that proteins required for the autophagy process are always present in the proliferating basal cells to facilitate the immediate autophagic response to external stresses as a protective mechanism for the basal layer ensuring epidermal function (see chapter 5).

To determine whether autophagy is important in the granular layer, I used mouse foetal epidermis covering the period of epidermal terminal differentiation and barrier formation (Fig. 3.3; Fig. 3.4). This model allows analysis of autophagy in epidermis before, during and after granular layer formation in the mouse foetus. Analysis of autophagy marker expression in this model shows that expression of autophagy proteins coincides with the skin's first attempts at terminal differentiation and granular formation during foetal epidermal development (Fig. 3.3; Fig. 3.4). These results strongly suggest that autophagy is required for epidermal terminal differentiation.

Autophagy is usually maintained at low levels in living cells and it is drastically up-regulated within minutes in response to starvation, stress or infection with

pathogens (Tanida 2011). Formation of LC3 aggregates only occurs with autophagy induction (Kabeya *et al.* 2000; Klionsky *et al.* 2012). However, in the absence of external stresses, LC3 aggregates are constitutively present in the epidermal granular layer (Fig. 3.2; Fig. 3.4). Therefore it is proposed that autophagy is part of the normal differentiation process in epidermis.

Published data characterising various LC3 positive vesicles shows that some organelles in some cell types use the autophagic machinery to form non-autophagic vesicles which are LC3 positive. Such organelles are lipid droplets, engulfed live cells within host cells and intracellular pathogens (Shibata *et al.* 2009). Therefore, I wanted to determine whether granular layer LC3 aggregates are other known organelles specific for terminally differentiating keratinocytes. Filaggrin is expressed in granular layer keratinocytes where it forms keratin bundles leading to the collapse and flattening of terminally differentiating cells. Lamellar bodies are organelles found in the granular layer where they secrete lipids, hydrolases, protease inhibitors and antimicrobial compounds during cornification (Menon *et al.* 1994; Ishida-Yamamoto *et al.* 1996; Ishida-Yamamoto *et al.* 2004; Raymond *et al.* 2008). I show that in adult human skin, LC3 aggregates do not colocalise with filaggrin granules or with the lamellar body marker CatD (Fig. 3.5; Fig. 3.6). Therefore, it can be concluded that LC3 puncta are not lamellar bodies and not filaggrin granules but most probably autophagosomes.

TEM analysis of 3-day old mouse epidermis shows double-membrane vesicles are present in both the lower proliferating basal layer as well as in the granular layer, confirming the presence of autophagic vesicles in epidermis (Fig. 3.7). However, immuno-EM analysis would be required to confirm that these double-membrane vesicles are positive for LC3. At the time this thesis is being written, immuno-EM for LC3 in mouse epidermis is work in progress.

These results from adult and foetal epidermis suggest that autophagy is constitutively active in the granular layer of epidermis. This led to the main hypothesis that autophagy is the mechanism by which granular layer keratinocytes degrade their organelles and undergo terminal differentiation, a specialised form of cell death.

As a first step in testing this hypothesis, I used monolayer primary keratinocytes as a model to mimic the different epidermal differentiation stages. *In vitro,* differentiation is induced by culturing keratinocytes in high calcium media (Hennings *et al.* 1983; fig. 3.8). Under these conditions, the undifferentiated keratinocyte population is predominantly K14 positive, a marker of proliferating basal keratinocytes. However, the differentiated population is a mix of K14 positive proliferating cells, K1 expressing differentiated supra-basal keratinocytes and filaggrin positive terminally differentiating granular layer cells.

Also, both undifferentiated and differentiated keratinocyte populations express autophagy proteins; however, there is no significant difference in total autophagy protein expression levels in both populations (Fig. 3.9). Due to the differentiated monolayer keratinocytes being a mix of different differentiation stages, a change in autophagy marker expression in one differentiation stage of keratinocytes may not be detected by Western blotting of lysates from this mixed population.

Immunofluorescence analysis shows that in the differentiated population, ULK1, LC3 and p62 appear to accumulate in peri-nuclear regions of some cells (Fig. 3.10). Closer examination of cell morphology reveals that the differentiated keratinocyte population is characterised by a proportion of cells having irregularly shaped nuclei with LC3/LAMP2 positive aggregates in regions of missing nuclei (Fig. 3.11; Fig. 3.13; Fig. 3.14). This indicates that regions of missing nuclear material are areas of high autophagic activity. LC3/LAMP2 aggregates are also positive for p62 (Fig. 3.15),

which strongly suggests targeted autophagic degradation in the differentiated keratinocyte culture. This form of autophagy in regions of missing nuclei of differentiated keratinocytes could be autophagic degradation of nuclear material.

From these results, I conclude that induction of differentiation in monolayer keratinocyte cultures is accompanied by the formation of peri-nuclear autolysosomes in some cells. This work shows that nucleophagy, which is autophagic degradation of nuclear material, occurs when differentiation is induced *in vitro*. However, only some cells of the differentiated population undergo nucleophagy. Similar forms of autophagic degradation have been observed in different organisms. Autophagic degradation of nuclear material has been reported in yeast, a bi-cellular organism *Tetrahymena thermophila* and in an osteosarcoma cell line where micro-nuclei are formed and these~~s~~ are then degraded (Krick *et al.* 2008; Liu and Yao 2012), (Rello-Varona *et al.* 2012). However, no formation of micronuclei is observed in terminally differentiating monolayer keratinocytes. In *C. elegans*, nucleophagy is responsible for degrading of whole nuclei in aging intestinal epithelia (McGee *et al.* 2011). This form of nucleophagy is more similar to the characteristics of autophagy in differentiating keratinocyte cultures. The observations made by Park *et al.* on nucleophagy in fibroblasts from a mouse model for nuclear envelopathies, is also very similar to the observations I have made in terminally differentiating keratinocytes (Park *et al.* 2009). However, nucleophagy in the reported mouse model is a pro-survival mechanism in response to DNA-damage (Park *et al.* 2009; Mijaljica *et al.* 2010). The results from this chapter show that nucleophagy in keratinocytes may be a terminal differentiation mechanism leading to keratinocyte cell death. Therefore, nucleophagy may be a keratinocyte cell death mechanism.

To measure autophagic flux, and to show that the autophagic process is completed, the degradation of autolysosomes is blocked with lysosomal inhibitors like BafA1

(Klionsky *et al.* 2012). In the keratinocyte cultures, BafA1 treatment blocks the late stages of autophagy and leads to accumulation of LC3 (LC3II/LC3I and LC3II/actin ratios) which I measured on the protein level as well as with immunofluorescence analysis (Fig. 3.16; Fig. 3.17). However, this measurement of autophagic flux shows that undifferentiated cells have a higher level of basal autophagy (higher LC3II/LC3I and LC3II/actin ratios) compared to differentiated keratinocytes (Fig. 3.16; Fig. 3.17). This is unexpected since immunofluorecence analysis of autophagy proteins in adult epidermis shows that granular layer keratinocytes have higher levels of autophagy proteins compared to keratinocytes of the other epidermal layers (Fig. 3.2), suggesting increased autophagy. This difference between keratinocyte monolayer cultures and adult epidermis may be due to the differentiated monolayer keratinocyte population being a mix of different differentiation stages, as well as incomplete terminal differentiation in keratinocyte monolayer cultures.

Western blot analysis shows that BafA1 has no significant effect on p62 levels in both undifferentiated and differentiated keratinocyte cultures (Fig. 3.16). However, immunofluorescence analysis shows stronger accumulation of p62 with BafA1 treatment in differentiated cells (Fig. 3.17). Therefore, from these results I conclude that in keratinocytes, the autophagic pathway is functional and is completed. But induction of differentiation in *in vitro* cultures does not increase the basal levels of autophagy. However, the striking feature of differentiating monolayer keratinocytes is autophagic degradation of the nucleus, which is probably the first step in organelle clearance characteristic for terminal differentiation.

Nucleophagic regions also contain the Heterochromatin Protein 1α (HP1α). HP1α is usually expressed in the nucleus as part of the chromatin (Maison and Almouzni 2004). In nucleophagic cells, HP1α is localised outside the nucleus but within autophagic vesicles in nucleophagic regions, indicating that these vesicles contain nuclear material (Fig. 3.18). These results are similar to published data on

nucleophagy in fibroblasts from a mouse model for nucear envelopthies (Park *et al.* 2009). However, nucleophagic regions of differentiated keratinocytes are not positive for acetylated histone H3 (Fig. 3.19). This indicates that nucleophagy is selective degradation of nuclear material and of specific nuclear regions which are HP1α positive and negative for acetylated histone H3. However, the mechanism by which the region of nucleus is selected and targeted for autophagy and engulfment by autophagic vesicles is not yet known. These results support my hypothesis that constitutive granular layer autophagy is the mechanism by which terminally differentiating keratinocytes degrade their organelles.

I determined the expression pattern of another nuclear protein, the nuclear membrane protein, LMNA. Nucleophagic regions do not contain LMNA (Fig. 3.20) however, closer examination of these cells showed that there is a much stronger expression of LMNA at the boundary to autophagic vesicles (Fig. 3.20b). This confirms that nucleophagic vesicles are outside the nuclear membrane of what is left of the partially degraded, DAPI-positive nucleus. Also, this data indicates that the nuclear membrane may play a role in the formation of these nucleophagic vesicles. My observations with LMNA are very similar to published data on nucleophagy in mouse laminopathies (Park *et al.* 2009).

To determine whether nucleophagy is due to DNA-damage, I analysed cultured keratinocytes for the expression of the DNA double-strand break marker γ-H2AX. Nucleophagic regions do not contain the protein γ-H2AX (Fig. 3.21) confirming that nucleophagy is not a response to DNA double-strand breaks. However, it is published that nucleophagy in laminopathies is required to degrade damaged DNA and ensure cell survival (Park *et al.* 2009). I show that nucleophagy during keratinocyte differentiation *in vitro* is not due to damaged DNA with double-strand breaks. However, the presence of other forms of DNA damage were not analysed and would be an aim for future work. These results support my hypothesis that

autophagy is a terminal differentiation mechanism in granular layer keratinocytes, leading to this specialised form of cell death. My PhD project is the first report showing nucleophagy in healthy mammalian cells under normal culture conditions, and not as a survival mechanism, but as a cell death mechanism.

Terminal differentiation in epidermis is characterised by loss of organelles and flattening of cells leading to cornification. To determine whether other organelles are also degraded by nucleophagy i*n vitro*, cultured keratinocytes were analysed for the expression of ER and Golgi markers. LC3 positive vesicles do not colocalise with ~~the~~ ER proteins (Fig. 3.22) but the Golgi sometimes is present within the autophagic vesicles at sites of nucleophagy (Fig. 3.23). This indicates that other organelles apart from the nucleus can be degraded via autophagy in terminally differentiating keratinocytes. However in monolayer culture, it is mainly the nuclei which are degraded via autophagy since autophagic degradation of other organelles like the Golgi is rarely observed.

To confirm that autophagy is responsible for degradation of nuclei in differentiating keratinocytes, results from siRNA-mediated autophagy inhibtion shows that in the absence of autophagy, the nuclei retain their orginal, rounded shape even after culturing under conditions inducing differentiation. ULK1 and WIPI were selected as suitable targets for a knockdown due to their strong granular layer expression in skin (Fig. 3.2; Fig. 3.24). So it is expected that a knockdown of these genes should not affect the proliferating, undifferentiated cells. I show that inhibition of autophagy in keratinocytes via siRNA knockdowns of ULK1 and WIPI1 and then inducing differentiation leads to a drastic reduction in the number of nucleophagic keratinocytes compared to cells with the non-targeting siRNA cultured under the same conditions (Fig. 3.25). Therefore, it can be concluded that autophagy is required for degradation of the nucleus during differentiation in keratinocyte monolayer cultures.

Blocking autophagy in keratinocyte monolayer cultures has no effect on the expression of the early epidermal differentiation markers like K1 (Fig. 3.26). This indicates that early epidermal differentiation does not depend on autophagy or autophagic degradation of organelles. So a block in autophagy may not affect the supra-basal keratinocytes which have very low basal autophagy levels. However, it is still unclear whether autophagy goes hand-in-hand with terminal differentiation or if it directly regulates induction of terminal differentiation.

In summary, this chapter shows that autophagy proteins are expressed in epidermis, and during foetal development their expression is induced at the time point when the granular layer is being formed. LC3 positive autophagic vesicles are mainly present in the granular layer, which is where keratinocytes degrade their organelles during terminal differentiation. *In vitro*, terminally differentiating keratinocyte cultures are characterised by cells having misshaped nuclei which is due to selective autophagic degradation of nuclear material, nucleophagy. Autophagy has no effect on early keratinocyte differentiation however its role in terminal differentiation of granular layer keratinocytes is not yet clear.

Chapter 4

RESULTS

mTOR regulation of autophagy in epidermis

mTOR regulation of autophagy in epidermis

Introduction

Immuno-suppressed organ transplant patients (OTRs) have a 65-fold higher incidence of cutaneous Squamous Cell Carcinoma (cSCC) (Berg & Otley, 2002). A new class of immunosuppressants, rapamycin and its analogues, have greatly reduced the incidence and progression of cSCCs in transplant patients (Geissler 2008; Wulff *et al.* 2008; McQuillan *et al.* 2009; Salgo *et al.* 2010; see section 1.1.6). These results from patient studies have been replicated using animal models. However, the mechanism by which rapamycin does this is not clear. In tumour-bearing mice which have undergone a heart transplant, rapamycin not only prevents allograft rejection, but also reduces proliferation and angiogenesis of already established solid tumours (Guba *et al.* 2002; Koehl *et al.* 2004; see section 1.1.6).

In epidermis, there are two active isoforms of AKT, AKT1 and AKT2 (Fig. 4.1). AKT1 plays an important regulatory role in terminally differentiating granular layer keratinocytes, whereas AKT2 is present in the less differentiated para-basal keratinocytes (Fig. 4.1; Calautti *et al.* 2005; Thrash *et al.* 2006; O'Shaughnessy *et al.* 2007; O'Shaughnessy *et al.* 2007b). In cSCC, AKT isoform expression and activity has been associated with tumour grade. With cSCC tumour progression, AKT1 expression and activity is reduced whereas AKT2 activity is up-regulated suggesting a tumour-suppressor role for AKT1 and possibly a tumour promoting role for AKT2 (O'Shaughnessy *et al.* 2007b).

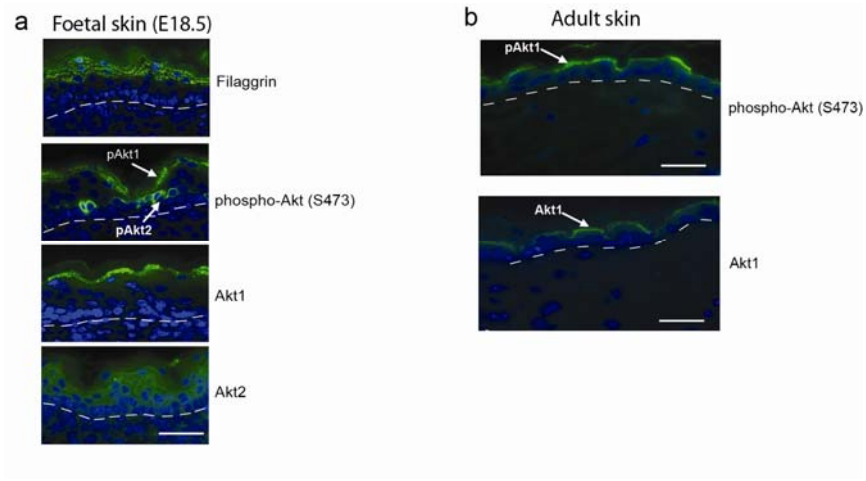

Figure 4.1: Expression pattern of epidermal AKT isoforms

(adapted from Sully *et al.* 2012)

(a) Immunofluorescence analysis of the terminal differentiation marker filaggrin shows that the granular layer is formed in mouse foetal epidermis at E18.5 suggesting epidermal terminal differentiation has been completed. Analysis of foetal mouse epidermis at E18.5 shows that the phospho-AKT (S473) expressing epidermal layers are spatially separated. Phospho-AKT is present in the granular layers which corresponds to the localisation of the AKT1 isoform. AKT2 is expressed in the supra-basal epidermal layers but is only phosphorylated in the para-basal layers.

(b) Immunofluorescence analysis of adult mouse epidermis shows that phospho-AKT mainly present in the granular layer which corresponds to the localisation of AKT1. Therefore, in adult epidermis, the predominant isoform is AKT1.

Bar = 50um. Dotted line = basement membrane

AKT is activated at the plasma membrane by PIP3, which is produced by the class I PI3K, resulting in phosphorylation of AKT at T308 (Fig. 1.4). For complete activation, AKT is phosphorylated at a second site, S473 by mTORC2 (Fig. 1.4). AKT then activates mTORC1 by blocking the inhibitory function of the TSC1-TSC2 complex (Fig. 1.4; section 1.1.7). mTORC1 regulates proliferation, growth, differentiation and also, autophagy.

Rapamycin inhibits mTORC1 activity. However it has been shown in a number of cells that a negative feedback loop exists between mTORC1 and the insulin receptor substrate-1 (IRS-1) resulting in increased phosphorylation of AKT when mTORC1 is inhibited (Fig. 1.4; Section 1.1.7; Harrington *et al.* 2004; Shah *et al.* 2004; Um *et al.* 2004). More recently in my lab, it has been shown that this negative feedback loop is also active in cultured keratinocytes (Sully *et al.* 2012). However there are two AKT isoforms in epidermis with differing roles during tumour progression. Therefore, it is important to find which AKT isoform is activated by rapamycin, with the prediction that rapamycin will exert anti-epidermal tumourigenic affects by selectively activating the pro-differentiation AKT1.

Autophagy is negatively regulated by mTORC1 and rapamycin inhibits mTORC1 activity resulting in reduced growth and increased autophagy. In the previous chapter it is shown that constitutive autophagy is involved in terminal differentiation of granular layer keratinocytes. Autophagy can be induced in all epidermal layers in response to stress and is shown in Chapter 5 (sections 5.2 and 5.3). Therefore, rapamycin may inhibit skin susceptibility to tumourigenesis by increasing one or both types of skin autophagy.

The main hypothesis behind the work presented in this chapter is that rapamycin prevents skin tumourigenesis by either affecting epidermal mTOR regulation of autophagy and/or selectively affecting epidermal AKT isoform activity. The aims of the work in this chapter were to investigate the effects of mTORC1 inhibitors on the

regulation of autophagy and also to determine which AKT isoform responds to rapamycin-mediated inhibition of mTORC1.

Results

4.1 The AKT1 isoform is selectively activated by rapamycin in epidermis

Not only do the AKT isoforms, AKT1 and AKT2 have different roles in epidermis (Fig. 4.1; ; section 1.1.7; Calautti *et al.* 2005; Thrash *et al.* 2006; O'Shaughnessy *et al.* 2007), but they also are important in cSCCs. The immunosuppressant rapamycin, which is also an mTORC1 inhibitor, has anti-tumourigenic properties (Geissler 2008; Wulff *et al.* 2008; McQuillan *et al.* 2009; Salgo *et al.* 2010). Therefore, it would be of great interest to determine the mechanism by which rapamycin reduces cancers in these patients.

In keratinocytes, rapamycin-mediated inhibition of the negative feedback loop between IRS-1 and mTORC1 leads to accumulation of activated and phosphorylated AKT (Sully *et al.* 2012; see section 1.1.7). Therefore, determining which AKT isoform responds to mTORC1 inhibition with increased phosphorylation may further explain rapamycin's anti-tumour properties.

I performed initial experiments in REK monolayer cultures (Baden and Kubilus 1983). One reason for using REKs is their ability to differentiate in organotypic cultures forming a complete barrier with a cornified layer, mimicking late epidermal differentiation (Marjukka Suhonen *et al.* 2003). REKs are also suitable for the establishment of stably transfected cell lines, which will be used to determine which AKT isoform responds to rapamycin treatment.

To determine which AKT isoform responds to rapamycin treatment, I over-expressed AKT1 and AKT2 in REKs and analysed their phosphorylation status after rapamycin treatment. The effect of rapamycin was confirmed by performing a stable knock-down of the endogenous AKT isoforms.

REKs stably transfected with HA-flag-tagged AKT1 (HA-flag-AKT) and HA-tagged AKT2 (HA-AKT) were treated with rapamycin. Western blotting of whole cell lysates (Fig. 4.2a) confirms over-expression of the AKT isoforms. The lower band of the double-bands for AKT1 in the HA-flag-AKT1 transfected cells represents endogenous AKT and the slightly larger band is the over-expressed HA-flag-AKT1. The probe for AKT2 shows increased intensity of AKT2 in HA-tagged AKT2 cells. HA-AKT2 is only a few base pairs larger than endogenous AKT2 therefore, endogenous and over-expressed AKT2 appear as a single band on the SDS gel (Fig. 4.2a).

The anti-HA antibody also confirms expression of these two isoforms. Reduced S6 phosphorylation with rapamycin treatment shows effective mTORC1 inhibition (Fig. 4.2a).

To determine which AKT isoform responds to rapamycin treatment via the negative feedback loop to IRS-1 (Fig. 4.1; see section1.1.7; Sully *et al.* 2012), ~~I immunoprecipitated the HA-tagged AKT isoforms from the cell lysates and analysed their~~ the phosphorylation status of immunoprecipitated HA-tagged AKT1 and AKT2 isoforms was analysed ~~-~~(Fig. 4.2b).

Immunoprecipitation of HA from cell lysates of vehicle-treated and rapamycin-treated transfected REKs shows that rapamycin increases phosphorylation of HA-flag-AKT1 compared to the vehicle-treated HA-flag-AKT1. However, HA-AKT2 phosphorylation levels are unaffected by rapamycin treatment when compared to the vehicle-treated HA-AKT2 (Fig. 4.2b). These results suggest that AKT1 responds to rapamycin-mediated mTORC1 inhibition and rapamycin-induced activation of the negative feedback loop to IRS-1 leading to increased AKT1 phosphorylation.

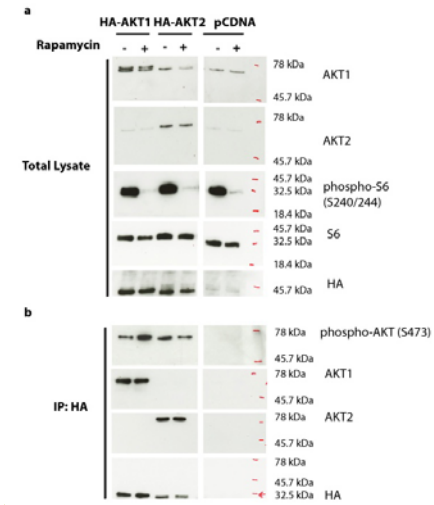

Figure 4.2: Rapamycin-mediated phosphorylation of AKT1 in REKs transfected with HA-flag-AKT1 and HA-AKT2.

(a) Western blotting of whole cell lysates from REKs transfected with HA-flag-AKT1 and HA-AKT2, treated with vehicle or rapamycin. ~~With an antibody specific for the AKT1 isoform,~~ Western blotting shows the presence of an AKT1 doublet in the HA-flag-AKT1 transfected cells representing endogenous AKT1 and the larger HA-flag-AKT1. HA-AKT2 and vector control transfected REKs express endogenous AKT1. ~~The anti-AKT2 antibody shows~~However, ~~increased AKT2 in~~ the HA-AKT2 transfected cells show increased AKT2. This is due to over-expressed HA-AKT2 which overlaps with the endogenous form of AKT2. HA-flag-AKT1 and vector control transduced REKs express lower levels of~~f only~~ endogenous AKT2. Reduced phosphorylation of S6 (S240/244) in the lysates of rapamycin-treated cells confirms effective mTORC1 inhibition. The anti-HA antibody shows expression of both HA-flag-AKT1 and HA-AKT2 in transfected cells whereas, HA is not expressed in ~~s. HA is not expressed in REKs transfected with~~ the vehicle control.

(b) Western blotting of immuno-precipitated HA-AKT isoforms from whole cell lysates of transfected REKs which had been treated with vehicle or rapamycin before harvesting. The anti-HA antibody shows that the IP for HA was successful. The anti-AKT1 and anti-AKT2 antibodies confirm the presence of HA-flag-AKT1 and HA-AKT2 in the immuno-precipitated protein from lysates of HA-flag-AKT1 and HA-AKT2 transfected REKs, respectively. Analysis of AKT phosphorylation levels shows that HA-flag-AKT1 responds to rapamycin-treatment

Formatted: Font: 12 pt

Formatted: Space After: 0 pt, Line spacing: single

with increased AKT phosphorylation (S473), but phosphorylation levels of HA-AKT2 are unaffected by rapamycin treatment.

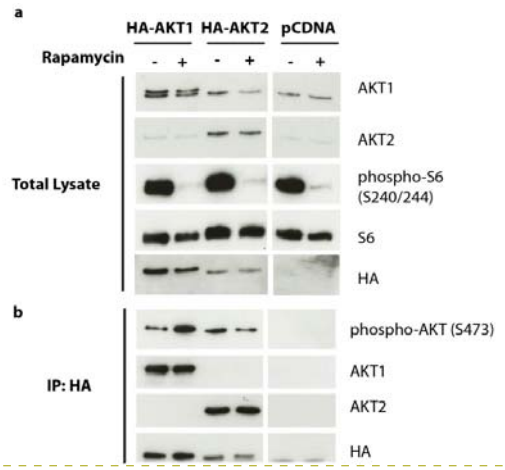

Formatted: Font: 12 pt

~~**Figure 4.2: Rapamycin-mediated phosphorylation of AKT1 in REKs transfected with HA-flag-AKT1 and HA-AKT2.**~~

~~**(a)** Western blotting of whole cell lysates from REKs transfected with HA-flag-AKT1 and HA-AKT2, treated with vehicle or rapamycin. With an antibody specific for the AKT1 isoform, Western blotting shows the presence of an AKT1 doublet in the HA-flag-AKT1 transfected cells representing endogenous AKT1 and the larger HA-flag-AKT1. HA-AKT2 and vector control transfected REKs express endogenous AKT1. The anti-AKT2 antibody shows increased AKT2 in the HA-AKT2 transfected cells. This is due to over-expressed HA-AKT2 which overlaps with the endogenous form of AKT2. HA-flag-AKT1 and vector control transduced REKs express lower levels of only endogenous AKT2. Reduced phosphorylation of S6 (S240/244) in the lysates of rapamycin-treated cells confirms effective mTORC1 inhibition. The anti-HA antibody shows expression of both HA-flag-AKT1 and HA-AKT2 in transfected cells. HA is not expressed in REKs transfected with the vehicle control.~~

~~**(b)** Western blotting of immuno-precipitated HA-AKT isoforms from whole cell lysates of transfected REKs which had been treated with vehicle or rapamycin before harvesting. The anti-HA antibody shows that the IP for HA was successful. The anti-AKT1 and anti-AKT2 antibodies confirm the presence of HA-flag-AKT1 and HA-AKT2 in the immuno-precipitated protein from lysates of HA-flag-AKT1 and HA-AKT2 transfected REKs, respectively. Analysis of AKT phosphorylation levels shows that HA-flag-AKT1 responds to rapamycin treatment~~

~~with increased AKT phosphorylation (S473), but phosphorylation levels of HA-AKT2 are unaffected by rapamycin treatment.~~

With these experiments, I show that in keratinocytes, over-expressed AKT1 responds to rapamycin-mediated mTORC1 inhibition and rapamycin-induced activation of the negative feedback loop to IRS-1. Over-expressed AKT2 is not affected by rapamycin treatment.

Next, I wanted to verify these findings by checking the effects of rapamycin on endogenous AKT phosphorylation levels. To do this, I performed a stable knockdown of endogenous AKT1 in REKs and determined whether rapamycin would have an effect on AKT2 phosphorylation levels.

REKs stably expressing two different shAKT1 (A1 and A3 shRNA) or scrambled shRNA were treated with rapamycin. Cell lysates were then harvested for Western blot analysis. Lysates from cells with scrambled shRNA show rapamycin induced AKT phosphorylation, whereas AKT phosphorylation is absent in lysates from rapamycin-treated REKs with either of the shAKT1 constructs (Fig. 4.3a). Although only a partial knockdown of endogenous AKT1 (~50%) was achieved (Fig. 4.3b), this shows that only endogenous AKT1 responds to rapamycin-induced phosphorylation in keratinocytes.

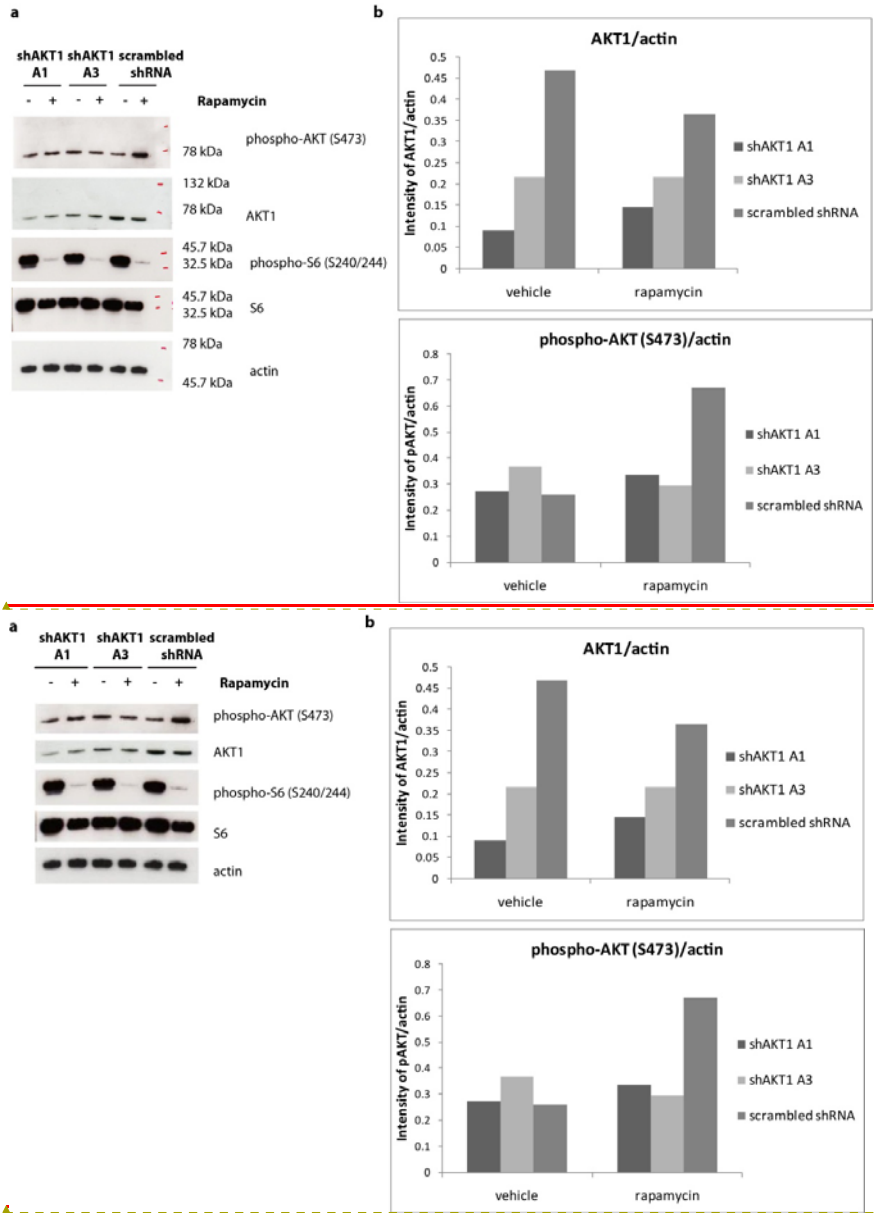

Figure 4.3: Rapamycin-induced phosphorylation of endogenous AKT1 in REKs.

(a) Western blotting of whole cells lysates from REKs with a stable knockdown of AKT1 treated with vehicle or rapamycin. A stable knockdown of AKT1 in REKs using two different

Formatted: Font: 12 pt, Bold

Formatted: Font: 12 pt, Bold

shRNA sequences shows reduced expression of AKT1 compared to cells with scrambled shRNA. Rapamycin treatment has no effect on AKT phosphorylation (S473) in cells with reduced AKT1 levels (shAKT1 cells). However, cells expressing the scrambled shRNA show increased phosphorylation of AKT (S473) confirming that AKT1 is the isoform which responds to mTORC1 inhibition with increased phosphorylation. The levels of phospho-S6 (S240/244) are strongly reduced in rapamycin-treated REKs confirming effective mTOR inhibition.

(b) Quantification of AKT1 levels normalised to actin (AKT1/actin) and phospho-AKT (S473) normalised to actin -(phospho-AKT/actin). AKT1/actin ratios show strong reduction of AKT1 levels in shAKT1-transfected REKs compared to cells transfected with scrambled shRNA. Quantification of phospho-AKT (S473) levels (phospho-AKT/actin) shows that only REKs transfected with scrambled shRNA respond to rapamycin treatment with increased phospho-AKT (S473). Rapamycin has no effects on phospho-AKT levels in REKs transfected with shAKT1 constructs.

Transfected REKs treated with 10nM rapamycin or vehicle for 2h before harvesting.

From these data, I show that only AKT1, and not AKT2, responds to rapamycin treatment which induces an increase in AKT1 phosphorylation levels in monolayer keratinocytes.

These findings have been confirmed in our lab by using immunohistochemistry using phospho-specific antibodies in foetal skin explant cultures (Sully *et al.* 2012). In epidermis AKT1 and AKT2 are expressed in different layers (Fig. 4.1) allowing direct observation of changes to these two isoforms. Rapamycin increases phospho-AKT1 levels dose-dependently in the granular layer, whereas para-basal phospho-AKT2 is unaffected (Sully *et al.* 2012).

I conclude that rapamycin inhibits mTORC1, and the mTORC1-dependent negative feedback loop leading to increased phospho-AKT1 in epidermal keratinocytes. AKT1, the isoform associated with granular layer keratinocytes, is the isoform which is sensitive to rapamycin-mediated mTORC1 inhibition. This suggests that rapamycin may exert its anti-tumourigenic effects on the epidermis by increasing AKT1

phosphorylation which is associated with more differentiated granular layer keratinocytes.

4.2 The effect of rapamycin on autophagy in keratinocyte cultures

Autophagy is downstream of the AKT/mTORC1 pathway. Rapamycin, an mTORC1 inhibitor, is routinely used to induce autophagy *in vitro*. Rapamycin is also an immuno-suppressant used in the clinic where it has reduced the amount of cSCCs rapamycin-treated transplant recipients develop. Therefore, I hypothesize that apart from its effect on angiogenesis and proliferation (Geissler 2008), rapamycin may reduce SCCs in patients by up-regulating autophagy in epidermis.

To investigate the role of rapamycin on autophagy in epidermis, I performed initial experiments in REK monolayer cultures (Baden et al, 1983) and then verified my findings in primary human keratinocyte monolayer cultures. Primary monolayer keratinocytes permit analysis of differentiated and undifferentiated cell populations which may more closely reflect the situation in patient skin.

4.2.1 The effect of rapamycin on autophagy in REK monolayer cultures

Initial experiments performed on the rat keratinocyte cell line, REKs, shows that REKs have very low levels of basal autophagy and rapamycin treatment may induce only a slight increase in autophagy levels (Appendix 12 and 13).

To determine whether the autophagic pathway is completed in REKs under normal culture conditions and also with rapamycin treatment, autophagy is inhibited with chloroquine (Fig. 4.4; Appendix 13). If the pathway is completed under normal culture conditions, chloroquine treatment would lead to accumulation of LC3II and LC3 positive autophagic vesicles. However, if the pathway is normally not completed, chloroquine would not affect LC3 levels.

Chloroquine ~~increases~~ reduces the acidity of autophagic and lysosomal vesicles which prevents function of lysosomal proteases thereby, inhibiting autophagic

degradation. Since chloroquine is a cheaper alternative to BafA1, another routinely used lysosomotropic agent, it was used for initial experiments in REKs before verification in primary keratinocytes. However, chloroquine has also been suggested to affect DNA synthesis and DNA repair (Solomon and Lee 2009) leading to other effects on cellular processes. Therefore, chloroquine was only used in initial experiments in keratinocytes.

Untreated, vehicle-treated and rapamycin-treated REKs were cultured with and without chloroquine to measure the turn-over of LC3I to LC3II. With chloroquine treatment (Fig. 4.4b), untreated cells show increased LC3II levels compared to the cells cultured without chloroquine (Fig. 4.4a). This shows that blocking the autophagy process with chloroquine leads to accumulation of autophagic vesicles and suggests that, in REKs under normal culture conditions, without chloroquine, the autophagic process is completed with degradation of autophagic vesicles.

Rapamycin treatment alone (Fig. 4.4a) leads to a low increase in LC3II levels compared to vehicle-treated cells (Fig. 4.4a). With chloroquine, the rapamycin-mediated increase in LC3II is much stronger (Fig. 4.4b). These results lead to two conclusions: First, in the untreated as well as in the rapamycin-treated REKs, the autophagy process is completed since blocking autophagy with chloroquine results in accumulation of LC3II. Second, rapamycin increases autophagy levels in REKs. In chloroquine-treated REKs (Fig. 4.4b), rapamycin increases LC3II levels compared to vehicle-treated REKs (Fig. 4.4b).

Formatted: Font: 12 pt

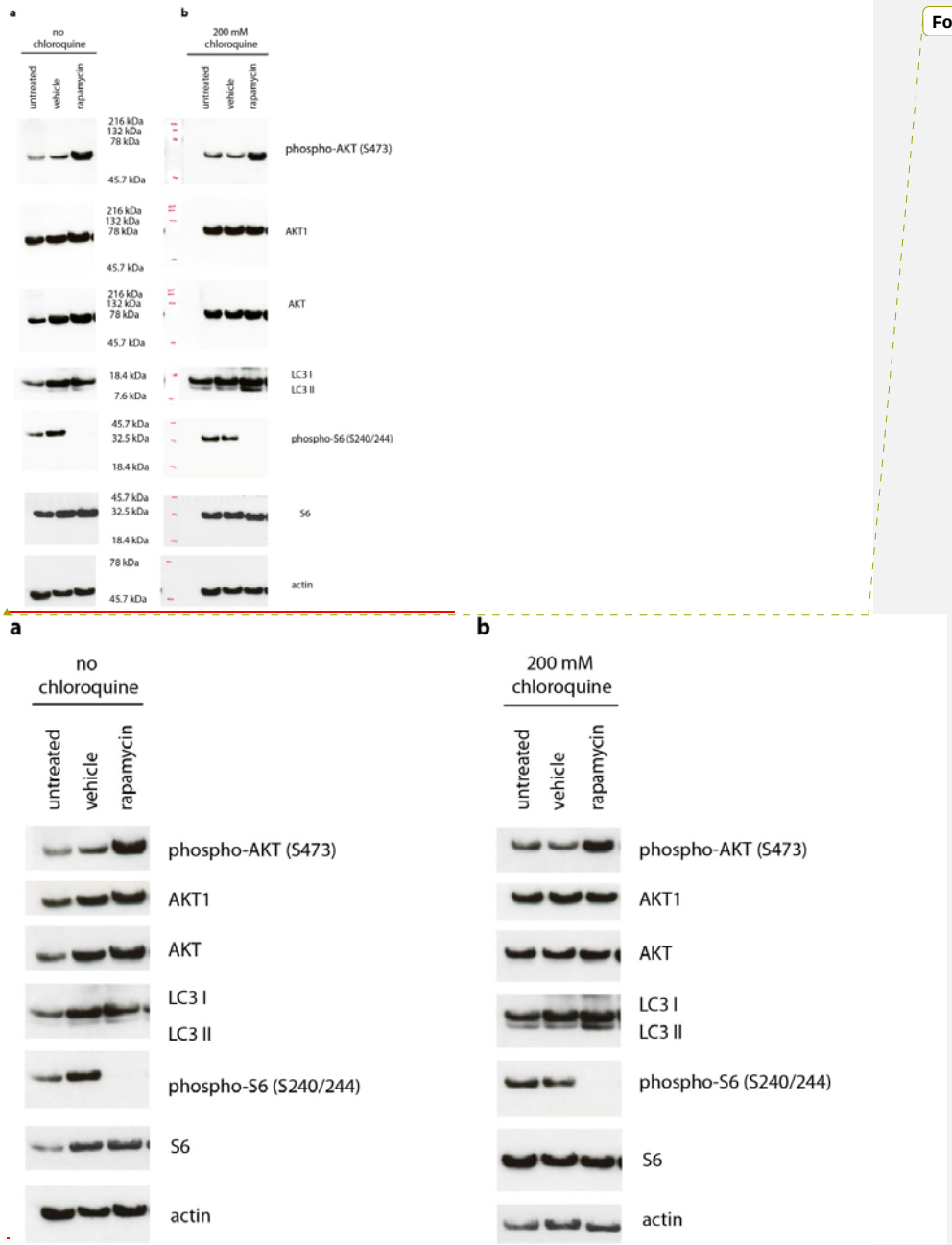

Figure 4.4: Analysis of autophagic flux in rapamycin-treated REKs with and without chloroquine.

REKs were treated with vehicle or rapamycin without chloroquine **(a)** or with chloroquine **(b)** before harvesting. Chloroquine is a drug which prevents degradation of autolysosomes leading to accumulation of autophagic vesicles and allowing measurement of autophagic flux.

With and without chloroquine **(a** and **b)**, rapamycin down-regulates S6 phosphorylation and also increases AKT phosphorylation confirming effective rapamycin-mediated mTORC1 inhibition. Compared to the cells without chloroquine **(a)**, the chloroquine- treated cells **(b)** show accumulation of LC3II in the untreated, vehicle-treated and rapamycin-treated cells. This is due to inhibition of the autophagy pathway at the last stage before degradation of autophagic vesicles. Blocking the autophagy pathway with chloroquine treatment **(b)**, shows that rapamycin increases the levels of LC3II when compared to chloroquine-treated vehicle and untreated cells.

REKs treated with 10nM rapamycin or vehicle for 4h before harvesting; 200 uM chloroquine added 2h before harvesting.

These results from Western blot analysis, as well as immunofluorescence staining for LC3 (Appendix 13 and 14) show that blocking autophagy in REKs with chloroquine leads to accumulation of LC3 positive vesicles. Therefore, under normal culture conditions, the autophagy process is completed in REKs. Rapamycin treatment not only increases turn-over of LC3I to LC3II increasing autophagic flux (Fig. 4.4), but also increases the amount of autophagic vesicles in REKs (Appendix 13). This suggests that keratinocytes are sensitive to rapamycin-induced autophagy.

As the next step, I wanted to verify these observations in primary human keratinocytes. One of the limitations of using REKs is that most commercially available antibodies against autophagy markers only recognise human proteins. Also, REKs are an immortalised cell line, so they may differ from primary keratinocytes, which are more relevant for the overall aim of my work to determine the role of autophagy in epidermis.

Appendix 14 shows results from experiments with primary keratinocyte cultures treated with rapamycin in the presence and absence of chloroquine. However,

chloroquine increases LC3I levels, suggesting it may have other effects other than increasing the lysosomal pH and preventing degradation of autophagic vesicles. Therefore, the effects of chloroquine alone mask any effect rapamycin may have on LC3II levels.

4.2.2 The effect of rapamycin on autophagy in primary keratinocyte monolayer cultures

The drug, Bafilomycin A1 (BafA1) selectively blocks the degradation of autophagic vesicles by preventing fusion of lysosomes with autophagosomes, and also inhibits the function of lysosomal enzymes (Bowman *et al.* 1988; Klionsky *et al.* 2008; Klionsky *et al.* 2012). Therefore, BafA1 is routinely used as an autophagy inhibitor for short-term *in vitro* experiments (Klionsky *et al.* 2008). Therefore, undifferentiated and differentiated primary monolayer keratinocyte cultures were treated with rapamycin and vehicle in the presence and absence of BafA1.

Western blot analysis of protein lysates shows that rapamycin treatment prevents phosphorylation of S6 indicating effective inhibition of mTORC1 activity (Fig. 4.5a). BafA1 treatment leads to accumulation of LC3II in both vehicle-treated and rapamycin-treated cells (Fig. 4.5a; Fig. 4.5b), suggesting inhibition of autophagic vesicle degradation.

Rapamycin does not affect total LC3II levels which are quantified as LC3II/actin ratios (Fig. 4.5b). In the presence of BafA1, rapamycin significantly increases the turn-over of LC3I to LC3II (LC3II/LC3I ratios) in the differentiated keratinocytes compared to the vehicle-treated differentiated cells (Fig. 4.5c). Therefore, rapamycin induces a higher rate of conversion of LC3I to LC3II, strongly suggesting rapamycin increases autophagic flux.

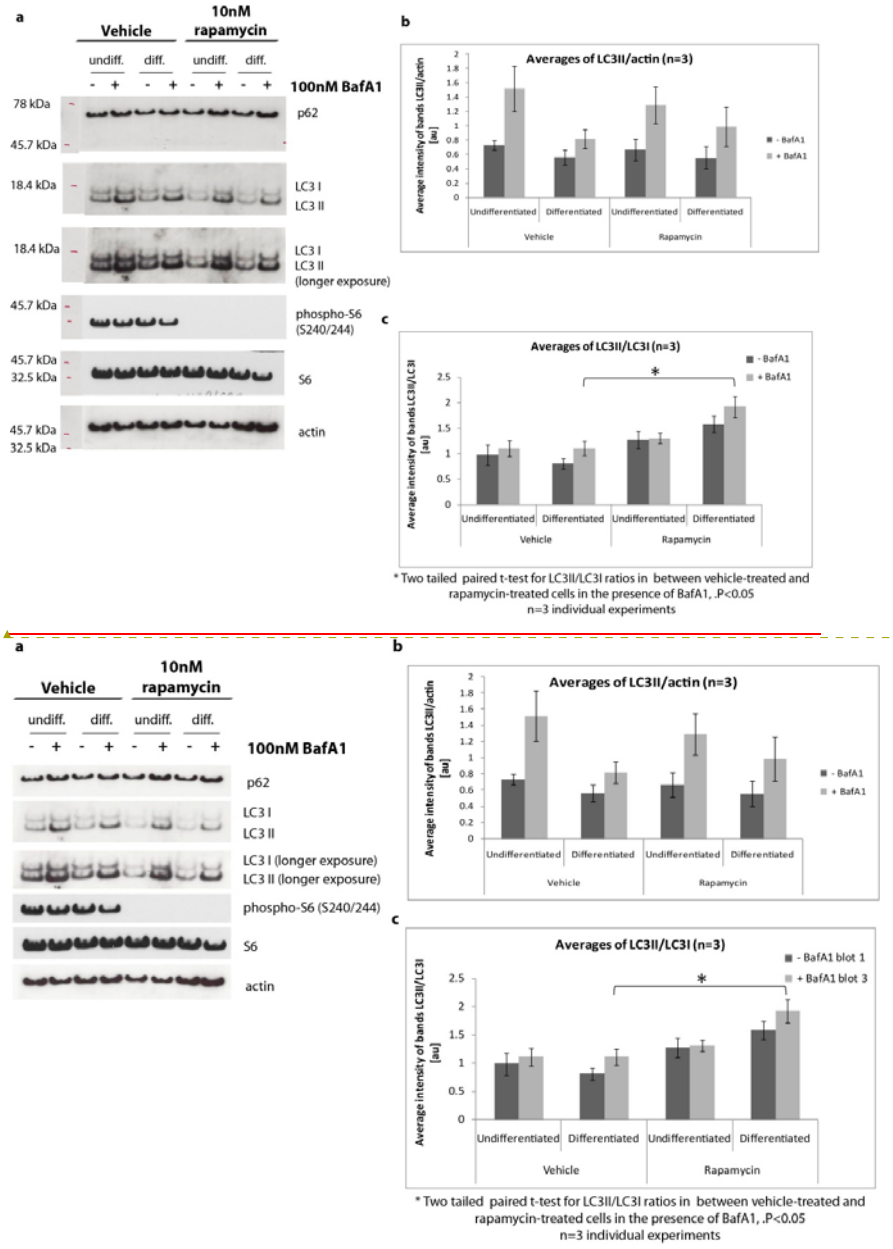

Figure 4.5: Analysis of autophagic flux in rapamycin-treated primary keratinocyte cultures with and without BafA1.

Formatted: Font: 12 pt

Formatted: Space After: 0 pt, Line spacing: single

(a) Monolayer keratinocyte cultures were treated with vehicle and with rapamycin in the presence and absence of BafA1. BafA1 is an autophagy specific inhibitor which prevents the fusion of lysosomes with autophagosomes and also inhibits the function of lysosomal proteases. Western blotting of protein lysates shows rapamycin-induced inhibition of S6 phosphorylation indicating effective mTORC1 inhibition. **(b)** In both undifferentiated and differentiated keratinocytes, BafA1 treatment leads to accumulation of LC3II. Quantification of total LC3II levels (LC3II/actin ratios) shows accumulation of LC3II with BafA1, however, rapamycin has no significant effects on LC3II/actin levels in the presence and absence of BafA1 when compared to vehicle-treated keratinocytes. **(c)** Quantification of LC3II/LC3I is a measure of the turn-over of LC3 in the cells. In the presence of BafA1, rapamycin induces a significant increase in LC3II/LC3I compared to vehicle-treated cells in the differentiated keratinocyte populations.

** Two-tailed t-test for means of LC3II/LC3I ratios in vehicle-treated and rapamycin-treated differentiated keratinocytes, P<0.05; n=3 experiments. Primary keratinocyte monolayers treated with 10nM rapamycin or vehicle for 4h before harvesting; 100nM BafA1 added 2h before harvesting. See appendix 17 for quantifications.*

With Western blot analysis, I show that blocking autophagy with BafA1 treatment allows detection of a rapamycin-induced increase in LC3 turn-over in both undifferentiated and differentiated keratinocytes (LC3II/LC3I ratios; Fig. 4.5c). However, total LC3II levels (LC3II/actin ratios; Fig. 4.5b) are unaffected by rapamycin treatment. This may be due to an incomplete block in autophagy with BafA1. As there is no way to measure the extent of autophagy inhibition, it is possible that BafA1 only partially inhibits the autophagy pathway and degradation of autophagic vesicles still occurs at a reduced rate. The concentration and duration of BafA1 treatment I used was the highest possible concentration to avoid toxicity to the cells and this is also within the range of specifications in the literature (Rubinsztein *et al.* 2009; Wang and Levine 2011).

These results suggest that rapamycin induces a ~~low but~~statistically significant increase in autophagic flux or LC3 turn-over in both undifferentiated and differentiated keratinocytes. Therefore, I verified these results with

immunofluorescence analysis of LC3 expression levels in rapamycin-treated monolayer keratinocyte cultures.

Immunofluorescence analysis confirms these observations by showing that BafA1 treatment of both undifferentiated and differentiated keratinocytes leads to increased LC3 levels (Fig. 4.6a, Fig. 4.6b). Rapamycin treatment combined with BafA1 induces a very strong increase in LC3 intensities/cell in both undifferentiated and differentiated keratinocytes compared to the vehicle-treated cells (Fig. 4.6a, Fig.4.6b). However, rapamycin with BafA1 has no effects on the number of LC3 aggregates/cell in the keratinocyte monolayer cultures (Fig. 4.6c). These results suggest that rapamycin strongly increases LC3 levels, but rapamycin does not affect the number of autophagic vesicles in keratinocytes.

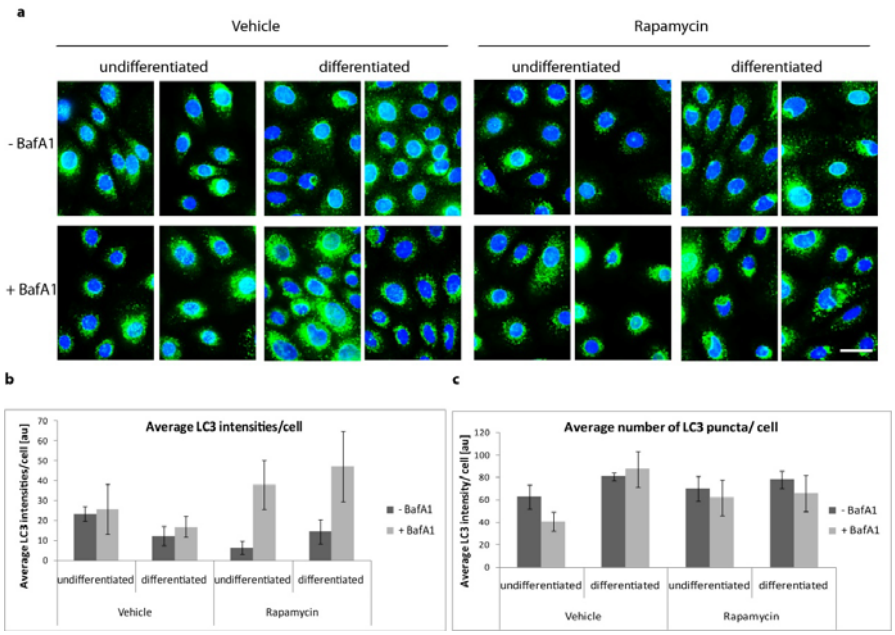

Figure 4.6: Analysis of the autophagosome marker, LC3 in rapamycin-treated primary keratinocyte cultures with and without BafA1 treatment.

(a) Monolayer primary keratinocyte cultures were treated with vehicle and rapamycin with and without BafA1. Immunofluorescence analysis of LC3 shows increased LC3 intensities in

BafA1 treated cells (also see quantification of LC3 intensities/cell). **(b)** BafA1 treatment increases the LC3 intensities/cell under all culture conditions. In both undifferentiated and differentiated keratinocytes, rapamycin treatment with BafA1 increases LC3 intensities/cell compared to vehicle-treated cells with BafA1. **(c)** However BafA1 has no effect on the number of LC3 puncta per cell.

Primary keratinocyte monolayers treated with 10nM rapamycin or vehicle for 4h before harvesting with or without 100 nm BafA1. See Appendix 16 for quantifications.

Bar = 20um.

For quantification, the total number of cells, the LC3 intensity values as well as the number of LC3 puncta were determined with ImageJ.

In this section I show that monolayer primary keratinocytes respond to rapamycin-induced autophagy. This effect of rapamycin becomes apparent when the autophagy process is blocked with BafA1. In both undifferentiated and differentiated keratinocytes, Western blot analysis shows increased rapamycin-induced turn-over of LC3 (LC3II/LC3I ratios; Fig. 4.5), suggesting the formation of more membrane-bound LC3. Immunofluorescence analysis of LC3 confirms that rapamycin induces an increase in LC3 levels (Fig. 4.6), but rapamycin does not affect the number of LC3 positive autophagic vesicles (Fig. 4.6). Therefore, these results suggest that in cultured keratinocytes, rapamycin increases LC3 turn-over and the rate of the autophagy process but, it does not affect the number of autophagosomes formed.

4.3 The effect of rapamycin on autophagy in 3D keratinocyte cultures

In the previous section, I show that monolayer primary keratinocyte cultures respond to rapamycin-induced autophagy with a significant increase in LC3 turn-over. Although, this effect of rapamycin is observed in both undifferentiated and differentiated keratinocyte cultures, these monolayer cultures may not give a true picture of what occurs in the epidermis. Therefore, I verified my observations from primary monolayer keratinocytes by using REK 3D-cultures.

REKs are suitable for organotypic cultures because they stratify and form all layers of the epidermis including the cornified layer which is difficult to obtain with 3D cultures of primary human keratinocytes. Organotypic cultures would also show the effects of rapamycin on autophagy in the different epidermal layers. In section 4.2, I also show that monolayer REK cultures respond to rapamycin-induced autophagy. Therefore, I treated REK organotypics with rapamycin and determined its effects on autophagy.

First, I characterised the REK organotypics by analysing the expression of epidermal differentiation markers. H&E staining of REK organotypics shows that the REK 3D cultures have stratified and formed a cornified layer (Fig. 4.7a). However, rapamycin-treated 3D cultures have a thinner cornified layer compared to vehicle-treated cultures (Fig. 4.7a). The cornified layer may have been lost during processing of the samples. Rapamycin may also affect cornification and lead to formation of a looser cornified layer which is then more easily lost during sample processing. But these possibilities have not yet been verified.

To determine whether differentiation and stratification has occurred in a manner similar to healthy adult epidermis, I performed immunofluorescence analysis for the expression of epidermal differentiation markers. The terminal differentiation marker filaggrin is expressed in the granular layers of the vehicle-treated REK 3D

cultures (Fig. 4.7b). The rapamycin-treated organotypics also show granular layer expression of filaggrin however, filaggrin appears to be confined to fewer upper epidermal layers than in the vehicle-treated cultures (Fig. 4.7b). This unexpected finding indicates that rapamycin affects granular layer keratinocytes. Loricrin, which is also a marker of the granular layer, is also present in the upper layers of REK organotypics (Fig. 4.7b). These results suggest that in both vehicle- and rapamycin-treated organotypics, the terminal differentiation pathway has been activated and the granular layers are present in the upper layers of the 3D cultures, similar to adult epidermis. However, filaggrin expression is slightly altered in rapamycin-treated organotypics.

A marker of early differentiation, K1, is expressed in the supra-basal layers of both vehicle- and rapamycin-treated REK organotypics (Fig. 4.7b). This expression pattern is very similar to healthy adult epidermis (Fig. 3.1) and shows the early differentiated supra-basal keratinocytes which are below the loricrin and filaggrin positive granular layers.

K14, a marker of proliferating keratinocytes of the basal layers in adult epidermis (Fig. 3.1), is strongly expressed in the basal and the supra-basal layers of the vehicle-treated REK organotypics (Fig. 4.7b). Rapamycin-treated organotypics show a similar K14 expression pattern to the vehicle-treated cultures. This unusual expression pattern of K14 shows that although the REK organotypics stratify and form all layers of epidermis, they do not mimic the epidermis completely.

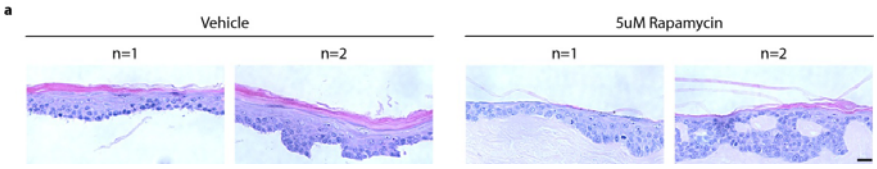

Figure 4.7: Expression pattern of epidermal differentiation markers in REK organotypics.

(a) H&E staining of REK organotypics showing epidermal stratification. Vehicle-treated organotypics have a thick cornified layer, whereas rapamycin-treated 3D-cultures have a much thinner one. It is not clear whether this thinner cornified layer is due to effects of rapamycin or if it was lost during processing of the sample.

Figure 4.7 continued on the next page.

REK organotypics treated with 5uM rapamycin or vehicle for 4 days before harvesting; Bar = 20um.

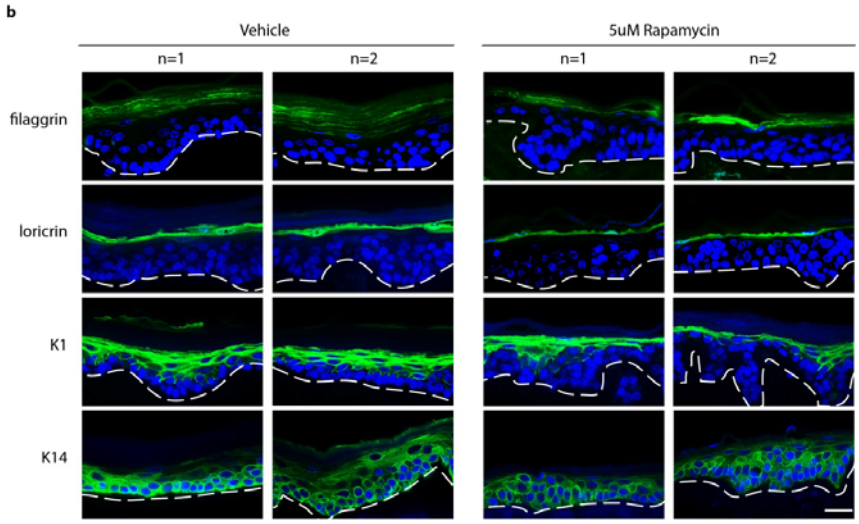

Figure 4.7: Expression pattern of epidermal differentiation markers in REK organotypics.

Figure 4.7 continued on the next page.

(b) Expression of epidermal differentiation markers in REK organotypics shows that the terminal differentiation marker filaggrin is expressed in the granular layers of both vehicle and rapamycin-treated 3D-cultures. Another terminal differentiation marker loricrin is also expressed in the granular layers of both vehicle and rapamycin-treated organotypics. The expression patterns of filaggrin and loricrin suggest activation of terminal differentiation and formation of the granular layers. K1, a marker of early differentiation is present in the supra-basal layers of both vehicle and rapamycin-treated organotypics. A marker of proliferating basal layer keratinocytes, K14 is expressed in the basal and supra-basal layers of the REK 3D-cultures. This expression pattern of K14 is rather unusual. In epidermis, K14 is present in the basal and para-basal layers.

REK organotypics treated with 5uM rapamycin or vehicle for 4 days before harvesting;
Bar = 20um. Dotted line = basement membrane.

I have shown that REK 3D cultures stratify and form all layers of the epidermis. However, rapamycin treatment alters the expression pattern of filaggrin, confining its expression to fewer upper layers compared to vehicle-treated organotypics. Next, I wanted to determine whether rapamycin has an effect on autophagy in 3D cultures.

First, I checked S6 phosphorylation which occurs down-stream of active mTORC1. Immunofluorescence analysis of phospho-S6 shows that vehicle-treated REK organotypics have strong S6 phosphorylation in the upper layers of the 3D cultures (Fig. 4.8a). With rapamycin, S6 phosphorylation is reduced and its expression is also confined to fewer layers (Fig. 4.8a).These results confirm that rapamycin strongly reduces mTORC1 activity in these 3D cultures.

Immunofluorescence analysis of the autophagosome marker, LC3, in vehicle-treated REK organotypics shows low levels of LC3 expression in all layers of the cultures but stronger LC3 intensities in the upper layers (Fig. 4.8b). With rapamycin-treatment, LC3 is still present at low levels in all the layers of the organotypics, but in the upper layers there is a very strong induction of LC3 in the granular layer (Fig. 4.8b). Also, granular layer LC3 is confined to fewer layers compared to upper layer LC3 in the vehicle-treated cultures (Fig. 4.8b).

WIPI1, with participates in the initial steps of autophagy, is expressed as puncta in the upper layers of the vehicle-treated REK organotypics (Fig. 4.8b). Rapamycin-treated REK 3D cultures show a similar expression pattern of WIPI1 (Fig. 4.8b). However, WIPI1 is also expressed in fewer layers in the rapamycin-treated organotypics compared to the vehicle-treated cultures (Fig. 4.8b). This rapamycin-induced change in WIPI1 expression pattern is similar to the effect of rapamycin on LC3 in REK organotypics.

The ATG5-ATG12 complex required for elongation of the double-membrane is expressed in all layers of the vehicle-treated REK 3D cultures (Fig. 4.8b). The expression of ATG5-ATG12 in the rapamycin-treated REK organotypics is very similar

to vehicle-treated cultures (Fig. 4.8b). Therefore, rapamycin has no effect on the expression pattern of ATG5-ATG12.

BECN1, which is important for the initiation of double-membrane formation, has a patchy expression pattern in all layers of vehicle-treated REK organotypics (Fig. 4.8b). Rapamycin has no effect on this patchy expression pattern of BECN1 in the REK 3D cultures (Fig. 4.8b).

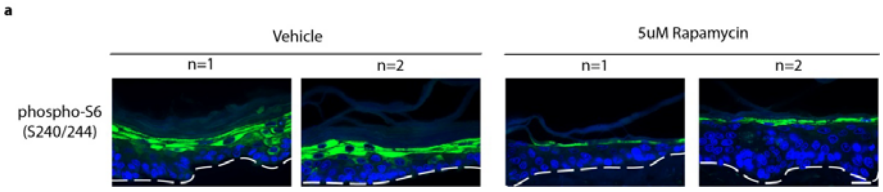

Figure 4.8: Expression pattern of autophagy markers in rapamycin-treated REK organotypics.

(a) Immunofluorescence analysis of S6 phosphorylation (S240/244) in REK organotypics shows phospho-S6 expression in the upper layers of vehicle-treated cultures. In the rapamycin-treated organotypics, phospho-S6 expression is restricted to less layers and the intensity of phospho-S6 is also reduced strongly.

Figure 4.8 continued on the next page.

REK organotypics treated with 5uM rapamycin or vehicle for 4 days before harvesting; Bar = 20um. Dotted line = basement membrane.

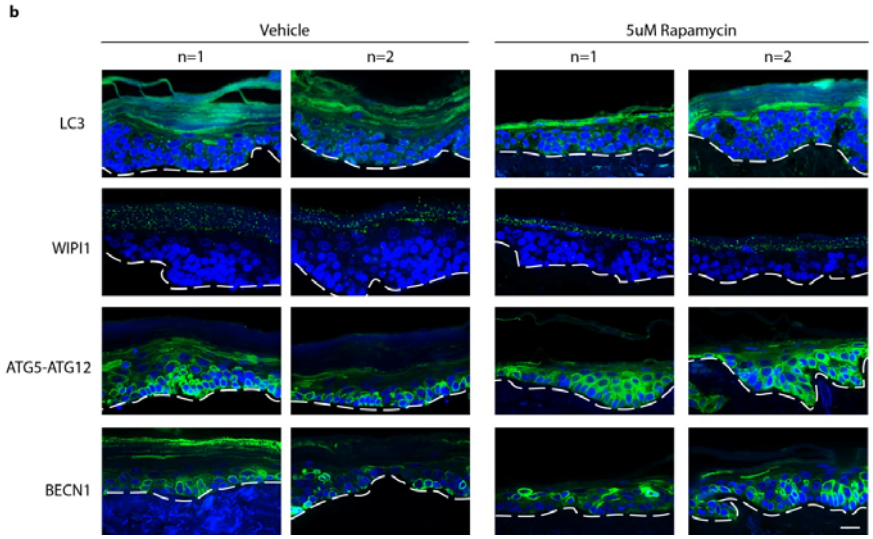

Figure 4.8: Expression pattern of autophagy markers in rapamycin-treated REK organotypics.

Figure 4.8 continued.

(b) In vehicle-treated 3D-cultures**,** the autophagosome marker LC3 is expressed at low levels in all layers of the organotypics. In the upper layers, LC3 expression is much stronger. In the rapamycin-treated organotypics, LC3 is present in all layers but its expression is strongly up-regulated in the granular layers, suggesting rapamycin-induced granular layer autophagy. With rapamycin, granular layer LC3 is expressed in fewer layers than in the vehicle-treated organotypics. WIPI1, which participates in double-membrane formation, is expressed as puncta in the upper layers of vehicle-treated REK organotypics. Rapamycin treatment restricts WIPI1 to fewer upper layers of the REK 3D-cultures. The ATG5-ATG12 complex, which is important for the elongation of the double-membrane, is strongly expressed in all layers of both vehicle-treated and rapamycin-treated REK 3D-cultures. So, rapamycin has no effect on ATG5-ATG12. BECN1, another complex required for the initiation stage of autophagy, has a patchy expression in all layers of the REK 3D-cultures. Rapamycin has no effect on the patchy expression pattern of BECN1. So, rapamycin-treatment has no strong effect on BECN1 expression in REK organotypics.

REK organotypics treated with 5uM rapamycin or vehicle for 4 days before harvesting;

Bar = 20um. Dotted line = basement membrane.

With these experiments I show that REK 3D-cultures are capable of rapamycin-induced autophagy. This confirms observations made with monolayer REK cultures and also monolayer primary keratinocyte cultures. Therefore, I conclude that monolayer keratinocytes respond to rapamycin-induced autophagy. However, ~~with~~ in the REK-3D cultures, ~~I show that it is~~only the granular layer keratinocytes ~~which up-regulate their LC3 levels suggesting an increase in autophagy in response~~ respond to rapamycin treatment and they do so by a marginal increase in LC3 levels. Therefore, I wanted to verify these results in epidermis.

4.4 The effect of mTORC1 inhibition on autophagy in mouse foetal skin explants

I observe that monolayer keratinocytes respond to rapamycin-induced autophagy (section 4.2) and in REK organotypics (section 4.3), rapamycin increases granular layer autophagy. Therefore, I wanted to determine whether epidermal granular layer autophagy also responds to rapamycin treatment in skin. For this, I cultured mouse foetal skin explants *in vitro* and treated them with rapamycin over the period of barrier acquisition. I used mouse foetal explants for these experiments because it was difficult to obtain a significant number of healthy human skin samples as well as to optimise their culture conditions. Instead of adult mouse epidermis, I used foetal mouse skin because this eliminates any complications due to hair or the many hair follicles in adult mouse skin. Also, foetal mouse epidermis is similar to adult human skin with regards to the number of epidermal layers which make it easier to observe any changes occurring in a specific epidermal layer. These mouse foetal explant cultures are a well established culture system for studying authentic skin differentiation (O'Shaughnessy *et al.* 2009; Byrne *et al.* 2010; Sully *et al.* 2012) without inducing a stress response (K. Sully unpublished results).

Mouse explants were harvested from E15.5 foetuses. At this time-point, mouse embryos do not have a granular layer or a *Stratum corneum* (see section 3.2). The explants are cultured for 72h at the air-liquid interface of media with vehicle or with two different rapamycin concentrations. The time-point of harvest corresponds to E18.5, which is just before birth and the granular layer and cornified layer are already formed (see section 3.2). The rapamycin concentration used was established to be the minimum dose required to effectively inhibit mTORC1 activity which is determined by analysis of S6 phosphorylation, a down-stream target of mTORC1. With this experiment using foetal explant epidermis, I wanted to determine whether healthy epidermis responds to rapamycin-induced autophagy and also, if rapamycin-induced autophagy has any effects on granular layer formation.

First I performed immunofluorescence analysis of epidermal differentiation markers to find out if epidermal terminal differentiation and granular layer formation has occurred in the explant cultures. The terminal differentiation marker filaggrin is expressed in the granular layer of vehicle-treated explants (Fig. 4.9). However, with rapamycin treatment, filaggrin expression is reduced and is present in fewer granular layers compared to vehicle-treated explants (Fig. 4.9). This confirms previous observations made with REK 3D-cultures but the effect of rapamycin on filaggrin in the epidermal explant cultures is much stonger than in the REK organotypics (Fig. 4.7b). However, rapamycin-treated explants still express filaggrin, only at lower levels, indicating that the granular layer is present. These results support observations made previously in my lab suggesting that rapamycin alters epidermal barrier properties due to mTORC1 modulation and increases in epidermal lipids (K. Sully, unpublished data). Therefore, the changes in the filaggrin expression pattern may be due to the rapamycin-mediated changes in the epidermal barrier.

Another epidermal terminal differentiation marker, Loricrin, is expressed in the granular layer of vehicle-treated explants (Fig. 4.9). Loricrin is also expressed in the granular layer of rapamycin-treated explants, and this expression pattern is very similar to the vehicle-treated cultures (Fig. 4.9). Therefore, in the foetal explant cultures, vehicle-treated as well as rapamycin-treated explants have undergone terminal differentiation and formation of the granular layer.

The early keratinocyte differentiation marker, K1, is expressed in the supra-basal layers of vehicle-treated and rapamycin-treated explants, indicating the presence of the spinous layer in the explants cultures (Fig. 4.9). The K1 expression pattern in rapamycin-treated explants is very similar to vehicle-treated cultures (Fig. 4.9).

K14, which is expressed by proliferating basal layer keratinocytes, is expressed strongly in the basal and para-basal layer of vehicle-treated and rapamycin-treated explants (Fig. 4.8). K14 is still present at lower levels in the other supra-basal layers of all explants cultures (Fig. 4.9).

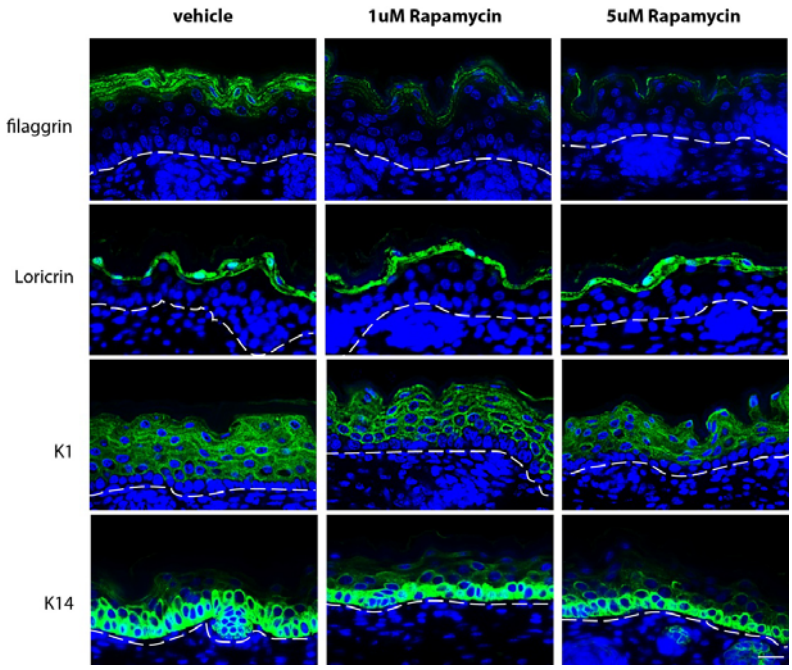

Figure 4.9: Expression pattern of epidermal differentiation markers in rapamycin-treated mouse foetal skin explants.

Immunofluorescence analysis of epidermal differentiation markers performed on mouse foetal skin explants treated with different concentrations of rapamycin shows that the terminal differentiation marker filaggrin is expressed in the granular layer of vehicle-treated explants. With rapamycin, filaggrin expression is reduced and its expression is confined to fewer granular layers. However, no dose-dependent effect of rapamycin is observed on filaggrin expression. Another terminal differentiation marker, Loricrin, is expressed in the granular layer of vehicle-treated and rapamycin-treated explants. K1, a marker of early differentiation is present in the supra-basal layers of both vehicle-treated and rapamycin-treated explants. A marker for the proliferating basal keratinocytes, K14, is expressed strongly in the basal and para-basal layers of both vehicle-treated and rapamycin-treated explants. K14 is also expressed at low levels in the spinous layer of vehicle-treated and rapamycin-treated explants. *Mouse skin explants from E15.5 foetuses were cultured in vitro for 72h at the air-liquid interface of media with vehicle or rapamycin.*

Bar = 20um. Dotted line = basement membrane.

These results confirm that epidermal differentiation has occurred in the vehicle-treated and the rapamycin-treated explants. Also, the different epidermal compartments express proteins which are characteristic for these layers. I conclude that the epidermal differentiation marker profile of foetal embryo explants cultures is similar to their expression patterns in healthy adult epidermis (see Fig. 3.1). However, rapamycin reduces filaggrin expression levels and changes its localisation to fewer granular layers. This suggests that rapamycin affects the granular layer and may also induce reorganisation of the epidermal granular layers. Loricrin, another protein expressed by terminally differentiating keratinocytes, is unaffected by rapamycin treatment. This shows that rapamycin-treated explants have a granular layer, but filaggrin expression is altered which may be due to other effects of rapamycin on the epidermal barrier.

Therefore, the next step was to analyse the expression profile of autophagy markers in these foetal explant cultures. I performed immunofluorescence analysis of S6 phosphorylation in mouse foetal explants to determine whether rapamycin treatment effectively blocked mTORC1 activity. Phospho-S6 (S240/244) is strongly expressed in the upper layers of vehicle-treated explants (Fig. 4.10a) whereas rapamycin reduces phospho-S6 (S240/244) levels (Fig. 4.10a). This confirms rapamycin-induced mTORC1 inhibition. ~~However, at the rapamycin concentrations used, there is still some S6 phosphorylation present showing that the concentrations of rapamycin used did not completely inhibit mTORC1 activity and there is no over dose of rapamycin.~~

The autophagy protein complex, ATG5-ATG12, which is required for the elongation of the double-membrane, is highly expressed in the basal layer of vehicle-treated explants. ATG5-ATG12 is also present at very low levels in the granular layer of vehicle-treated explants (Fig. 4.10b). Rapamycin treatment had no effect on the basal layer expression of ATG5-ATG12, but granular layer ATG5-ATG12 expression is slightly increased (Fig. 4.10b). However, no dose-dependent effect of rapamycin is

observed on granular layer ATG5-ATG12 levels (Fig. 4.10b). This may be due to the very low levels of this complex in the granular layer and a small rapamycin dose-dependent increase may not be detected with immunofluorescence analysis.

BECN1, which has different roles in autophagy depending on its binding partners, is required for autophagic double-membrane formation. Immunofluorescence analysis of BECN1 shows a very strong basal layer expression in the vehicle-treated and rapamycin-treated explants (Fig. 4.10b). BECN1 is also present at very low levels in the granular layer of vehicle-treated explants (Fig. 4.10b). Rapamycin treatment increases granular layer BECN1 but it does not affect basal BECN1 (Fig. 4.10b). With immunofluorescence analysis, I could not detect any dose-dependent effects of rapamycin on granular layer BECN1 levels (Fig. 4.10b). The BECN1 expression pattern in these explants is similar to the expression profile of the ATG5-ATG12 complex.

Another autophagy protein required for the initiation step is WIPI1. Immunofluorescence analysis of WIPI1 expression shows it is present as puncta in the upper layers of vehicle-treated and rapamycin-treated foetal explants (Fig. 4.10c). Rapamycin treatment concentrates WIPI1 puncta to fewer granular layers compared to vehicle-treated explants (Fig. 4.10c).

ULK1, which is also required for one of the autophagy initiation complexes, is present in the upper layers of vehicle-treated explants (Fig. 4.10c). Rapamycin treatment induces an up-regulation of granular layer ULK1 expression and it is also more concentrated in the granular layer (Fig. 4.10c).

The autophagosome marker LC3 is expressed strongly in granular layer of vehicle-treated explants (Fig. 4.10c). Rapamycin increases granular layer LC3 dose-dependently (Fig. 4.10c). This suggests rapamycin-induced up-regulation of autophagy and increased formation of autophagic vesicles.

These experiments show that autophagy markers are present in the granular layer of foetal explant cultures and rapamycin alters the granular layer expression profile of autophagy markers as well as induces the formation of LC3 aggregates.

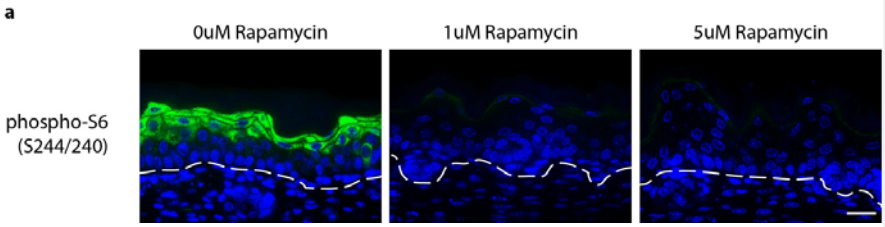

Figure 4.10: Expression pattern of autophagy markers in rapamycin-treated mouse foetal skin explants.

(a) Immunofluorescence analysis of phospho-S6 in vehicle-treated and rapamycin-treated mouse foetal skin explants shows S6 phosphorylation in the upper layers of vehicle-treated explants. Rapamycin strongly reduces S6 phosphorylation levels.

Figure 4.10 continued on the next page.

Mouse skin explants were harvested from E15.5 foetuses and cultured in vitro for 72h at the air-liquid interface of media with vehicle or rapamycin.

Bar = 20um. Dotted line = basement membrane.

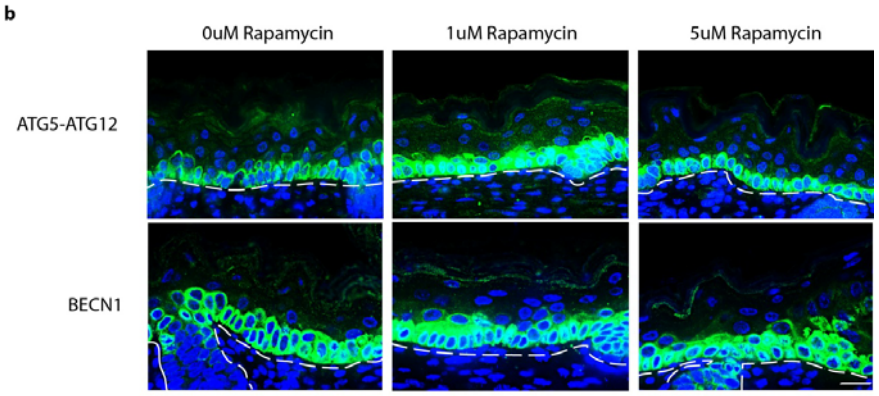

Figure 4.10: Expression pattern of autophagy markers in rapamycin-treated mouse foetal skin explants.

Figure 4.10 continued.

(b) The ATG5-ATG12 complex required for autophagome membrane elongation is strongly expressed in the basal layers of all explants cultures. ATG5-ATG12 is also present in the upper layers of vehicle-treated explant cultures at low levels. Rapamycin increases granular layer ATG5-ATG12 expression but it does not affect basal ATG5-ATG12 levels. However, with immunofluorescence, no dose-dependent effect of rapamycin is observed on granular layer ATG5-ATG12. BECN1, which plays an important role in initiation of the autophagy process, is expressed strongly in the basal and para-basal layers of all explants cultures. BECN1 is also present in the upper layers of vehicle-treated explants, and rapamycin increases granular layer BECN1 levels.

Figure 4.10 continued on the next page.

Mouse skin explants were harvested from E15.5 foetuses and cultured in vitro for 72h at the air-liquid interface of media with vehicle or rapamycin.

Bar = 20um. Dotted line = basement membrane.

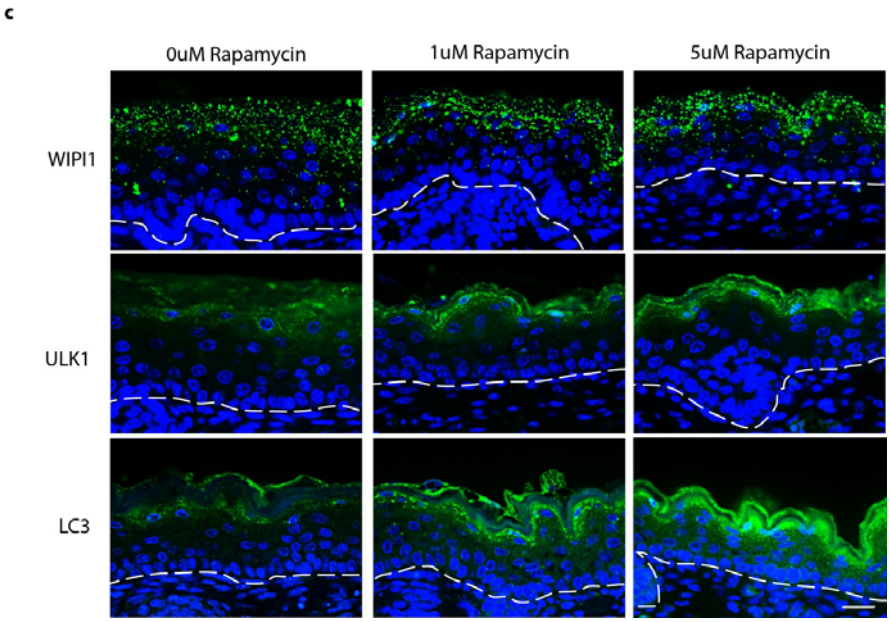

Figure 4.10: Expression pattern of autophagy markers in rapamycin-treated mouse foetal skin explants.

Figure 4.10 continued.

(c) WIPI1, another protein important for autophagy initiation, is present as puncta in the upper layers of vehicle-treated explants. Rapamycin changes WIPI1 expression pattern slightly by ~~confining it to the granular layer where it is more concentrated~~reducing its expression to fewer layers. ULK1, which participates in autophagosome double-membrane formation and is also directly regulated by mTORC1, is present in the upper layers of vehicle-treated explant cultures. Rapamycin increases ULK1 expression levels in the granular layer. The autophagosome marker LC3 is expressed in all epidermal layers of vehicle-treated explants but is more concentrated in the granular layers. Rapamycin treatment strongly up-regulates granular layer LC3 levels dose-dependently.

Mouse skin explants were harvested from E15.5 foetuses and cultured in vitro for 72h at the air-liquid interface of media with vehicle or rapamycin.

Bar = 20um. Dotted line = basement membrane.

Using mouse foetal skin explants cultures I show that rapamycin has no effect on basal layer BECN1 and ATG5-ATG12 levels. However, rapamycin increases granular layer BECN1 and granular layer ATG5-ATG12. Rapamycin also increases ULK1 expression with is mainly present in the granular layer. Therefore, rapamycin changes the granular layer expression patterns of BECN1, ATG5-ATG12, WIPI1 and ULK1. Granular layer LC3 expression is up-regulated does-dependently with rapamycin and more LC3 aggregates are formed.

To confirm that the rapamycin-induced increase in granular layer LC3 levels and LC3 aggregates formation is due to increased autophagy, I performed Western blot analysis of the epidermis from foetal skin explants. The foetal epidermis was separated from the dermis of the explant cultures before protein extraction. Western blotting shows that the lower concentration of rapamycin (1uM) strongly reduces phospho-S6 in the foetal epidermis (Fig. 4.11a), confirming mTORC1 inhibition as well as observations made with immunofluorescence analysis (Fig. 4.10). Compared to the vehicle-treated explant, Western blotting shows that rapamycin ~~increases~~ may increase the level of LC3II/LC3I ratios (Fig. 4.11b), suggesting a higher turn-over of LC3I to LC3II in the rapamycin-treated foetal explant epidermis. Therefore, rapamycin-induced autophagy occurs in the epidermis of the foetal explant cultures.

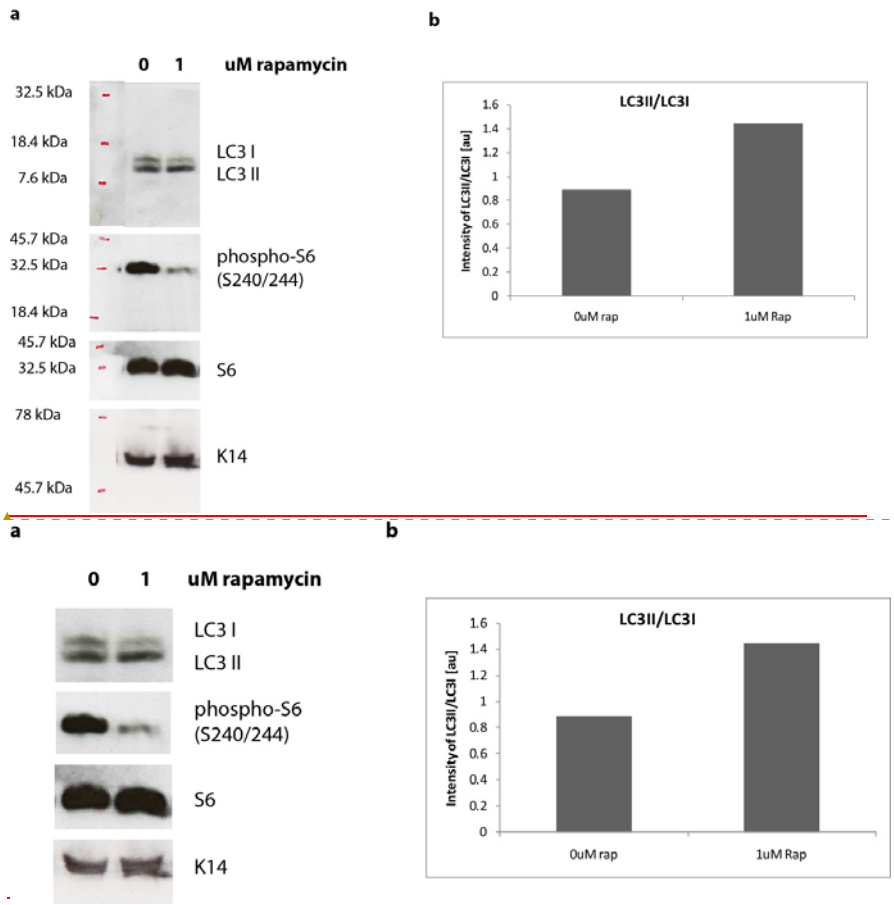

Figure 4.11: Expression of autophagosome marker LC3 in the epidermis of rapamycin-treated mouse foetal skin explants.

(a) Mouse foetal explants isolated at E15.5 were treated with vehicle and rapamycin for 72h before harvesting. Western blotting of epidermis lysates from mouse foetal skin explant cultures shows down-regulation of S6 phosphorylation with 1uM rapamycin, indicating effective mTORC1 inhibition. Rapamycin treatment increases LC3II levels in the foetal explant epidermis.

(b) Quantification of LC3II/LC3I shows increased rapamycin-induced LC3 turn-over.

Formatted: Font: 12 pt

Mouse skin explants were harvested from E15.5 foetuses and cultured in vitro for 72h at the air-liquid interface of media with vehicle or rapamycin. Foetal explant epidermis was separated from dermis and lysed for Western blotting.

In conclusion, in mouse foetal explants cultures, rapamycin increases granular layer autophagy marker expression levels and also changes expression patterns of autophagy markers in the granular layer. Rapamycin also increases LC3 turn-over (LC3I to LC3II) suggesting rapamycin induced autophagosome formation. This data supports previous observations made in monolayer keratinocyte cultures and REK organotypics. Therefore, I conclude that granular layer autophagy responds to rapamycin-mediated mTORC1 inhibition.

As a next step, I wanted to find out if rapamycin-induced granular layer autophagy is due to rapamycin-mediated mTORC1 inhibition or if this increase in granular autophagy is due to other effects rapamycin has in epidermis. So, I used another mTOR inhibitor, Torin1. At low concentrations Torin1 inhibits mTORC1, whereas it blocks mTORC2 activity at higher concentrations (Thoreen *et al.* 2009). Foetal skin explants were harvested at E15.5, which is before epidermal barrier formation, and cultured *in vitro* for 72h in the presence of vehicle, Torin1 or rapamycin.

Initially I determined the expression pattern of epidermal differentiation markers to find out if the foetal explants had formed a granular and cornified layer in culture. The terminal differentiation markers in the Torin1-treated explants were expressed in a similar manner to vehicle treated explants (Fig. 4.12). However, Torin1 induces expression of filaggrin in fewer granular layers where it is more concentrated (Fig. 4.12), whereas rapamycin treatment leads to an overall reduction in filaggrin expression levels in all layers (Fig. 4.12).

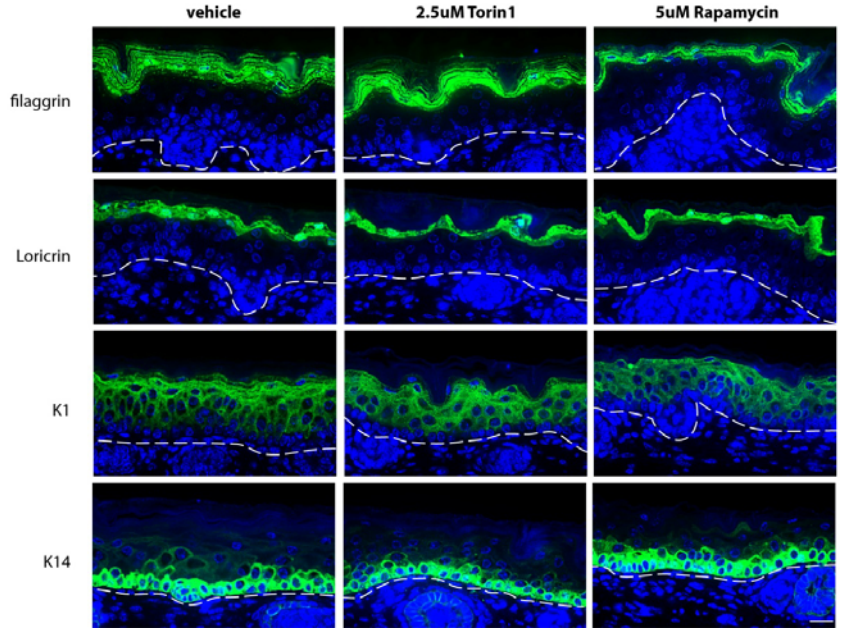

Figure 4.12: Expression pattern of epidermal differentiation markers in Torin1-treated mouse foetal skin explants.

Mouse foetal explants isolated at E15.5 were treated with vehicle, Torin1 or rapamycin for 72h before harvesting. Immunofluorescence analysis of epidermal differentiation markers shows expression of the terminal differentiation marker filaggrin in the granular layers of vehicle-treated and torin1-treated explants. However, filaggrin expression levels are reduced in rapamycin-treated explants and it is expressed in fewer layers compared to vehicle-treated explants. Loricrin, another terminal differentiation marker is expressed at similar levels in the granular layers of vehicle-treated, Torin1-treated and rapamycin-treated explants, suggesting formation of granular layers in all explant cultures. A marker for early keratinocyte differentiation, K1, is expressed in the supra-basal layers of vehicle-treated explants, torin1-treated and rapamycin-treated explants. K14, usually expressed in proliferating basal keratinocytes, is present in the basal and para-basal layers of vehicle-treated, Torin1-treated and rapamycin-treated explant cultures. K14 expression is still present in the supra-basal layers of all explants, but at very low levels. *Mouse skin explants were harvested from E15.5 foetuses and cultured in vitro for 72h at the air-liquid interface of media with vehicle, Torin1 or rapamycin.Bar = 20um. Dotted line = basement membrane.*

The foetal explant cultures used in this experiment were isolated from embryos at a time-point before barrier formation and cultured *in vitro* over the period of granular and cornified layer formation. I show that these explants have activated their terminal differentiation pathways and developed granular layers *in vitro*. The expression profile of epidermal terminal differentiation markers shows that these explants have normal stratification like in healthy adult epidermis. Therefore, I proceeded to analyse the effects of Torin1-mediated mTORC1 inhibition on epidermal autophagy, compared to rapamycin-induced granular layer autophagy.

Phospho-S6 is strongly expressed in the upper layers of vehicle-treated explants showing active mTORC1 signalling (Fig. 4.13a). Torin1 ~~confines phospho-S6 to fewer epidermal layers (Fig. 4.13a). R~~and rapamycin strongly reduce~~s~~ phospho-S6 levels (Fig. 4.13a). These results suggest that Torin1 and rapamycin down-regulate mTORC1 activity in epidermis.

The ATG5-ATG12 complex is strongly expressed in the basal layers of all explant cultures (Fig. 4.13b). ATG5-ATG12 is also present in the granular layers of vehicle-treated explants but at much lower levels (Fig. 4.13b). Similar to rapamycin, Torin1 increases granular layer ATG5-ATG12 expression, whereas basal ATG5-ATG12 is unaffected (Fig. 4.13b). Therefore, mTORC1 inhibition via Torin1 or rapamycin has similar effects on granular layer ATG5-ATG12.

BECN1 is strongly expressed in the basal and para-basal layers of all foetal epidermal explants (Fig. 4.13b). Like rapamycin, Torin1 has no effect on basal layer BECN1 expression levels however, compared to vehicle-treated explants, both drugs increase granular layer BECN1 expression (Fig. 4.13b). This effect of Torin1 and rapamycin on BECN1 expression is similar to their effects on ATG5-ATG12.

WIPI1 is strongly expressed as puncta in the upper layers of vehicle-treated explants (Fig. 4.13c). Both Torin1 and rapamycin lead to a reduction in the number of WIPI1 expressing layers compared to vehicle-treated explants (Fig. 4.13c). Also, both drugs increase the expression levels of WIPI1 in the granular layer (Fig. 4.13c).

ULK1, which is directly regulated by mTORC1 activity, is expressed in the upper layers of vehicle-treated explants (Fig. 4.13c). Torin1 increases ULK1 expression intensity in the upper layers (Fig. 4.13c), whereas rapamycin treatment not only increases ULK1 expression levels, but also reduces the number of ULK1 expressing epidermal layers (Fig. 4.13c).

The autophagosome marker LC3 is expressed in all epidermal layers of vehicle-treated explants with the highest levels in the granular layers where it is present as aggregates (Fig. 4.13c). Torin1 treatment strongly up-regulates granular layer LC3 expression and also increases LC3 aggregate formation (Fig. 4.13c). Rapamycin also increases granular layer LC3 levels however its effect is not as strong as with Torin1 (Fig. 4.13c).

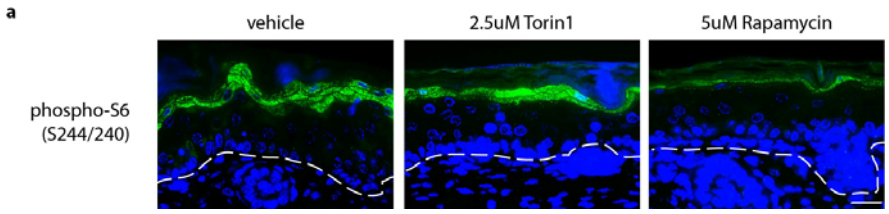

Figure 4.13: Expression pattern of autophagy markers in Torin1-treated mouse foetal skin explants.

(a) Immunofluorescence analysis of phospho-S6 (S240/244) shows strong expression in the upper layers of the vehicle-treated explants. Torin1 treatment has no effects on S6 phosphorylation levels however, S6 is expressed in fewer layers compared to vehicle-treated explant cultures. Rapamycin treatment reduces phospho-S6 levels and confines S6 phosphorylation to fewer epidermal layers. These results show that Torin1-induced and rapamycin-induced mTORC1 inhibitions have different effects on epidermal S6 phosphorylation.

Figure 4.13 continued on the next page.

Mouse skin explants were harvested from E15.5 foetuses and cultured in vitro for 72h at the air-liquid interface of media with vehicle, Torin1 or rapamycin.

Bar = 20um. Dotted line = basement membrane.

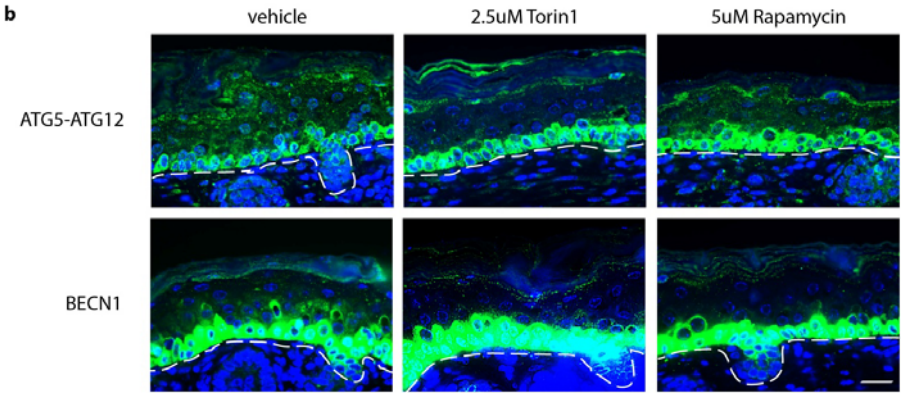

Figure 4.13: Expression pattern of autophagy markers in Torin1-treated mouse foetal skin explants.

Figure 4.13 continued.

(b) The ATG5-ATG12 complex required for elongation of the autophagosomal membrane is strongly expressed in the basal layer of vehicle-treated, Torin1-treated and rapamycin-treated foetal explants. ATG5-ATG12 is also present in the granular layer of vehicle-treated explants. Torin1 as well as rapamycin treatment increase granular layer ATG5-ATG12 expression levels. BECN1 is also strongly expressed in the basal layers of vehicle-treated, Torin1-treated and rapamycin-treated explants. Torin1 and rapamycin have no effects on basal layer BECN1 expression. BECN1 is also present in the upper layers of vehicle-treated explants at lower levels. Torin1 and rapamycin induce an increase in granular layer BECN1 expression.

Figure 4.13 continued on the next page.

Mouse skin explants were harvested from E15.5 foetuses and cultured in vitro for 72h at the air-liquid interface of media with vehicle, Torin1 or rapamycin.

Bar = 20um. Dotted line = basement membrane.

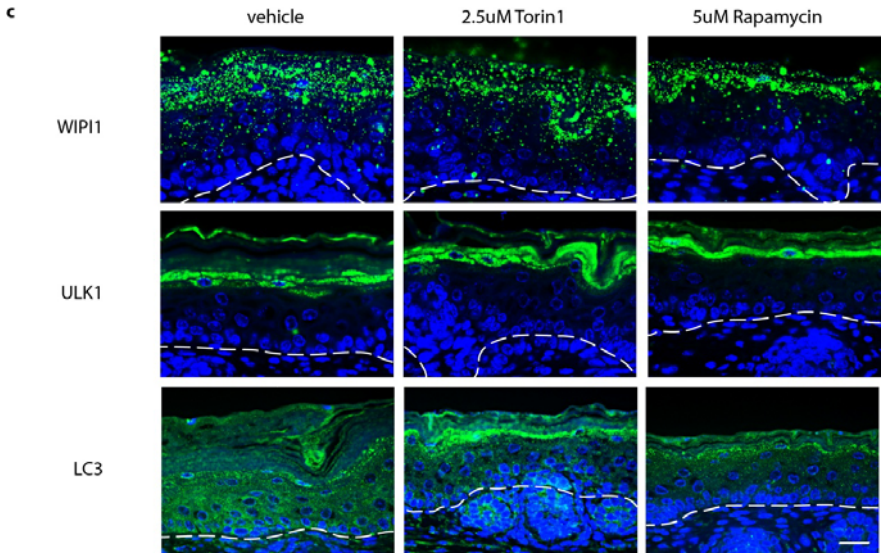

Figure 4.13: Expression pattern of autophagy markers in Torin1-treated mouse foetal skin explants.

Figure 4.13 continued.

(c) In the Torin1-treated explants, WIPI1 is also expressed as puncta in the upper layers but, WIPI1 expression is restricted to fewer layers and is also concentrated in the granular layers of the explants. Rapamycin-treated explants show a similar WIPI1 expression pattern to Torin1-treated explants cultures. ULK1 is strongly expressed in the upper layers of vehicle-treated explants. Torin1 and rapamycin treatment increase granular layer ULK1 expression. LC3 is expressed in all layers of vehicle-treated explants with the strongest expression levels in the granular layer where it is present as LC3 puncta. Torin1 treatment induces a very strong increase in granular layer LC3 levels, where LC3 is also present as puncta. Compared to vehicle treatment, rapamycin also increases LC3 in the granular layer however its effect is not as striking as Torin1 treatment.

Mouse skin explants were harvested from E15.5 foetuses and cultured in vitro for 72h at the air-liquid interface of media with vehicle, Torin1 or rapamycin.

Bar = 20um. Dotted line = basement membrane.

Therefore, Torin1 and rapamycin-induced mTORC1 inhibition have similar effects on autophagy in epidermis. However, Torin1 induces a much stronger increase in granular layer LC3 expression intensities and LC3 aggregate formation. Both drugs change the expression patterns and also increase the expression levels of granular layer ULK1, WIPI1, BECN1 and ATG5-ATG12 strongly suggesting mTORC1 regulates constitutive granular layer autophagy. The basal layer expression of BECN1 and ATG5-ATG12 is unaffected by Torin1 or rapamycin treatment. This indicates that BECN1 and ATG5-ATG12 have different roles in the basal layer compared to granular layer autophagy proteins (see chapter 5).

Both rapamycin and Torin1 have similar effects on granular layer autophagy in mouse foetal skin explants. This shows that the initial observations on the effects of rapamycin on epidermis, leading to increased granular layer autophagy, is not due to other unknown effects of rapamycin, but it is due to rapamycin-mediated mTORC1 inhibition. I conclude that constitutively active granular layer autophagy is sensitive to mTORC1 mediated autophagy.

Discussion

At the beginning of this chapter I set out to determine which AKT isoform is sensitive to rapamycin treatment in epidermis. Rapamycin and is analogues are used as immunosuppressants for organ-transplant recipients (OTRs). One of the benefits of using rapamycin over other immunosuppressants is that the patients develop less cSCCs. Rapamycin is also an mTORC1 inhibitor. AKT which is upstream of mTORC1 plays an important role in epidermal development and differentiation. Moreover, the AKT1 isoform, which is associated with terminally differentiating keratinocytes (Fig. 4.1; Calautti *et al.* 2005; Thrash *et al.* 2006) is down-regulated in cSCCs (O'Shaughnessy *et al.* 2007b).

I show that in keratinocytes, rapamycin-treatment inhibits mTORC1 activity and increases AKT1 phosphorylation (Fig. 4.2 and Fig. 4.3). This indicates that in epidermis, it is the AKT1 expressing terminally differentiating keratinocytes which respond to rapamycin treatment (Fig. 4.2 and Fig. 4.3). In my lab, these observations were verified and confirmed by using a mouse foetal explant model (Sully *et al.* 2012). Therefore, these findings indicate that in immunosuppressed patients, rapamycin may increase epidermal AKT1 phosphorylation and activity, promoting terminal differentiation and reducing cSCCs.

Autophagy is regulated by different cell signalling pathways. However, in epidermis the AKT/mTORC1 pathway is a key regulator of epidermal development and differentiation (see section 2.2.; Calautti *et al.* 2005; Thrash *et al.* 2006; O'Shaughnessy *et al.* 2007). Therefore, most mTORC1 probably also regulates epidermal autophagy. In the previous chapter I show that autophagy is a mechanism of organelle degradation during epidermal terminal differentiation. Therefore, I wanted to determine whether rapamycin has an effect on epidermal autophagy and epidermal differentiation, which may contribute to the beneficial effects of rapamycin on cSCC development in OTRs.

Initial experiments with REK monolayer cultures show that rapamycin treatment increases LC3II protein levels (Fig. 4.4; Appendix 12). Immunofluorescence analysis of these cells shows a rapamycin-induced increase in total LC3 expression levels and LC3 aggregate formation (Fig. 4.4, Fig. 4.5, Fig. 4.6). These results show that keratinocytes are capable of rapamycin-induced autophagy. In the previous chapter I used monolayer primary keratinocytes as a model to show that autophagy is a mechanism of organelle degradation in terminally differentiating keratinocytes. Therefore, in this chapter I wanted to find verify whether primary human keratinocytes also respond to rapamycin-induced autophagy.

In primary human keratinocyte cultures, both undifferentiated and differentiated keratinocytes respond to rapamycin treatment with an increase in LC3 turn-over (LC3II/LC3I ratios, Fig. 4.5). Immunofluorescence analysis of LC3 in primary monolayer cultures shows that rapamycin increases LC3 intensities/cell but it does not affect the numbers of LC3 aggregates/cell (Fig. 4.6). Therefore, I conclude that undifferentiated and differentiated monolayer keratinocytes respond to rapamycin induced autophagy.

Although both undifferentiated and differentiated monolayer keratinocyte cultures represent different keratinocyte differentiation stages, these cells cannot reflect exactly what happens in the epidermis. The differentiated monolayer culture is a mix of K14 positive proliferating cells, early differentiated K1 expressing cells and filaggrin positive terminally differentiating keratinocytes (Fig. 3.8). So, analysis of the differentiated monolayer keratinocyte population does not show exactly which epidermal differentiation stage responds to rapamycin treatment. As a next step I analysed the effects of rapamycin on autophagy in REK organotypic cultures.

REKs stratify in 3D cultures forming a granular and cornified layer, like in epidermis. In REK organotypics, WIPI1 is present as puncta in the upper layers of vehicle-treated 3D cultures (Fig. 4.8). Rapamycin confines WIPI1 to fewer epidermal layers. In REK organotypics, granular layer LC3 is up-regulated but is also restricted to

fewer layers after rapamycin treatment. These results show that rapamycin affects the expression pattern of autophagy markers in the upper layers and increases granular layer LC3 expression and LC3 aggregate formation. Therefore, in REK 3D cultures granular layer keratinocytes responds to rapamycin-induced autophagy.

Although REK organotypics are very similar to epidermis, they cannot completely mimic the epidermis. Therefore, I treated mouse foetal explant cultures with different doses of rapamycin to determine whether rapamycin affects epidermal autophagy. In mouse foetal explants, rapamycin changes the expression pattern of only granular layer autophagy markers, whereas basal BECN1 and ATG5-ATG12 are unaffected by rapamycin treatment (Fig. 4.10b). LC3 expression and LC3 aggregate formation in the granular layers of foetal explants is dose-dependently up-regulated with rapamycin (Fig. 4.10c and Fig. 4.11). These results show that in epidermis, mainly granular layer keratinocytes respond to rapamycin-induced autophagy. However, it is unclear whether this rapamycin-induced increase in autophagy marker expression and LC3 aggregate formation is due to rapamycin-mediated mTORC1 inhibition or other effects of rapamycin. Therefore, I used another mTOR inhibitor Torin1 to verify this.

At low concentrations, Torin1 blocks mTORC1 activity, whereas at higher concentrations it inhibits both mTORC1 and mTORC2 (Thoreen *et al.* 2009). I compared the effects of low Torin1 concentrations on foetal explants cultures to rapamycin and vehicle-treated explants. Torin1 has similar effects on autophagy marker expression and LC3 levels compared to rapamycin. Both Torin1 and rapamycin change granular layer autophagy marker expression patterns and increase LC3 expression levels as well as the amount of LC3 aggregates in the granular layer (Fig. 4.13c). However, Torin1 has a much stronger effect on granular layer LC3 expression and LC3 vesicle formation (Fig. 4.13c). These results confirm that the rapamycin-mediated increase in granular layer autophagy is due to rapamycin-induced mTORC1 inhibition. Therefore, I show that constitutive granular

layer autophagy is up-regulated by rapamycin-mediated mTORC1 inhibition in epidermis.

My findings suggest that rapamycin and its analogues may exert their anti-carcinogenic effects on treated transplant patients by increasing epidermal AKT1 activity as well as epidermal autophagy levels. Epidermal AKT1 is associated with more differentiated keratinocytes (Fig. 4.1) and in my previous chapter I show that constitutive granular layer autophagy is a mechanism of organelle degradation during terminal differentiation in epidermis. Therefore, promoting AKT1 activity as well as increasing granular layer autophagy may support epidermal terminal differentiation in OTRs, preventing formation and progression of cSCCs.

Chapter 5

RESULTS

Functional importance of autophagy in epidermis

Functional importance of autophagy in epidermis

Introduction

Autophagy, which can be a pro-survival or a cell death mechanism, has been implicated in a number of cellular processes including starvation, differentiation, immunity, aging, and tumourigenesis. In chapters 3 and 4, I show that autophagy is constitutively active in the granular layer of the epidermis where terminal differentiation occurs, and this constitutive autophagy is sensitive to mTORC1 inhibition. Also, autophagy is a mechanism of nucleus degradation during keratinocyte terminal differentiation *in vitro*. Therefore, one of the aims of this chapter is to determine whether autophagy plays a role in epidermal barrier defect diseases due to incomplete keratinocyte terminal differentiation, like psoriasis.

One of the main functions of the epidermis is to protect the organism from UV irradiation however UV exposure also increases the risk of developing cutaneous Squamous Cell Carcinomas (cSCCs) (Alam and Ratner 2001; Eberle *et al.* 2007; Leiter and Garbe 2008). HPV infections have also been implicated in SCC formation (Storey and Simmonds 2009; Neale *et al.* 2013). Therefore, other aims of this chapter are to determine the effects of UV irradiation on autophagy marker expression in healthy mouse epidermis as well as during HPV8-induced cSCC formation in transgenic mice. Also, the expression pattern of the autophagosome marker, LC3 was analysed in cSCC patient samples. The results from these experiments may have future therapeutic implications in the treatment of barrier defects and epidermal SCCs.

Results

5.1 Expression of autophagy markers in an epidermal barrier defect disease, psoriasis

Psoriasis vulgaris or plaque psoriasis is a skin barrier defect which is characterized by keratinocyte hyperproliferation and abnormal terminal differentiation, as well as infiltration of immune cells into the dermis and epidermis, and increased vascularisation (reviewed in Raychaudhuri 2012).

H&E staining of psoriatic and healthy human epidermis show hyperproliferative and thicker epidermis in lesional psoriatic skin (involved skin) compared to non-lesional psoriasis (uninvolved skin) and healthy epidermis (Fig. 5.1a). Also, the cornified layer of the psoriatic lesion is thicker and still contains nuclei compared to the cornified layers in non-lesional psoriasis and healthy skin where nuclei are completely absent (blue vertical line, Fig. 5.1b). There is also no clear granular layer in the involved skin compared to uninvolved epidermis and healthy epidermis where the granular layer is clearly defined (blue arrows, Fig. 5.1b).

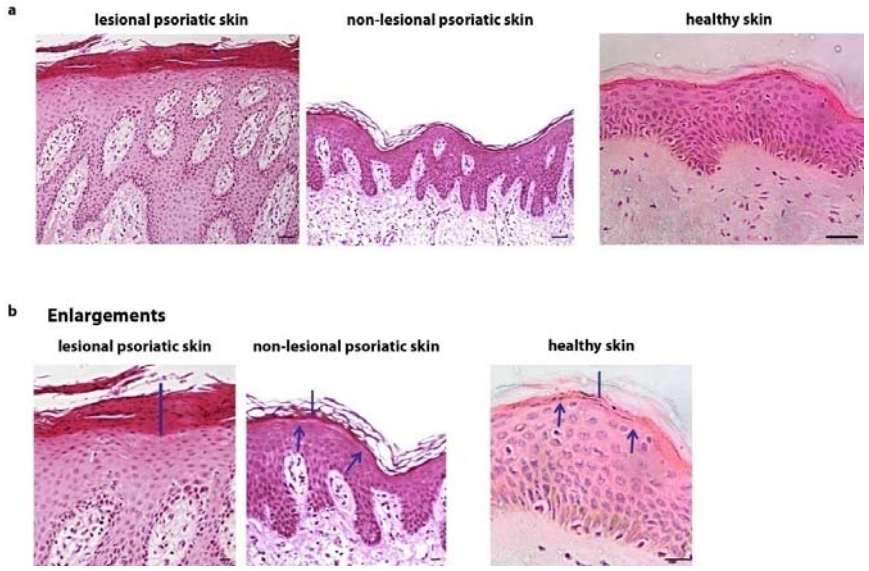

Figure 5.1: H&E staining of lesional and non-lesional psoriatic skin, and healthy skin.

(a) H&E staining of non-lesional and lesional psoriatic epidermis, and healthy epidermis shows thicker epidermis in lesional psoriatic skin compared to non-lesional psoriasis and healthy epidermis. The uppermost layer of lesional psoriatic epidermis is para-keratotic with nuclei still present in the cornified envelope, whereas non-lesional and healthy epidermis has corneocytes without nuclei.

Black bar = 50um

(b) Enlargements of H&E staining of psoriatic lesion, non-lesional psoriasis and healthy epidermis show thicker uppermost layer and nuclei retention in psoriatic lesion (blue vertical line), whereas the cornified layer of non-lesional psoriatic skin and healthy epidermis are completely free from nuclei (blue vertical line). Also, in psoriatic lesions, there is no clear granular layer compared to non-lesional psoriatic skin and healthy epidermis (blue arrows).

Black bar = 20um. Blue vertical line = cornified layer. Blue arrows = granular layer.

The figure is representative of n=6 different samples of psoriatic lesions and n=5 different samples of healthy adult epidermis.

These results show that in psoriatic lesions, the granular layer is absent and the cornified layer is para-keratotic suggesting incomplete terminal differentiation. This results in improper barrier function of the epidermis, which is characteristic for psoriasis. However, in uninvolved skin, there is a clearly defined granular layer and corneocytes have no nuclei similar to healthy epidermis.

Therefore I wanted to verify my hypothesis, that autophagy is a mechanism for organelle degradation during terminal differentiation in epidermis, by determining whether the autophagosome maker LC3 is present in psoriatic lesions and also, by analysing the expression pattern of other autophagy markers.

Immunofluorescence analysis of healthy adult epidermis shows that LC3 is expressed in all layers of the epidermis with the strongest expression in the granular layers (Fig. 3.2; Fig. 5.2). In psoriatic lesions which are characterised by parakeratosis, LC3 is completely absent from all layers of the epidermis, including the upper layers (Fig. 5.2). In non-lesional psoriatic epidermis where cornification occurs, LC3 is present in the granular layer where it forms aggregates. However, the expression level of LC3 in all epidermal layers of non-lesional psoriasis is strongly reduced compared to healthy epidermis (Fig. 5.2). This suggests that in the epidermis of psoriatic lesions, which are characterised by nuclei retention in the uppermost epidermal layers, there are no autophagic vesicles. However, in non-lesional psoriatic epidermis, where there is no nuclei retention in the uppermost layers and cornification can occur, there are LC3 positive autophagic vesicles in the granular layer.

WIPI1 is not expressed in any layers of lesional psoriatic epidermis, whereas it is expressed at low levels in the upper layers of non-lesional psoriatic epidermis, similar to healthy epidermis (Fig. 5.2). However, WIPI1 expression levels are much lower in non-lesional psoriatic epidermis compared to healthy epidermis (Fig. 5.2). This suggests that where cornification can occur, like in non-lesional psoriatic skin and healthy skin, WIPI1 is expressed in the upper layers.

In healthy skin, ULK1 is expressed in all layers of the epidermis with highest expression levels in the upper layers (Fig. 3.2; Fig. 5.2). In non-lesional psoriatic epidermis, ULK1 is expressed in the supra-basal and granular layers with an expression intensity which is much higher than in healthy epidermis (Fig. 5.2). In lesional psoriatic epidermis, ULK1 is highly expressed in all epidermal layers except in the parakeratotic uppermost layers (Fig. 5.2). This shows that in both lesional and non-lesional psoriatic epidermis, ULK1 expression is deregulated.

Immunofluorescence analysis of BECN1 expression in healthy epidermis shows that BECN1 is predominantly expressed in the proliferating basal layer (Fig. 3.2; Fig. 5.2). In non-lesional psoriatic skin, BECN1 is present in the basal and para-basal layers, whereas BECN1 is expressed strongly in the supra-basal layers of lesional psoriatic skin (Fig. 5.2).

The expression pattern of ATG5-ATG12 is similar to BECN1 with a strong basal layer expression of ATG5-ATG12 in healthy epidermis (Fig. 3.2; Fig. 5.2). In non-lesional psoriatic skin, ATG5-ATG12 is also mainly expressed in the basal layer (Fig. 5.2). However, in lesional psoriatic epidermis, ATG5-ATG12 is expressed in the supra-basal layers (Fig. 5.2). These results suggest that both BECN1 and ATG5-ATG12 are highly over-expressed in lesional psoriatic epidermis.

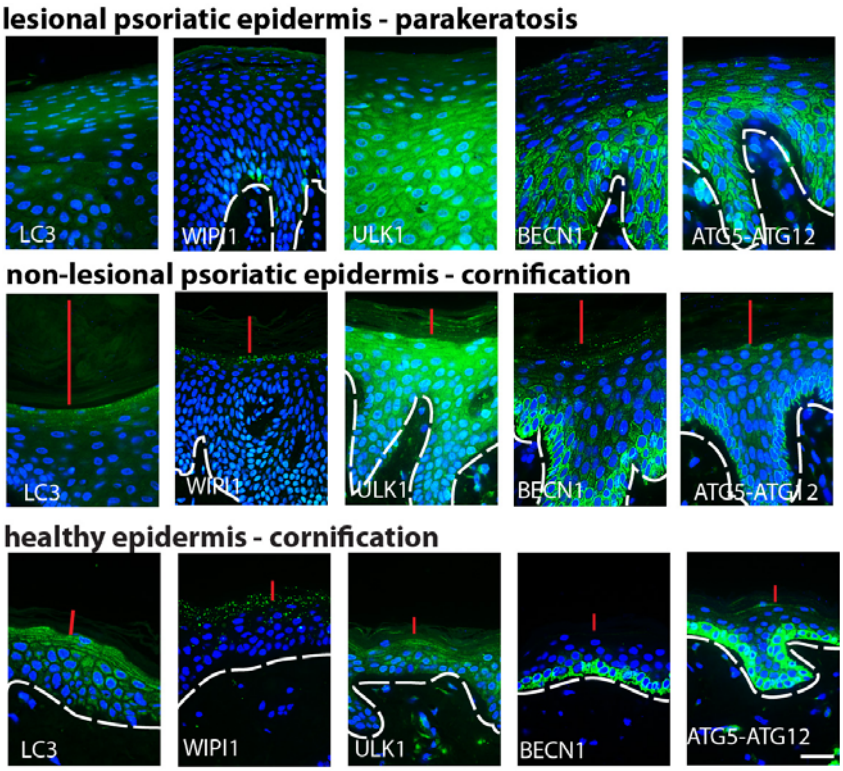

Figure 5.2: Autophagy marker expression profile in non-lesional and lesional psoriatic skin compared to healthy skin.

Immunofluorescence analysis of autophagy markers was performed on lesional psoriatic skin compared to non-lesional psoriatic skin and healthy epidermis. In lesional psoriatic skin LC3 and WIPI1 are not expressed. However, in non-lesional psoriatic skin, LC3 and WIPI1 are expressed in the upper layers, similar to the LC3 and WIPI1 expression patterns in healthy epidermis. In both lesional and non-lesional psoriatic epidermis, ULK1 expression is strongly up-regulated in the supra-basal layers compared to healthy epidermis. BECN1 and ATG5-ATG12, which are strongly expressed in the basal layer of healthy epidermis and in the basal and para-basal layers of non-lesional psoriatic epidermis, are up-regulated in the supra-basal layers of lesional psoriatic epidermis.

This figure is representative of n=6 samples of psoriatic lesions and n=5 samples of healthy epidermis. Red vertical bars = cornified layers. Black bar = 20 um.

Therefore, I conclude that immunofluorescence analysis of autophagy markers in psoriatic skin shows that autophagy marker expression is deregulated in psoriatic lesions compared to healthy epidermis. In non-lesional psoriasis, autophagy marker expression pattern is similar to healthy epidermis however, autophagy marker expression levels are still altered. Also, the autophagosome marker LC3, which is expressed in all layers of healthy epidermis with the highest intensity in the granular layers, is completely absent from the epidermis of psoriatic lesions. Non-lesional psoriatic epidermis expresses LC3 in the granular layers but at lower levels compared to healthy epidermis.

In conclusion, I observe that in psoriatic skin, were cornification occurs, granular layer autophagy markers are expressed in a manner similar to healthy epidermis, and LC3 is present in the granular layers. However, in psoriatic lesions where there is improper cornification with nuclear retention, autophagy marker expression is deregulated and there is no LC3 expression in the upper layers.

5.2 Expression of autophagy markers in mouse epidermis during recovery from UV exposure.

One of the main hazards the epidermis is exposure~~exposed~~ to ~~is~~ UV. UV has been shown to induce epidermal hyperproliferation as well as altered AKT isoform expression which is important for keratinocyte differentiation (Kinouchi *et al.* 2002; O'Shaughnessy *et al.* 2007b; Sully *et al.* 2012). Therefore, I wanted to determine whether autophagy also plays a role in the epidermal response to UV exposure.

Dorsal mouse epidermis was exposed to solar-simulated UV irradiation (10 J/cm^2 UVA and 1 J/cm^2 UVB) and harvested at different time-points. H&E staining shows UV-induced hyperproliferation 3 days (d3) after UV exposure compared to the epidermis before UV exposure (d0) (Fig. 5.3a). At d10 hyperproliferation is reduced suggesting that the epidermis is recovering from UV exposure (Fig. 5.3a). At d24, the epidermis has fully recovered and the initial thickness of the epidermis is restored (Fig. 5.3a).

Immunofluorescence analysis of epidermal differentiation markers shows that the terminal differentiation marker, loricrin, is strongly expressed in the granular layer of mouse epidermis at all the time-points before and after UV exposure (Fig. 5.3b). This suggests that terminal differentiation is not affected by UV exposure.

K1, a marker for early keratinocyte differentiation, is expressed in the supra-basal layers at d0 (Fig. 5.3b). At d3, the time point when epidermal hyper-proliferation is highest in my samples, K1 is only expressed at low levels in the uppermost layers of the epidermis (Fig. 5.3b). However, at d10, K1 expression is restored in the supra-basal layers, and this expression pattern is maintained at d24 (Fig. 5.3b). These results show that UV-induced hyperproliferation coincides with reduced expression of K1.

A marker for proliferating keratinocytes, K14 is strongly expressed in the basal layer of epidermis at d0 (Fig. 5.3b). K14 expression is strongly up-regulated in all layers of

the hyperproliferative epidermis at d3 and is no more confined to the basal layer (Fig. 5.3b). As the epidermis recovers at d10, K14 is present in the basal layer and at lower levels in the supra-basal layers. At d24, K14 is mainly expressed in the basal layer (Fig. 5.3b). These results suggest that UV exposure increases the K14 expressing proliferative compartment of epidermis, which coincides with epidermal hyperproliferation.

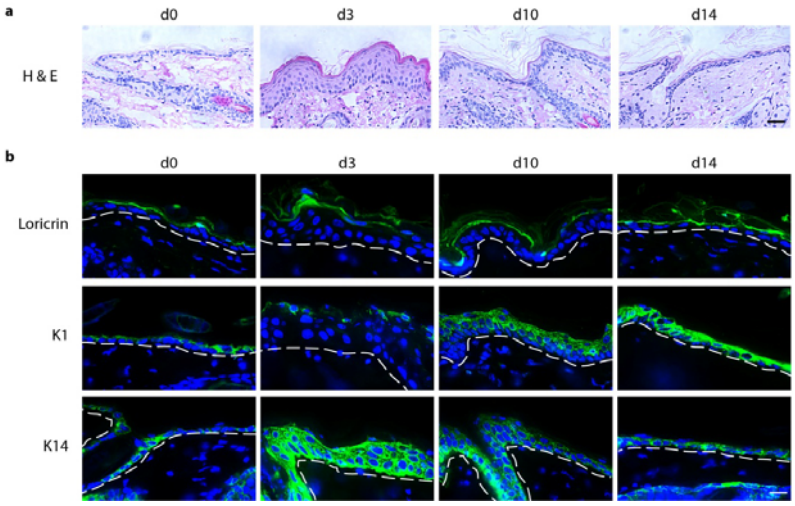

Figure 5.3: Expression of epidermal differentiation markers in UV-exposed healthy adult mouse epidermis.

(a) H&E staining of UV-exposed adult epidermis covering the period before UV irradiation (d0) to 24 days after UV exposure (d24). At d3 the epidermis is thicker and hyperproliferative compared to d0. Epidermal hyperproliferation and thickness is reduced at d10 compared to d3, but is still thicker than at d0. At d24, epidermal thickness has returned to normal, similar to d0.

(b) Expression of epidermal differentiation markers loricrin, K1 and K14 in UV-exposed mouse epidermis shows expression of the terminal differentiation marker loricrin in the granular layers of d0, d3, d10 and d24. K1, a marker of early epidermal differentiation is expressed in the supra-basal layers at d0. However, at d3 when UV induced hyperproliferation is highest, K1 is only expressed at very low levels in the upper epidermal layers. At d10 and d24, K1 expression is back to the supra-basal layers of the epidermis. A marker for proliferating basal keratinocytes, K14, is strongly expressed in the basal layer of d0 epidermis. At d3, K14 is strongly expressed in all layers of the epidermis. At d10, K14 expression is reduced but is still present in all epidermal layers. However at d24, K14 expression is mainly in the lower epidermal layers.

Formatted: Normal, Indent: Left: 2 cm, No bullets or numbering

~~*This figure is representative of n=2 different samples of mouse epidermis. Bar = 20 um.*~~

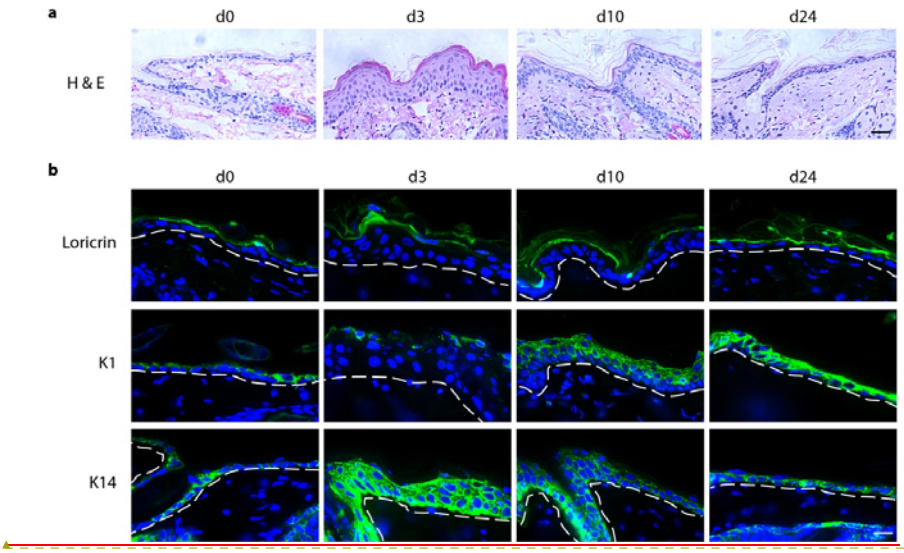

Formatted: Indent: Left: 2 cm

Formatted: Font: Italic

Figure 5.3: Expression of epidermal differentiation markers in UV-exposed healthy adult mouse epidermis.

~~(c)~~(a) H&E staining of UV exposed adult epidermis covering the period before UV irradiation (d0) to 24 days after UV exposure (d24). At d3 the epidermis is thicker and hyperproliferative compared to d0. Epidermal hyperproliferation and thickness is reduced at d10 compared to d3, but is still thicker than at d0. At d24, epidermal thickness has returned to normal, similar to d0.

~~(d)~~(b) Expression of epidermal differentiation markers loricrin, K1 and K14 in UV exposed mouse epidermis shows expression of the terminal differentiation marker loricrin in the granular layers of d0, d3, d10 and d24. K1, a marker of early epidermal differentiation is expressed in the supra-basal layers at d0. However, at d3 when UV induced hyperproliferation is highest, K1 is only expressed at very low levels in the upper epidermal layers. At d10 and d24, K1 expression is back to the supra-basal layers of the epidermis. A marker for proliferating basal keratinocytes, K14, is strongly expressed in the basal layer of d0 epidermis. At d3, K14 is strongly expressed in all layers of the epidermis. At d10, K14 expression is reduced but is still present in all epidermal layers. However at d24, K14 expression is mainly in the lower epidermal layers.

This figure is representative of n=2 different samples of mouse epidermis. Bar = 20 um.

Therefore, I conclude that exposure of the epidermis to solar-simulated UV has no effect on epidermal terminal differentiation but it drastically reduces the K1 positive, early differentiating keratinocytes of the supra-basal layer. This is accompanied by UV-induced expansion of the K14 expressing proliferative compartment. As the epidermis recovers and hyperproliferation is reduced, normal expression of epidermal differentiation markers is restored.

As the next step, I proceeded to analyse the expression of autophagy markers in response to UV. At d0 before UV exposure, LC3 is expressed strongly in the granular layers and ULK1 is expressed all through the epidermis with slightly stronger expression intensity in the granular layers (Fig. 5.4). The ATG5-ATG12 complex and BECN1 are strongly expressed in the basal layer at d0 (Fig. 5.4). WIPI1 shows a punctate expression pattern in the upper layer of d0 epidermis (Fig. 5.4).

At d3, when UV-induced epidermal hyperproliferation is at its peak in the time points analysed, LC3 is highly expressed in all layers of the epidermis (Fig. 5.4). At this time-point ULK1, ATG5-ATG12 and BECN1 are also strongly expressed all through the epidermis (Fig. 5.4). However, WIPI1, usually present as puncta in the uppermost layers, is unaffected by UV irradiation and shows punctate expression in the upper layers of d3 epidermis (Fig. 5.4). This WIPI1 expression pattern is maintained throughout recovery of the epidermis from UV exposure (Fig. 5.4).

At d10, when hyperproliferation is reduced and the epidermis has partially recovered from UV, LC3 expression returns to the granular layers (Fig. 5.4). ULK1 is also mainly expressed in the granular layer (Fig. 5.4). The ATG5-ATG12 complex and BECN1 are strongly expressed in the basal and para-basal layers (Fig. 5.4).

At d24 when the epidermis has recovered and epidermal thickness has returned to normal, LC3 is strongly expressed in the granular layer and ULK1 expression is reduced in all epidermal layers, similar to d0 (Fig. 5.4). At d24, the ATG5-ATG12

complex and BECN1 are mainly expressed in the basal layer like before UV exposure at d0 (Fig. 5.4).

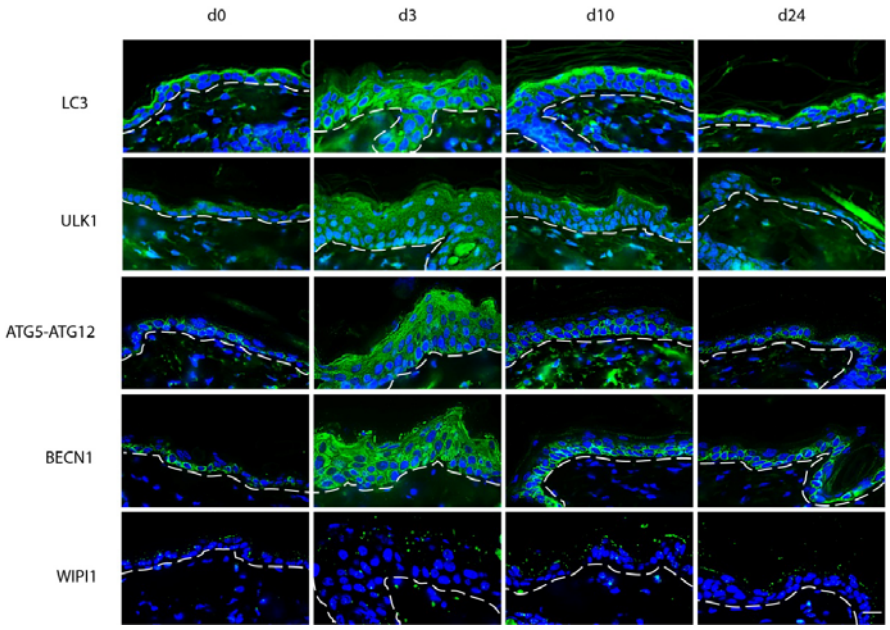

Figure 5.4: Expression of autophagy markers in UV-exposed healthy adult mouse epidermis.

UV exposed adult epidermis covering the period before UV irradiation (d0) to 24 days after UV exposure (d24) shows granular layer expression of LC3, and WIPI1 at d0 and ULK1 is expressed all through the epidermis. At d0, ATG5-ATG12 and BECN1 are strongly expressed in the basal layer. The epidermis is thicker and hyperproliferative at d3, reflecting a strong signal for LC3, ULK1, BECN1 and ATG5-ATG12, whereas WIPI1 is down-regulated and only present in the uppermost layers. At d10, LC3 and ULK1 expression is reduced in the supra-basal layers and are more concentrated in the granular layers. Also at d10, WIPI1 is expressed in the upper layers similar to d0 and, supra-basal ATG5-ATG12 and BECN1 expression is also reduced. The epidermis has recovered from UV-induced hyperproliferation at d24 and also shows normal autophagy marker expression like at d0.

This figure is representative of n=2 different samples of adult mouse epidermis.

Bar = 20 um.

Immunofluorescence analysis of autophagy markers during the recovery of adult mouse epidermis from UV shows that UV induces a deregulation in autophagy marker expression patterns which coincides with epidermal hyperproliferation. UV-induced hyperproliferation goes hand in hand with over-expression of LC3, ULK1, BECN1 and ATG5-ATG12 in all layers of the epidermis compared to non-irradiated epidermis. This shows that all epidermal layers can express autophagy proteins, suggesting all epidermal layers are capable of autophagy. Therefore, solar-simulated UV ~~is an~~can induce~~r of~~ autophagy in all layers of the epidermis.

In this section, I show that UV induces hyperproliferation of the epidermis with expansion of the proliferating K14 expressing compartment and reduction in the early differentiated K1 positive cells, which coincides with a deregulation in autophagy markers. As the epidermis recovers, the proliferating compartment returns to the basal layer and the early differentiated supra-basal layer is restored. Also, autophagy marker expression returns to normal.

5.3 Expression of autophagy markers in mouse ear epidermis in response to culture stress

Exposure to UV is an external stress which I have shown to induce a deregulation in autophagy marker expression. Therefore, for further experiments analysing the UV response of epidermis, I planned to use adult ear epidermal explant cultures. The benefit of using adult ear epidermis over epidermis from other body sites is the ease in isolation of the skin and its culturing compared to epidermis from other body regions which have more hair and hair follicles which would also interfere with UV experiments.

However, as an initial experiment, adult mouse ear epidermis was isolated and cultured for 48h before harvesting. *In vitro* culturing of adult ear skin is a drastic change in environment as well as in the supply of nutrients. Therefore, it was of great interest to determine whether *in vitro* culturing of adult ear epidermis has any effects on the expression of the epidermal stress marker Keratin6 (K6), and on autophagy markers.

To determine whether isolating and culturing adult ear epidermis induces stress, the expression of K6 was analysed. K6 is usually expressed in the hair follicle and in palmo-plantar epidermis as well as in stressed skin (Stark *et al.* 1987; Rothnagel *et al.* 1999). Immunofluorescence analysis of K6 in cultured mouse epidermis shows that K6 is only present in the hair follicles at 0h culture, indicating healthy and unstressed epidermis (Fig. 5.5). At 24h culture, K6 is expressed in the basal layer of the ear epidermal explants (Fig. 5.5). After 48h in culture epidermal K6 expression is further up-regulated (Fig. 5.5). This suggests that *in vitro* culturing of adult mouse ear epidermis induces a stress response and K6 expression.

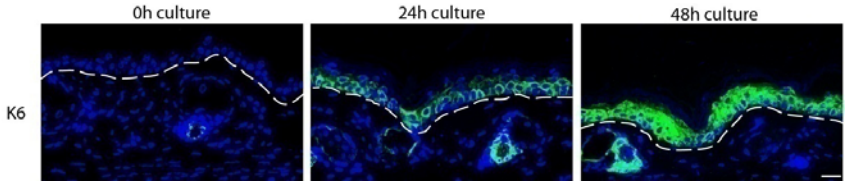

Figure 5.5: Expression of Keratin6 (K6) in cultured adult mouse ear epidermis.

Adult ear epidermis was cultured for 24h and 48h before harvesting. Immunofluorescence analysis of K6 expression shows it is absent in uncultured skin (0h culture). Culturing the epidermis for 24h induces expression of K6 which is further up-regulated after 48h in culture. These results suggest that culturing epidermis *in vitro* induces expression of the epidermal stress marker K6.

This figure is representative of n=2 different samples of adult mouse epidermis.

Bar = 20 um.

Immunofluorescence analysis of K6 expression in adult mouse ear explant cultures shows that the stress response of the epidermis increases with pro-longed *in vitro* culturing. As a next step, I wanted to determine whether epidermal differentiation in ear explant epidermis is affected by culture stress.

Immunofluorescence analysis of epidermal differentiation markers in adult ear explant cultures shows that the terminal differentiation marker loricrin is strongly expressed in the granular layer of uncultured ear explant epidermis (Fig.5.6). Ear explants cultured for 24h and 48h show a similar granular layer expression pattern of loricrin, suggesting terminal differentiation is unaffected by culture stress (Fig.5.6).

A marker of early keratinocyte differentiation, K1, which is usually expressed in the supra-basal layer of body epidermis, is expressed in all layers of uncultured adult ear epidermis with stronger expression around the hair follicles (Fig.5.6). This suggests that the expression pattern of K1 in mouse ear epidermis is slightly different from other body regions. However, after 24h in culture, K1 is still expressed in all layers of the explant epidermis but at very slightly higher expression levels compared to uncultured ear epidermis (Fig.5.6). The expression intensity of K1 is further marginally increased after 48h in culture (Fig.5.6). These results suggest that culture stress may affect~~s~~ K1 expression in adult ear explant cultures.

K14, a marker for proliferating keratinocytes is strongly expressed in the basal layer of uncultured adult ear epidermis (Fig.5.6) which is similar to K14 expression in body epidermis. After 24h in culture, K14 expression is very slightly reduced in the ear explant cultures (Fig.5.6) and these reduced K14 expression levels are maintained in the basal layer at 48h (Fig.5.6). Therefore, culturing adult ear explants *in vitro* marginally reduces the K14 expression levels in the basal layer~~ slightly~~, but this is not further ~~reduced~~ affected with pro-longed culture.

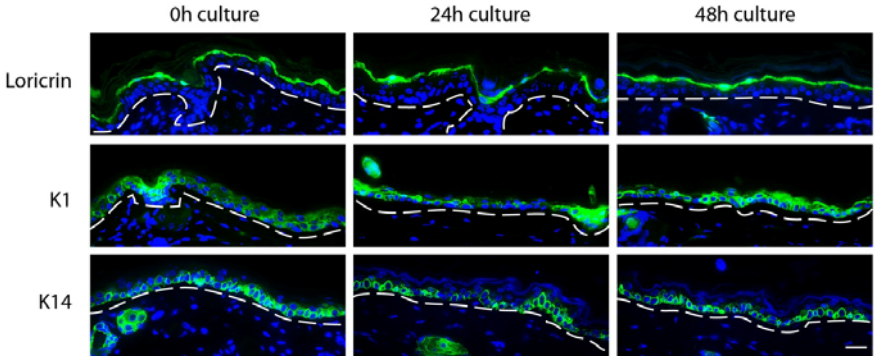

Figure 5.6: Expression of epidermal differentiation markers in cultured adult mouse ear epidermis.

Adult ear epidermis was cultured for 24h and 48h before harvesting. Immunofluorescence analysis of the terminal differentiation marker loricrin shows granular layer expression of loricrin in uncultured epidermis, as well as at 24h and 48h. K1, a marker for early keratinocyte differentiation, is expressed in all epidermal layers of uncultured ear epidermis, with a stronger expression around the developing hair follicle. At 24h and 48h, K1 is also expressed in all layers of the epidermis with increased expression intensity. K14, a marker for proliferating basal layer keratinocytes, is strongly expressed in the lower epidermal layers of uncultured ear explant skin. At 24h and 48h, K14 is still expressed in the basal layers of the ear explants, however at slightly lower expression levels compared to uncultured epidermis.

This figure is representative of n=2 different samples of adult mouse epidermis.

Bar = 20 um.

Culturing mouse ear epidermis *in vitro* induces a stress response which leads to a ~~slight~~ marginal increase in K1 expression levels accompanied by a very slight decrease in K14 expression intensities. However, the K1 and K14 expressing compartments are not changed, only the expression intensities are altered. The loricrin positive terminally differentiating keratinocytes are unaffected by culture stress. This suggests that in adult ear epidermal explants, the layers of epidermis representing different keratinocyte differentiation stages are still maintained, but there is a change in the expression levels of epidermal differentiation markers.

Therefore, mouse ear epidermal explant cultures are a suitable model to analyse the effects of *in vitro* culture stress on the epidermis. The expression of autophagy markers, in this model for epidermal culture stress, was then analysed.

Immunofluorescence analysis shows that at 0h culture, there is very low expression of LC3 in the ear epidermis however LC3 is highly expressed in the hair follicles and sebaceous glands (Fig. 5.7). WIPI1 is strongly expressed in the granular and cornified layers of uncultured epidermis (Fig. 5.7). The ATG5-ATG12 complex as well as BECN1, show low expression levels in the basal layer of uncultured ear epidermis. However, BECN1 and ATG5-ATG12 are strongly expressed in the hair follicles and the sebaceous glands of the ear explant epidermis (Fig. 5.7).

24h after *in vitro* culture of ear epidermis explants, which shows K6 expression (Fig. 5.5), LC3 is strongly up-regulated in all layers of the ear explant epidermis (Fig. 5.7). BECN1 and ATG5-ATG12 expression is also increased however their expression is still confined to the basal layer (Fig. 5.7).

Ear explant epidermis cultured for 48h maintains the LC3 expression in all layers of the epidermis however the intensity of LC3 expression is increased (Fig. 5.7). BECN1 and ATG5-ATG12 are still highly expressed in the basal layers of the ear explant cultures, similar to ear epidermis explants cultured for 24h (Fig. 5.7). WIPI1 expression is unaffected by culture stress and is still present as puncta in the upper layers of the ear epidermis explants (Fig. 5.7).

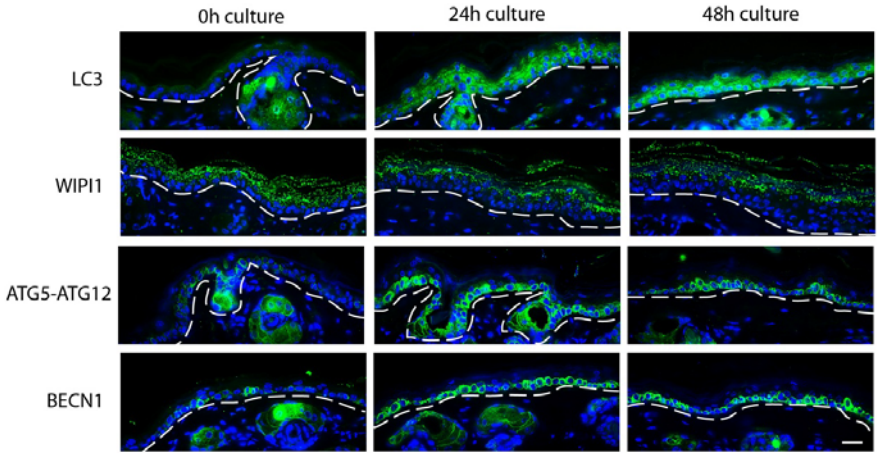

Figure 5.7: Immunofluorescence analysis of autophagy markers in cultured adult mouse ear epidermis.

Immunofluorescence analysis of LC3 expression shows it is expressed at low levels in the epidermis of uncultured skin (0h culture). After 24h in culture, LC3 expression is highly up-regulated in all layers of the epidermis and these high levels of LC3 are maintained at 48h. However under all culture conditions, LC3 is strongly expressed in the hair follicles and in the sebaceous glands. At 0h culture, WIPI1 is strongly expressed in the upper layers of ear epidermis. However, 24h and 48h culture induces a slight reduction in WIPI1 levels. ATG5-ATG12 is mainly expressed in the hair follicle in uncultured ear skin. After 24h and 48h culture, ATG5-ATG12 is strongly expressed in the basal layer of the ear epidermis. At 0h, BECN1 shows a patchy basal layer expression pattern which is then up-regulated and continuously expressed in the basal layer of 24h and 48h cultured epidermis. ATG5-ATG12 and BECN1 are also present in hair follicles and sebaceous glands of the ear epidermis.

This figure is representative of n=2 different samples of adult mouse epidermis.

Bar = 20 um.

These results show that ear epidermis is stressed by *in vitro* culturing and this induces the expression of K6. Uncultured ear epidermis does not express K6 and shows low expression levels of LC3, ATG5-ATG12 and BECN1. *In vitro* cultures of ear epidermis explants show high expression levels of LC3 in all layers of the epidermis and increased basal layer expression of ATG5-ATG12 and BECN1. This shows that culturing of adult ear epidermis induces stress as well as increases expression of autophagy markers. The high expression levels of LC3 in stressed ear epidermis suggest increased levels of autophagy in all epidermal layers.

To determine whether autophagy levels are up-regulated in stressed ear explants, I performed Western blot analysis of ear epidermis explant lysates. Culturing ear epidermis for 24h induces an increase in LC3II levels compared to LC3II at 0h (Fig. 5.8). This suggests increased autophagosome formation and higher autophagy levels induced by the stress of *in vitro* culturing. BECN1 is also up-regulated in ear explants cultured for 24h compared to 0h (Fig. 5.8). However, no changes in the ATG5-ATG12 expression level was detected with Western blot analysis (Fig. 5.8). The expression levels of ATG5-ATG12 at both 0h and 24h are very high, so any subtle change in ATG5-ATG12 expression levels may not be detected.

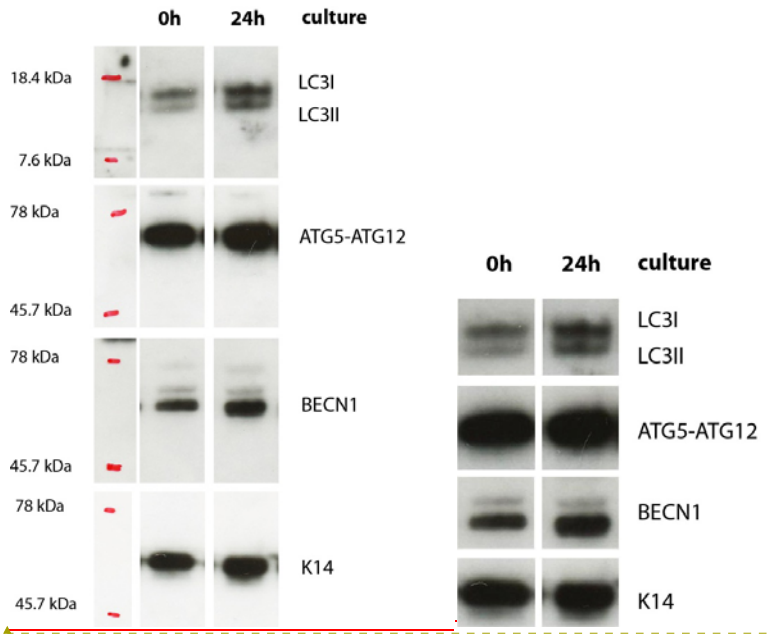

Formatted: Font: 12 pt

Figure 5.8: Western blot analysis of autophagy markers in cultured adult mouse ear epidermis.

The expression levels of autophagy markers LC3, BECN1 and ATG5-ATG12 were analysed in epidermal protein lysates of cultured ear explants using Western blot analysis. The expression levels of BECN1 are increased after 24h culture compared to BECN1 levels in uncultured epidermis. The ATG5-ATG12 complex is expressed at very high levels at both 0h and 24h cultures so, any subtle change in ATG5-ATG12 levels is not clear. After 24h culture, the level of LC3II is increased compared to the uncultured epidermis.

This figure is representative of n=2 different samples of adult mouse epidermis.

In vitro culturing of adult ear epidermis explants induces K6 expression suggesting the culture conditions trigger a stress response in the ear epidermis explants. Immunofluorescence analysis of LC3 shows that culture stress induces a high up-regulation of LC3 in all epidermal layers. This was confirmed by Western blot analysis which shows increased LC3 cleavage after 24h in culture, suggesting increased autophagosome formation in stressed epidermis. Both immunofluorescence and Western blot analysis show that culture stress also increases BECN1 levels, which is predominantly expressed in the basal layers of ear epidermis. Immunofluorescence analysis also shows higher ATG5-ATG12 expression in the basal layer of stressed ear epidermis explants. However, Western blot analysis could not confirm this.

The ear epidermis contains numerous hair follicles and sebaceous glands which may contaminate epidermal protein lysates analysed by Western blotting although the dermis was separated from the epidermis before protein lysates were prepared. However, immunofluoresence analysis of autophagy markers in ear epidermis explants also shows that the expression of these proteins in hair follicles and in sebaceous glands does not vary in response to culture stress.

Therefore, in this section I show that *in vitro* culturing of adult ear epidermis induces stress as well as an increase in autophagy levels. Therefore, autophagy may be an epidermal stress response which occurs in all layers of the epidermis, similar to UV-induced autophagy. This model was therefore not suitable for my initial plan to analyse the effects of UV on epidermal autophagy.

5.4 Expression of autophagy markers during HPV8-induced cSCC formation in adult mouse epidermis.

There is some controversy in the research field as to whether cutaneous HPV infections are linked to SCC formation (Harwood *et al.* 2004; Arron *et al.* 2011; commentary in Schiller and Buck 2011; reviewed in McLaughlin-Drubin *et al.* 2012; Neale *et al.* 2013). However, HPV8 transgenic mice expressing the complete early region of HPV8 (HPV8-CER) under the K14 promoter have been shown to develop epidermal dysplasias, papillomas and cSCCs with age and also, after UV exposure (Schaper *et al.* 2005; Marcuzzi *et al.* 2009; Hufbauer *et al.* 2010).

Paraffin-embedded mouse tissue samples of transgenic hemizygous mice expressing all early genes of HPV8 (HPV8-CER) under the control of the K14 promoter backcrossed into the FVB/N background were kindly provided by B. Akguel (Schaper *et al.* 2005; Hufbauer *et al.* 2010). HPV8-CER transgenic mice were shaved and exposed to a combination of 10 J/cm^2 UVA and 1 J/cm^2 UVB on 4 cm^2 areas of skin.

The transgene is controlled by the human K14 promoter and this restricts HPV8-CER expression to mainly the basal layer and reduced expression in the spinous layer. UV exposure increases epidermal K14 expression and induces hyperproliferation and expansion of the K14 expressing keratinocytes (Fig. 5.3; Kinouchi *et al.* 2002). So, in HPV8-transgenic mice, UV exposure activates K14 as well as HPV8-CER. As wild-type epidermis recovers from UV exposure, K14 expression and hyperplasia is reduced (Fig. 5.3), whereas in the transgenic mice, HPV8-CER expression is further increased with proliferation of HPV8-CER expressing keratinocytes. This leads to formation of papillomas and also SCCs (Marcuzzi *et al.* 2009; Hufbauer *et al.* 2010).

I decided to use this mouse model to determine whether autophagy marker expression is changed during HPV8-mediated SCC formation. UV exposed HPV8-CER transgenic mouse skin was harvested just before UV irradiation (d0) and then at different time points after UV exposure. H&E staining of HPV-8 mouse skin samples shows 3 days (d3) after UV irradiation, the epidermis is hyperproliferative compared

to d0 (Fig. 5.9a). This is similar to the UV-induced hyperplasia observed in healthy mouse epidermis at d3 (Fig 5.3). However, at d10 in HPV8 mice, epidermal hyperproliferation is increased and the epidermis is thicker than at d3. At d24, papillomas are formed (Fig. 5.9a). These results show that UV-induced hyperproliferation does not recover in HPV8-transgenic mice but leads to the formation of papillomas, confirming published data (Hufbauer *et al.* 2010).

Next, I wanted to determine the expression pattern of epidermal differentiation markers during HPV8-induced papilloma formation. The terminal differentiation marker, loricrin is strongly expressed in the granular layer of non-irradiated HPV8-CER mouse epidermis (Fig. 5.9b). At d3, loricrin is still present in the granular layer of the hyperproliferative epidermis however its expression intensity is reduced (Fig. 5.9b). At d10, loricrin is strongly expressed in the upper layers of the dysplastic epidermis and also in the keratin whorls of the papillomas at d24 (Fig. 5.9b). This suggests that where cornification can occur, in the uppermost layers of the epidermis, or within the papillomas, loricrin is expressed.

K1, a marker for early keratinocyte differentiation is expressed in the supra-basal layers of untreated HPV8-CER mouse epidermis (Fig. 5.9b). At d3, K1 is only expressed in very few supra-basal keratinocytes of the hyperproliferative epidermis (Fig. 5.9b). At d10, when epidermal hyperproliferation is further increased, K1 is still expressed in only a few supra-basal cells (Fig. 5.9b). In the papillomas at d24, K1 is expressed at low levels in a few keratinocytes (Fig. 5.9b). These results suggest that hyperproliferation induced by UV exposure and activation of the transgene HPV8-CER, lead to a reduction in K1 expression.

In untreated transgenic mouse epidermis, K14, a marker for proliferating keratinocytes, is mainly expressed in the basal layer and in the hair follicle (Fig. 5.9b). At d3, corresponding to the first signs of epidermal hyperplasia in the time points analysed, K14 expression is highly up-regulated in all layers of the epidermis (Fig. 5.9b). At d10, when epidermal thickness and hyperproliferation is further

increased, K14 is still expressed in all epidermal layers (Fig. 5.9b). and is maintained in the papillomas at d24 (Fig. 5.9b). This suggests that UV exposure of HPV8-CER transgenic mouse skin induces high expression of K14 and expansion of the K14 expressing keratinocytes, which are still present in the fully formed papillomas.

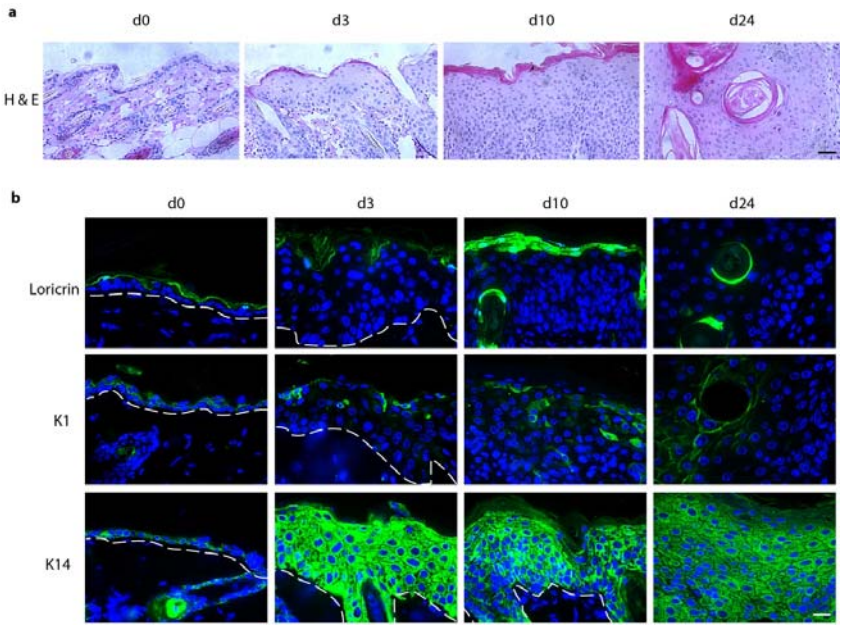

Figure 5.9: Expression of epidermal differentiation markers during HPV8-induced papilloma formation in mice.

(a) H&E staining of mouse epidermis before and during UV-mediated HPV8-induced papilloma formation shows the healthy epidermis at d0, epidermal hyperproliferation at d3 which is further increased at d10 and papilloma formation at d24.

(b) Immunofluorescence analysis of epidermal differentiation markers shows expression of the terminal differentiation marker, loricrin in the granular layers of d0 epidermis. Loricrin expression is down-regulated at d3, but is still present in the granular layers. Granular layer loricrin expression is restored at d10 and, at d24 loricrin is also present in the whorls of the papillomas. K1, a marker for early epidermal differentiation is expressed in the supra-basal layers of epidermis at d0. At d3 and d10, K1 expression is strongly down-regulated with a few supra-basal keratinocytes still expressing K1. K1 remains down-regulated at d24 with a very low expression in some regions of the papillomas. K14, a marker for proliferating keratinocytes is expressed in the basal layer of d0 epidermis. At d3, K14 expression is strongly up-regulated in all epidermal layers and is maintained at d10 and d24.

This figure is representative of n=2 different samples of adult mouse epidermis.

Bar = 20 um.

During UV-induced constitutive expression of the HPV8-CER transgene in mouse epidermis, which induces epidermal hyperproliferation and papilloma formation, the K1 positive differentiated keratinocyte compartment is down-regulated and the K14 expressing undifferentiated and proliferating keratinocyte compartment is expanded. Therefore, I determined the expression pattern of autophagy markers during HPV8-CER induced epidermal papilloma formation.

In the untreated HPV8-CER transgenic mouse epidermis, the autophagosome marker LC3 is strongly expressed in the granular layers (Fig. 5.10). ULK1 and WIPI1 also show a granular layer expression pattern similar to their expression pattern in wild type mouse skin (Fig. 5.10; see section 3.2 and section 5.2). The ATG5-ATG12 complex and BECN1, which are predominantly expressed in the basal layer of wild-type mouse epidermis (Fig. 5.4) as well as in human epidermis (Fig. 3.2), are also strongly expressed in the basal layer of untreated HPV8-CER mouse epidermis (Fig. 5.10). These results show that untreated HPV8-CER transgenic mouse epidermis has an autophagy marker expression profile similar to untreated wild-type epidermis.

At d3, LC3 expression is up-regulated in all layers of the hyperproliferative epidermis (Fig. 5.10). ATG5-ATG12 and BECN1 expression is also increased and is present in all layers of the hyperproliferative epidermis (Fig. 5.10). ULK1 and WIPI1, which show a strong granular layer expression pattern in untreated epidermis, are strongly down-regulated in the hyperproliferative epidermis at d3 (Fig. 5.10).

At d10, when epidermal thickness and hyperproliferation is further increased in HPV8-transgenic mouse epidermis, LC3 is still highly expressed in all epidermal layers (Fig. 5.10). BECN1 and the ATG5-ATG12 complex are also expressed in all layers of the hyperproliferative epidermis however their expression intensities are reduced compared to the earlier time point at d3 (Fig. 5.10). ULK1 and WIPI1 which were not expressed in the upper epidermal layers at d3 are expressed at low levels in the upper layers of d10 transgenic mouse epidermis (Fig. 5.10).

At d24, when papillomas are formed, LC3 is still strongly expressed in the papillomas, as well as BECN1 and ULK1 (Fig. 5.10). The ATG5-ATG12 complex is down-regulated but is still present in the papillomas and WIPI1 cannot be detected in the papillomas with immunofluorescence analysis (Fig. 5.10).

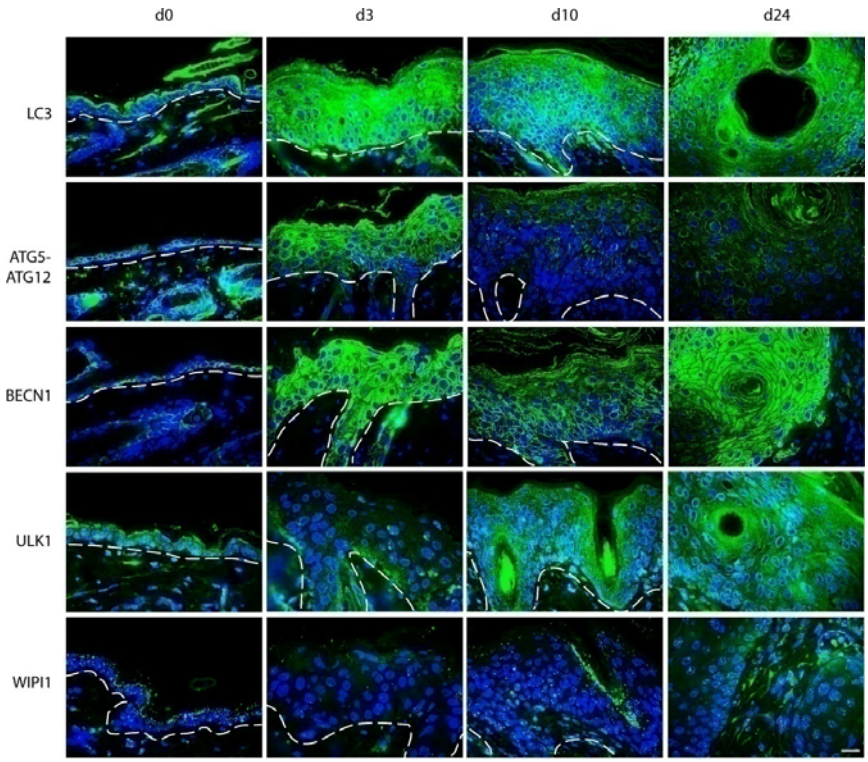

Figure 5.10: Expression of autophagy markers during HPV8-induced papilloma formation in mice.

Immunofluorescence analysis of LC3 shows strong granular layer expression at d0. At d3 and d10, LC3 expression is strongly up-regulated in layers of the epidermis. LC3 is slightly reduced but is still present in the papillomas at d24. The expression pattern of ATG5-ATG12 and BECN1 are very similar with strong basal layer expression at d0. At d3, both ATG5-ATG12 and BECN1 are highly up-regulated in all layers of the epidermis. At d10 ATG5-ATG12 and BECN1 are still present in all layers of the hyperproliferative epidermis but their expression is reduced. This expression pattern is maintained in the papillomas at d24. ULK1 and WIPI1 which are strongly expressed in the granular layer at d0, are down-regulated in the hyperproliferative epidermis at d3. At d10, both ULK1 and WIPI1 are still expressed at low levels in the upper epidermal layers. However, in the papillomas at d24, ULK1 and WIPI1 are absent.

This figure is representative of n=2 samples of adult mouse epidermis. Bar = 20 um.

Therefore, during UV-induced HPV8-CER over-expression in mouse epidermis resulting in papilloma formation, LC3 expression is up-regulated in epidermal hyperplasia as well as in the papillomas which later develop. Similarly, BECN1 expression is increased in hyperproliferating epidermis and its expression is maintained in papillomas. The ATG5-ATG12 complex is initially up-regulated after UV exposure of the HPV8-transgenic mouse epidermis, but then its expression is reduced in the hyperproliferative epidermis and in papillomas. Both ULK1 and WIPI1 expression is down-regulated in the hyperproliferative epidermis of the transgenic mouse skin. However, as the epidermal hyperplasia progresses, ULK1 expression recovers and is present in the papillomas. WIPI1 expression recovers in some regions of the dysplastic epidermis but is absent in the papillomas.

In conclusion, UV-induced over-expression of HPV8-CER in mouse epidermis induces a reduction in the differentiated keratinocyte compartment and an expansion of the undifferentiated proliferating keratinocytes but, it does not affect the terminally differentiating keratinocytes. During UV-induced epidermal hyperplasia and papilloma formation in HPV8-CER mouse epidermis, autophagy marker expression is deregulated. However, LC3 expression levels are constantly increased. This does not indicate an increase in overall autophagy levels, but it suggests that the autophagy pathway may be involved during epidermal hyperproliferation and its progression to papillomas.

5.5 Expression of autophagy markers in human epidermal SCCs

Immunosuppressed organ-transplant recipients (OTRs) have a 60-100-fold higher incidence of cSCCs compared to the healthy population (Berg and Otley 2002; Hofbauer *et al.* 2010). cSCCs are characterised by abnormal keratinocyte morphology, high keratinocyte proliferation, disrupted keratinocyte differentiation and invasion of the neighbouring tissue by abnormal keratinocytes (reviewed in Ratushny *et al.* 2012).

In the previous section I show that autophagy may be involved in the development of HPV8-induced papillomas. However, expression of the HPV8-transgene may affect autophagy levels and this may not reflect the true autophagy levels in non-HPV8 tumours. Also, most of the samples analysed are still papillomas and not fully developed cSCCs. Therefore, I wanted to determine whether the autophagy marker LC3 is expressed in human cSCCs and whether there is any correlation between human OTR cSCC tumours grade and LC3 expression levels.

Immunoflu~~r~~orescence analysis of LC3 was performed on cSCC tumour samples from OTRs treated with azathioprine, cyclosporine, prednisolone and acitretin, of which the first three reduce patient immune response and the last, is a retinoid which induces keratinocyte differentiation and reduces epidermal hyperplasia. Tumour grade is a histological diagnosis which depends on tumour cell differentiation stage, levels of necrosis, levels of mitotic activity and depth of invasion (Tufaro *et al.* 2011). The higher the tumour grade, the more aggressive the cSCC is, leading to worse patient prognosis. The tumour differentiation stage reflects the degree of keratinization and poor tumour differentiation is associated with a worse prognosis. Therefore, I wanted to determine whether there is any correlation between SCC tumour differentiation stage, which is a factor determining tumour grade, and LC3 expression in the tumours.

In well differentiated cSCCs, from OTRs LC3 is highly expressed (Fig. 5.11, **a-e**). However, there are variations in LC3 expression intensities within the individual

tumours, but overall, there is a high expression of LC3 (Fig. 5.11, **a-e**). A well differentiated cSCC from an immunocompetent individual has much lower levels of LC3 expression compared to LC3 levels in well differentiated cSCCs from OTRs (Fig. 5.11, **a-f**).

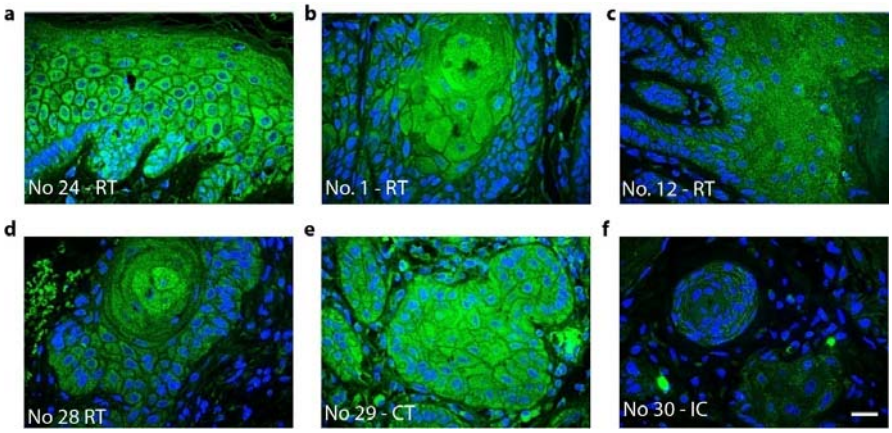

Figure 5.11: Expression of LC3 in well differentiated cSCCs.

Immunofluorescence analysis of LC3 was performed on well differentiated cSCCs from immunosuppressed OTRs (**a-e**) and compared to a low grade cSCC tumour from an immuno-competent individual (**f**). Expression levels of LC3 within the same tumour vary but overall, LC3 is highly expressed in well differentiated cSCCs from immuno-suppressed OTRs (**a-e**) compared to a well differentiated cSCC tumour from an immuno-competent individual (**f**).

This figure is representative of 3 images from n=6 cSCCs from OTRs and 3 images from n=1 cSCC from an immuno-competent patient.

RT = renal transplant; CT = cardiac transplant; IC = immuno-competent.

White bar = 20um

These results suggest that LC3 is expressed in well differentiated cSCCs of both immuno-suppressed and immuno-competent patients. However, in immuno-suppressed patients LC3 expression is highly up-regulated.

Therefore, the next step was to analyse LC3 expression in poorly differentiated cSCCs of both immuno-suppressed and immuno-competent patients (Fig. 5.12). Immunofluorescence analysis of LC3 shows that LC3 is expressed in poorly differentiated cSCCs of OTRs however LC3 expression levels vary from patient to patient (Fig. 5.12, **g-k**). A poorly differentiated cSCC from an immuno-competent individual shows LC3 expression, but LC3 expression levels are lower than in poorly differentiated cSCCs from immuno-suppressed OTRs (Fig. 5.12, **g-l**).

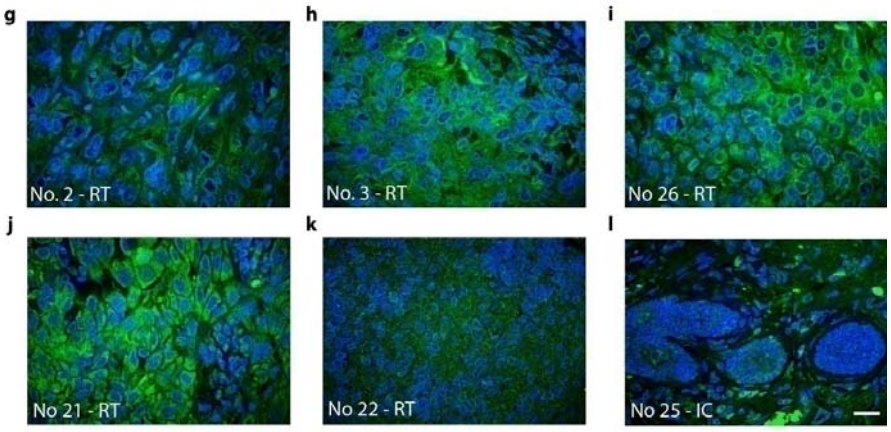

Figure 5.12: Expression of LC3 in poorly differentiated cSCCs.

Immunofluorescence analysis of LC3 was performed on poorly differentiated cSCCs from immunosuppressed OTRs (**g-k**) and compared to a poorly differentiated cSCC tumour from an immuno-competent individual (**l**). LC3 is expressed in poorly differentiated cSCCs from OTRs however LC3 expression intensities vary from tumour to tumour. Compared to poorly differentiated cSCC from an immuno-competent individual, poorly differentiated cSCCs from OTRs express higher levels of LC3.

This figure is representative of 3 images from n=7 cSCCs from OTRs and 3 images from n=1 cSCC from an immuno-competent patient.

RT = renal transplant; IC = immuno-competent.

White bar = 20um.

Poorly differentiated SCCs are characterised by expansion of undifferentiated cells which invade the nearby tissues. LC3 is expressed in poorly differentiated cSCCs of OTRs, however LC3 expression levels vary from patient to patient. A poorly differentiated cSCC from an immuno-competent patient is also positive for LC3, but LC3 expression levels are much lower compared to poorly differentiated cSCCs from OTRs. Therefore, in both well differentiated and poorly differentiated cSCCs, LC3 expression levels are higher in OTRs compared to immuno-competent patients. This suggests that other factors including immune status influence LC3 expression levels.

Poorly differentiated cSCCs are associated with worse patient prognosis whereas well differentiated cSCCs are not as invasive and are associated with higher patient recovery. Therefore, I wanted to determine whether there is any correlation between LC3 expression levels and SCC tumour differentiation stage.

In Fig. 5.11 and 5.12, it has been established that both well differentiated and poorly differentiated cSCCs of immuno-suppressed OTRs have higher LC3 expression levels compared to well differentiated and poorly differentiated cSCCs of immuno-competent patients respectively. However, in immuno-suppressed OTRs, LC3 expression levels in well differentiated cSCCs are much higher than in poorly differentiated cSCCs (Fig. 5.13, **m-n**; **p-q**). In immuno-competent patients, the LC3 expression intensities are reversed with lower LC3 levels in well differentiated cSCCs compared to LC3 expression intensities in poorly differentiated cSCCs (Fig. 5.13, **o**; **r**).

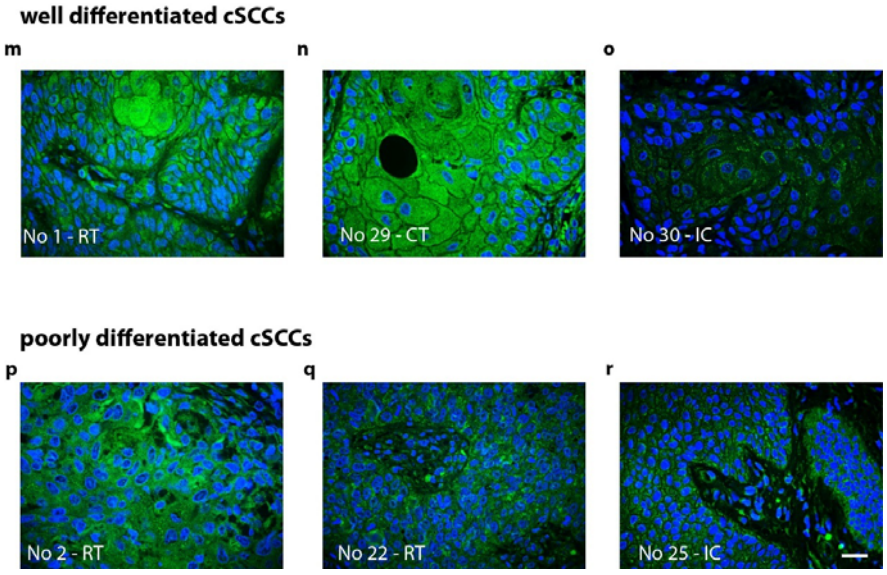

Figure 5.13: Comparison of LC3 expression in well differentiated and in poorly differentiated cSCCs.

Immunofluorescence analysis of LC3 in well differentiated and in poorly differentiated cSCCs from both immunosuppressed OTRs and in immuno-competent patients shows that LC3 is highly expressed in well differentiated cSCCs from OTRs (**m-n**) compared to LC3 levels in cSCC from immuno-competent patients (**o**).

In poorly differentiated cSCCs from OTRs (**p-q**), LC3 is also expressed but at lower levels compared to well differentiated cSCCs from OTRs (**m-n**). However, LC3 expression levels in poorly differentiated cSCCs from OTRs vary from patient to patient (**p-q**).

But compared to the LC3 expression intensity in the poorly differentiated cSCC from the immuno-competent individual (**r**), poorly differentiated cSCCs from OTRs have higher expression levels of LC3 (**p-q**).

This figure is representative of 3 images from n=6 well differentiated and n=7 poorly differentiated cSCCs from OTRs. And 3 images each from n=1 well differentiated cSCC and n=1 poorly differentiated cSCC from different immuno-competent patients.

RT = renal transplant; CT = cardiac transplant; IC = immuno-competent.

White bar = 20um

Immunofluorescence analysis of LC3 expression in cSCCs suggests that in OTRs, LC3 expression levels are higher in well differentiated cSCCs compared to poorly differentiated cSCCs. But in immuno-competent individuals, it is the opposite with poorly differentiated cSCCs showing higher expression of LC3 compared to well differentiated cSCCs.

In conclusion, immunofluorescence analysis of LC3 expression in cSCCs shows that LC3 expression levels depend on immune status and also on tumour differentiation grade.

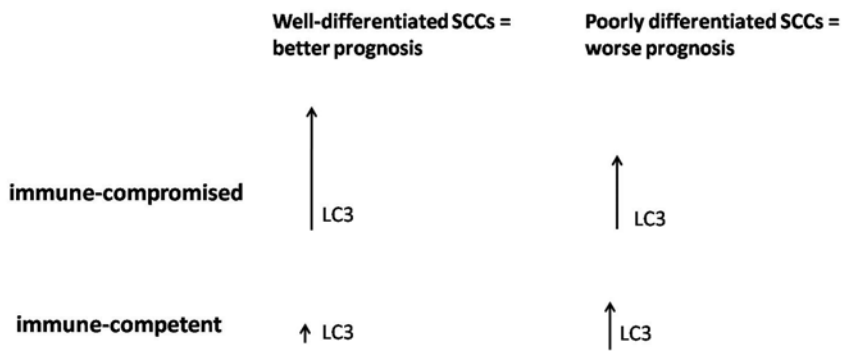

Figure 5.14: A scheme representing the LC3 expression levels in well differentiated and in poorly differentiated cSCCs from both immune-compromised and immune-competent patients.

In immunosuppressend OTRs, LC3 is present at higher levels in well differentiated cSCCs compared to the LC3 levels in poorly differentiated cSCCs. In immune-competent patients, LC3 is expressed at much lower levels in well-differentiated cSCCs compared to poorly differentiated cSCCs. However, LC3 levels in both tumour differentiation grades are higher in cSCCs from immune-compromised patients compared to cSCCs from immuno-competent patients.

In this chapter, I have shown that in the epidermal barrier defect diseases psoriasis, granular layer LC3 expression is absent in psoriatic lesions characterised by improper terminal differentiation. Autophagy can also be an epidermal stress response, induced by UV or culture stress, which alters autophagy marker expression and increases LC3 levels in all epidermal layers suggesting that all layers of the epidermis are capable of autophagy. During papilloma and cSCC formation, autophagy marker expression is altered suggesting autophagy may play a role in the formation of epidermal SCCs. However, in patient cSCCs, LC3 expression is higher in well differentiated tumours compared to poorly differentiated tumours of OTRs. And compared to cSCCs from immuno-competent individuals, LC3 levels are higher in OTRs.

Discussion

In chapter 3, I show that autophagy is a mechanism of nucleus degradation in terminally differentiating keratinocytes in culture. As a first step to test this *in vivo*, I analysed the autophagy marker expression pattern in a skin disease due to barrier defects, psoriasis. Psoriasis is characterised by epidermal hyperproliferation and incomplete terminal differentiation, infiltration of immune cells and increased vascularisation (reviewed in Raychaudhuri 2012).

H&E staining of psoriatic epidermis shows that there is no clear granular layer in the lesional skin compared to the non-lesional epidermis where the granular layer is clearly defined (Fig. 5.1). Also LC3, which is strongly expressed in the granular layer of adult epidermis, is not expressed in psoriatic lesions where cornification does not occur. However, in non-lesional psoriatic skin where cornification occurs, LC3 is expressed in the granular layers (Fig. 5.2). These results suggest that where constitutive granular layer autophagy is present, cornification occurs.

However, immunofluorescence analysis of LC3 expression levels does not determine whether the autophagy process occurs or whether autophagy is functional. My results show that LC3, which is required for autophagosome formation, is not present in psoriatic lesions. This suggests that autophagy cannot occur in lesional psoriatic skin, and autophagy can be activated in non-lesional skin where LC3 is expressed. However, analysis of LC3 cleavage in psoriatic epidermal lysates, using Western blotting, would indicate whether autophagosome formation takes place in psoriatic epidermis. Also, the small samples size (6 patients) I used for my investigations should be enlarged for further analysis. The psoriasis samples used were archive material therefore there is no patient information available like age, body site and treatment, since these can affect severity of the disease and possibly also autophagy marker expression.

Published data using gene expression and proteomics analysis to characterise psoriatic epidermis has not revealed any deregulated autophagy genes (Cargill *et al.* 2007; Piruzian *et al.* 2010; Mitsui *et al.* 2012). Therefore, incompetent autophagy in psoriasis may be a consequence of other pathways being deregulated.

Most of my work has focused on characterising constitutive autophagy and its role in keratinocyte terminal differentiation. But I also show that in epidermis, autophagy is induced in response to stress like UV exposure and culture shock. Published data shows that UV induces epidermal hyperproliferation and epidermal thickening, and affects epidermal AKT isoform expression (Kinouchi *et al.* 2002; O'Shaughnessy *et al.* 2007b; Sully *et al.* 2012). AKT is a key regulator of epidermal development and differentiation (Calautti *et al.* 2005; Thrash *et al.* 2006; O'Shaughnessy *et al.* 2007) and it can also affect the autophagy pathway via mTORC1.

In mouse epidermis exposed to solar-simulated UV (10 J/cm^2 UVA and 1 J/cm^2 UVB), autophagy marker expression is deregulated and LC3, ULK1, ATG5-ATG12 and BECN1 are expressed in all layers of the epidermis (Fig. 5.4). This shows that all layers of the epidermis can express LC3 as well as other autophagy proteins, suggesting that all layers of the epidermis are capable of autophagy. UV-induced hyperproliferation coincides with increased autophagy marker expression in all epidermal layers. As, the epidermis recovers and hyperproliferation is reduced, autophagy marker expression also returns to normal (Fig. 5.3; Fig. 5.4). These results suggest that autophagy plays a role in the UV response of epidermis.

Excessive UV exposure can lead to increased ROS levels, DNA damage, apoptosis and formation of sunburn cells. However, the epidermal basal layer is well protected from UV-induced DNA damage, and sunburn cells usually form in the supra-basal layers (Karen L Agnew and Christopher). In healthy, non-irradiated epidermis, ATG5-ATG12 and BECN1 are strongly expressed in the basal layer where other autophagy markers are not expressed (Fig. 3.2; Fig. 5.4). Basal layer ATG5-

Field Code Changed

ATG12 and BECN1 are unaffected by mTORC1 inhibition in monolayer experiments as well as in foetal epidermal explants, suggesting they are not involved in constitutive granular layer autophagy (see chapter 4). However, solar-simulated UV induces an increase in ATG5-ATG12 and BECN1 in the basal layer as well as in the other epidermal layers (Fig. 5.4). These results suggest that other mechanisms regulate basal layer ATG5-ATG12 and BECN1 expression. Also, basal layer ATG5-ATG12 and BECN1 may be involved in the UV response of the epidermis suggesting that they may have a role in ensuring epidermal recovery and survival from UV damage. But it is unclear whether UV-induced ROS levels or UV-induced DNA damage, or both are the trigger for increased autophagy marker expression in my samples of UV-exposed epidermis. However, ROS also acts as a signalling molecule, inducing autophagy under starvation conditions (Scherz-Shouval and Elazar 2007; Scherz-Shouval *et al.* 2007) and, UV-induced DNA damage has also been shown to activate autophagy via AMPK in epidermal cells (Yang *et al.* 2012; Qiang *et al.* 2013).

Autophagy can also be an epidermal stress response to *in vitro* culture conditions, which deregulate autophagy marker expression patterns in adult ear explant epidermis (Fig. 5.7; Fig. 5.8). Culture stress also induced high LC3 expression in all layers of the epidermis similar to the UV response of adult epidermis (Fig. 5.7; Fig. 5.4). These results also suggest that all layers of the epidermis may be capable of autophagy.

The change from *in vivo* to *in vitro* nutrient supply and also, the high oxygen and moisture levels in the tissue incubator may have stressed the adult ear explant cultures which expressed increasing levels of K6, as well as high LC3 levels, with prolonged culture (Fig. 5.5; Fig. 5.7; Fig. 5.8). Normal culture conditions within the incubator are 5% CO_2/ 95% air (21% O_2) which is a much higher oxygen concentration than cells are exposed to *in vivo* (Adams 2009). ~~healthy tissues are exposed to (3-6% oxygen) (Klionsky *et al.*).~~ It has been published that in *in vitro* cultures of primary mammalian cells, the cells are exposed to high levels of stress or

Formatted: Font: Italic

Formatted: Font color: Auto

Formatted: Font color: Auto

"culture shock" which leads to their senescence (Sherr and DePinho 2000). This culture stress is due to high ROS levels which induces DNA damage and affects cellular signalling pathways (reviewed in Adams 2009). ROS is also a known inducer of autophagy in cultured cells (Scherz-Shouval and Elazar 2007; Scherz-Shouval *et al.* 2007). Therefore, this increase in autophagy markers observed in cultured ear epidermis explants, may be due to the ROS levels the explants are exposed to under the culture conditions which trigger a stress response and induce autophagy.

However, foetal epidermal explants previously used (see chapter 4) did not express K6 (work done by K. Sully; Appendix 21) and prolonged culture did not affect LC3 levels (see chapter 4). An explanation for this may be that, foetal epidermal explants, which were harvested before birth, were still growing in the amniotic fluid, so the high moisture levels within the incubator were suitable for these foetal explants. Also, foetal explants may adapt more easily to a change in environmental conditions, similar to the change at birth.

With these experiments, I show that the epidermis is also capable of induced autophagy in all epidermal layers, which may be required to ensure epidermal survival under stress conditions. This induced autophagy may be due to high ROS levels like in the ear explant cultures, or a combination of ROS and UV-induced DNA damage, like in the UV exposed mouse epidermis.

HPV infections ~~have been implicated~~play a role in cervical cancers, anogenital cancers and head and neck cancers (Shamanin *et al.* 1996; zur Hausen 1996; Gillison and Shah 2001; Burd 2003; Gillison and Lowy 2004). However, whether HPV infections are implicated in~~the~~ SCCs is still controversial (Harwood *et al.* 2004; Underbrink *et al.* 2008; Arron *et al.* 2011; Schiller and Buck 2011; McLaughlin-Drubin *et al.* 2012). A transgenic mouse model expressing HPV8-CER under the K14 promoter has been characterised and published showing that UV and age lead to formation of papillomas and in some cases, cSCCs (Schaper *et al.* 2005; Marcuzzi *et al.* 2009; Hufbauer *et al.* 2010). During HPV8-induced papilloma formation in

transgenic mice, autophagy marker expression is also deregulated and high LC3 and BECN1 levels are maintained in the papillomas (Fig. 5.10). This suggests a role for autophagy during the development of papillomas and possibly, SCCs.

However, it is unclear whether over-expression of HPV8 directly induces autophagy marker expression levels, or whether the change in autophagy markers is due to the papilloma formation. Two recent studies show controversial results on the effects of HPV16 on keratinocyte autophagy. One publication shows that HPV16 induces autophagy in primary keratinocytes as a host defence mechanism to protect against HPV16 infections (Griffin *et al.* 2013), whereas another study shows that HPV16 infections activate AKT/mTORC1 signalling inhibiting autophagy in keratinocytes (Surviladze *et al.* 2013).

Therefore, I wanted to determine whether there is any correlation between LC3 levels in patient cSCCs and the tumour differentiation status which is a factor determining tumour grade. Immuno-suppressed OTRs have a 65-100 fold higher risk of developing cSCCs (Berg and Otley 2002; Hofbauer *et al.* 2010). I analysed the LC3 expression levels in cSCCs from OTRs treated with a combined therapy of azathioprine and cyclosporine. In cSCCs from OTRs, well differentiated cSCCs express higher levels of LC3 than the poorly differentiated tumours (Fig. 5.13 and Fig. 5.14). However, in immuno-competent patients, the LC3 levels are reversed with higher LC3 levels in the poorly differentiated tumours compared to well differentiated cSCCs (Fig. 5.13 and Fig. 5.14). But, both poorly differentiated and well differentiated cSCCs from OTRs have higher LC3 levels than the tumours from immuno-competent patients (Fig. 5.11; Fig. 5.12; Fig.5.13). These results suggest that autophagy levels may vary in cSCCs depending on the immune status of the patients and the cSCC differentiation stage. This may have implications for the treatment of cSCCs with autophagy inhibitors like rapamycin and its analogues, which are known to reduce cSCC formation and progression in OTRS (Wulff *et al.* 2008; McQuillan *et al.* 2009; Salgo *et al.* 2010).

Rapamycin mediated-mTORC1 inhibition has been shown to reduce tumour proliferation and angiogenesis which probably contributes to rapamycin-mediated cSCC reduction (Guba *et al.* 2002; Koehl *et al.* 2004; Geissler 2008). However, further experiments are required to verify whether autophagy levels in cSCCs respond to mTOR inhibitors and if this increase in autophagy can lead to tumour cell death. Increased autophagy in healthy epidermis may also be a protective mechanism preventing formation of more cSCCs. However, my conclusions are based on findings using a small sample size which should be enlarged for future analysis.

My findings in this chapter show autophagy marker expression patterns in disease conditions as well as in response to stresses like UV exposure and culture schock. Modulation of constitutive granular layer autophagy may be important in the treatment of epidermal barrier diseases like psoriasis. Also, autophagy may play a role in the epidermal response to UV exposure which is also a high risk factor contributing to epidermal SCCs. Autophagy levels in cSCCs depend on immune status and tumour differentiation stage which may also have future therapeutic implications.

Chapter 6

Final Discussion

Final Discussion

The initial reason for investigating autophagy in epidermis, was the observation that OTRs on a new class of immunosuppressants, rapamycin and its analogues, develop less cSCCs. Rapamycin is an mTOR inhibitor which is also used routinely to induce autophagy (Klionsky *et al.* 2012). Rapamycin has been shown to reduce tumour proliferation and angiogenesis, as well as change the lipid composition of the epidermal cornified layer (unpublished data, K.Sully). However, the effects of rapamycin on epidermal autophagy have not yet been analysed. Therefore, since there was no published data on autophagy protein expression in the different epidermal compartments, the first step was to establish the autophagy marker expression profile in healthy epidermis.

The epidermis is made up of basal layer keratinocytes capable of self-renewal as well as differentiation forming the upper epidermal layers. In the granular layer, keratinocytes undergo terminal differentiation, a specialised form of cell death, characterised by loss of organelles and formation of squames. The epidermal autophagy marker expression pattern (ULK1, WIPI1, BECN1, ATG5-ATG12 and LC3) suggests that autophagy plays an important role in the terminal differentiation process of granular layer keratinocytes. Also, induction of autophagy marker expression during foetal development coincides with the initiation of epidermal terminal differentiation. These results suggest that autophagy is constitutively active in granular layer keratinocytes and may be important for granular layer formation. TEM analysis of 3 day old epidermis shows that autophagy vesicles ~~are~~ may be present in both the basal and granular layers. However, quantification of autophagic vesicles with TEM was not possible. Based on this data, I hypothesized

that constitutive autophagy is a mechanism of terminal differentiation in granular layer keratinocytes, where organelle degradation occurs.

To investigate this, *in vitro* experiments were carried out using monolayer primary keratinocyte cultures which were stimulated to differentiate by the well established method of increasing the calcium concentration in the culture media (Hennings *et al.* 1983; Menon *et al.* 1985; Yuspa *et al.* 1989; Elias *et al.* 2002). Analysis of autophagy during keratinocyte differentiation in monolayer cultures shows that the autophagy process occurs however, there are no striking differences in autophagy levels between undifferentiated and differentiated cultures. Closer analysis of the monolayer cultures revealed that differentiating keratinocytes undergo nucleophagy, autophagic degradation of the nucleus. This is different from micro-nucleophagy whereby satellite nuclei are formed due to stress or genome instability and are then engulfed by autophagosomes (Krick *et al.* 2008; Rello-Varona *et al.* 2012). Nucleophagy is characterised by engulfment of pieces of the nucleus leading to the complete removal of the nucleus (Park *et al.* 2009).

Nucleophagy in differentiating monolayer keratinocytes is characterised by accumulation of LC3/LAMP2/p62 positive autolysosomes which are DAPI negative but contain HP1α positive cargo in the regions of missing nuclei, suggesting selective autophagic degradation of nuclear material. HP1α is a non-histone chromosomal protein which is associated with highly condensed, transcriptionally inactive regions (James and Elgin 1986; James *et al.* 1989). However, while analysing the nucleophagic regions, a very low DAPI signal could sometimes be detected in the nucleophagic regions. But the intensity of DAPI was so low that imaging was impossible and could not be documented. This loss of DAPI in the nucleophagic regions could be due to conformational changes in the chromatin leading to the inability of DAPI to incorporate in the DNA. These observations of reduced or absent DAPI in the nucleophagic regions is similar to published data on autophagic degradation of nuclei in the aging intestinal epithelia in *C. elegans,* which may be

due to age-related changes in LMNA and compromised nuclear integrity (McGee *et al.* 2011).

In monolayer keratinocyte cultures, nucleophagic vesicles do not colocalise with LMNA, a nuclear envelope protein, suggesting they are outside the partially degraded nucleus. However, LMNA accumulates at the border between the still intact nucleus and the autophagic vesicles, suggesting a role for the nuclear membrane during keratinocyte nucleophagy. These observations are similar to observations made in fibroblasts isolated from a mouse model for nuclear envelopathies (Park *et al.* 2009).

However, in this mouse model, nucleophagy degrades γ-H2AX positive nuclear regions. γ-H2AX is a marker for DNA double-strand breaks and also plays a role in the recognition and repair of the damaged DNA (Fillingham *et al.* 2006). However, keratinocyte nucleophagy is not due to γ-H2AX positive DNA double-strand breaks. The HP1 proteins are known play important roles in chromatin formation and maintenance. More recently, HP1 proteins have been implicated in the cellular response to DNA damage. HP1 proteins localise to sites of UV-induced DNA damage, DNA double strand breaks and sites of oxidative DNA damage independently of other DNA damage repair proteins or mechanisms (Luijsterburg *et al.* 2009). This suggests that nuclear material within the autophagosome may be damaged or modified nuclear material, bound to HP1α, which is targeted for autophagic degradation. However, other markers of DNA damage were not analysed and would be an aim for future work.

Nucleophagy in monolayer keratinocytes is characterised by autophagic degradation starting at a specific region of the nucleus. The signal which specifies the exact region for the beginning of nucleophagy was not investigated. One possibility is that HP1α accumulation in specific regions of unwanted nuclear material could be the trigger for nucleophagy. There is also mounting evidence that HP1 proteins can be phosphorylated regulating their functions (LeRoy *et al.* 2009;

Hiragami-Hamada *et al.* 2011). Therefore, further analysis of HP1α posttranslational modifications in the nucleophagic regions may explain what signal determines the site of nucleophagy in monolayer keratinocytes.

In the epidermis, there is a calcium gradient which is lowest in the basal layer and increases gradually until it peaks in the granular layer before dropping drastically in the cornified layer (Menon *et al.* 1985; Elias *et al.* 2002b). Terminal differentiation is regulated by hormone signalling, transcription factors and lipids (Eckert *et al.* 1997). Epidermal calcium also regulates lamellar body secretion as well as expression of epidermal differentiation markers, the terminal differentiation process and barrier formation (Menon *et al.* 1985; Elias *et al.* 2002). Therefore, terminal differentiation probably is regulated by the interplay of various stimuli. Calcium levels also influence autophagy with some reports claiming calcium induces autophagy and others showing it inhibits autophagy (reviewed in Decuypere *et al.* 2011). Therefore, it is possible that the epidermal calcium levels and the changes in calcium concentrations between the layers, which play a role in regulating epidermal terminal differentiation, also influence constitutive granular layer autophagy.

For *in vitro* monolayer experiments, keratinocyte differentiation was also induced with high calcium concentrations in the media. *In vivo*, terminal differentiation is probably controlled by a combination of various stimuli including calcium. Therefore, future work should compare the effects of other methods of *in vitro* induction of terminal differentiation on autophagy, such as culturing keratinocytes in suspension cultures or exposure to TPA (reviewed in Watt 1988).

Cultured cells are exposed to high levels of cell stress due to the unsuitable culture conditions which cannot replace the optimal *in vivo* conditions. This culture stress or “culture shock” is responsible for the limited population doublings cultured primary cells are capable of before becoming senescent (Sherr and DePinho 2000; reviewed in Adams 2009). In my work, I show that *in vitro* culturing of adult ear explant epidermis induces high levels of stress which increase with time in culture.

This is also accompanied by a dramatic increase in LC3 expression levels and LC3 processing, suggesting increased autophagy due to culture stress. However, foetal epidermis does not express K6 in culture, suggesting it is not stressed (K. Sully, unpolished data). This may be due to the similar high moisture levels of the *ex vivo* and *in vivo* conditions. Foetal epidermis may also be more resistant to stress or may be able to adapt to changing environmental conditions more easily than adult epidermis.

Both undifferentiated and differentiated primary monolayer keratinocyte cultures were cultured under the same conditions therefore, both keratinocyte cultures were exposed to equal amounts of culture stress. Nucleophagy observed and characterised in differentiated keratinocytes is therefore not due to culture stress. However, culture stress or "culture shock" must always be considered when performing *in vitro* assays with cultured cells or tissues.

In monolayer keratinocyte cultures, impaired autophagy mediated by siRNA knockdowns of key autophagy genes prevents nucleophagy even after inducing terminal differentiation in culture. However, differentiated keratinocyte cultures are comprised of keratinocytes at different stages of differentiation including proliferating K14 positive keratinocytes, K1 expressing early differentiated cells and filaggrin positive terminally differentiating keratinocytes. In the differentiated culture, a fraction (~11%) of the keratinocytes undergoes nucleophagy at the time point of analysis. Since terminal differentiation in the epidermis is characterised by loss of organelles including the nuclei, it is possible that the nucleophagic monolayer keratinocyte fraction are those undergoing terminal differentiation in culture. Therefore, these findings show that autophagy may be a mechanism of nucleus degradation in differentiating keratinocytes. Future work would include analysing the expression of terminal differentiation markers in nucleophagic keratinocytes as well as in the other fractions of the differentiated keratinocyte cultures.

The epidermal AKT isoforms regulate epidermal proliferation and differentiation. AKT1 has been associated with differentiated keratinocytes whereas AKT2 is expressed in the less differentiated keratinocyes and has been associated with high SCC tumour grade (Fig. 4.1; Brash *et al.* 1991; Calautti *et al.* 2005; O'Shaughnessy *et al.* 2007b). Treatment of OTRs with rapamycin, an mTORC1 inhibitor, reduces the incidence and progression of SCCs (Wulff *et al.* 2008; McQuillan *et al.* 2009; Salgo *et al.* 2010). mTORC1 is down-stream of AKT and is also a key regulator of autophagy. I show that in cultured keratinocytes rapamycin inhibits the negative feedback loop between mTORC1 and IRS-1 leading to increased phosphorylation of AKT1. This supports published data showing that in epidermal explant cultures only AKT1, which is mainly expressed in the upper epidermal layers, and not AKT2, responds to rapamycin treatment with increased phosphorylation (Sully *et al.* 2012). This suggests that in addition to rapamycins anti-proliferative and anti-angiogenic effects, rapamycin may also exert its anti-tumourigenic potential through increased AKT1 activity promoting epidermal differentiation.

Rapamycin is a commonly used autophagy inducer for cultured cells. In my work I show that drug-induced mTORC1 inhibition, using rapamycin and Torin1, in organotypics and in epidermal explant cultures, leads to a strong increase in granular layer LC3 levels. This may be another benefit of treating OTRs with rapamycin, which may increase constitutive granular layer autophagy levels promoting epidermal terminal differentiation, further contributing to rapamycins anti-tumour properties.

I also observe that rapamycin treatment alters filaggrin expression in keratinocyte 3D-cultures and in mouse foetal epidermal explant cultures, by restricting filaggrin expression to fewer granular layers and also reducing its expression intensity. During terminal differentiation, filaggrin is degraded to urocanic acid, an important component of the natural moisturising factor which is required for epidermal hydration and protection from UV (Rawlings *et al.* 1994; Rawlings and Harding

2004). Therefore, an explanation for this may be that rRapamycin may speed up the processing of filaggrin to urocanic acid, reducing the amount of filaggrin still present in the upper epidermal layers. However, rapamycin also affects the lipid components in the cornified layer increasing the lipid content of the epidermis (K. Sully, unpublished data). Rapamycin also changes the expression pattern of the ATP-binding cassette transporter A12 (ABCA12) required for lipid transport. Loss of ABCA12 is associated with the skin barrier defect Harlequin ichthyosis, which is characterised by severe hyperkeratosis (Akiyama *et al.* 2005; Kelsell *et al.* 2005; Yanagi *et al.* 2008). Therefore, the effects of rapamycin on filaggrin expression may be a consequence of rapamycin-mediated changes in epidermal barrier properties.

To verify my hypothesis that autophagy is a terminal differentiation mechanism in granular layer keratinocytes *in vivo*, an epidermal barrier defect condition, psoriasis was used. Psoriasis is characterised by keratinocyte hyperproliferation, abnormal terminal differentiation and parakeratosis, inflammation and abnormal vascularisation (Griffiths and Barker 2007; Raychaudhuri 2012). Due to the incomplete and deregulated terminal differentiation in psoriatic plaques, the epidermal barrier is defective. I show that in the both lesional and non-lesional psoriatic epidermis, autophagy marker expression is deregulated. However, LC3 puncta are still present in the granular layer of non-lesional psoriatic epidermis but at a much lower expression level compared to healthy adult epidermis. In lesional psoriatic skin, LC3 is not expressed. These results show that LC3 is only expressed in epidermis which is capable of complete terminal differentiation. Therefore, autophagy may play an important role in terminal differentiation. Published data on mTOR in psoriasis shows that mTOR activity is deregulated in both lesional and non-lesional psoriatic epidermis, however, in lesional psoriasis, mTORC1 activity is increased (Kjellerup *et al.* 2009; Buerger *et al.* 2013). Autophagy is negatively regulated by mTORC1. Hyperactivation of mTORC1 would inhibit autophagy and this may explain why the autophagosome marker, LC3 aggregate formation is not detected with immunofluorescence analysis in psoriatic lesions.

In addition to this, published data shows that activation of Toll-Like-Receptor (TLR) signalling on keratinocytes causes inflammation. TLR signalling also induces p62 expression which further increases TLR signalling and, hyperproliferation and inflammation. In healthy keratinocytes, autophagy regulates epidermal p62 levels preventing inflammation. However, psoriatic epidermis expresses high levels of p62 which may be responsible for the high levels of inflammation in this disease (Miller 2008; Lee *et al.* 2011). My findings showing the autophagy process is absent or in complete in psoriatic lesions, may provide an explanation for the published work showing high p62 levels in psoriatic keratinocytes causing excessive inflammation.

Therefore, patients with epidermal barrier defect diseases such as psoriasis may profit from treatments with mTORC1 inhibitors. These could restore constitutive epidermal autophagy which may lead to normal terminal differentiation and barrier formation and, reduced inflammation and hyperproliferation. Another effect of the mTOR inhibitor, rapamycin, is a reduction in filaggrin protein levels in the upper epidermal layers. I hypothesize that this may be due to increased degradation of filaggrin to urocanic acid, a component of the natural moisturising factor, supporting epidermal barrier function.

Immunosuppressed OTRs treated with rapamycin and its analogues may also profit from similar effects of rapamycin on epidermal autophagy which protects the patients from acquiring new cSCCs and also prevents progression of already acquired cSCCs. Rapamycin may increase constitutive granular layer autophagy, supporting keratinocyte terminal differentiation and preventing the proliferation of potential and already existing cancer cells. Rapamycins effects on filaggrin and epidermal lipids (K. Sully, unpublished data) may also increase barrier protection against UV, one of the major risk factors for SCC formation. There are a number of ongoing clinical trials to determine the efficacy of mTOR inhibitors in treating skin cancers in OTRs (the TUMORAPA trial, the RESCUE study, the PROSKIN trial)

(Leblanc *et al.* 2011). However, the numerous side effects of rapamycin treatment reduce its popularity as an immunosuppressant (Leblanc *et al.* 2011).

To determine whether there is any correlation between cSCC differentiation grade and autophagy levels, I analysed the expression of LC3 in poorly differentiated and well differentiated non-rapamycin-treated cSCCs from OTRs. LC3 is expressed in both cSCC differentiation grades. However, LC3 expression levels are higher in well differentiated cSCCs compared to poorly differentiated tumours. And compared to cSCCs from immuno-competent patients, LC3 levels are higher in cSCCs from OTRs. These results suggest that autophagy levels in cSCCs may depend on tumour differentiation grade and on immune status of the patient.

My results, and published data, suggest that OTRs may profit from treatments with mTOR inhibitors, which have a preventive effect on cSCCs formation and progression rather than attempting to cure the acquired cSCCs. However, the development of newer mTOR inhibitors with milder side effects would be of a great benefit in treating these patients.

UV exposure, one of the main hazards the epidermis is exposed to is also a major risk factor contributing cSCC formation (Leiter and Garbe 2008). Solar-simulated UV is a mixture of UVA and UVB, which induce oxidative stress leading to high ROS levels, damaged DNA, proteins and lipids, which can induce autophagy (Yang *et al.* 2012; Qiang *et al.* 2013; Zhao *et al.* 2013). UV induces epidermal hyperproliferation and changes the AKT1 expression patterns in epidermis, which is a key regulator of keratinocyte differentiation (Kinouchi *et al.* 2002; O'Shaughnessy *et al.* 2007b; Sully *et al.* 2012). My data shows that autophagy marker expression patterns are deregulated in solar-simulated UV-exposed epidermis. LC3 which is confined to the granular layer of healthy unexposed epidermis is expressed in all epidermal layers in response to UV exposure. This shows that all epidermal layers are capable of LC3 expression and possibly also of autophagy. However, as the epidermis recovers and hyperproliferation is reduced, autophagy marker expression patterns return to

normal. These results suggest that stress-induced autophagy plays a role in the epidermal response to UV and may have a protective function ensuring recovery from UV-induced ROS and DNA damage.

Therefore, in epidermis, constitutive autophagy is associated with terminally differentiating keratinocytes of the granular layer where organelle degradation occurs, and inducible autophagy which occurs in all epidermal layers is a stress response.

In conclusion, the work presented in this thesis shows that autophagy is an important fundamental process in keratinocytes which contributes to the regulation of keratinocyte differentiation ensuring epidermal function. Autophagy may be a mechanism by which terminally differentiating keratinocytes of the epidermal granular layer degrade their organelles which is required for barrier formation. This may have implications for the treatment of patients with barrier defects. In immunosuppressed OTRs, autophagy may contribute to the anti-tumour properties of the drug, rapamycin and may be a preventive treatment against cSCCs. This could be of interest for the pharmaceutical industry in the development of anti-cancer treatments for patients at risk of developing skin cancers.

References

Adams, P. D. (2009). "Healing and hurting: molecular mechanisms, functions, and pathologies of cellular senescence." Mol Cell 36(1): 2-14.

Ahlberg, J., L. Marzella, et al. (1982). "Uptake and degradation of proteins by isolated rat liver lysosomes. Suggestion of a microautophagic pathway of proteolysis." Lab Invest 47(6): 523-532.

Akiyama, M., Y. Sugiyama-Nakagiri, et al. (2005). "Mutations in lipid transporter ABCA12 in harlequin ichthyosis and functional recovery by corrective gene transfer." J Clin Invest 115(7): 1777-1784.

Alam, M. and D. Ratner (2001). "Cutaneous squamous-cell carcinoma." N Engl J Med 344(13): 975-983.

Aldabagh, B., J. G. Angeles, et al. (2013). "Cutaneous squamous cell carcinoma and human papillomavirus: is there an association?" Dermatol Surg 39(1 Pt 1): 1-23.

Alessi, D. R., S. R. James, et al. (1997). "Characterization of a 3-phosphoinositide-dependent protein kinase which phosphorylates and activates protein kinase Balpha." Curr Biol 7(4): 261-269.

Amaravadi, R. K., J. Lippincott-Schwartz, et al. (2011). "Principles and current strategies for targeting autophagy for cancer treatment." Clin Cancer Res 17(4): 654-666.

Andjelkovic, M., D. R. Alessi, et al. (1997). "Role of translocation in the activation and function of protein kinase B." J Biol Chem 272(50): 31515-31524.

Antonsson, A., S. Karanfilovska, et al. (2003). "General acquisition of human papillomavirus infections of skin occurs in early infancy." J Clin Microbiol 41(6): 2509-2514.

Arias, E. and A. M. Cuervo (2011). "Chaperone-mediated autophagy in protein quality control." Curr Opin Cell Biol 23(2): 184-189.

Arron, S. T., J. G. Ruby, et al. (2011). "Transcriptome sequencing demonstrates that human papillomavirus is not active in cutaneous squamous cell carcinoma." J Invest Dermatol 131(8): 1745-1753.

Arstila, A. U. and B. F. Trump (1968). "Studies on cellular autophagocytosis. The formation of autophagic vacuoles in the liver after glucagon administration." Am J Pathol 53(5): 687-733.

Axe, E. L., S. A. Walker, et al. (2008). "Autophagosome formation from membrane compartments enriched in phosphatidylinositol 3-phosphate and dynamically connected to the endoplasmic reticulum." J Cell Biol 182(4): 685-701.

Aymard, E., V. Barruche, et al. (2011). "Autophagy in human keratinocytes: an early step of the differentiation?" Exp Dermatol 20(3): 263-268.

Baden, H. P. and J. Kubilus (1983). "The growth and differentiation of cultured newborn rat keratinocytes." J Invest Dermatol 80(2): 124-130.

Berg, D. and C. C. Otley (2002). "Skin cancer in organ transplant recipients: Epidemiology, pathogenesis, and management." J Am Acad Dermatol 47(1): 1-17; quiz 18-20.

Bickers, D. R. and M. Athar (2006). "Oxidative stress in the pathogenesis of skin disease." J Invest Dermatol 126(12): 2565-2575.

Bjedov, I., J. M. Toivonen, et al. (2010). "Mechanisms of life span extension by rapamycin in the fruit fly Drosophila melanogaster." Cell Metab 11(1): 35-46.

Blank, I. H. (1953). "Further observations on factors which influence the water content of the stratum corneum." J Invest Dermatol 21(4): 259-271.

Blommaart, E. F., J. J. Luiken, et al. (1995). "Phosphorylation of ribosomal protein S6 is inhibitory for autophagy in isolated rat hepatocytes." J Biol Chem 270(5): 2320-2326.

Bodemann, B. O., A. Orvedahl, et al. (2011). "RalB and the exocyst mediate the cellular starvation response by direct activation of autophagosome assembly." Cell 144(2): 253-267.

Boissy, R. E., J. R. Smyth, Jr., et al. (1983). "Progressive cytologic changes during the development of delayed feather amelanosis and associated choroidal defects in the DAM chicken line. A vitiligo model." Am J Pathol 111(2): 197-212.

Bowman, E. J., A. Siebers, et al. (1988). "Bafilomycins: a class of inhibitors of membrane ATPases from microorganisms, animal cells, and plant cells." Proc Natl Acad Sci U S A 85(21): 7972-7976.

Boya, P., R. A. Gonzalez-Polo, et al. (2005). "Inhibition of macroautophagy triggers apoptosis." Mol Cell Biol 25(3): 1025-1040.

Brash, D. E., J. A. Rudolph, et al. (1991). "A role for sunlight in skin cancer: UV-induced p53 mutations in squamous cell carcinoma." Proc Natl Acad Sci U S A 88(22): 10124-10128.

Broers, J. L., F. C. Ramaekers, et al. (2006). "Nuclear lamins: laminopathies and their role in premature ageing." Physiol Rev 86(3): 967-1008.

Buerger, C., B. Malisiewicz, et al. (2013). "mTOR and its downstream signalling components are activated in psoriatic skin." Br J Dermatol.

Burd, E. M. (2003). "Human papillomavirus and cervical cancer." Clin Microbiol Rev 16(1): 1-17.

Byrne, C., A. A. Avilion, et al. (2010). "Whole-mount assays for gene induction and barrier formation in the developing epidermis." Methods Mol Biol 585: 271-286.

Calautti, E., J. Li, et al. (2005). "Phosphoinositide 3-kinase signaling to Akt promotes keratinocyte differentiation versus death." J Biol Chem 280(38): 32856-32865.

Camisa, C. (2000). "Psoriasis: a clinical update on diagnosis and new therapies." Cleve Clin J Med 67(2): 105-106, 109-113, 117-109.

Campbell, C., A. G. Quinn, et al. (1993). "p53 mutations are common and early events that precede tumor invasion in squamous cell neoplasia of the skin." J Invest Dermatol 100(6): 746-748.

Candi, E., R. Schmidt, et al. (2005). "The cornified envelope: a model of cell death in the skin." Nat Rev Mol Cell Biol 6(4): 328-340.

Cargill, M., S. J. Schrodi, et al. (2007). "A large-scale genetic association study confirms IL12B and leads to the identification of IL23R as psoriasis-risk genes." Am J Hum Genet 80(2): 273-290.

Cecconi, F. and B. Levine (2008). "The role of autophagy in mammalian development: cell makeover rather than cell death." Dev Cell 15(3): 344-357.

Chan, E. Y., S. Kir, et al. (2007). "siRNA screening of the kinome identifies ULK1 as a multidomain modulator of autophagy." J Biol Chem 282(35): 25464-25474.

Chan, E. Y. and S. A. Tooze (2009). "Evolution of Atg1 function and regulation." Autophagy 5(6): 758-765.

Chen, S., S. K. Rehman, et al. (2010). "Autophagy is a therapeutic target in anticancer drug resistance." Biochim Biophys Acta 1806(2): 220-229.

Cho, H., J. Mu, et al. (2001b). "Insulin resistance and a diabetes mellitus-like syndrome in mice lacking the protein kinase Akt2 (PKB beta)." Science 292(5522): 1728-1731.

Cho, H., J. L. Thorvaldsen, et al. (2001). "Akt1/PKBalpha is required for normal growth but dispensable for maintenance of glucose homeostasis in mice." J Biol Chem 276(42): 38349-38352.

Christopher Potten, J. W.

Claerhout, S., L. Verschooten, et al. (2010). "Concomitant inhibition of AKT and autophagy is required for efficient cisplatin-induced apoptosis of metastatic skin carcinoma." Int J Cancer 127(12): 2790-2803.

Codogno, P., M. Mehrpour, et al. (2012). "Canonical and non-canonical autophagy: variations on a common theme of self-eating?" Nat Rev Mol Cell Biol 13(1): 7-12.

Codogno, P. and A. J. Meijer (2006). "Atg5: more than an autophagy factor." Nat Cell Biol 8(10): 1045-1047.

Conway, K. L., P. Kuballa, et al. (2013). "ATG5 regulates plasma cell differentiation." Autophagy 9(4).

Copp, J., G. Manning, et al. (2009). "TORC-specific phosphorylation of mammalian target of rapamycin (mTOR): phospho-Ser2481 is a marker for intact mTOR signaling complex 2." Cancer Res 69(5): 1821-1827.
Crotzer, V. L. and J. S. Blum (2009). "Autophagy and its role in MHC-mediated antigen presentation." J Immunol 182(6): 3335-3341.
Cuervo, A. M., E. Knecht, et al. (1995). "Activation of a selective pathway of lysosomal proteolysis in rat liver by prolonged starvation." Am J Physiol 269(5 Pt 1): C1200-1208.
Daido, S., T. Kanzawa, et al. (2004). "Pivotal role of the cell death factor BNIP3 in ceramide-induced autophagic cell death in malignant glioma cells." Cancer Res 64(12): 4286-4293.
Debnath, J., E. H. Baehrecke, et al. (2005). "Does autophagy contribute to cell death?" Autophagy 1(2): 66-74.
Decuypere, J. P., G. Bultynck, et al. (2011). "A dual role for Ca(2+) in autophagy regulation." Cell Calcium 50(3): 242-250.
Degenhardt, K., R. Mathew, et al. (2006). "Autophagy promotes tumor cell survival and restricts necrosis, inflammation, and tumorigenesis." Cancer Cell 10(1): 51-64.
Deretic, V. (2008). "Autophagosome and phagosome." Methods Mol Biol 445: 1-10.
Di Cesare, A., P. Di Meglio, et al. (2009). "The IL-23/Th17 axis in the immunopathogenesis of psoriasis." J Invest Dermatol 129(6): 1339-1350.
Diepgen, T. L. and V. Mahler (2002). "The epidemiology of skin cancer." Br J Dermatol 146 Suppl 61: 1-6.
Doorbar, J. (2005). "The papillomavirus life cycle." J Clin Virol 32 Suppl 1: S7-15.
Eberle, J., L. F. Fecker, et al. (2007). "Apoptosis pathways as promising targets for skin cancer therapy." Br J Dermatol 156 Suppl 3: 18-24.
Eckert, R. L., J. F. Crish, et al. (1997). "The epidermal keratinocyte as a model for the study of gene regulation and cell differentiation." Physiol Rev 77(2): 397-424.
Egawa, K. (2003). "Do human papillomaviruses target epidermal stem cells?" Dermatology 207(3): 251-254.
Elias, P., S. Ahn, et al. (2002b). "Origin of the epidermal calcium gradient: regulation by barrier status and role of active vs passive mechanisms." J Invest Dermatol 119(6): 1269-1274.
Elias, P. M. (2012). "Structure and function of the stratum corneum extracellular matrix." J Invest Dermatol 132(9): 2131-2133.
Elias, P. M., S. K. Ahn, et al. (2002). "Modulations in epidermal calcium regulate the expression of differentiation-specific markers." J Invest Dermatol 119(5): 1128-1136.
Elias, P. M. and B. E. Brown (1978). "The mammalian cutaneous permeability barrier: defective barrier function is essential fatty acid deficiency correlates with abnormal intercellular lipid deposition." Lab Invest 39(6): 574-583.
English, L., M. Chemali, et al. (2009). "Autophagy enhances the presentation of endogenous viral antigens on MHC class I molecules during HSV-1 infection." Nat Immunol 10(5): 480-487.
Fader, C. M., D. Sanchez, et al. (2008). "Induction of autophagy promotes fusion of multivesicular bodies with autophagic vacuoles in k562 cells." Traffic 9(2): 230-250.
Fass, E., E. Shvets, et al. (2006). "Microtubules support production of starvation-induced autophagosomes but not their targeting and fusion with lysosomes." J Biol Chem 281(47): 36303-36316.
Fillingham, J., M. C. Keogh, et al. (2006). "GammaH2AX and its role in DNA double-strand break repair." Biochem Cell Biol 84(4): 568-577.
Florey, O., S. E. Kim, et al. (2011). "Autophagy machinery mediates macroendocytic processing and entotic cell death by targeting single membranes." Nat Cell Biol 13(11): 1335-1343.

Frech, M., M. Andjelkovic, et al. (1997). "High affinity binding of inositol phosphates and phosphoinositides to the pleckstrin homology domain of RAC/protein kinase B and their influence on kinase activity." J Biol Chem 272(13): 8474-8481.

Fuchs, E. and D. W. Cleveland (1998). "A structural scaffolding of intermediate filaments in health and disease." Science 279(5350): 514-519.

Fujita, N., T. Itoh, et al. (2008). "The Atg16L complex specifies the site of LC3 lipidation for membrane biogenesis in autophagy." Mol Biol Cell 19(5): 2092-2100.

Ganesan, A. K., H. Ho, et al. (2008). "Genome-wide siRNA-based functional genomics of pigmentation identifies novel genes and pathways that impact melanogenesis in human cells." PLoS Genet 4(12): e1000298.

Gani, O. A. and R. A. Engh (2010). "Protein kinase inhibition of clinically important staurosporine analogues." Nat Prod Rep 27(4): 489-498.

Ganley, I. G., H. Lam du, et al. (2009). "ULK1.ATG13.FIP200 complex mediates mTOR signaling and is essential for autophagy." J Biol Chem 284(18): 12297-12305.

Ganley, I. G., P. M. Wong, et al. (2011). "Distinct autophagosomal-lysosomal fusion mechanism revealed by thapsigargin-induced autophagy arrest." Mol Cell 42(6): 731-743.

Gaugel, A., D. Bakula, et al. (2012). "Defining regulatory and phosphoinositide-binding sites in the human WIPI-1 beta-propeller responsible for autophagosomal membrane localization downstream of mTORC1 inhibition." J Mol Signal 7(1): 16.

Geissler, E. K. (2008). "The impact of mTOR inhibitors on the development of malignancy." Transplant Proc 40(10 Suppl): S32-35.

Gelfand, J. M., A. L. Neimann, et al. (2006). "Risk of myocardial infarction in patients with psoriasis." JAMA 296(14): 1735-1741.

Gillison, M. L. and D. R. Lowy (2004). "A causal role for human papillomavirus in head and neck cancer." Lancet 363(9420): 1488-1489.

Gillison, M. L. and K. V. Shah (2001). "Human papillomavirus-associated head and neck squamous cell carcinoma: mounting evidence for an etiologic role for human papillomavirus in a subset of head and neck cancers." Curr Opin Oncol 13(3): 183-188.

Gonzalez-Polo, R. A., P. Boya, et al. (2005). "The apoptosis/autophagy paradox: autophagic vacuolization before apoptotic death." J Cell Sci 118(Pt 14): 3091-3102.

Griffin, L. M., L. Cicchini, et al. (2013). "Human papillomavirus infection is inhibited by host autophagy in primary human keratinocytes." Virology 437(1): 12-19.

Griffiths, C. E. and J. N. Barker (2007). "Pathogenesis and clinical features of psoriasis." Lancet 370(9583): 263-271.

Griffiths, R. E., S. Kupzig, et al. (2012). "Maturing reticulocytes internalize plasma membrane in glycophorin A-containing vesicles that fuse with autophagosomes before exocytosis." Blood 119(26): 6296-6306.

Guan, J. L., A. K. Simon, et al. (2013). "Autophagy in stem cells." Autophagy 9(6).

Guba, M., P. von Breitenbuch, et al. (2002). "Rapamycin inhibits primary and metastatic tumor growth by antiangiogenesis: involvement of vascular endothelial growth factor." Nat Med 8(2): 128-135.

Gutierrez, M. G., D. B. Munafo, et al. (2004). "Rab7 is required for the normal progression of the autophagic pathway in mammalian cells." J Cell Sci 117(Pt 13): 2687-2697.

Hailey, D. W., A. S. Rambold, et al. (2010). "Mitochondria supply membranes for autophagosome biogenesis during starvation." Cell 141(4): 656-667.

Hara, K., K. Yonezawa, et al. (1998). "Amino acid sufficiency and mTOR regulate p70 S6 kinase and eIF-4E BP1 through a common effector mechanism." J Biol Chem 273(23): 14484-14494.

Hara, T., A. Takamura, et al. (2008). "FIP200, a ULK-interacting protein, is required for autophagosome formation in mammalian cells." J Cell Biol 181(3): 497-510.
Hardie, D. G., F. A. Ross, et al. (2012). "AMPK: a nutrient and energy sensor that maintains energy homeostasis." Nat Rev Mol Cell Biol 13(4): 251-262.
Hardman, M. J., L. Moore, et al. (1999). "Barrier formation in the human fetus is patterned." J Invest Dermatol 113(6): 1106-1113.
Hardman, M. J., P. Sisi, et al. (1998). "Patterned acquisition of skin barrier function during development." Development 125(8): 1541-1552.
Harrington, L. S., G. M. Findlay, et al. (2004). "The TSC1-2 tumor suppressor controls insulin-PI3K signaling via regulation of IRS proteins." J Cell Biol 166(2): 213-223.
Harris, J., M. Hartman, et al. (2011). "Autophagy controls IL-1beta secretion by targeting pro-IL-1beta for degradation." J Biol Chem 286(11): 9587-9597.
Harris, J., J. C. Hope, et al. (2009). "Autophagy and the immune response to TB." Transbound Emerg Dis 56(6-7): 248-254.
Harrison, D. E., R. Strong, et al. (2009). "Rapamycin fed late in life extends lifespan in genetically heterogeneous mice." Nature 460(7253): 392-395.
Harwood, C. A., T. Surentheran, et al. (2004). "Increased risk of skin cancer associated with the presence of epidermodysplasia verruciformis human papillomavirus types in normal skin." Br J Dermatol 150(5): 949-957.
Hawley, S. A., D. A. Pan, et al. (2005). "Calmodulin-dependent protein kinase kinase-beta is an alternative upstream kinase for AMP-activated protein kinase." Cell Metab 2(1): 9-19.
Hayashi-Nishino, M., N. Fujita, et al. (2009). "A subdomain of the endoplasmic reticulum forms a cradle for autophagosome formation." Nat Cell Biol 11(12): 1433-1437.
Hennings, H., K. A. Holbrook, et al. (1983). "Factors influencing calcium-induced terminal differentiation in cultured mouse epidermal cells." J Cell Physiol 116(3): 265-281.
Hiragami-Hamada, K., K. Shinmyozu, et al. (2011). "N-terminal phosphorylation of HP1{alpha} promotes its chromatin binding." Mol Cell Biol 31(6): 1186-1200.
Ho, H., R. Kapadia, et al. (2011). "WIPI1 coordinates melanogenic gene transcription and melanosome formation via TORC1 inhibition." J Biol Chem 286(14): 12509-12523.
Hodgkinson, C. P., E. M. Sale, et al. (2002). "Characterization of PDK2 activity against protein kinase B gamma." Biochemistry 41(32): 10351-10359.
Hofbauer, G. F., J. N. Bouwes Bavinck, et al. (2010). "Organ transplantation and skin cancer: basic problems and new perspectives." Exp Dermatol 19(6): 473-482.
Hojo, M., T. Morimoto, et al. (1999). "Cyclosporine induces cancer progression by a cell-autonomous mechanism." Nature 397(6719): 530-534.
Hosokawa, N., Y. Hara, et al. (2007). "Generation of cell lines with tetracycline-regulated autophagy and a role for autophagy in controlling cell size." FEBS Lett 581(15): 2623-2629.
Hovnanian, A. (2005). "Harlequin ichthyosis unmasked: a defect of lipid transport." J Clin Invest 115(7): 1708-1710.
Hufbauer, M., D. Lazic, et al. (2010). "Enhanced human papillomavirus type 8 oncogene expression levels are crucial for skin tumorigenesis in transgenic mice." Virology 403(2): 128-136.
Hutchison, C. J. (2002). "Lamins: building blocks or regulators of gene expression?" Nat Rev Mol Cell Biol 3(11): 848-858.
Ichihashi, M., M. Ueda, et al. (2003). "UV-induced skin damage." Toxicology 189(1-2): 21-39.
Ichimura, Y., T. Kirisako, et al. (2000). "A ubiquitin-like system mediates protein lipidation." Nature 408(6811): 488-492.
Ichimura, Y. and M. Komatsu (2011). "Pathophysiological role of autophagy: lesson from autophagy-deficient mouse models." Exp Anim 60(4): 329-345.

Iizuka, H., H. Takahashi, et al. (2004). "Unique keratinization process in psoriasis: late differentiation markers are abolished because of the premature cell death." J Dermatol 31(4): 271-276.

Inoki, K., Y. Li, et al. (2002). "TSC2 is phosphorylated and inhibited by Akt and suppresses mTOR signalling." Nat Cell Biol 4(9): 648-657.

Ishida-Yamamoto, A., R. A. Eady, et al. (1996). "Immunoelectron microscopic analysis of cornified cell envelope formation in normal and psoriatic epidermis." J Histochem Cytochem 44(2): 167-175.

Ishida-Yamamoto, A., M. Kishibe, et al. (2007). "Rab11 is associated with epidermal lamellar granules." J Invest Dermatol 127(9): 2166-2170.

Ishida-Yamamoto, A., M. Simon, et al. (2004). "Epidermal lamellar granules transport different cargoes as distinct aggregates." J Invest Dermatol 122(5): 1137-1144.

Itakura, E., C. Kishi, et al. (2008). "Beclin 1 forms two distinct phosphatidylinositol 3-kinase complexes with mammalian Atg14 and UVRAG." Mol Biol Cell 19(12): 5360-5372.

Itakura, E. and N. Mizushima (2010). "Characterization of autophagosome formation site by a hierarchical analysis of mammalian Atg proteins." Autophagy 6(6): 764-776.

Itoh, K., T. Chiba, et al. (1997). "An Nrf2/small Maf heterodimer mediates the induction of phase II detoxifying enzyme genes through antioxidant response elements." Biochem Biophys Res Commun 236(2): 313-322.

Itoh, K., N. Wakabayashi, et al. (1999). "Keap1 represses nuclear activation of antioxidant responsive elements by Nrf2 through binding to the amino-terminal Neh2 domain." Genes Dev 13(1): 76-86.

Jackson, M., S. E. Howie, et al. (1999). "Psoriatic keratinocytes show reduced IRF-1 and STAT-1alpha activation in response to gamma-IFN." FASEB J 13(3): 495-502.

Jain, A., T. Lamark, et al. (2010). "p62/SQSTM1 is a target gene for transcription factor NRF2 and creates a positive feedback loop by inducing antioxidant response element-driven gene transcription." J Biol Chem 285(29): 22576-22591.

Jain, R. and W. Weninger (2013). "Shedding light on cutaneous innate immune responses: the intravital microscopy approach." Immunol Cell Biol.

James, T. C., J. C. Eissenberg, et al. (1989). "Distribution patterns of HP1, a heterochromatin-associated nonhistone chromosomal protein of Drosophila." Eur J Cell Biol 50(1): 170-180.

James, T. C. and S. C. Elgin (1986). "Identification of a nonhistone chromosomal protein associated with heterochromatin in Drosophila melanogaster and its gene." Mol Cell Biol 6(11): 3862-3872.

Jewell, J. L. and K. L. Guan (2013). "Nutrient signaling to mTOR and cell growth." Trends Biochem Sci.

Johansen, T. and T. Lamark (2011). "Selective autophagy mediated by autophagic adapter proteins." Autophagy 7(3): 279-296.

Johnson, S. C., P. S. Rabinovitch, et al. (2013). "mTOR is a key modulator of ageing and age-related disease." Nature 493(7432): 338-345.

Jones, S. A., K. H. Mills, et al. (2013). "Autophagy and inflammatory diseases." Immunol Cell Biol 91(3): 250-258.

Jung, C. H., C. B. Jun, et al. (2009). "ULK-Atg13-FIP200 complexes mediate mTOR signaling to the autophagy machinery." Mol Biol Cell 20(7): 1992-2003.

Kabeya, Y., N. Mizushima, et al. (2000). "LC3, a mammalian homologue of yeast Apg8p, is localized in autophagosome membranes after processing." EMBO J 19(21): 5720-5728.

Kabeya, Y., N. Mizushima, et al. (2004). "LC3, GABARAP and GATE16 localize to autophagosomal membrane depending on form-II formation." J Cell Sci 117(Pt 13): 2805-2812.

Karantza-Wadsworth, V., S. Patel, et al. (2007). "Autophagy mitigates metabolic stress and genome damage in mammary tumorigenesis." Genes Dev 21(13): 1621-1635.

Karen L Agnew, B. A. G. and B. B. Christopher.

Karim, M. R., T. Kanazawa, et al. (2007). "Cytosolic LC3 ratio as a sensitive index of macroautophagy in isolated rat hepatocytes and H4-II-E cells." Autophagy 3(6): 553-560.

Kelsell, D. P., E. E. Norgett, et al. (2005). "Mutations in ABCA12 underlie the severe congenital skin disease harlequin ichthyosis." Am J Hum Genet 76(5): 794-803.

Kim, P. K., D. W. Hailey, et al. (2008). "Ubiquitin signals autophagic degradation of cytosolic proteins and peroxisomes." Proc Natl Acad Sci U S A 105(52): 20567-20574.

Kinouchi, M., H. Takahashi, et al. (2002). "Ultraviolet B irradiation increases keratin 5 and keratin 14 expression through epidermal growth factor receptor of SV40-transformed human keratinocytes." Arch Dermatol Res 293(12): 634-641.

Kirisako, T., Y. Ichimura, et al. (2000). "The reversible modification regulates the membrane-binding state of Apg8/Aut7 essential for autophagy and the cytoplasm to vacuole targeting pathway." J Cell Biol 151(2): 263-276.

Kirkin, V., T. Lamark, et al. (2009). "A role for NBR1 in autophagosomal degradation of ubiquitinated substrates." Mol Cell 33(4): 505-516.

Kjellerup, R. B., L. Iversen, et al. (2009). "The expression and phosphorylation of eukaryotic initiation factor 4E are increased in lesional psoriatic skin." Br J Dermatol 161(5): 1059-1066.

Klionsky, D. J., F. C. Abdalla, et al. (2012). "Guidelines for the use and interpretation of assays for monitoring autophagy." Autophagy 8(4): 445-544.

Klionsky, D. J., H. Abeliovich, et al. (2008). "Guidelines for the use and interpretation of assays for monitoring autophagy in higher eukaryotes." Autophagy 4(2): 151-175.

Klionsky, D. J., A. M. Cuervo, et al. (2007). "How shall I eat thee?" Autophagy 3(5): 413-416.

Klionsky, D. J., Z. Elazar, et al. (2008). "Does bafilomycin A1 block the fusion of autophagosomes with lysosomes?" Autophagy 4(7): 849-950.

Koehl, G. E., J. Andrassy, et al. (2004). "Rapamycin protects allografts from rejection while simultaneously attacking tumors in immunosuppressed mice." Transplantation 77(9): 1319-1326.

Komatsu, M., H. Kurokawa, et al. (2010). "The selective autophagy substrate p62 activates the stress responsive transcription factor Nrf2 through inactivation of Keap1." Nat Cell Biol 12(3): 213-223.

Kovacina, K. S., G. Y. Park, et al. (2003). "Identification of a proline-rich Akt substrate as a 14-3-3 binding partner." J Biol Chem 278(12): 10189-10194.

Krick, R., Y. Muehe, et al. (2008). "Piecemeal microautophagy of the nucleus requires the core macroautophagy genes." Mol Biol Cell 19(10): 4492-4505.

Kuma, A., M. Hatano, et al. (2004). "The role of autophagy during the early neonatal starvation period." Nature 432(7020): 1032-1036.

Lamark, T., V. Kirkin, et al. (2009). "NBR1 and p62 as cargo receptors for selective autophagy of ubiquitinated targets." Cell Cycle 8(13): 1986-1990.

Landmann, L. (1988). "The epidermal permeability barrier." Anat Embryol (Berl) 178(1): 1-13.

Lapaquette, P., A. L. Glasser, et al. (2010). "Crohn's disease-associated adherent-invasive E. coli are selectively favoured by impaired autophagy to replicate intracellularly." Cell Microbiol 12(1): 99-113.

Lavieu, G., F. Scarlatti, et al. (2006). "Regulation of autophagy by sphingosine kinase 1 and its role in cell survival during nutrient starvation." J Biol Chem 281(13): 8518-8527.

Lavieu, G., F. Scarlatti, et al. (2007). "Is autophagy the key mechanism by which the sphingolipid rheostat controls the cell fate decision?" Autophagy 3(1): 45-47.

Leblanc, K. G., Jr., M. P. Hughes, et al. (2011). "The role of sirolimus in the prevention of cutaneous squamous cell carcinoma in organ transplant recipients." Dermatol Surg 37(6): 744-749.

Lee, H. M., D. M. Shin, et al. (2011). "Autophagy negatively regulates keratinocyte inflammatory responses via scaffolding protein p62/SQSTM1." J Immunol 186(2): 1248-1258.

Lee, S. H., E. H. Choi, et al. (1998). "Iontophoresis itself on hairless mouse skin induces the loss of the epidermal calcium gradient without skin barrier impairment." J Invest Dermatol 111(1): 39-43.

Leiter, U. and C. Garbe (2008). "Epidemiology of melanoma and nonmelanoma skin cancer--the role of sunlight." Adv Exp Med Biol 624: 89-103.

LeRoy, G., J. T. Weston, et al. (2009). "Heterochromatin protein 1 is extensively decorated with histone code-like post-translational modifications." Mol Cell Proteomics 8(11): 2432-2442.

Levine, B. and D. J. Klionsky (2004). "Development by self-digestion: molecular mechanisms and biological functions of autophagy." Dev Cell 6(4): 463-477.

Levine, B. and G. Kroemer (2008). "Autophagy in the pathogenesis of disease." Cell 132(1): 27-42.

Liang, C., J. S. Lee, et al. (2008). "Beclin1-binding UVRAG targets the class C Vps complex to coordinate autophagosome maturation and endocytic trafficking." Nat Cell Biol 10(7): 776-787.

Liu, M. L. and M. C. Yao (2012). "The role of ATG8 and autophagy in programmed nuclear degradation in Tetrahymena thermophila." Eukaryot Cell.

Locke, M. and A. K. Sykes (1975). "The role of the Golgi complex in the isolation and digestion of organelles." Tissue Cell 7(1): 143-158.

Luijsterburg, M. S., C. Dinant, et al. (2009). "Heterochromatin protein 1 is recruited to various types of DNA damage." J Cell Biol 185(4): 577-586.

Maison, C. and G. Almouzni (2004). "HP1 and the dynamics of heterochromatin maintenance." Nat Rev Mol Cell Biol 5(4): 296-304.

Manabe, M., M. Sanchez, et al. (1991). "Interaction of filaggrin with keratin filaments during advanced stages of normal human epidermal differentiation and in ichthyosis vulgaris." Differentiation 48(1): 43-50.

Manning, B. D. and L. C. Cantley (2007). "AKT/PKB signaling: navigating downstream." Cell 129(7): 1261-1274.

Marcuzzi, G. P., M. Hufbauer, et al. (2009). "Spontaneous tumour development in human papillomavirus type 8 E6 transgenic mice and rapid induction by UV-light exposure and wounding." J Gen Virol 90(Pt 12): 2855-2864.

Mari, M., J. Griffith, et al. (2010). "An Atg9-containing compartment that functions in the early steps of autophagosome biogenesis." J Cell Biol 190(6): 1005-1022.

Marjukka Suhonen, T., S. Pasonen-Seppanen, et al. (2003). "Epidermal cell culture model derived from rat keratinocytes with permeability characteristics comparable to human cadaver skin." Eur J Pharm Sci 20(1): 107-113.

Martinez, J., J. Almendinger, et al. (2011). "Microtubule-associated protein 1 light chain 3 alpha (LC3)-associated phagocytosis is required for the efficient clearance of dead cells." Proc Natl Acad Sci U S A 108(42): 17396-17401.

Masoro, E. J. (2009). "Caloric restriction-induced life extension of rats and mice: a critique of proposed mechanisms." Biochim Biophys Acta 1790(10): 1040-1048.

Mathew, R., C. M. Karp, et al. (2009). "Autophagy suppresses tumorigenesis through elimination of p62." Cell 137(6): 1062-1075.

Mathew, R., S. Kongara, et al. (2007). "Autophagy suppresses tumor progression by limiting chromosomal instability." Genes Dev 21(11): 1367-1381.

Mathew, R. and E. White (2011). "Autophagy in tumorigenesis and energy metabolism: friend by day, foe by night." Curr Opin Genet Dev 21(1): 113-119.

Matsunaga, K., E. Morita, et al. (2010). "Autophagy requires endoplasmic reticulum targeting of the PI3-kinase complex via Atg14L." J Cell Biol 190(4): 511-521.

Matsunaga, K., T. Saitoh, et al. (2009). "Two Beclin 1-binding proteins, Atg14L and Rubicon, reciprocally regulate autophagy at different stages." Nat Cell Biol 11(4): 385-396.

Maycotte, P., S. Aryal, et al. (2012). "Chloroquine sensitizes breast cancer cells to chemotherapy independent of autophagy." Autophagy 8(2): 200-212.

McGee, M. D., D. Weber, et al. (2011). "Loss of intestinal nuclei and intestinal integrity in aging C. elegans." Aging Cell 10(4): 699-710.

McLaughlin-Drubin, M. E., J. Meyers, et al. (2012). "Cancer associated human papillomaviruses." Curr Opin Virol 2(4): 459-466.

McMahon, M., K. Itoh, et al. (2003). "Keap1-dependent proteasomal degradation of transcription factor Nrf2 contributes to the negative regulation of antioxidant response element-driven gene expression." J Biol Chem 278(24): 21592-21600.

McQuillan, R. F., C. M. O'Seaghdha, et al. (2009). "The effect of switching from calcineurin inhibitor to sirolimus on the incidence of skin cancers in kidney transplant recipients." J Eur Acad Dermatol Venereol 23(3): 330-331.

Menon, G. K., G. W. Cleary, et al. (2012). "The structure and function of the stratum corneum." Int J Pharm 435(1): 3-9.

Menon, G. K., S. Grayson, et al. (1985). "Ionic calcium reservoirs in mammalian epidermis: ultrastructural localization by ion-capture cytochemistry." J Invest Dermatol 84(6): 508-512.

Menon, G. K., L. F. Price, et al. (1994). "Selective obliteration of the epidermal calcium gradient leads to enhanced lamellar body secretion." J Invest Dermatol 102(5): 789-795.

Mijaljica, D., M. Prescott, et al. (2010). "The intricacy of nuclear membrane dynamics during nucleophagy." Nucleus 1(3): 213-223.

Miller, L. S. (2008). "Toll-like receptors in skin." Adv Dermatol 24: 71-87.

Mitsui, H., M. Suarez-Farinas, et al. (2012). "Combined use of laser capture microdissection and cDNA microarray analysis identifies locally expressed disease-related genes in focal regions of psoriasis vulgaris skin lesions." J Invest Dermatol 132(6): 1615-1626.

Mizushima, N. (2005). "The pleiotropic role of autophagy: from protein metabolism to bactericide." Cell Death Differ 12 Suppl 2: 1535-1541.

Mizushima, N. (2007). "Autophagy: process and function." Genes Dev 21(22): 2861-2873.

Mizushima, N. and M. Komatsu (2011). "Autophagy: renovation of cells and tissues." Cell 147(4): 728-741.

Mizushima, N. and B. Levine (2010). "Autophagy in mammalian development and differentiation." Nat Cell Biol 12(9): 823-830.

Mizushima, N., T. Noda, et al. (1998). "A protein conjugation system essential for autophagy." Nature 395(6700): 395-398.

Mizushima, N., A. Yamamoto, et al. (2001). "Dissection of autophagosome formation using Apg5-deficient mouse embryonic stem cells." J Cell Biol 152(4): 657-668.

Mizushima, N., T. Yoshimori, et al. (2011). "The role of Atg proteins in autophagosome formation." Annu Rev Cell Dev Biol 27: 107-132.

Moreau, K., B. Ravikumar, et al. (2012). "Arf6 promotes autophagosome formation via effects on phosphatidylinositol 4,5-bisphosphate and phospholipase D." J Cell Biol 196(4): 483-496.

Moreau, K., B. Ravikumar, et al. (2011). "Autophagosome precursor maturation requires homotypic fusion." Cell 146(2): 303-317.

Muench, P., S. Probst, et al. (2010). "Cutaneous papillomavirus E6 proteins must interact with p300 and block p53-mediated apoptosis for cellular immortalization and tumorigenesis." Cancer Res 70(17): 6913-6924.

Murase, D., A. Hachiya, et al. (2013). "Autophagy Has a Significant Role in Determining Skin Color by Regulating Melanosome Degradation in Keratinocytes." J Invest Dermatol.

Nakagawa, I., A. Amano, et al. (2004). "Autophagy defends cells against invading group A Streptococcus." Science 306(5698): 1037-1040.

Nakamura, N., A. Matsuura, et al. (1997). "Acidification of vacuoles is required for autophagic degradation in the yeast, Saccharomyces cerevisiae." J Biochem 121(2): 338-344.

Nakamura, N., C. Rabouille, et al. (1995). "Characterization of a cis-Golgi matrix protein, GM130." J Cell Biol 131(6 Pt 2): 1715-1726.

Nakatogawa, H., Y. Ichimura, et al. (2007). "Atg8, a ubiquitin-like protein required for autophagosome formation, mediates membrane tethering and hemifusion." Cell 130(1): 165-178.

Neale, R. E., S. Weissenborn, et al. (2013). "Human Papilloma Virus load in eyebrow hair follicles and risk of cutaneous squamous cell carcinoma." Cancer Epidemiol Biomarkers Prev.

Nicola, A. M., P. Albuquerque, et al. (2012). "Macrophage autophagy in immunity to Cryptococcus neoformans and Candida albicans." Infect Immun 80(9): 3065-3076.

Nishida, Y., S. Arakawa, et al. (2009). "Discovery of Atg5/Atg7-independent alternative macroautophagy." Nature 461(7264): 654-658.

Noda, T. and Y. Ohsumi (1998). "Tor, a phosphatidylinositol kinase homologue, controls autophagy in yeast." J Biol Chem 273(7): 3963-3966.

O'Donovan, P., C. M. Perrett, et al. (2005). "Azathioprine and UVA light generate mutagenic oxidative DNA damage." Science 309(5742): 1871-1874.

O'Shaughnessy, R. F., B. Akgul, et al. (2007b). "Cutaneous human papillomaviruses down-regulate AKT1, whereas AKT2 up-regulation and activation associates with tumors." Cancer Res 67(17): 8207-8215.

O'Shaughnessy, R. F., J. C. Welti, et al. (2007). "AKT-dependent HspB1 (Hsp27) activity in epidermal differentiation." J Biol Chem 282(23): 17297-17305.

O'Shaughnessy, R. F., J. C. Welti, et al. (2009). "Akt-dependent Pp2a activity is required for epidermal barrier formation during late embryonic development." Development 136(20): 3423-3431.

Obara, K., T. Noda, et al. (2008). "Transport of phosphatidylinositol 3-phosphate into the vacuole via autophagic membranes in Saccharomyces cerevisiae." Genes Cells 13(6): 537-547.

Oren, A., T. Ganz, et al. (2003). "In human epidermis, beta-defensin 2 is packaged in lamellar bodies." Exp Mol Pathol 74(2): 180-182.

Ortonne, J. P. (2002). "From actinic keratosis to squamous cell carcinoma." Br J Dermatol 146 Suppl 61: 20-23.

Pankiv, S., T. H. Clausen, et al. (2007). "p62/SQSTM1 binds directly to Atg8/LC3 to facilitate degradation of ubiquitinated protein aggregates by autophagy." J Biol Chem 282(33): 24131-24145.

Pankiv, S., T. Lamark, et al. (2010). "Nucleocytoplasmic shuttling of p62/SQSTM1 and its role in recruitment of nuclear polyubiquitinated proteins to promyelocytic leukemia bodies." J Biol Chem 285(8): 5941-5953.

Park, Y. E., Y. K. Hayashi, et al. (2009). "Autophagic degradation of nuclear components in mammalian cells." Autophagy 5(6): 795-804.

Pattingre, S., A. Tassa, et al. (2005). "Bcl-2 antiapoptotic proteins inhibit Beclin 1-dependent autophagy." Cell 122(6): 927-939.

Pelham, H. R. (1990). "The retention signal for soluble proteins of the endoplasmic reticulum." Trends Biochem Sci 15(12): 483-486.

Peng, X. D., P. Z. Xu, et al. (2003). "Dwarfism, impaired skin development, skeletal muscle atrophy, delayed bone development, and impeded adipogenesis in mice lacking Akt1 and Akt2." Genes Dev 17(11): 1352-1365.

Peterson, R. T., P. A. Beal, et al. (2000). "FKBP12-rapamycin-associated protein (FRAP) autophosphorylates at serine 2481 under translationally repressive conditions." J Biol Chem 275(10): 7416-7423.

Pfeffer, S. R. (2001). "Rab GTPases: specifying and deciphering organelle identity and function." Trends Cell Biol 11(12): 487-491.

Piruzian, E., S. Bruskin, et al. (2010). "Integrated network analysis of transcriptomic and proteomic data in psoriasis." BMC Syst Biol 4: 41.

Polson, H. E., J. de Lartigue, et al. (2010). "Mammalian Atg18 (WIPI2) localizes to omegasome-anchored phagophores and positively regulates LC3 lipidation." Autophagy 6(4).

Porter, R. M. and E. B. Lane (2003). "Phenotypes, genotypes and their contribution to understanding keratin function." Trends Genet 19(5): 278-285.

Proby, C. M., K. J. Purdie, et al. (2000). "Spontaneous keratinocyte cell lines representing early and advanced stages of malignant transformation of the epidermis." Exp Dermatol 9(2): 104-117.

Proikas-Cezanne, T., S. Ruckerbauer, et al. (2007). "Human WIPI-1 puncta-formation: a novel assay to assess mammalian autophagy." FEBS Lett 581(18): 3396-3404.

Proikas-Cezanne, T., S. Waddell, et al. (2004). "WIPI-1alpha (WIPI49), a member of the novel 7-bladed WIPI protein family, is aberrantly expressed in human cancer and is linked to starvation-induced autophagy." Oncogene 23(58): 9314-9325.

Proksch, E., J. M. Brandner, et al. (2008). "The skin: an indispensable barrier." Exp Dermatol 17(12): 1063-1072.

Pua, H. H., J. Guo, et al. (2009). "Autophagy is essential for mitochondrial clearance in mature T lymphocytes." J Immunol 182(7): 4046-4055.

Purdie, K. J., C. J. Sexton, et al. (1993). "Malignant transformation of cutaneous lesions in renal allograft patients: a role for human papillomavirus." Cancer Res 53(21): 5328-5333.

Qiang, L., C. Wu, et al. (2013). "Autophagy controls p38 activation to promote cell survival under genotoxic stress." J Biol Chem 288(3): 1603-1611.

Qu, X., J. Yu, et al. (2003). "Promotion of tumorigenesis by heterozygous disruption of the beclin 1 autophagy gene." J Clin Invest 112(12): 1809-1820.

Quivy, J. P., A. Gerard, et al. (2008). "The HP1-p150/CAF-1 interaction is required for pericentric heterochromatin replication and S-phase progression in mouse cells." Nat Struct Mol Biol 15(9): 972-979.

Ramos, J., J. Villa, et al. (2004). "UV dose determines key characteristics of nonmelanoma skin cancer." Cancer Epidemiol Biomarkers Prev 13(12): 2006-2011.

Ratushny, V., M. D. Gober, et al. (2012). "From keratinocyte to cancer: the pathogenesis and modeling of cutaneous squamous cell carcinoma." J Clin Invest 122(2): 464-472.

Ravikumar, B., A. Acevedo-Arozena, et al. (2005). "Dynein mutations impair autophagic clearance of aggregate-prone proteins." Nat Genet 37(7): 771-776.

Ravikumar, B., K. Moreau, et al. (2010). "Plasma membrane contributes to the formation of pre-autophagosomal structures." Nat Cell Biol 12(8): 747-757.

Ravikumar, B., C. Vacher, et al. (2004). "Inhibition of mTOR induces autophagy and reduces toxicity of polyglutamine expansions in fly and mouse models of Huntington disease." Nat Genet 36(6): 585-595.

Rawlings, A. V. and C. R. Harding (2004). "Moisturization and skin barrier function." Dermatol Ther 17 Suppl 1: 43-48.

Rawlings, A. V., I. R. Scott, et al. (1994). "Stratum corneum moisturization at the molecular level." J Invest Dermatol 103(5): 731-741.

Raychaudhuri, S. P. (2012). "A Cutting Edge Overview: Psoriatic Disease." Clin Rev Allergy Immunol.

Raymond, A. A., A. Gonzalez de Peredo, et al. (2008). "Lamellar bodies of human epidermis: proteomics characterization by high throughput mass spectrometry and possible involvement of CLIP-170 in their trafficking/secretion." Mol Cell Proteomics 7(11): 2151-2175.

Reggiori, F., I. Monastyrska, et al. (2010). "Coronaviruses Hijack the LC3-I-positive EDEMosomes, ER-derived vesicles exporting short-lived ERAD regulators, for replication." Cell Host Microbe 7(6): 500-508.

Reggiori, F., T. Shintani, et al. (2005). "Atg9 cycles between mitochondria and the pre-autophagosomal structure in yeasts." Autophagy 1(2): 101-109.

Rello-Varona, S., D. Lissa, et al. (2012). "Autophagic removal of micronuclei." Cell Cycle 11(1): 170-176.

Rogakou, E. P., C. Boon, et al. (1999). "Megabase chromatin domains involved in DNA double-strand breaks in vivo." J Cell Biol 146(5): 905-916.

Rogakou, E. P., D. R. Pilch, et al. (1998). "DNA double-stranded breaks induce histone H2AX phosphorylation on serine 139." J Biol Chem 273(10): 5858-5868.

Ropolo, A., D. Grasso, et al. (2007). "The pancreatitis-induced vacuole membrane protein 1 triggers autophagy in mammalian cells." J Biol Chem 282(51): 37124-37133.

Rosner, M. and M. Hengstschlager (2010). "Evidence for cell cycle-dependent, rapamycin-resistant phosphorylation of ribosomal protein S6 at S240/244." Amino Acids 39(5): 1487-1492.

Rothnagel, J. A., T. Seki, et al. (1999). "The mouse keratin 6 isoforms are differentially expressed in the hair follicle, footpad, tongue and activated epidermis." Differentiation 65(2): 119-130.

Rubinsztein, D. C., A. M. Cuervo, et al. (2009). "In search of an "autophagomometer"." Autophagy 5(5): 585-589.

Rubinsztein, D. C., T. Shpilka, et al. (2012). "Mechanisms of autophagosome biogenesis." Curr Biol 22(1): R29-34.

Saitoh, T., N. Fujita, et al. (2008). "Loss of the autophagy protein Atg16L1 enhances endotoxin-induced IL-1beta production." Nature 456(7219): 264-268.

Sakurai, T., G. He, et al. (2008). "Hepatocyte necrosis induced by oxidative stress and IL-1 alpha release mediate carcinogen-induced compensatory proliferation and liver tumorigenesis." Cancer Cell 14(2): 156-165.

Sale, E. M. and G. J. Sale (2008). "Protein kinase B: signalling roles and therapeutic targeting." Cell Mol Life Sci 65(1): 113-127.

Salemi, S., S. Yousefi, et al. (2012). "Autophagy is required for self-renewal and differentiation of adult human stem cells." Cell Res 22(2): 432-435.

Salgo, R., J. Gossmann, et al. (2010). "Switch to a sirolimus-based immunosuppression in long-term renal transplant recipients: reduced rate of (pre-)malignancies and nonmelanoma skin cancer in a prospective, randomized, assessor-blinded, controlled clinical trial." Am J Transplant 10(6): 1385-1393.

Salt, I. P., G. Johnson, et al. (1998). "AMP-activated protein kinase is activated by low glucose in cell lines derived from pancreatic beta cells, and may regulate insulin release." Biochem J 335 (Pt 3): 533-539.

Sancak, Y., T. R. Peterson, et al. (2008). "The Rag GTPases bind raptor and mediate amino acid signaling to mTORC1." Science 320(5882): 1496-1501.

Sanjuan, M. A., C. P. Dillon, et al. (2007). "Toll-like receptor signalling in macrophages links the autophagy pathway to phagocytosis." Nature 450(7173): 1253-1257.

Sanjuan, M. A., S. Milasta, et al. (2009). "Toll-like receptor signaling in the lysosomal pathways." Immunol Rev 227(1): 203-220.

Sarbassov, D. D., D. A. Guertin, et al. (2005). "Phosphorylation and regulation of Akt/PKB by the rictor-mTOR complex." Science 307(5712): 1098-1101.

Scarlatti, F., C. Bauvy, et al. (2004). "Ceramide-mediated macroautophagy involves inhibition of protein kinase B and up-regulation of beclin 1." J Biol Chem 279(18): 18384-18391.

Scarpa, R., F. Ayala, et al. (2006). "Psoriasis, psoriatic arthritis, or psoriatic disease?" J Rheumatol 33(2): 210-212.

Schaper, I. D., G. P. Marcuzzi, et al. (2005). "Development of skin tumors in mice transgenic for early genes of human papillomavirus type 8." Cancer Res 65(4): 1394-1400.

Scherz-Shouval, R. and Z. Elazar (2007). "ROS, mitochondria and the regulation of autophagy." Trends Cell Biol 17(9): 422-427.

Scherz-Shouval, R., E. Shvets, et al. (2007). "Reactive oxygen species are essential for autophagy and specifically regulate the activity of Atg4." EMBO J 26(7): 1749-1760.

Schiller, J. T. and C. B. Buck (2011). "Cutaneous squamous cell carcinoma: a smoking gun but still no suspects." J Invest Dermatol 131(8): 1595-1596.

Seglen, P. O. and P. B. Gordon (1982). "3-Methyladenine: specific inhibitor of autophagic/lysosomal protein degradation in isolated rat hepatocytes." Proc Natl Acad Sci U S A 79(6): 1889-1892.

Segrelles, C., S. Ruiz, et al. (2002). "Functional roles of Akt signaling in mouse skin tumorigenesis." Oncogene 21(1): 53-64.

Sehgal, S. N. (2003). "Sirolimus: its discovery, biological properties, and mechanism of action." Transplant Proc 35(3 Suppl): 7S-14S.

Shah, O. J., Z. Wang, et al. (2004). "Inappropriate activation of the TSC/Rheb/mTOR/S6K cassette induces IRS1/2 depletion, insulin resistance, and cell survival deficiencies." Curr Biol 14(18): 1650-1656.

Shaid, S., C. H. Brandts, et al. (2013). "Ubiquitination and selective autophagy." Cell Death Differ 20(1): 21-30.

Shamanin, V., H. zur Hausen, et al. (1996). "Human papillomavirus infections in nonmelanoma skin cancers from renal transplant recipients and nonimmunosuppressed patients." J Natl Cancer Inst 88(12): 802-811.

Sherr, C. J. and R. A. DePinho (2000). "Cellular senescence: mitotic clock or culture shock?" Cell 102(4): 407-410.

Shi, C. S., K. Shenderov, et al. (2012). "Activation of autophagy by inflammatory signals limits IL-1beta production by targeting ubiquitinated inflammasomes for destruction." Nat Immunol 13(3): 255-263.

Shi, M., T. Zhang, et al. (2013). "Calpain, Atg5 and Bak play important roles in the crosstalk between apoptosis and autophagy induced by influx of extracellular calcium." Apoptosis 18(4): 435-451.

Shibata, M., K. Yoshimura, et al. (2009). "The MAP1-LC3 conjugation system is involved in lipid droplet formation." Biochem Biophys Res Commun 382(2): 419-423.

Shintani, T. and D. J. Klionsky (2004). "Autophagy in health and disease: a double-edged sword." Science 306(5698): 990-995.

Smith, C. H. and J. N. Barker (1995). "Cell trafficking and role of adhesion molecules in psoriasis." Clin Dermatol 13(2): 151-160.

Smith, J. W., A. Koshoffer, et al. (2005). "Membranous complexes characteristic of melanocytes derived from patients with Hermansky-Pudlak syndrome type 1 are macroautophagosomal entities of the lysosomal compartment." Pigment Cell Res 18(6): 417-426.

Solomon, V. R. and H. Lee (2009). "Chloroquine and its analogs: a new promise of an old drug for effective and safe cancer therapies." Eur J Pharmacol 625(1-3): 220-233.

Sondell, B., L. E. Thornell, et al. (1995). "Evidence that stratum corneum chymotryptic enzyme is transported to the stratum corneum extracellular space via lamellar bodies." J Invest Dermatol 104(5): 819-823.

Stark, H. J., D. Breitkreutz, et al. (1987). "Keratins of the human hair follicle: "hyperproliferative" keratins consistently expressed in outer root sheath cells in vivo and in vitro." Differentiation 35(3): 236-248.

Steven, A. C., M. E. Bisher, et al. (1990). "Biosynthetic pathways of filaggrin and loricrin--two major proteins expressed by terminally differentiated epidermal keratinocytes." J Struct Biol 104(1-3): 150-162.

Steven, A. C. and P. M. Steinert (1994). "Protein composition of cornified cell envelopes of epidermal keratinocytes." J Cell Sci 107 (Pt 2): 693-700.

Storey, A. and M. Simmonds (2009). "Interaction between ultraviolet radiation and human papillomavirus." Cancer Treat Res 146: 159-167.

Strelkov, S. V., H. Herrmann, et al. (2003). "Molecular architecture of intermediate filaments." Bioessays 25(3): 243-251.

Sully, K., O. Akinduro, et al. (2012). "The mTOR inhibitor rapamycin opposes carcinogenic changes to epidermal Akt1/PKBalpha isoform signaling." Oncogene.

Surviladze, Z., R. T. Sterk, et al. (2013). "Cellular Entry of Human Papillomavirus Type 16 Involves Activation of the Phosphatidylinositol 3-Kinase/Akt/mTOR Pathway and Inhibition of Autophagy." J Virol 87(5): 2508-2517.

Takahashi, Y., C. L. Meyerkord, et al. (2011). "Bif-1 regulates Atg9 trafficking by mediating the fission of Golgi membranes during autophagy." Autophagy 7(1): 61-73.

Takahashi, Y., M. M. Young, et al. (2013). "SNAPping off Golgi membranes for autophagosome formation." Cell Cycle 12(1): 15-16.

Tanaka, Y., G. Guhde, et al. (2000). "Accumulation of autophagic vacuoles and cardiomyopathy in LAMP-2-deficient mice." Nature 406(6798): 902-906.

Tanida, I. (2011). "Autophagosome formation and molecular mechanism of autophagy." Antioxid Redox Signal 14(11): 2201-2214.

Tanida, I., T. Ueno, et al. (2004). "Human light chain 3/MAP1LC3B is cleaved at its carboxyl-terminal Met121 to expose Gly120 for lipidation and targeting to autophagosomal membranes." J Biol Chem 279(46): 47704-47710.

Tanida, I., T. Ueno, et al. (2008). "LC3 and Autophagy." Methods Mol Biol 445: 77-88.

Thomas, A. C., D. Tattersall, et al. (2009). "Premature terminal differentiation and a reduction in specific proteases associated with loss of ABCA12 in Harlequin ichthyosis." Am J Pathol 174(3): 970-978.

Thoreen, C. C., S. A. Kang, et al. (2009). "An ATP-competitive mammalian target of rapamycin inhibitor reveals rapamycin-resistant functions of mTORC1." J Biol Chem 284(12): 8023-8032.

Thrash, B. R., C. W. Menges, et al. (2006). "AKT1 provides an essential survival signal required for differentiation and stratification of primary human keratinocytes." J Biol Chem 281(17): 12155-12162.

Tobin, D. J. (2008). "Human hair pigmentation--biological aspects." Int J Cosmet Sci 30(4): 233-257.

Tolmachova, T., M. Abrink, et al. (2007). "Rab27b regulates number and secretion of platelet dense granules." Proc Natl Acad Sci U S A 104(14): 5872-5877.

Tooze, S. A., H. B. Jefferies, et al. (2010). "Trafficking and signaling in mammalian autophagy." IUBMB Life 62(7): 503-508.

Tsukada, M. and Y. Ohsumi (1993). "Isolation and characterization of autophagy-defective mutants of Saccharomyces cerevisiae." FEBS Lett 333(1-2): 169-174.

Tsukamoto, S., A. Kuma, et al. (2008). "The role of autophagy during the oocyte-to-embryo transition." Autophagy 4(8): 1076-1078.

Tsukamoto, S., A. Kuma, et al. (2008). "Autophagy is essential for preimplantation development of mouse embryos." Science 321(5885): 117-120.

Tufaro, A. P., J. C. Chuang, et al. (2011). "Molecular markers in cutaneous squamous cell carcinoma." Int J Surg Oncol 2011: 231475.
Um, S. H., F. Frigerio, et al. (2004). "Absence of S6K1 protects against age- and diet-induced obesity while enhancing insulin sensitivity." Nature 431(7005): 200-205.
Underbrink, M. P., H. L. Howie, et al. (2008). "E6 proteins from multiple human betapapillomavirus types degrade Bak and protect keratinocytes from apoptosis after UVB irradiation." J Virol 82(21): 10408-10417.
Van Den Bossche, K., J. M. Naeyaert, et al. (2006). "The quest for the mechanism of melanin transfer." Traffic 7(7): 769-778.
van Weeren, L., A. M. de Graaff, et al. (2004). "Rab3D and actin reveal distinct lamellar body subpopulations in alveolar epithelial type II cells." Am J Respir Cell Mol Biol 30(3): 288-295.
Vander Haar, E., S. I. Lee, et al. (2007). "Insulin signalling to mTOR mediated by the Akt/PKB substrate PRAS40." Nat Cell Biol 9(3): 316-323.
Vazquez, P., A. I. Arroba, et al. (2012). "Atg5 and Ambra1 differentially modulate neurogenesis in neural stem cells." Autophagy 8(2): 187-199.
Wakabayashi, N., K. Itoh, et al. (2003). "Keap1-null mutation leads to postnatal lethality due to constitutive Nrf2 activation." Nat Genet 35(3): 238-245.
Wang, M. and R. A. Miller (2012). "Fibroblasts from long-lived mutant mice exhibit increased autophagy and lower TOR activity after nutrient deprivation or oxidative stress." Aging Cell 11(4): 668-674.
Wang, R. C. and B. Levine (2011). "Calcipotriol induces autophagy in HeLa cells and keratinocytes." J Invest Dermatol 131(4): 990-993.
Wang, X., L. E. Campbell, et al. (1998). "Amino acid availability regulates p70 S6 kinase and multiple translation factors." Biochem J 334 (Pt 1): 261-267.
Wang, Y. and Z. H. Qin (2013). "Coordination of autophagy with other cellular activities." Acta Pharmacol Sin.
Watt, F. M. (1988). "Keratinocyte cultures: an experimental model for studying how proliferation and terminal differentiation are co-ordinated in the epidermis." J Cell Sci 90 (Pt 4): 525-529.
Watt, F. M. (1998). "Epidermal stem cells: markers, patterning and the control of stem cell fate." Philos Trans R Soc Lond B Biol Sci 353(1370): 831-837.
Weedon, D., J. Searle, et al. (1979). "Apoptosis. Its nature and implications for dermatopathology." Am J Dermatopathol 1(2): 133-144.
White, E. (2012). "Deconvoluting the context-dependent role for autophagy in cancer." Nat Rev Cancer.
White, E. and R. S. DiPaola (2009). "The double-edged sword of autophagy modulation in cancer." Clin Cancer Res 15(17): 5308-5316.
Wilkinson, J. E., L. Burmeister, et al. (2012). "Rapamycin slows aging in mice." Aging Cell 11(4): 675-682.
Wu, X., B. C. Nguyen, et al. (2010). "Opposing roles for calcineurin and ATF3 in squamous skin cancer." Nature 465(7296): 368-372.
Wu, Y. T., H. L. Tan, et al. (2010). "Dual role of 3-methyladenine in modulation of autophagy via different temporal patterns of inhibition on class I and III phosphoinositide 3-kinase." J Biol Chem 285(14): 10850-10861.
Wulff, C. N., M. Thygesen, et al. (2008). "Case management used to optimize cancer care pathways: a systematic review." BMC Health Serv Res 8: 227.
Xie, R., S. Nguyen, et al. (2010). "Acetylated microtubules are required for fusion of autophagosomes with lysosomes." BMC Cell Biol 11: 89.

Yamamoto, H., S. Kakuta, et al. (2012). "Atg9 vesicles are an important membrane source during early steps of autophagosome formation." J Cell Biol 198(2): 219-233.

Yanagi, T., M. Akiyama, et al. (2008). "Harlequin ichthyosis model mouse reveals alveolar collapse and severe fetal skin barrier defects." Hum Mol Genet 17(19): 3075-3083.

Yang, Y., H. Wang, et al. (2012). "GSK3beta signaling is involved in ultraviolet B-induced activation of autophagy in epidermal cells." Int J Oncol 41(5): 1782-1788.

Yang, Z. Z., O. Tschopp, et al. (2003). "Protein kinase B alpha/Akt1 regulates placental development and fetal growth." J Biol Chem 278(34): 32124-32131.

Yen, W. L., T. Shintani, et al. (2010). "The conserved oligomeric Golgi complex is involved in double-membrane vesicle formation during autophagy." J Cell Biol 188(1): 101-114.

Yla-Anttila, P., H. Vihinen, et al. (2009). "Monitoring autophagy by electron microscopy in Mammalian cells." Methods Enzymol 452: 143-164.

Young, A. R., E. Y. Chan, et al. (2006). "Starvation and ULK1-dependent cycling of mammalian Atg9 between the TGN and endosomes." J Cell Sci 119(Pt 18): 3888-3900.

Yousefi, S., R. Perozzo, et al. (2006). "Calpain-mediated cleavage of Atg5 switches autophagy to apoptosis." Nat Cell Biol 8(10): 1124-1132.

Yue, Z., S. Jin, et al. (2003). "Beclin 1, an autophagy gene essential for early embryonic development, is a haploinsufficient tumor suppressor." Proc Natl Acad Sci U S A 100(25): 15077-15082.

Yuspa, S. H., A. E. Kilkenny, et al. (1989). "Expression of murine epidermal differentiation markers is tightly regulated by restricted extracellular calcium concentrations in vitro." J Cell Biol 109(3): 1207-1217.

Zhao, Y., C. F. Zhang, et al. (2013). "Autophagy Is Induced by UVA and Promotes Removal of Oxidized Phospholipids and Protein Aggregates in Epidermal Keratinocytes." J Invest Dermatol.

zur Hausen, H. (1996). "Papillomavirus infections--a major cause of human cancers." Biochim Biophys Acta 1288(2): F55-78.

Appendix

Appendix 1: Expression of epidermal differentiation markers in undifferentiated and differentiated monolayer keratinocytes

Differentiation in primary human monolayer keratinocyte cultures is induced by culturing keratinocytes in media with high calcium content. Western blot analysis for epidermal differentiation markers was performed to confirm differentiation had occurred in cultured cells.

The expression pattern of the proteins filaggrin, K1 and K14 shows that the undifferentiated keratinocyte population consists mainly of K14 positive, proliferating keratinocytes. However, the differentiated population consists of K14 expressing proliferating cells, K1 positive early differentiated keratinocytes and filaggrin positive terminally differentiated keratinocytes. Therefore, the differentiated keratinocytes is a mix of cells at different stages in their differentiation.

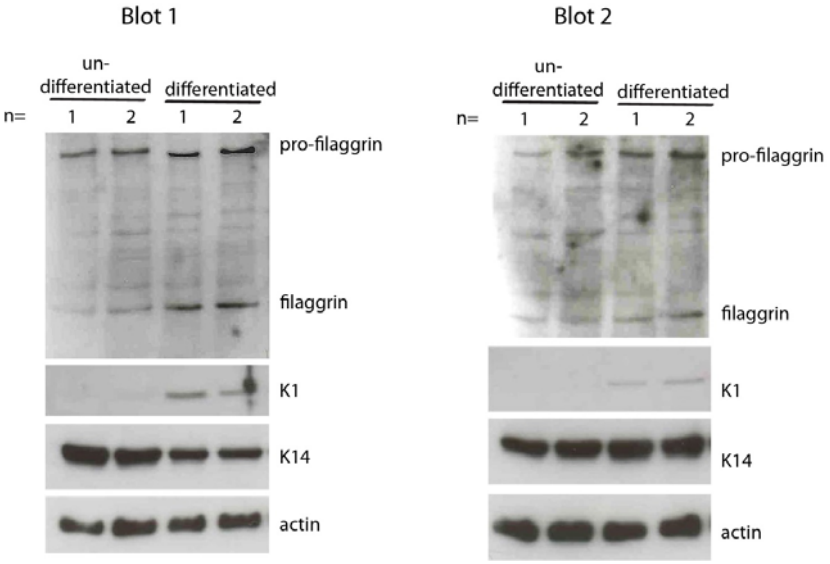

Appendix 1: Expression of epidermal differentiation markers in undifferentiated and differentiated monolayer keratinocytes.

Processed filaggrin, usually present in the granular layer of epidermis, is strongly expressed in differentiated keratinocytes, indicating activation of terminal differentiation. However the filaggrin precursor, pro-filaggrin, is present in both undifferentiated and differentiated keratinocytes. K1, a marker of early differentiation in keratinocytes of the spinous layer, is absent in undifferentiated cells but is expressed in the differentiated population. K14, a marker of the basal layer, is expressed in both undifferentiated and differentiated keratinocyte cultures.

This figure represents n=2 blots for Figure 3.7.

Appendix 2: Comparison of autophagy marker expression in undifferentiated and differentiated keratinocyte monolayer cultures

Western blot analysis of autophagy marker expression levels in undifferentiated and differentiated keratinocytes shows that there is no striking difference in the expression levels of autophagy proteins in both keratinocyte populations. However, LC3 turn-over (LC3II/LC3I) and total LC3II levels (LC3II/actin) are higher in the undifferentiated keratinocyte population compared to the differentiated cells. This suggests a higher rate of autophagy in the undifferentiated cells.

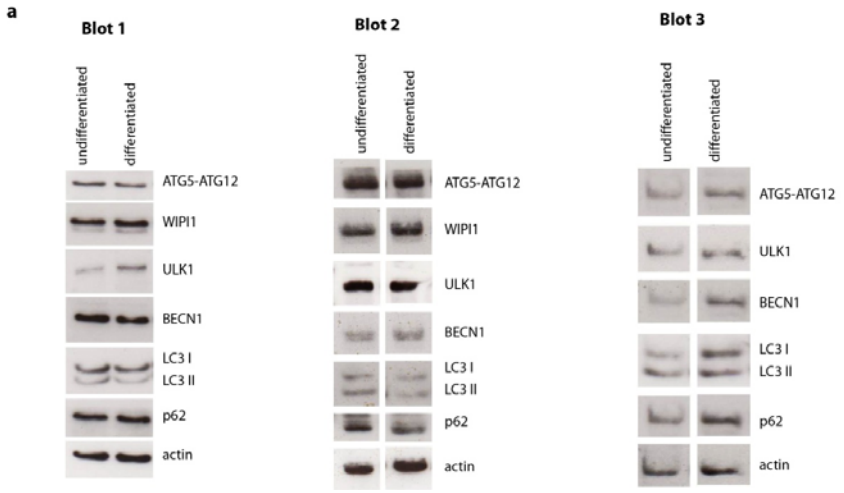

Appendix 2: Comparison of autophagy marker expression in undifferentiated and differentiated keratinocyte monolayer cultures.

(d) n=3 experiments were performed to determine the expression levels of autophagy markers in undifferentiated and differentiated primary monolayer keratinocytes. There is no striking difference in autophagy marker expression levels between undifferentiated and differentiated keratinocytes. However, blot 1 shows higher ULK1 levels in the differentiated keratinocytes. This was not observed in the other two repetitions of the experiment (blot 2 and blot 3). With each experiment, there is some variation in autophagy marker expression levels in monolayer keratinocyte cultures.

Appendix 2 continued on the next page.

b

Quantification of blots n=3 - average values

	undifferentiated		differentiated	
	LC3II/LC3I	LC3II/actin	LC3II/LC3I	LC3II/actin
blot 1	0.71	0.87	0.48	0.44
blot 2	0.74	0.64	0.65	0.28
blot 3	1.51	0.62	0.7	0.31
Averages	***0.99***	***0.71***	***0.61***	***0.34***
Std Error	0.2618099	0.0802081	0.0665833	0.0491031

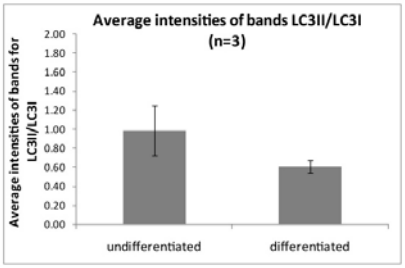

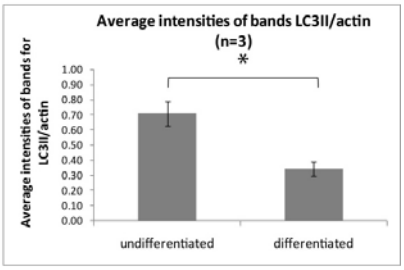

Two tailed paired t-test for average band intensities of LC3II/actin (n=3 experiments) undifferentiated and differentiated keratinocytes: $P<0.05$

Appendix 2: Comparison of autophagy marker expression in undifferentiated and differentiated keratinocyte monolayer cultures.

Appendix 2 continued.

(e) Quantification LC3 turn-over from LC3I to LC3II (LC3II/LC3I) and quantification of total LC3II levels (LC3II/actin). The table shows the individual values for LC3II/LC3I and LC3II/actin for each of n=3 blots from n=3 individual experiments. Graphs show average values for LC3II/LC3I band intensities and LC3II/actin band intensities for n=3 individual experiments. The values for the ratios of LC3II/LC3I and LC3II/actin are lower in the differentiated keratinocytes compared to the undifferentiated keratinocytes. This suggests a reduced turn-over of LC3 and less total amounts of LC3II in the differentiated keratinocyte population. This difference is statistically significant for the LC3II/actin levels, $P<0.05$.

Quantification of bands was done with ImageJ.

Appendix 2 continued on the next page.

c t-Test: Paired Two Sample for Means of LC3II/LC3I, n=3 experiments

	Variable 1	*Variable 2*
Mean	0.986666667	0.61
Variance	0.205633333	0.0133
Observations	3	3
Pearson Correlation	0.699855705	
Hypothesized Mean Di	0	
df	2	
t Stat	1.708985456	
P(T<=t) one-tail	0.114789639	
t Critical one-tail	2.91998558	
P(T<=t) two-tail	0.229579279	
t Critical two-tail	4.30265273	

t-Test: Paired Two Sample for Means of LC3II/actin, n=3 experiments

	Variable 1	*Variable 2*
Mean	0.71	0.343333
Variance	0.0193	0.007233
Observations	3	3
Pearson Correlation	0.969075452	
Hypothesized Mean Difference	0	
df	2	
t Stat	10.53608914	
P(T<=t) one-tail	0.00444417	
t Critical one-tail	2.91998558	
P(T<=t) two-tail	0.00888834	
t Critical two-tail	4.30265273	

Appendix 2: Comparison of autophagy marker expression in undifferentiated and differentiated keratinocyte monolayer cultures.

Appendix 2 continued.

(f) Results for the paired t-test for the means of LC3II/LC3I and LC3II/actin for n=3 experiments.

This figure represents n=3 blots for Figure 3.9.

Appendix 3: Changes in nucleus shape in differentiated keratinocytes compared to undifferentiated cells

Immunofluorescence analysis of DAPI-stained nuclei in undifferentiated and differentiated keratinocytes shows some cells have misshaped nuclei in the differentiated cell culture. Quantification of the number of misshaped nuclei in both keratinocyte populations shows that there is a significantly higher number of cells with misshaped nuclei in the differentiated kerainocytes compared to the undifferentiated cultures.

a

Experiment 07/2012

	undifferentiated	differentiated
misshaped nuclei	8	35
total cells	277	278

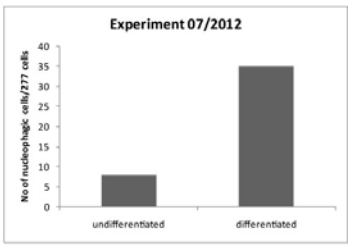

b

Experiment 08/2012

	undifferentiated	differentiated
misshaped nuclei	7	36
total cells	281	287

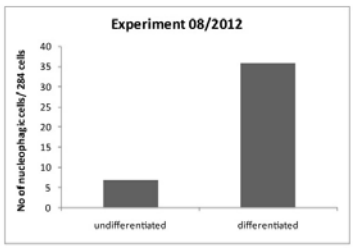

c

Experiment 12/2012

	undifferentiated	differentiated
misshaped nuclei	0	20
total cells	280	280

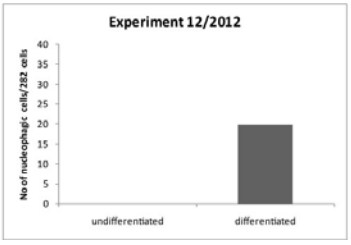

Appendix 3: Changes in nucleus shape in differentiated keratinocytes compared to undifferentiated cells.

(a, b, c) Immunofluorescence analysis of DAPI-stained nuclei in undifferentiated and differentiated keratinocytes shows some cells have misshaped nuclei in the differentiated cell culture. The number of cells with misshaped nuclei per total of ~280 cells in both undifferentiated and differentiated keratinocyte cultures was counted for n=3 experiments. The total number of cells was determined using ImageJ and the number of cells with misshaped nuclei was counted manually.

Appendix 3 continued on the next page.

d

Summary	Number of misshaped nuclei		
	undifferentiated	differentiated	total number of cells/ population
Experiment 12/2012	0	20	280
Experiment 07/2012	8	35	277
Experiment 08/2012	7	36	284
average no of misshaped nuclei	**5**	**30.33333333**	**280.3333333**
Std Error	*2.516611478*	*5.174724899*	

e

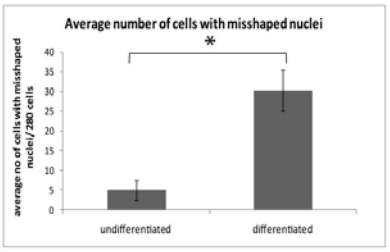

Two tailed paired t-test for number of misshaped nuclei in undifferentiated and differentiated keratinocytes: P<0.05

f

t-Test: Paired Two Sample for Means of cells with misshaped nuclei, n=3

	Variable 1	*Variable 2*
Mean	5	30.33333333
Variance	19	80.33333333
Observations	3	3
Pearson Correlation	0.98545327	
Hypothesized Mean Difference	0	
df	2	
t Stat	-9.284877771	
P(T<=t) one-tail	0.005700859	
t Critical one-tail	2.91998558	
P(T<=t) two-tail	0.011401717	
t Critical two-tail	4.30265273	

Appendix 3: Changes in nucleus shape in differentiated keratinocytes compared to undifferentiated cells.

Appendix 3 continued.

(d) The table shows the number of cells with misshaped nuclei per total of ~280 cells in both undifferentiated and differentiated keratinocyte cultures of each of the n=3 experiments, as well as the average of the three experiments.

(e) The graph shows the average values of n=3 experiments for the number of nucleophagic keratinocytes in the undifferentiated and differentiated keratinocyte cultures. A two-tailed paired t-test shows that these differences are significant with a P<0.05.

(f) Results from the paired t-test.

This figure represents n=3 experiments for Figure 3.11.

Appendix 4: Expression of the apoptosis marker, cleaved Caspase-3 in undifferentiated and differentiated keratinocyte monolayer cultures

To determine whether an apoptotic cell death in differentiated cultures is a cause for the misshaped nuclei, the monolayer keratinocyte cultures were analysed for the expression for cleaved Caspase-3 (cl. C-3).

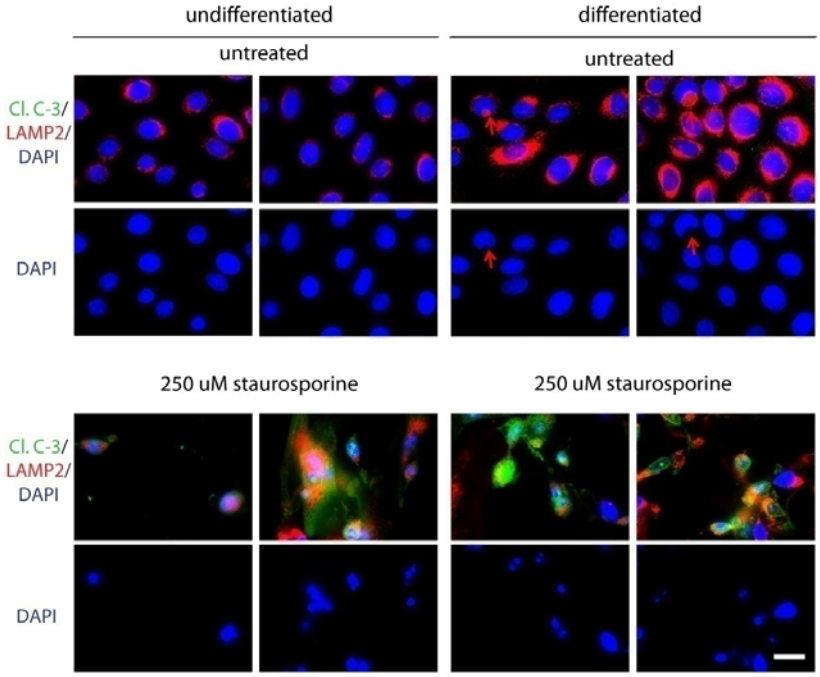

Appendix 4: Immunofluorescence analysis of cl. C-3 (green) and LAMP2 (red) in undifferentiated and differentiated keratinocytes.

As a positive control for apoptosis, both undifferentiated and differentiated keratinocytes were treated with staurosporine to induce apoptotic cell death. Cl. C-3 as well as LAMP2 is expressed in the positive controls for apoptosis of both keratinocyte populations. However, untreated undifferentiated and differentiated keratinocytes do not express cl. C-3. Also, cells with misshaped nuclei (red arrows) are not positive for cl. C-3.

Bar = 20um. Red arrows = misshaped nuclei.

This figure represents n=3 experiments for Figure 3.12.

Appendix 5: Localisation of LC3 in primary keratinocyte monolayer cultures

Initially, there did not appear to be any obvious difference in autophagy marker expression patterns between undifferentiated and differentiated keratinocytes (Fig. 3.9). However, closer examination of the keratinocyte monolayer cultures shows that in the differentiated keratinocyte cultures, the regions of missing DAPI nuclear stain of the misshaped nuclei are replaced by an accumulation of LC3 aggregates (Fig. 3.13). This suggests that the regions of missing nuclear material may be sites of high autophagic activity.

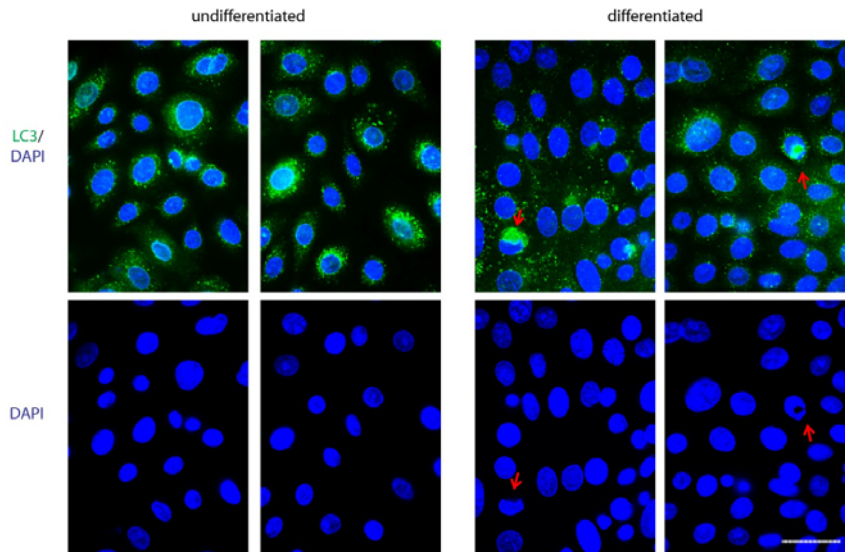

Appendix 5: Localisation of LC3 in undifferentiated and differentiated keratinocytes

DAPI staining of keratinocyte nuclei shows cells with misshaped nuclei (red arrows) in the differentiated population, whereas undifferentiated kerationocytes have regular nuclei. Immunofluorescence analysis of LC3 expression shows accumulation of LC3 in regions of missing nuclear material.

Bar = 20um. Red arrows = regions of misshaped nuclei with peri-nuclear LC3 accumulation.

This figure represents n=5 experiments for Figure 3.13.

Appendix 6: Analysis of autophagic flux in undifferentiated and differentiated primary keratinocyte cultures using chloroquine

Autophagy is a dynamic process therefore determining the amounts of autophagy proteins at one time point is not a reliable read out for autophagy levels. Autophagic flux is a measure of the rate at which autophagic cargo and autophagy proteins are processed over a certain period of time. The autophagic flux is usually analysed by measuring LC3 turn-over in the presence and in the absence of drugs which prevent degradation of autophagic vesicles by interfering with lysosomal function.

For an initial experiment, chloroquine was used to block the autophagy process. Chloroquine increases lysosomal pH preventing function of lysosomal proteases (Klionsky *et al.* 2008). This would show whether the autophagic pathway is completed and functional in the keratinocyte monolayer cultures, and this would also allow measurement of autophagic flux in undifferentiated and differentiated keratinocytes.

a

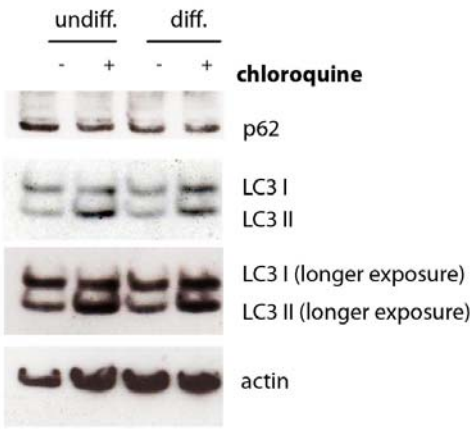

b Quantification of band intensities

	LC3I	LC3II	actin	LC3II/LC3I	LC3II/actin
undifferentiated	8868.225	4469.477	6738.497	0.50398778	0.66327506
undifferentiated + chl	9692.276	9510.79	11897.18	0.98127519	0.79941583
differentiated	8034.861	5511.255	12368.83	0.6859179	0.44557603
differentiated + chl	11209.1	7974.598	11690.08	0.71143938	0.68216825

Appendix 6: Analysis of LC3 and p62 levels in undifferentiated and differentiated keratinocytes after chloroquine treatment.

(a) An initial experiment was performed to determine whether p62 and LC3 levels were affected when autophagy was blocked with chloroquine. In both undifferentiated and differentiated keratinocyte populations, chloroquine treatment leads to an increase in LC3II band intensities.

(b) Quantification of the LC3I, LC3II, p62 and actin was done with ImageJ.

Appendix 6 continued on the next page.

c

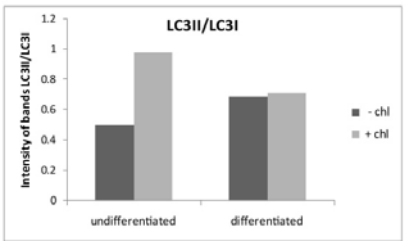

d

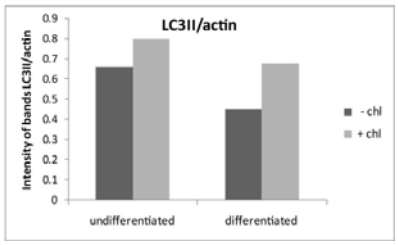

Appendix 6: Analysis of LC3 and p62 levels in undifferentiated and differentiated keratinocytes after chloroquine treatment.

Appendix 6 continued.

(c) Quantification of LC3II/LC3I ratios is a measure for the turn-over of LC3I to LC3II. In the undifferentiated keratinocyte culture, chloroquine treatment leads to an increase in LC3II/LC3I compared to untreated cells. However, in the differentiated keratinocytes chloroquine has no effect on LC3II/LC3I levels.

(d) Quantification of LC3II/actin ratios are a read-out for the total amount of membrane-bound LC3 (LC3II) in the cells. In both undifferentiated and differentiated keratinocyte cultures, chloroquine treatment leads to an increase in LC3II/actin ratios. However, LC3II/actin levels are slightly higher in the undifferentiated keratinocyte populations compared to the differentiated cultures.

This figure represents n=1 blots referred to in section 3.6.

Appendix 7: Monolayer primary keratinocyte cultures are capable of starvation-induced autophagy

Withdrawal of essential growth factors can induce autophagy therefore, keratinocytes were cultured in medium without essential growth factors. Starvation due to withdrawal of glucose also leads to autophagy induction via activation of AMPK (Fig. 1.5; Salt *et al.* 1998; Hardie *et al.* 2012). However, starvation experiments were only carried out under conditions of growth factor withdrawal due to limitations of the medium components from the supplier.

Chloroquine was used to block the autophagy process to determine whether autophagy is induced and is also completed under conditions of growth factor withdrawal.

Under conditions of growth factor withdrawal (starvation), the LC3II/LC3I ratios remain unchanged in both undifferentiated and differentiated keratinocytes (Appendix 7c). The total LC3II levels (LC3II/actin) appear to be less under conditions of growth factor withdrawal in both undifferentiated and differentiated keratinocytes compared to normal culture conditions (Appendix 7d). Therefore, this experiment shows that withdrawal of essential growth factors does not induce autophagy in primary keratinocyte cultures.

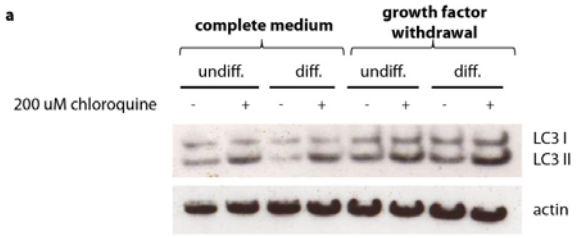

b Quantification of band intensities

	LC3I	LC3II	actin	LC3II/LC3I	LC3II/actin
undifferentiated	8868.225	4469.477	6738.497	0.50398778	0.66327506
undifferentiated + chl	9692.276	9510.79	11897.18	0.98127519	0.79941583
differentiated	8034.861	5511.255	12368.83	0.6859179	0.44557603
differentiated + chl	11209.1	7974.598	11690.08	0.71143938	0.68216825
Starved undifferentiated	7184.447	4909.062	12629.54	0.68329017	0.38869685
Starved undifferentiated + chl	8255.74	7260.841	15559	0.87949003	0.46666517
Starved differentiated	6193.205	4619.012	14067.54	0.74581933	0.32834542
Starved differentiated + chl	5184.719	4104.134	11749.47	0.79158273	0.34930382

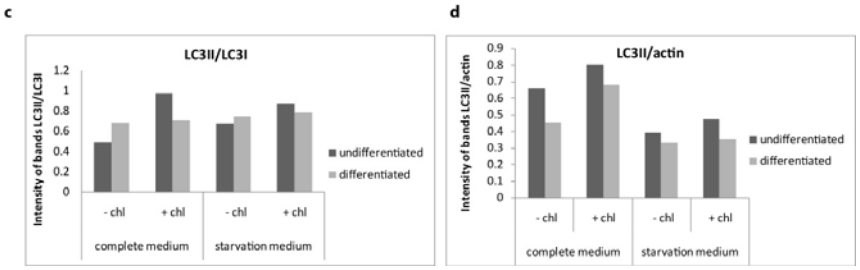

Appendix 7: Monolayer keratinocyte cultures do not respond to starvation-induced (growth factor withdrawal) autophagy

(a) Both undifferentiated and differentiated keratinocytes were cultured in complete medium as well as in medium lacking essential growth factors. Western blot analysis shows LC3 protein levels in keratinocytes under growth factor withdrawal compared to normal culture conditions in the presence and absence of chloroquine.

(b) Band intensities of LC3I, LC3II and actin were quantified using ImageJ.

(c) Quantification of LC3II/LC3II shows that growth factor withdrawal does not have an effect on LC3II/LC3I levels in both keratinocyte populations in the presence and absence of chloroquine.

(d) Quantification of LC3II/actin shows that there is less LC3II under conditions of growth factor withdrawal in both undifferentiated and differentiated keratinocyte cultures.

Appendix 8: Western blot analysis of autophagy protein expression in undifferentiated and differentiated keratinocytes after BafA1 treatment

Autophagy is a very dynamic process. Therefore, to measure the rate of autophagy turn-over over a certain period of time, the autophagy pathway is inhibited to allow measurement of the accumulated autophagy protein and autophagic cargo. Drugs like BafA1, which inhibits lysosomal protease function as well as prevents fusion of autophagosomes with autolysosomes (Klionsky *et al.* 2008), are used.

Western blot analysis shows that in both undifferentiated and differentiated keratinocytes BafA1 treatment leads to accumulation of LC3II bands. This shows that under normal culture conditions the autophagy process is completed in both keratinocyte cultures. The ratios of LC3II/LC3I and LC3II/actin are higher in the BafA1-treated undifferentiated compared to the BafA1-treated differentiated keratinocytes. This suggests that undifferentiated keratinocytes have a higher rate of autophagic flux compared to the differentiated cells. However, quantification of p62 levels (p62/actin ratios) shows that blocking the autophagy pathway with BafA1 does not affect p62 turn-over.

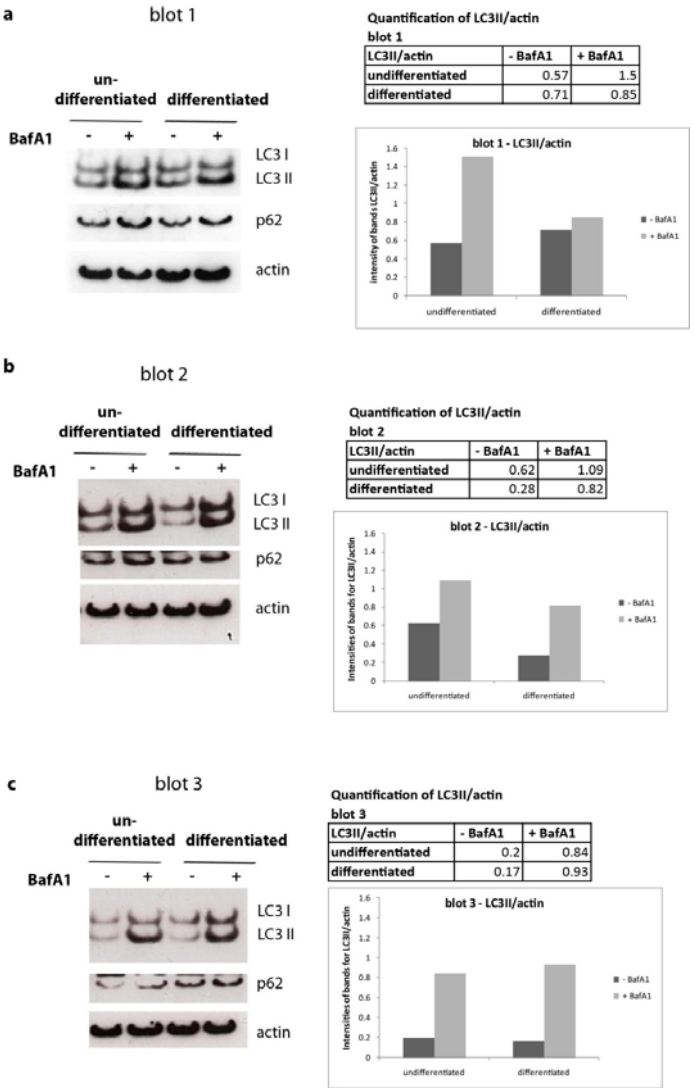

Appendix 8: Analysis of LC3 and p62 levels in undifferentiated and differentiated keratinocytes after BafA1 treatment.

(a, b, c) Western blot analysis of primary keratinocyte cultures treated with and without BafA1 for n=3 individual experiments. Quantification of LC3II/actin ratios and graphs for each experiment shows increased LC3II/actin in the BafA1 treated cells.

Appendix 8 continued on the next page.

d

Average of LC3II/actin (n=3)

LC3II/actin	- BafA1	+ BafA1
undifferentiated	0.463333	1.143333
differentiated	0.386667	0.866667

Average error of LC3II/actin (n=3)

LC3II/actin	- BafA1	+ BafA1
undifferentiated	0.132455	0.192383
differentiated	0.164756	0.03283

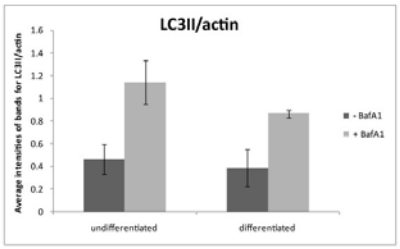

e

t-Test: Paired Two Sample for Means of BafA1-treated keratinocytes, undifferentiated vs differentiated

	Variable 1	*Variable 2*
Mean	1.166666667	0.866666667
Variance	0.137633333	0.003233333
Observations	3	3
Pearson Correlation	-0.564895009	
Hypothesized Mean Difference	0	
df	2	
t Stat	1.280368799	
P(T<=t) one-tail	0.164421972	
t Critical one-tail	2.91998558	
P(T<=t) two-tail	0.328843943	
t Critical two-tail	4.30265273	

Appendix 8: Analysis of LC3 and p62 levels in undifferentiated and differentiated keratinocytes after BafA1 treatment.

Appendix 8 continued.

(g) Table shows average values for LC3II/actin and standard errors for n=3 individual experiments. Graph shows that the LC3II/actin values in the undifferentiated keratinocytes are higher than in the differentiated keratinocyte population.

(h) Paired two tailed t-test for average values of BafA1-treated keratinocytes shows that the difference in LC3II/actin ratios between undifferentiated and differentiated keratinocytes is not statistically significant.

Appendix 8 continued on the next page.

f

Quantification of LC3II/LC3I
blot 1

LC3II/LC3I	- BafA1	+ BafA1
undifferentiated	1.02	1.13
differentiated	0.98	1.29

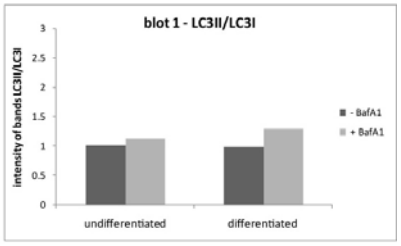

g

Quantification of LC3II/LC3I
blot 2

LC3II/LC3I	- BafA1	+ BafA1
undifferentiated	0.85	1.22
differentiated	0.46	0.72

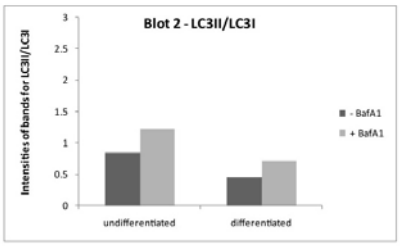

h

Quantification of LC3II/LC3I
blot 3

LC3II/LC3I	- BafA1	+ BafA1
undifferentiated	0.61	1.55
differentiated	0.4	1.05

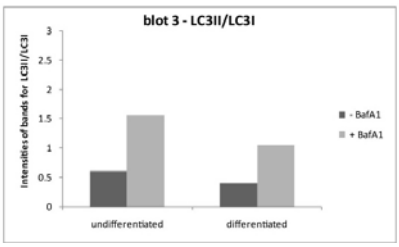

Appendix 8: Analysis of LC3 and p62 levels in undifferentiated and differentiated keratinocytes after BafA1 treatment.

Appendix 8 continued.

(f, g, h) Quantification of LC3II/LC3I ratios and graphs for each of the n=3 individual experiments shows increased LC3II/actin in the BafA1 treated cells.

Appendix 8 continued on the next page.

i

Average of LC3II/LC3I (n=3)

LC3II/LC3I	- BafA1	+ BafA1
undifferentiated	0.826667	1.3
differentiated	0.613333	1.02

Average error of LC3II/LC3I (n=3)

LC3II/LC3I	- BafA1	+ BafA1
undifferentiated	0.11893	0.127671
differentiated	0.18415	0.165227

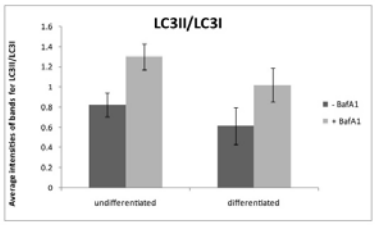

j

t-Test: Paired Two Sample for Means of LC3II/LC3I in BafA1-treated keratinocytes, undifferentiated vs differentiated

	Variable 1	*Variable 2*
Mean	1.3	1.02
Variance	0.0489	0.0819
Observations	3	3
Pearson Correlation	-0.11377219	
Hypothesized Mean Difference	0	
df	2	
t Stat	1.272727273	
P(T<=t) one-tail	0.165527061	
t Critical one-tail	2.91998558	
P(T<=t) two-tail	0.331054123	
t Critical two-tail	4.30265273	

Appendix 8: Analysis of LC3 and p62 levels in undifferentiated and differentiated keratinocytes after BafA1 treatment.

Appendix 8 continued.

(i) Table shows average values for LC3II/LC3I and standard errors for n=3 individual experiments. Graph shows that the LC3II/LC3I values in the undifferentiated keratinocytes are higher than in the differentiated keratinocyte population.

(j) Paired two tailed t-test for average values of BafA1-treated keratinocytes shows that the difference in LC3II/LC3I ratios between undifferentiated and differentiated keratinocytes is not statistically significant.

Appendix 8 continued on the next page.

k

Quantification of p62/actin
blot 1

p62/actin	- BafA1	+ BafA1
undifferentiated	0.582	0.943
differentiated	0.503	0.511

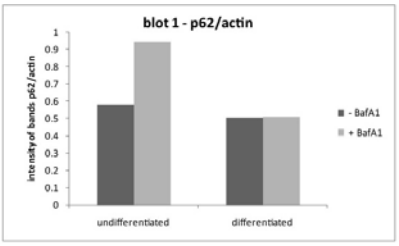

l

Quantification of p62/actin
blot 2

p62/actin	- BafA1	+ BafA1
undifferentiated	0.29	0.35
differentiated	0.33	0.29

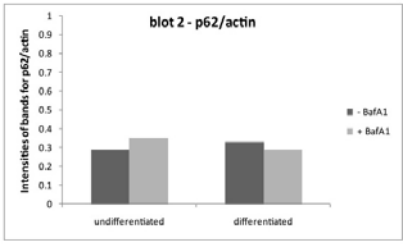

m

Quantification of p62/actin
blot 3

p62/actin	- BafA1	+ BafA1
undifferentiated	0.13	0.26
differentiated	0.41	0.42

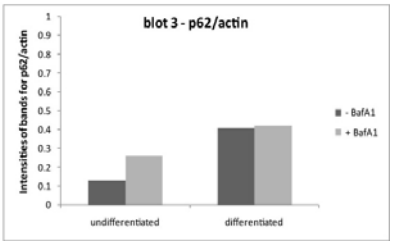

Appendix 8: Analysis of LC3 and p62 levels in undifferentiated and differentiated keratinocytes after BafA1 treatment.

Appendix 8 continued.

(k, l, m) Quantification of p62/actin ratios and graphs for each of the n=3 individual experiments shows an increase in p62/actin in the indifferentiated BafA1-treated cells. However, in the differentiated keratinocytes, BafA1 does not have an effect on p62/actin levels.

Appendix 8 continued on the next page.

n

Average of p62/actin (n=3)

p62/actin	- BafA1	+ BafA1
undifferentiated	0.334	0.517667
differentiated	0.414333	0.407

Average error of p62/actin (n=3)

p62/actin	- BafA1	+ BafA1
undifferentiated	0.132323	0.214248
differentiated	0.049988	0.064127

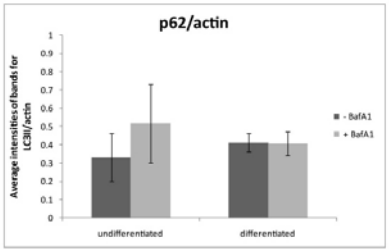

o

t-Test: Paired Two Sample for Means of p62/actin in BafA1-treated keratinocytes, undifferentiated vs differentiated

	Variable 1	*Variable 2*
Mean	0.517666667	0.407
Variance	0.137706333	0.012337
Observations	3	3
Pearson Correlation	0.733935671	
Hypothesized Mean Difference	0	
df	2	
t Stat	0.640568647	
P(T<=t) one-tail	0.293700777	
t Critical one-tail	2.91998558	
P(T<=t) two-tail	0.587401554	
t Critical two-tail	4.30265273	

Appendix 8: Analysis of LC3 and p62 levels in undifferentiated and differentiated keratinocytes after BafA1 treatment.

Appendix 8 continued.

(n) Table shows average values for p62/actin and standard errors for n=3 individual experiments. Graph shows that the p62/actin values in the undifferentiated keratinocytes are higher than in the differentiated keratinocyte population.

(o) Paired two tailed t-test for average values of BafA1-treated keratinocytes shows that the difference in p62/actin ratios between undifferentiated and differentiated keratinocytes is not statistically significant.

This figure represents n=3 blots referred to in Figure 3.16.

Appendix 9: Analysis of cellular protein expression patterns in undifferentiated and differentiated keratinocytes after BafA1 treatment

The observations made with Western blot analysis in BafA1-treated and untreated keratinocyte cultures were verified using immunofluorescence analysis. BafA1 treatment increases the LC3 expression intensities per cell in both undifferentiated and differentiated keratinocyte populations. This increase in LC3 intensities is statistically significant in the differentiated keratinocytes with $P<0.05$. However, the LC3 intensities per cell are nearly equal in both undifferentiated and differentiated keratinocytes when treated with BafA1. Therefore, immunofluorescence analysis shows that the LC3 intensities per cell in undifferentiated and differentiated cells does not vary greatly. Therefore, no statistical test was performed in the LC3 intensities in the BafA1-treated cells of both keratinocyte populations.

BafA1 treatment also increases the p62 expression intensities per cell in both keratinocyte populations and this increase is statistically significant in the undifferentiated cells with $P<0.05$. However, the difference in p62 intensities per cell in the BafA1-treated undifferentiated keratinocytes compared to the BafA1-treated differentiated cells is not statistically significant.

These results show that under normal culture conditions, the autophagy process is completed since blocking it with BafA1 leads to an increase in LC3 and p62 levels. However, there is no significant difference in LC3 and p62 expression intensities in undifferentiated and differentiated keratinocytes.

Quantification of LC3 intensities per cell (n=1)

Label	IntDen	No of cells	Average intensity per cell
high Ca 48h nHEKs P2 LC3_g p62_r 60x 21122012 image 1g.tif	462.73	15	30.84866667
high Ca 48h nHEKs P2 LC3_g p62_r 60x 21122012 image 2g.tif	1225.81	13	94.29307692
high Ca 48h nHEKs P2 LC3_g p62_r 60x 21122012 image 4g.tif	769.72	11	69.97454545
Sum	2458.26	39	
Average LC3 intensity per cell	**63.03231**		
Std Error	18.48035		

Label	IntDen	No of cells	Average intensity per cell
high Ca + Baf 48h nHEKs P2 LC3_g p62_r 60x 21122012 image 1g.tif	1750.8	12	145.9
high Ca + Baf 48h nHEKs P2 LC3_g p62_r 60x 21122012 image 4g.tif	1144.84	13	88.06461538
important! high Ca + Baf 48h nHEKs P2 LC3_g p62_r 60x 21122012 image 3g.tif	2119.23	14	151.3735714
Sum	5014.87	39	
Average LC3 intensity per cell	**128.5864**		
Std Error	20.25246		

Label	IntDen	No of cells	Average intensity per cell
low Ca 48h nHEKs P2 LC3_g p62_r 60x 21122012 image 1g.tif	682.57	13	52.50538462
low Ca 48h nHEKs P2 LC3_g p62_r 60x 21122012 image 3g.tif	1025.72	11	93.24727273
low Ca 48h nHEKs P2 LC3_g p62_r 60x 21122012 image 4g.tif	1290.07	10	129.007
Sum	2998.36	34	
Average LC3 intensity per cell	**88.18706**		
Stnd Error	22.09972		

Label	IntDen	No of cells	Average intensity per cell
low Ca + Baf 48h nHEKs P2 LC3_g p62_r 60x 21122012 image 1g.tif	1856.32	9	206.2577778
low Ca + Baf 48h nHEKs P2 LC3_g p62_r 60x 21122012 image 2g.tif	1644.86	11	149.5327273
low Ca + Baf 48h nHEKs P2 LC3_g p62_r 60x 21122012 image 3g.tif	1984.07	11	180.37
Sum	5485.25	31	
Average LC3 intensity per cell	**176.9435**		
Std Error	16.39588		

Appendix 9 Table 1: Analysis of LC3 expression in undifferentiated and differentiated keratinocytes after BafA1 treatment for n=1 experiments.

Keratinocyte monolayer cultures treated with and without BafA1. The LC3 expression intensities were analysed with immunofluorescence analysis and quantified with ImageJ. The average LC3 intensity per cell was calculated for each culture condition.

Appendix 9 continued on the next page.

Quantification of LC3 intensities per cell (n=2)

	IntDen	No of cells	Average intensity per cell
Untreated high Ca LC3_g Lamp2_r 23112012 image 1gb.tif (green)	60.79	14	4.342142857
Untreated high Ca LC3_g Lamp2_r 23112012 image 2gb.tif (green)	206.29	10	20.629
Untreated high Ca LC3_g Lamp2_r 23112012 image 4gb.tif (green)	49.19	7	7.027142857
sum	316.27	31	
average	105.4233		
Intensity per cell	**10.20226**		
Stdn Error	5.041392		

	IntDen	No of cells	Average intensity per cell
Untreated + Baf high Ca LC3_g Lamp2_r 23112012 image 1gb.tif (green)	799.67	6	133.2783333
Untreated + Baf high Ca LC3_g Lamp2_r 23112012 image 4gb.tif (green)	597.34	7	85.33428571
Untreated + Baf high Ca LC3_g Lamp2_r 23112012 image 3gb.tif (green)	417.73	8	52.21625
sum	1814.74	21	
average	604.9133		
Intensity per cell	**86.41619**		
Stdn Error	23.53071		

	IntDen	No of cells	Average intensity per cell
Untreated low Ca LC3_g Lamp2_r 23112012 image 3gb.tif (green)	77.69	7	11.09857143
Untreated low Ca LC3_g Lamp2_r 23112012 image 4gb.tif (green)	163.18	6	27.19666667
Untreated low Ca LC3_g Lamp2_r 23112012 image 2gb.tif (green)	76.28	6	12.71333333
sum	317.15	19	
average	105.7167		
Intensity per cell	**16.69211**		
Stdn Error	5.118176		

	IntDen	No of cells	Average intensity per cell
Untreated + Baf low Ca LC3_g Lamp2_r 23112012 image 1gb.tif (green)	449.09	4	112.2725
Untreated + Baf low Ca LC3_g Lamp2_r 23112012 image 2gb.tif (green)	809.6	6	134.9333333
Untreated + Baf low Ca LC3_g Lamp2_r 23112012 image 3gb.tif (green)	568.16	10	56.816
sum	1826.85	20	
average	608.95		
Intensity per cell	**91.3425**		
Stdn Error	23.20351		

Appendix 9 Table 2: Analysis of LC3 expression in undifferentiated and differentiated keratinocytes after BafA1 treatment for n=2 experiments.

Appendix 9 continued.

Keratinocyte monolayer cultures treated with and without BafA1. The LC3 expression intensities were analysed with immunofluorescence analysis and quantified with ImageJ. The average LC3 intensity per cell was calculated for each culture condition.

Appendix 9 continued on the next page.

Quantification of LC3 intensities per cell (n=3)

Label	IntDen	No of cells	Average intensity per cell
high Ca 48h nHEKs P2 LC3_g LAMP2_r 60x 21122012 image 2g.tif	234.29	15	15.61933333
high Ca 48h nHEKs P2 LC3_g LAMP2_r 60x 21122012 image 4g.tif	180.14	9	20.01555556
high Ca 48h nHEKs P2 LC3_g LAMP2_r 60x 21122012 image 6g.tif	344.41	16	21.525625
Sum	758.84	40	
Average LC3 intensity per cell	**18.971**		
Stnd Error	1.771555512		

Label	IntDen	No of cells	Average intensity per cell
high Ca + BafA1 48h nHEKs P2 LC3_g LAMP2_r 60x 21122012 image 2g.tif	1955.32	18	108.6288889
high Ca + BafA1 48h nHEKs P2 LC3_g LAMP2_r 60x 21122012 image 4g.tif	1402.08	14	100.1485714
high Ca + BafA1 48h nHEKs P2 LC3_g LAMP2_r 60x 21122012 image 5g.tif	2654.62	12	221.2183333
Sum	6012.02	44	
Average LC3 intensity per cell	**136.6368182**		
Stnd Error	39.02007036		

Label	IntDen	No of cells	Average intensity per cell
low Ca 48h nHEKs P2 LC3_g LAMP2_r 60x 21122012 image 1g.tif	616.05	11	56.00454545
low Ca 48h nHEKs P2 LC3_g LAMP2_r 60x 21122012 image 2g.tif	863.64	12	71.97
low Ca 48h nHEKs P2 LC3_g LAMP2_r 60x 21122012 image 4g.tif	984.38	12	82.03166667
Sum	2464.07	35	
Average LC3 intensity per cell	**70.402**		
Stnd Error	7.577539595		

Label	IntDen	No of cells	Average intensity per cell
low Ca + BafA1 48h nHEKs P2 LC3_g LAMP2_r 60x 21122012 image 1g.tif	1419.02	14	101.3585714
low Ca + BafA1 48h nHEKs P2 LC3_g LAMP2_r 60x 21122012 image 2g.tif	1136.39	16	71.024375
low Ca + BafA1 48h nHEKs P2 LC3_g LAMP2_r 60x 21122012 image 3g.tif	1714.75	14	122.4821429
Sum	4270.16	44	
Average LC3 intensity per cell	**97.04909091**		
Stnd Error	14.9336879		

Appendix 9 Table 3: Analysis of LC3 expression in undifferentiated and differentiated keratinocytes after BafA1 treatment for n=3 experiments.

Appendix 9 continued.

Keratinocyte monolayer cultures treated with and without BafA1. The LC3 expression intensities were analysed with immunofluorescence analysis and quantified with ImageJ. The average LC3 intensity per cell was calculated for each culture condition.

Appendix 9 continued on the next page.

a

Average LC3 intensity per cell (n=1)

	- BafA1	+ BafA1
undifferentiated	88.2	176.9
differentiated	63	128.6

Std Error per cell (n=1)

	- BafA1	+ BafA1
undifferentiated	22.1	16.4
differentiated	18.5	20.3

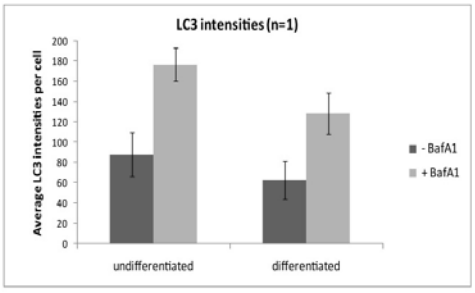

b

Average LC3 intensity per cell (n=2)

	- BafA1	+ BafA1
undifferentiated	16.7	91.3
differentiated	10.2	86.4

Std Error per cell (n=2)

	- BafA1	+ BafA1
undifferentiated	5.11	23.2
differentiated	5.04	23.5

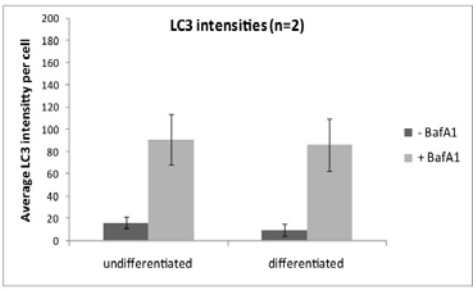

c

Average LC3 intensity per cell (n=3)

	- BafA1	+ BafA1
undifferentiated	70.4	97.05
differentiated	18.97	136.64

Std Error per cell (n=3)

	- BafA1	+ BafA1
undifferentiated	7.58	14.93
differentiated	1.77	39.02

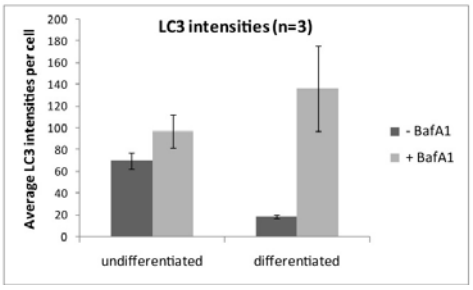

Appendix 9: Analysis of LC3 expression in undifferentiated and differentiated keratinocytes after BafA1 treatment for n=3 experiments.

Appendix 9 continued.

(a, b, c) Keratinocyte monolayer cultures were treated with and without BafA1 in n=3 experiments. The average LC3 intensities per cell for each experiment, n=1, 2, 3 are shown in tables on the left and the corresponding graphs for the values are in the graphs on the right.

Appendix 9 continued on the next page.

d

Average LC3 intensity per cell of 3 experiments (n=1, 2, 3)

	- BafA1	+ BafA1
undifferentiated	58.43333	121.75
differentiated	30.72333	117.2133

Std error of average LC3 intensity per cell of 3 experiments (n=1, 2, 3)

	- BafA1	+ BafA1
undifferentiated	21.49002	27.62491
differentiated	16.3357	15.58051

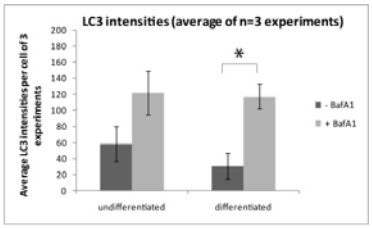

e

t-Test: Paired Two Sample for Means for LC3 intensities in undifferentiated cells with and without BafA1

	Variable 1	*Variable 2*
Mean	58.43333333	121.75
Variance	1385.463333	2289.4075
Observations	3	3
Pearson Correlation	0.73466149	
Hypothesized Mean Difference	0	
df	2	
t Stat	-3.371541287	
P(T<=t) one-tail	0.038919462	
t Critical one-tail	2.91998558	
P(T<=t) two-tail	0.077838924	
t Critical two-tail	4.30265273	

f

t-Test: Paired Two Sample for Means for LC3 intensities in differentiated cells with and without BafA1

	Variable 1	*Variable 2*
Mean	30.72333333	117.2133333
Variance	800.5656333	728.2565333
Observations	3	3
Pearson Correlation	0.505259779	
Hypothesized Mean Difference	0	
df	2	
t Stat	-5.443915627	
P(T<=t) one-tail	0.01606268	
t Critical one-tail	2.91998558	
P(T<=t) two-tail	0.032125361	
t Critical two-tail	4.30265273	

Appendix 9: Analysis of LC3 expression in undifferentiated and differentiated keratinocytes after BafA1 treatment for n=3 experiments.

Appendix 9 continued.

(d) Average values for LC3 intensities per cell of n=3 experiments, with the values on the left and the graph on the right.

(e) The results of a paired t-test for undifferentiated keratinocytes without BafA1 compared to BafA1 treated cells, shows that the difference in LC3 expression intensities is not significant.

(f) The results of a paired t-test for differentiated keratinocytes without BafA1 compared to BafA1 treated cells, shows that the difference in LC3 expression intensities is significant, $P<0.05$. **Appendix 9 continued on the next page.**

Quantification of p62 intensities per cell (n=1)

Label	IntDen	No of cells	Average intensity per cell
low Ca 48h nHEKs P2 LC3_g p62_r 60x 21122012 image 4.tif (RGB) (red)	12.89	10	1.289
low Ca 48h nHEKs P2 LC3_g p62_r 60x 21122012 image 3.tif (RGB) (red)	38.11	13	2.931538462
low Ca 48h nHEKs P2 LC3_g p62_r 60x 21122012 image 2.tif (RGB) (red)	76.62	13	5.893846154
low Ca 48h nHEKs P2 LC3_g p62_r 60x 21122012 image 1.tif (RGB) (red)	29.57	13	2.274615385
sum	157.19	49	
average	39.2975		
Average intensity per cell		**3.20795918**	
Stdn Error		**0.99141759**	
low Ca + Baf 48h nHEKs P2 LC3_g p62_r 60x 21122012 image 4.tif (RGB) (red)	346.76	10	34.676
low Ca + Baf 48h nHEKs P2 LC3_g p62_r 60x 21122012 image 3.tif (RGB) (red)	341.91	12	28.4925
low Ca + Baf 48h nHEKs P2 LC3_g p62_r 60x 21122012 image 2.tif (RGB) (red)	288.64	11	26.24
low Ca + Baf 48h nHEKs P2 LC3_g p62_r 60x 21122012 image 1.tif (RGB) (red)	350.29	10	35.029
sum	1327.6	43	
average	331.9		
Intensity per cell		**30.8744186**	
Stdn Error		**2.21063946**	
high Ca 48h nHEKs P2 LC3_g p62_r 60x 21122012 image 3_1.tif (RGB) (red)	113.7	15	7.58
high Ca 48h nHEKs P2 LC3_g p62_r 60x 21122012 image 3.tif (RGB) (red)	424.47	10	42.447
high Ca 48h nHEKs P2 LC3_g p62_r 60x 21122012 image 2.tif (RGB) (red)	515.8	15	34.38666667
high Ca 48h nHEKs P2 LC3_g p62_r 60x 21122012 image 1.tif (RGB) (red)	134.17	16	8.385625
sum	1188.14	56	
average	297.035		
Intensity per cell		**21.2167857**	
Stdn Error		**8.93979225**	
important! high Ca + Baf 48h nHEKs P2 LC3_g p62_r 60x 21122012 image 3.tif (RGB	921.51	13	70.88538462
high Ca + Baf 48h nHEKs P2 LC3_g p62_r 60x 21122012 image 4_1.tif (RGB) (red)	597.07	10	59.707
important! high Ca + Baf 48h nHEKs P2 LC3_g p62_r 60x 21122012 image 3_2.tif (R	623.16	9	69.24
high Ca + Baf 48h nHEKs P2 LC3_g p62_r 60x 21122012 image 1.tif (RGB) (red)	677.57	13	52.12076923
sum	2819.31	45	
average	704.8275		
Intensity per cell		**62.6513333**	
Stdn Error		**4.38099925**	

Appendix 9 Table 4: Analysis of p62 expression in undifferentiated and differentiated keratinocytes after BafA1 treatment for n=1 experiments.

Appendix 9 continued.

Keratinocyte monolayer cultures treated with and without BafA1. The p62 expression intensities were analysed with immunofluorescence analysis and quantified with ImageJ. The average p62 intensity per cell was calculated for each culture condition.

Appendix 9 continued on the next page.

Quantification of p62 intensities per cell (n=2)			
Label	**IntDen**	**No of cells**	**Intensity per cell**
low Ca LC3_g Lp62_r 60x 22022013 image 1.tif (RGB) (red)	122.81	4	30.7025
low Ca LC3_g Lp62_r 60x 22022013 image 2.tif (RGB) (red)	16.82	7	2.402857143
low Ca LC3_g Lp62_r 60x 22022013 image 3.tif (RGB) (red)	35.55	8	4.44375
low Ca LC3_g Lp62_r 60x 22022013 image 4.tif (RGB) (red)	3.97	6	0.661666667
sum	179.15	25	
average	44.7875		
Intensity per cell		**7.166**	
Stdn Error		**7.0921678**	
low Ca + baf LC3_g Lp62_r 60x 22022013 image 1.tif (RGB) (red)	143.19	6	23.865
low Ca + baf LC3_g Lp62_r 60x 22022013 image 2.tif (RGB) (red)	173.04	7	24.72
low Ca + baf LC3_g Lp62_r 60x 22022013 image 3.tif (RGB) (red)	303.95	6	50.65833333
low Ca + baf LC3_g Lp62_r 60x 22022013 image 1_2.tif (RGB) (red)	263.35	7	37.62142857
sum	883.53	26	
average	220.8825		
Intensity per cell		**33.981923**	
Stdn Error		**6.3197078**	
high Ca LC3_g Lp62_r 60x 22022013 image 1.tif (RGB) (red)	216.37	6	36.06166667
high Ca LC3_g Lp62_r 60x 22022013 image 2.tif (RGB) (red)	75.46	11	6.86
high Ca LC3_g Lp62_r 60x 22022013 image 3.tif (RGB) (red)	86.44	14	6.174285714
high Ca LC3_g Lp62_r 60x 22022013 image 4.tif (RGB) (red)	104.56	10	10.456
sum	482.83	41	
average	120.7075		
Intensity per cell		**11.776341**	
Stdn Error		**7.1200678**	
high Ca + Baf LC3_g Lp62_r 60x 22022013 image 1.tif (RGB) (red)	272.28	10	27.228
high Ca + Baf LC3_g Lp62_r 60x 22022013 image 2.tif (RGB) (green)	192.18	5	38.436
high Ca + Baf LC3_g Lp62_r 60x 22022013 image 3.tif (RGB) (red)	391.71	7	55.95857143
high Ca + Baf LC3_g Lp62_r 60x 22022013 image 1_2.tif (RGB) (red)	238.5	6	39.75
sum	1094.67	28	
average	273.6675		
Intensity per cell		**39.095357**	
Stdn Error		**5.9149359**	

Appendix 9 Table 5: Analysis of p62 expression in undifferentiated and differentiated keratinocytes after BafA1 treatment for n=2 experiments.

Appendix 9 continued.

Keratinocyte monolayer cultures treated with and without BafA1. The p62 expression intensities were analysed with immunofluorescence analysis and quantified with ImageJ. The average p62 intensity per cell was calculated for each culture condition.

Appendix 9 continued on the next page.

g

Average p62 intensity per cell (n=1)

	Undifferentiated	Differentiated
- BafA1	3.21	21.22
+ BafA1	30.87	62.65

Std error per cell per cell (n=1)

	Undifferentiated	Differentiated
- BafA1	0.99	8.94
+ BafA1	2.21	4.38

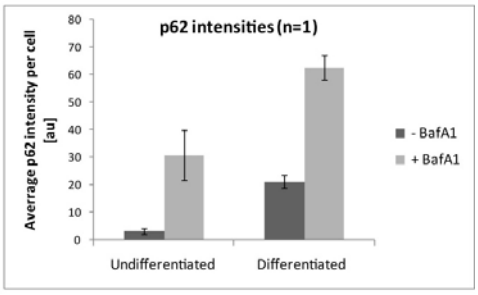

h

Average p62 intensity per cell (n=2)

	Undifferentiated	Differentiated
- BafA1	7.17	11.78
+ BafA1	33.98	39.1

Std error per cell per cell (n=2)

	Undifferentiated	Differentiated
- BafA1	7.09	7.12
+ BafA1	6.32	5.91

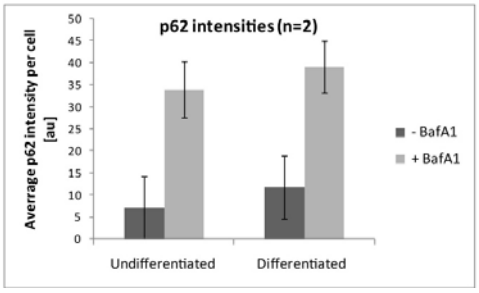

Appendix 9: Analysis of p62 expression in undifferentiated and differentiated keratinocytes after BafA1 treatment for n=2 experiments.

Appendix 9 continued.

(g, h) Keratinocyte monolayer cultures were treated with and without BafA1 in n=2 experiments. The average p62 intensities per cell for each experiment, n=1, 2 are shown in tables on the left and the corresponding graphs for the values are in the graphs on the right.

Appendix 9 continued on the next page.

i

Average p62 intensity per cell of 2 experiments (n=1, 2)

	Undifferentiated	Differentiated
- BafA1	5.19	16.5
+ BafA1	32.425	50.875

Std errors p62 intensity per cell per cell of 2 experiments (n=1, 2)

	Undifferentiated	Differentiated
- BafA1	1.98	4.7
+ BafA1	1.56	11.78

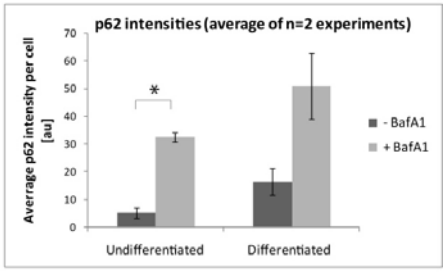

j

t-Test: Paired Two Sample for Means for p62 intensities in undifferentiated keratinocytes without and with BafA1

	Variable 1	*Variable 2*
Mean	5.19	32.425
Variance	7.8408	4.83605
Observations	2	2
Pearson Correlation	1	
Hypothesized Mean Difference	0	
df	1	
t Stat	-64.082353	
P(T<=t) one-tail	0.0049668	
t Critical one-tail	6.31375151	
P(T<=t) two-tail	0.00993359	
t Critical two-tail	12.7062047	

k t-Test: Paired Two Sample for Means for p62 intensities in differentiated keratinocytes without and with BafA1

	Variable 1	*Variable 2*
Mean	16.5	50.875
Variance	44.5568	277.30125
Observations	2	2
Pearson Correlation	1	
Hypothesized Mean Difference	0	
df	1	
t Stat	-4.8724309	
P(T<=t) one-tail	0.06443401	
t Critical one-tail	6.31375151	
P(T<=t) two-tail	0.12886802	
t Critical two-tail	12.7062047	

Appendix 9: Analysis of p62 expression in undifferentiated and differentiated keratinocytes after BafA1 treatment for n=2 experiments.

Appendix 9 continued.

(i) Average values for p62 intensities per cell of n=2 experiments, with the values on the left and the graph on the right.

(j) The results of a paired t-test for undifferentiated keratinocytes without BafA1 compared to BafA1 treated cells, shows statistically significant difference in p62 expression intensities, $P<0.05$

(k) The results of a paired t-test for differentiated keratinocytes without BafA1 compared to BafA1 treated cells, shows that the difference in p62 expression intensities is not significant.

I

t-Test: Paired Two Sample for Means for p62 intensities BafA1 treated cells, undifferentiated vs differentiated keratinocytes

	Variable 1	*Variable 2*
Mean	32.425	50.875
Variance	4.83605	277.30125
Observations	2	2
Pearson Correlation	-1	
Hypothesized Mean Difference	0	
df	1	
t Stat	-1.384096024	
P(T<=t) one-tail	0.199154757	
t Critical one-tail	6.313751514	
P(T<=t) two-tail	0.398309513	
t Critical two-tail	12.70620473	

Appendix 9: Analysis of p62 expression in undifferentiated and differentiated keratinocytes after BafA1 treatment for n=2 experiments.

Appendix 9 continued.

(I) The results of a paired t-test for BafA1-treated keratinocytes, undifferentiated cells compared differentiated cells, shows no statistically significant difference

This figure represents n=3 experiments referred to in Figure 3.17.

Appendix 10: Inhibition of autophagy via siRNA knockdowns of ULK1 and WIPI1, and its effects on nucleophagy in differentiating keratinocytes

In order to find out if autophagy is essential for degradation of nuclei, during differentiation *in vitro*, a knockdown of key autophagy proteins was carried out using siRNAs against ULK1 and WIPI1. Monolayer proliferating undifferentiated keratinocytes were transfected with the different siRNAs. 24h after transfection, differentiation was induced for a further 48h by increasing the calcium content of the media (corresponding to 72h after the siRNA transfection). The end-concentration of siRNAs used was 50nM. Titrations for lower contentrations (10nM and 25nM) showed that lower siRNA concentrations did not efficiently down-regulate target gene expression. Undifferentiated keratinocytes were cultured in medium with low calcium for the period before harvesting.

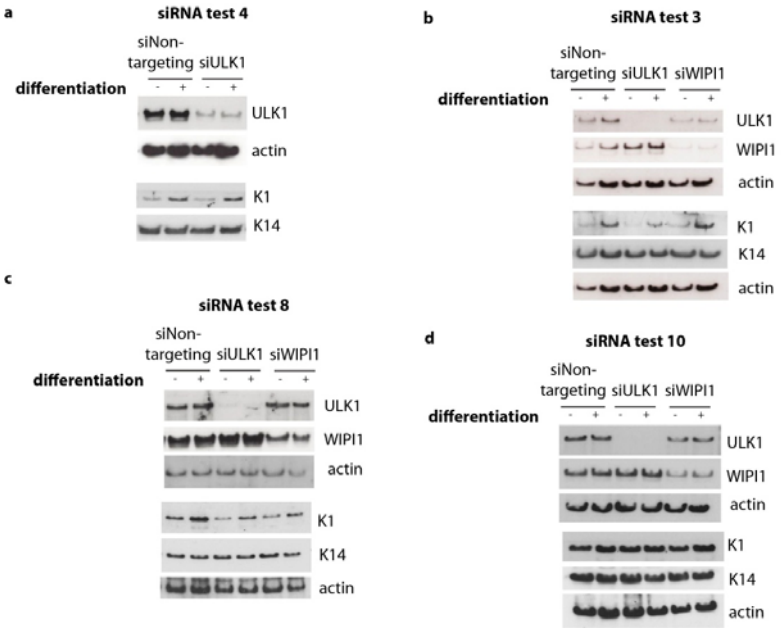

Appendix 10: Inhibition of autophagy via siRNA knockdowns of ULK1 and WIPI1 and, its effects on the expression of keratinocyte differentiation markers.

(a, b, c, d) Western blotting of lysates from four different experiments of keratinocytes transfected with non-targeting, ULK1 and WIPI1 siRNA shows effective knockdown of ULK1 and WIPI1 in the siULK1 and siWIPI1 cells. Western blot analysis of differentiation markers K1 and K14 shows that in keratinocytes with non-targeting siRNA, K1 is expressed at lower levels in the undifferentiated keratinocytes compared to the differentiated keratinocytes. Both siULK1 and siWIPI1 cells show a similar K1 expression pattern. Western blot analysis of K14 expression shows relatively constant K14 expression levels in both undifferentiated and differentiated siNon-targeting, siULK1 and siWIPI1 cells.

Appendix 10 continued on the next page.

e

siRNA test5

	siNon-targeting	siULK1	siWIPI1
undifferentiated	3.9	1.1	1.2
differentiated	14.8	6.8	2.6

siRNA test7

	siNon-targeting	siULK1	siWIPI1
undifferentiated	1.8	2.9	0
differentiated	16.5	13.4	2.4

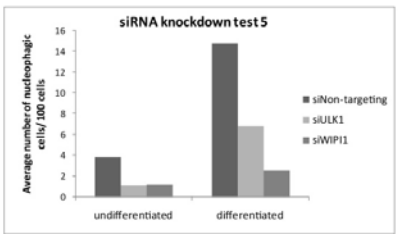

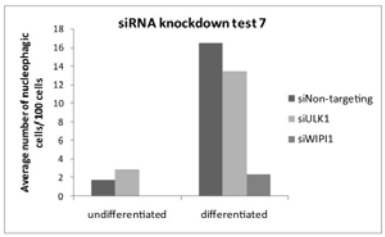

Appendix 10: Inhibition of autophagy via siRNA knockdowns of ULK1 and WIPI1, and its effects on nucleophagy in differentiating keratinocytes.

Appendix 10 continued.

(e) Quantification of nucleophagic keratinocytes in both undifferentiated and differentiated cultures of cells transfected with non-targeting, ULK1 and WIPI1 siRNAs in two independent transfections shows there is a reduction in the proportion of nucleophagic cells in the differentiated siULK1 and siWIPI1 knockdown cells compared to differentiated cells with non-targeting siRNA.

Total number of cells determined with ImageJ and number of nucleophagic cells counted manually.

Appendix 10 continued on the next page.

f

Average number of nucleophagic cells/ 100 cells

undifferentiated

	siNon-targeting	siULK1	siWIPI1
test 5	3.9	1.1	1.2
test 7	1.8	2.9	0
Average	**2.85**	**2**	**0.6**
Std Error	*1.05*	*0.9*	*0.6*

differentiated

	siNon-targeting	siULK1	siWIPI1
test 5	**14.8**	**6.8**	**2.6**
test 7	**16.5**	**13.4**	**2.4**
Average	**15.65**	**10.1**	**2.5**
Std Error	*0.85*	*3.3*	*0.1*

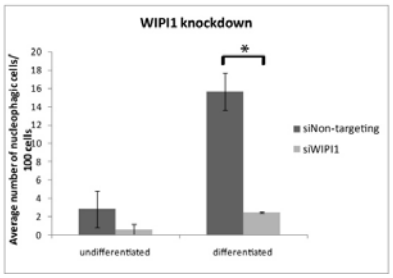

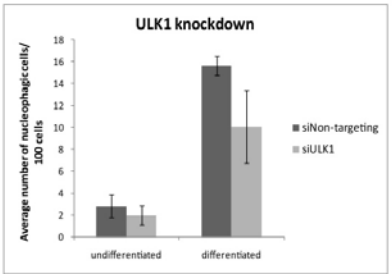

Appendix 10: Inhibition of autophagy via siRNA knockdowns of ULK1 and WIPI1, and its effects on nucleophagy in differentiating keratinocytes.

Appendix 10 continued.

(f) The average number of nucleophagic keratinocytes of the n=2 experiments, ~10% in siULK1 cells, ~3% in siWIPI1 cells and ~16% in siNon-targeting cells, shows that a knockdown of key autophagy genes reduces the number of nucleophagic keratinocytes in the differentiated keratinocyte population. This reduction in nucleophagic cells is statistically significant ($P<0.05$) in the differentiated keratinocytes with siWIPI compared to the non-targeting siRNA cells.

Appendix 10 continued on the next page.

g

t-Test: Paired Two Sample for Means of differentiated cells - siNon-targeting vs siULK11

	Variable 1	*Variable 2*
Mean	15.65	10.1
Variance	1.445	21.78
Observations	2	2
Pearson Correlation	1	
Hypothesized Mean Difference	0	
df	1	
t Stat	2.26530612	
P(T<=t) one-tail	0.13232584	
t Critical one-tail	6.31375151	
P(T<=t) two-tail	0.26465167	
t Critical two-tail	12.7062047	

t-Test: Paired Two Sample for Means of differentiated cells - siNon-targeting vs siWIPI1

	Variable 1	*Variable 2*
Mean	15.65	2.5
Variance	1.445	0.02
Observations	2	2
Pearson Correlation	-1	
Hypothesized Mean Difference	0	
df	1	
t Stat	13.842105	
P(T<=t) one-tail	0.0229559	
t Critical one-tail	6.3137515	
P(T<=t) two-tail	0.0459118	
t Critical two-tail	12.706205	

Appendix 10: Inhibition of autophagy via siRNA knockdowns of ULK1 and WIPI1, and its effects on nucleophagy in differentiating keratinocytes.

Appendix 10 continued.

(g) A paired t-test for the average number of nucleophagic keratinocytes in differentiated keratinocytes, shows that the reduction in nucleophagic keratinocytes in siWIPI1 transfected cells, compared to the siNon-targeting cells, is statistically significant with $P<0.05$. However, the reduction in nucleophagic keratinocytes in the differentiated population of siULK1 transfected keratinocytes compared to the siNon-targeting cells is not statistically significant.

This figure represents n=2 experiments for Figure 3.25 and 3.26.

Appendix 11: The effects of 3-MA on class I and class III PI3kinases in REKs.

Western blot analysis was performed to determine whether 3-MA specifically blocks the autophagy pathway in REKs. 3-MA is routinely used as an autophagy inhibitor, however, in some cell types and under certain conditions, 3-MA also inhibits the class I PI3kinase. Therefore, initial experiments were performed to determine whether 3-MA affects the class I or the class III PI3kinase, or both, in keratinocytes. Initial experiments were done with REKs.

However, my results show that in REKs, 3-MA inhibits the class I PI3kinase which is up-stream of AKT and regulates AKT activity and its down-stream targets like S6 phosphorylation. 3-MA does not affect LC3 processing and so does not inhibit the class III PI3kinase in REKs. Therefore, 3-MA is not a suitable autophagy inhibitor for keratinocytes under the culture conditions used in my experiments.

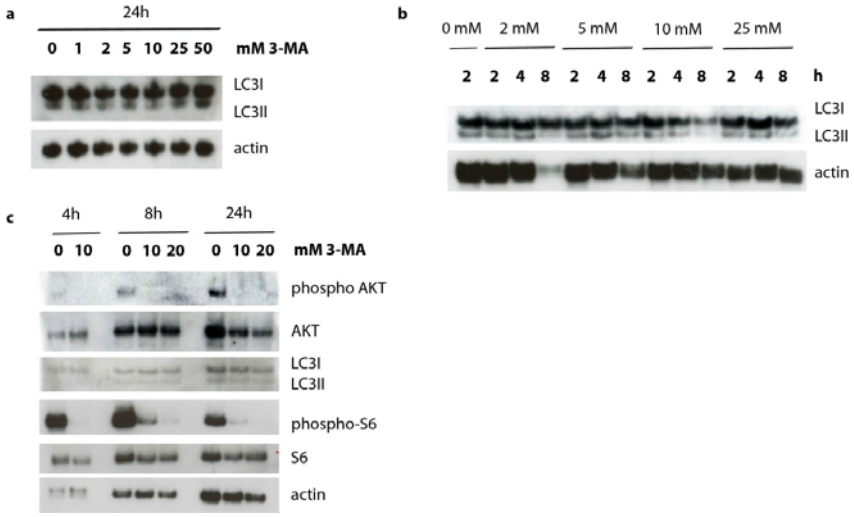

Appendix 11: The effects of 3-MA on class I and class III PI3kinases in REKs.

(a) Western blotting of lysates from REKs treated with 0-50mM 3-MA for 24h shows that concentrations of 3-MA have no effects on LC3 processing.

(b) REKs were also treated with 0-25 mM 3-MA and harvested after 2h, 4h and 8h. After 8h treatment, LC3I and LC3II are decreased with 10 mM and 25 mM 3-MA. However, this effect of 3-MA on LC3 processing is very mild.

(c) Western blotting of REK lysates treated with 0-20 mM 3-MA and harvested at 4h, 8h and 24h shows a dramatic reduction in phospho-AKT (S473) and also in phospho-S6 (S240/244). However, 3-MA had no effect on LC3 processing.

This figure represents n=2 experiments for Figure 3.23.

Appendix 12: The effect of rapamycin on autophagy in REK monolayer cultures

First, I wanted to determine whether REK monolayer cultures are capable of rapamycin-induced autophagy. REKs were treated with rapamycin or its vehicle DMSO, before harvesting. Western blot analysis of REK protein lysates shows that with rapamycin treatment S6 phosphorylation, which is a down-stream target of mTORC1 activity, is inhibited. This confirms that rapamycin treatment effectively blocks mTORC1. Phospho-AKT levels increase with rapamycin due to inactivation of the negative feed-back loop between mTORC1 and the IRS-1 receptor (Sully *et al.* 2012), further confirming effective rapamycin treatment.

Analysis of LC3 by Western blotting shows that untreated REKs have low levels of LC3II (Appendix 12a), suggesting low levels of basal autophagy in these cells. Compared to vehicle-treated cells, rapamycin induces a slight increase in LC3II, indicating an increase in the number of autophagosomes (Appendix 12a). However, due to the very low intensities of the LC3II bands, quantification was not possible.

These results were verified using immunofluorescence analysis for LC3 expression in the REK cultures (Appendix 12b). Immunofluorescence analysis of LC3 shows a low intensity of LC3 expression in REK monolayers, suggesting low basal levels of autophagy. This confirms observations made by Western blotting with very low levels of LC3II in the REK protein lysates. However, the punctate expression pattern of LC3 indicates the presence of autophagic vesicles (Appendix 12b). But with immunofluorescence analysis, I observed no effects of rapamycin treatment on LC3 levels or LC3 puncta when compared to the vehicle-treated cells (Appendix 12b).

These results indicate that REKs have very low levels of basal autophagy and rapamycin treatment may induce a slight increase in autophagy levels, however, this is difficult to detect with Western blotting and with immunofluorescence analysis.

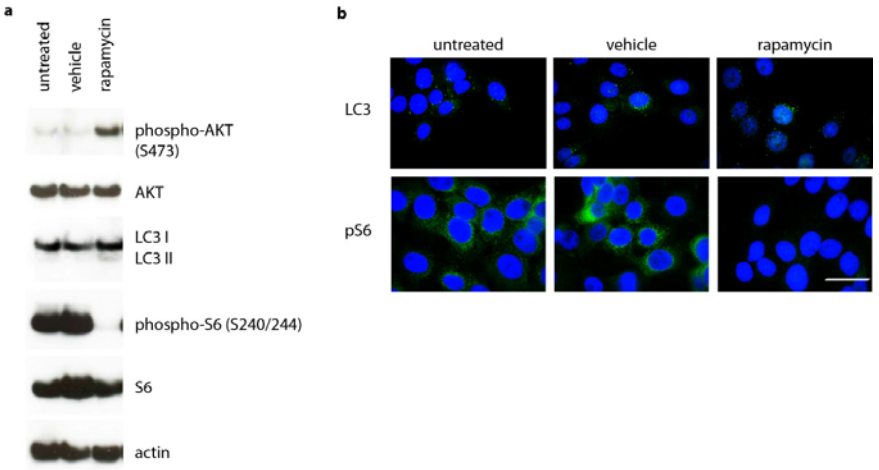

Appendix 12: Effects of rapamycin on expression of autophagosome marker, LC3, in REKs.

(a) Western blotting of whole cell lysates of REKs treated with vehicle or rapamycin shows that rapamycin down-regulates S6 phosphorylation indicating effective mTORC1 inhibition. With rapamycin treatment, AKT phosphorylation is increased suggesting rapamycin-mediated inhibition of the negative feedback loop and effective mTORC1 inhibition. Compared to the untreated and vehicle-treated cells, rapamycin induces a very slight up-regulation of LC3II however, due to the very low intensities of LC3II bands, quantification cannot be done.

(b) Immuno-fluorescence staining for LC3 and phospho-S6 (S240/244) on REK monolayer cultures shows reduced phospho-S6 levels with rapamycin treatment, showing effective mTORC1 inhibition and confirming observations made by Western blotting. LC3 is expressed at low levels in untreated and vehicle-treated cells. However, any changes in LC3 induced by rapamycin are not detected with immuno-fluorescence staining. Staining for LC3 shows a punctate expression pattern in all cells indicating the presence of autophagic vesicles.

REKs treated with 10nM rapamycin or vehicle for 4h before harvesting.

Bar = 20um.

This figure is reference in section 4.2.

Appendix 13: Immunofluorescence analysis showing the effect of rapamycin on autophagy in REK monolayer treated with and without chloroquine

Rapamycin alone induces an increase in LC3 expression levels compared to vehicle-treated cells (Appendix 13a; Appendix 13b), which is further increased with chloroquine (Appendix 13a; Appendix 13b). Rapamycin treatment also leads to formation of more LC3 aggregates compared to vehicle treated REKs (Appendix 13c). Blocking autophagic degradation with chloroquine leads to a further increase in rapamycin-induced LC3 puncta formation (Appendix 13c). These results show that rapamycin up-regulates the autophagy pathway in REKs leading to formation of more LC3 positive vesicles.

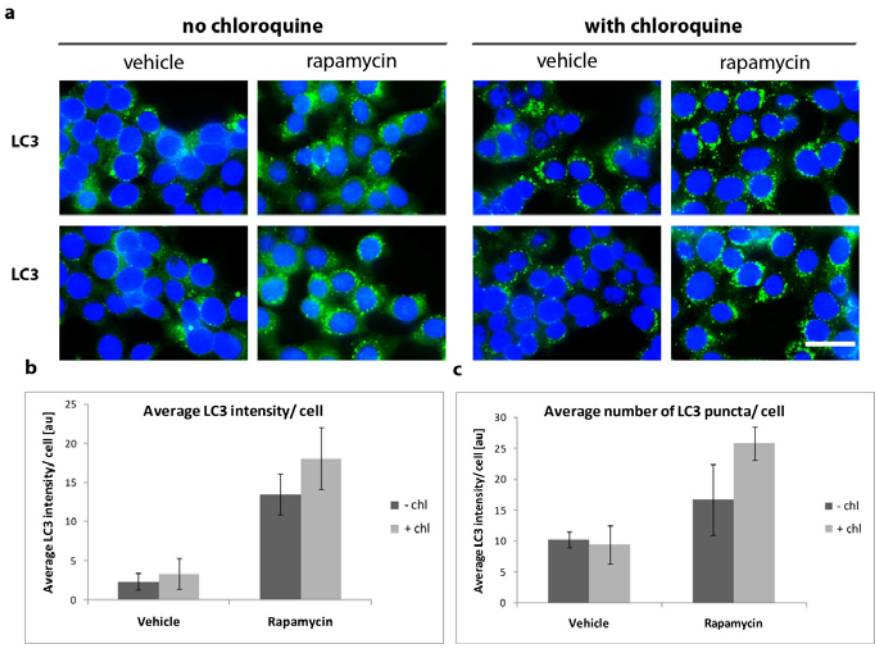

Appendix 13: Analysis of the autophagosome marker LC3, in rapamycin-treated REKs with and without chloroquine.

(a) REKs were treated with vehicle or rapamycin with or without chloroquine before harvesting. Immunofluorescence analysis of LC3 expression in REK monolayer cultures treated with vehicle alone and with rapamycin alone (without chloroquine) shows that rapamycin increases LC3 expression. Chloroquine-treatment leads to accumulation of LC3 in vehicle-treated and in rapamycin-treated REKs.

(b) Quantification of the LC3 expression intensity per cell shows that chloroquine treatment increases the LC3 intensities/cell. Compared to vehicle-treated REKs, rapamycin strongly increase the LC3 intensity/cell and this is further increased in the presence of chloroquine.

(c) Rapamycin-treatment also increases the number of LC3 aggregates/cell and this is further increased with chloroquine. Since this is a preliminary experiment, only a small sample size was analysed and statistical relevance could not be assessed.

Appendix 13 continued on the next page.

REKs treated with 10nM rapamycin or vehicle for 4h before harvesting; 200uM chloroquine added 2h before harvesting. Bar = 20um.

Average LC3 puncta per cell (2 fields per condition)

	Count	IntDen	No of cells per image	count/ cell
REKs 20052010 DMSO LC3 perm + Me_Ac. 60x image 1_1_1.tif (green)	170	0.13	19	8.94736842
REKs 20052010 DMSO LC3 perm + Me_Ac. 60x image 3_1_1.tif (green)	251	0.19	22	11.4090909
Sum	**421**		41	
Average LC3 intensity per cell	**10.26829**			
Std Error				**10.27**

	Count	IntDen	No of cells per image	count/ cell
REKs 20052010 DMSO + chl LC3 perm + Me_Ac. 60x image 1_1_1.tif (green)	286	0.41	22	13.00
REKs 20052010 DMSO + chl LC3 perm + Me_Ac. 60x image 2_1_1.tif (green)	186	0.23	28	6.64
Sum	**472**		50	
Average LC3 intensity per cell	**9.44**			
Std Error				**3.18**

	Count	IntDen	No of cells per image	count/ cell
REKs 20052010 Rap LC3 perm + Me_Ac. 60x image 2_1_1.tif (green)	319	0.3	14	22.79
REKs 20052010 Rap LC3 perm + Me_Ac. 60x image 2_1_1_2.tif (green)	182	0.33	16	11.375
Sum	**501**		30	
Average LC3 intensity per cell	**16.7**			
Std Error				**5.71**

	Count	IntDen	No of cells per image	count/ cell
REKs 20052010 Rap + chl LC3 perm + Me_Ac. 60x image 1_1_1.tif (green)	419	0.49	18	23.2777778
REKs 20052010 Rap + chl LC3 perm + Me_Ac. 60x image 2_1_1.tif (green)	458	0.41	16	28.625
Sum	**877**		34	
Average LC3 intensity per cell	**25.79412**			
Std Error				**2.67**

Appendix 13 Table 1: Analysis of the autophagosome marker LC3, in rapamycin-treated REKs with and without chloroquine.

Appendix 13 continued.

Quantification of LC3 puncta per cell for 2 fields of view.

Quantification of LC3 puncta per field of view was done with imageJ. However, number of cells per field of view was determined by eye.

Appendix 13 continued on the next page.

Average LC3 intensities per cell (2 fields per condition)

Label	IntDen	No of cells per image	Int/cell
REKs 20052010 DMSO LC3 perm + Me_Ac. 60x image 1_1_1.tif (green)	23.98	19	1.262105
REKs 20052010 DMSO LC3 perm + Me_Ac. 60x image 3_1_1.tif (green)	73.27	22	3.330455
Sum	97.25	41	
Average LC3 intensity per cell	**2.37195122**		
Std Error			1.034175

Label	IntDen	No of cells per image	Int/cell
REKs 20052010 DMSO + chl LC3 perm + Me_Ac. 60x image 1_1_1.tif (green)	124.12	22	5.641818
REKs 20052010 DMSO + chl LC3 perm + Me_Ac. 60x image 2_1_1.tif (green)	46.04	28	1.644286
Sum	170.16	50	
Average LC3 intensity per cell	**3.4032**		
Std Error			1.998766

Label	IntDen	No of cells per image	Int/cell
REKs 20052010 Rap LC3 perm + Me_Ac. 60x image 2_1_1.tif (green)	228.84	14	16.34571
REKs 20052010 Rap LC3 perm + Me_Ac. 60x image 2_1_1_2.tif (green)	177.22	16	11.07625
Sum	406.06	30	
Average LC3 intensity per cell	**13.5353333**		
Std Error			2.634732

Label	IntDen	No of cells per image	Int/cell
REKs 20052010 Rap + chl LC3 perm + Me_Ac. 60x image 1_1_1.tif (green)	259.11	18	14.395
REKs 20052010 Rap + chl LC3 perm + Me_Ac. 60x image 2_1_1.tif (green)	356.59	16	22.28688
Sum	615.7	34	
Average LC3 intensity per cell	**18.1088235**		
Std Error			3.945938

Appendix 13 Table 2: Analysis of the autophagosome marker LC3, in rapamycin-treated REKs with and without chloroquine.

Appendix 13 continued.

Quantification of LC3 intensities per cell for 2 fields of view.

Quantification of LC3 intensities per field of view was done with imageJ. However, number of cells per field of view was determined by eye.

Appendix 13 continued on the next page.

f Average no of LC3 puncta/ cell

	- chl	+ chl
Vehicle	10.27	9.44
Rapamycin	16.70	25.79

Std error of LC3 puncta/ cell

	- chl	+ chl
Vehicle	1.23	3.18
Rapamycin	5.71	2.67

g Average LC3 intensity/ cell

	- chl	+ chl
Vehicle	2.37195122	3.4032
Rapamycin	13.5353333	18.10882

Std error of LC3 intensity/ cell

	- chl	+ chl
Vehicle	1.03	2.00
Rapamycin	2.63	3.95

h t-Test: Paired Two Sample for Means of LC3 puncta in REKs with chloroquine treated with vehicle vs rapamycin

	Variable 1	*Variable 2*
Mean	9.821428571	25.9513889
Variance	20.20663265	14.2963927
Observations	2	2
Pearson Correlation	-1	
Hypothesized Mean Difference	0	
df	1	
t Stat	-2.756229869	
P(T<=t) one-tail	0.110786126	
t Critical one-tail	6.313751514	
P(T<=t) two-tail	0.221572253	
t Critical two-tail	12.70620473	

i t-Test: Paired Two Sample for Means of LC3 intensities in REKs with chloroquine treated with vehicle vs rapamycin

	Variable 1	*Variable 2*
Mean	3.6430519	18.34094
Variance	7.9901329	31.14085
Observations	2	2
Pearson Correlation	-1	
Hypothesized Mean Difference	0	
df	1	
t Stat	-2.4724337	
P(T<=t) one-tail	0.1223408	
t Critical one-tail	6.3137515	
P(T<=t) two-tail	0.2446817	
t Critical two-tail	12.706205	

Appendix 13: Analysis of the autophagosome marker LC3, in rapamycin-treated REKs with and without chloroquine.

Appendix 13 continued.

(f) Table showing average LC3 puncta per cell and the standard errors

(g) Table showing average LC3 intensities per cell and the standard errors

(h) Results from the paired t-test for LC3 intensities per cell performed on REKs with chloroquine, treated with vehicle compared to rapamycin

(i) Results from the paired t-test for LC3 intensities per cell performed on REKs with chloroquine, treated with vehicle compared to rapamycin

This figure is referenced in section 1.2.

Appendix 14: ~~The~~ Western blot analysis of the effects of rapamycin on autophagy in primary keratinocyte monolayer cultures treated with and without chloroquine

To determine whether primary monolayer keratinocytes respond to rapamycin-induced autophagy, I treated both undifferentiated and differentiated primary keratinocyte cultures with rapamycin in the presence and absence of chloroquine. If rapamycin increases autophagy in primary keratinocytes, a much stronger increase in LC3 levels would be expected with chloroquine.

Western blotting of lysates from primary human monolayer keratinocyte cultures shows that rapamycin treatment down-regulates phosphorylation of S6, indicating effective mTORC1 inhibition (Appendix 14a).

Chloroquine increases LC3II levels in both vehicle-treated and rapamycin-treated keratinocyte cultures, suggesting chloroquine blocks the autophagy pathway leading to accumulation of LC3 (Appendix 14a). Quantification of LC3/actin ratios shows that rapamycin treatment in the absence of chloroquine leads to a small increase the LC3II levels in both the undifferentiated and differentiated keratinocyte populations (Appendix 14b). Combined treatment with chloroquine and rapamycin does not further increase LC3II/actin levels (Appendix 14b).

Quantification of LC3 turn-over (LC3II/LC3I), shows that chloroquine treatment leads to an increase in LC3II/LC3I ratios in both undifferentiated and differentiated keratinocyte populations. However, rapamycin treatment alone and combined with chloroquine, has no significant effect on LC3II/LC3I levels when compared to vehicle-treated cells (Appendix 14c). Chloroquine-treatment also leads to the accumulation of LC3I in both vehicle-treated and rapamycin-treated keratinocytes (Appendix 14d). This is an unexpected effect of chloroquine, since it should only affect the late stages of autophagy preventing degradation of autophagic vesicles. In keratinocytes, chloroquine may affect other pathways up-stream of autophagy

leading to more LC3I in the cells. However, rapamycin treatment in the presence of chloroquine leads to a strong increase in LC3I levels (Appendix 14d). This effect of chloroquine on the rapamycin-induced increase in LC3I may also be a reason why LC3 turn-over appears to be reduced with rapamycin treatment (Appendix 14d).

These results show that chloroquine is not a suitable autophagy inhibitor to measure LC3 turn over in keratinocytes. Any effect of rapamycin on LC3II levels cannot be measured because chloroquine also increases LC3I levels which may be due to other effects of chloroquine.

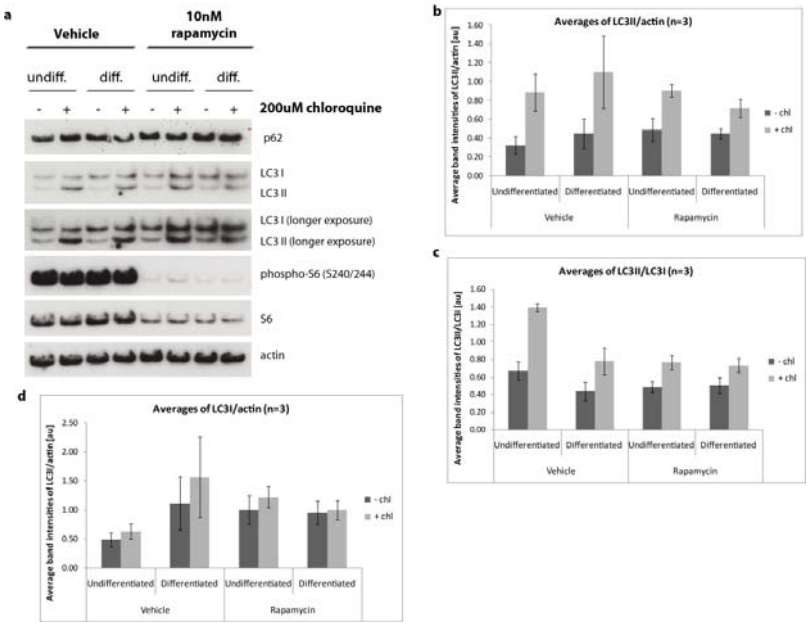

Appendix 14: Analysis of autophagic flux in rapamycin-treated primary keratinocyte cultures with and without chloroquine.

(a) Undifferentiated and differentiated monolayer primary keratinocytes were treated with vehicle or rapamycin in the presence and absence of chloroquine. Western blot analysis of protein lysates shows that with rapamycin treatment, S6 phosphorylation is down-regulated confirming effective mTOR inhibition. Chloroquine treatment blocks degradation of autophagic vesicles leading to accumulation of LC3II in both vehicle-treated and rapamycin-treated cells.

(b) Total levels of LC3II are quantified as LC3II/actin. Chloroquine treatment leads to increased LC3II/actin. Rapamycin treatment alone has no significant effect on LC3II levels however rapamycin treatment with chloroquine does not increase LC3II/actin levels.

(c) LC3II turn-over is quantified as LC3II/LC3I ratios. Chloroquine treatment increases the LC3II/LC3I ratios. Rapamycin treatment alone has no effect on LC3II/LC3I levels, and with chloroquine, rapamycin also has no significant effects on LC3 turn-over.

(d) LC3I turn-over quantified as LC3I/actin shows that chloroquine treatment also increases LC3I levels slightly in both undifferentiated and differentiated keratinocytes.

Appendix 14 continued on the next page.

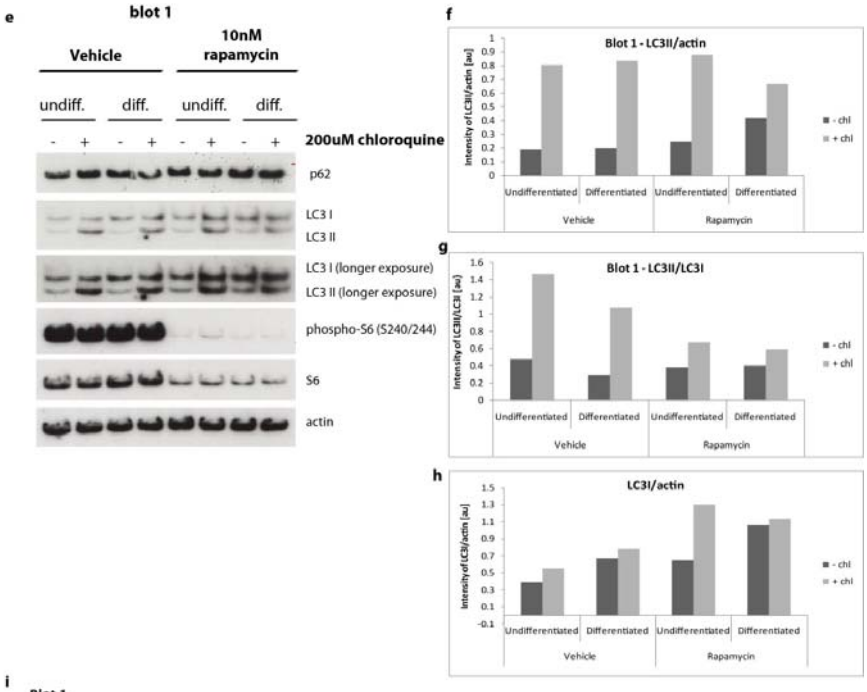

i

Blot 1

	LC3I	LC3II	LC3II/LC3I	actin	LC3I/actin	LC3II/actin
Undifferentiated Vehicle	5142.468	2454.548	***0.48***	13121.267	***0.39***	***0.19***
Undifferentiated Vehicle + chl.	6468.225	9513.347	***1.47***	11767.832	***0.55***	***0.81***
Differentiated Vehicle	7693.589	2303.598	***0.30***	11531.66	***0.67***	***0.20***
Differentiated Vehicle + chl.	9373.489	10161.59	***1.08***	12048.489	***0.78***	***0.84***
Undifferentiated Rapamycin	8772.317	3399.841	***0.39***	13593.196	***0.65***	***0.25***
Undifferentiated Rapamycin + chl	15436.27	10455.28	***0.68***	11840.489	***1.30***	***0.88***
Differentiated Rapamycin	14502.51	5742.376	***0.40***	13714.095	***1.06***	***0.42***
Differentiated Rapamycin + chl	14173.44	8414.276	***0.59***	12596.489	***1.13***	***0.67***

Appendix 14: Analysis of autophagic flux in rapamycin-treated primary keratinocyte cultures with and without chloroquine.

Appendix 14 continued.

(e) Western blot n=1 analysis of undifferentiated and differentiated monolayer primary keratinocytes treated with vehicle or rapamycin with or without of chloroquine.

(f) Graph of quantification for LC3II/LC3I for blot 1

(g) Graph of quantification for LC3II/actin for blot 1

(h) Graph of quantification for LC3I/actin for blot 1

(i) Quantification of LC3I, LC3II, actin and the LC3II/LC3I and LC3II/actin ratios for n=1 blots

Appendix 14 continued on the next page.

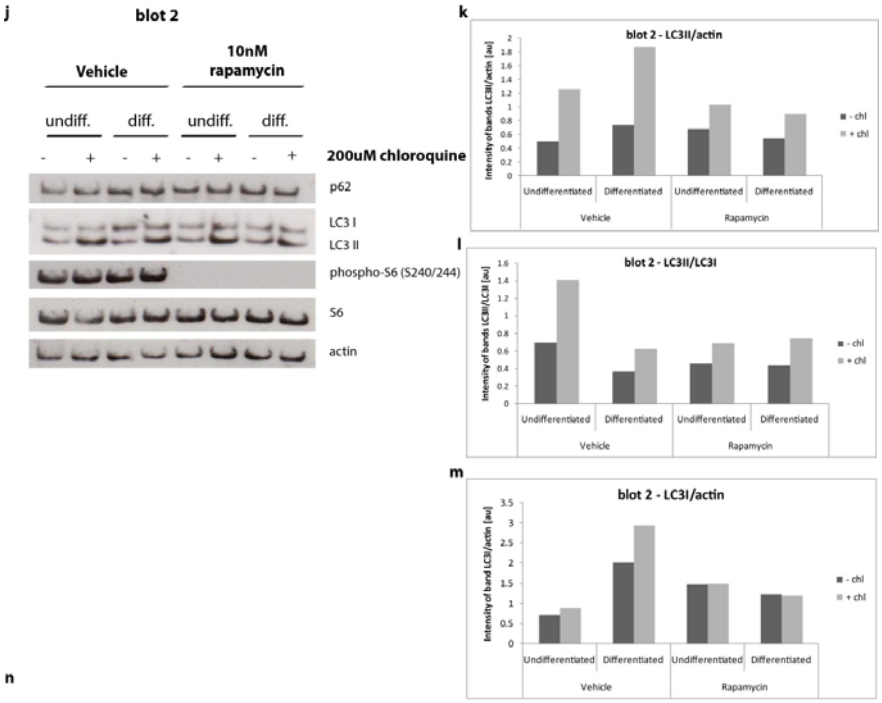

n

Blot 2

	LC3I	LC3II	LC3II/LC3I	actin	LC3I/actin	LC3II/actin
Undifferentiated Vehicle	2326.062	1629.406	***0.70***	3249.74	***0.72***	***0.50***
Undifferentiated Vehicle + chl.	3078.134	4351.77	***1.41***	3452.841	***0.89***	***1.26***
Differentiated Vehicle	6049.912	2215.234	***0.37***	2984.234	***2.03***	***0.74***
Differentiated Vehicle + chl.	6206.983	3912.284	***0.63***	2102.113	***2.95***	***1.86***
Undifferentiated Rapamycin	3850.79	1758.335	***0.46***	2604.113	***1.48***	***0.68***
Undifferentiated Rapamycin + chl	6317.104	4373.456	***0.69***	4232.184	***1.49***	***1.03***
Differentiated Rapamycin	4401.497	1956.92	***0.44***	3573.891	***1.23***	***0.55***
Differentiated Rapamycin + chl	3687.426	2740.87	***0.74***	3061.012	***1.20***	***0.90***

Appendix 14: Analysis of autophagic flux in rapamycin-treated primary keratinocyte cultures with and without chloroquine.

Appendix 14 continued.

(j) Western blot n=2 analysis of undifferentiated and differentiated monolayer primary keratinocytes treated with vehicle or rapamycin with or without of chloroquine.

(k) Graph of quantification for LC3II/LC3I for blot 2

(l) Graph of quantification for LC3II/actin for blot 2

(m) Graph of quantification for LC3I/actin for blot 2

(n) Quantification of LC3I, LC3II, actin and the LC3II/LC3I and LC3II/actin ratios for n=2 blots

Appendix 14 continued on the next page.

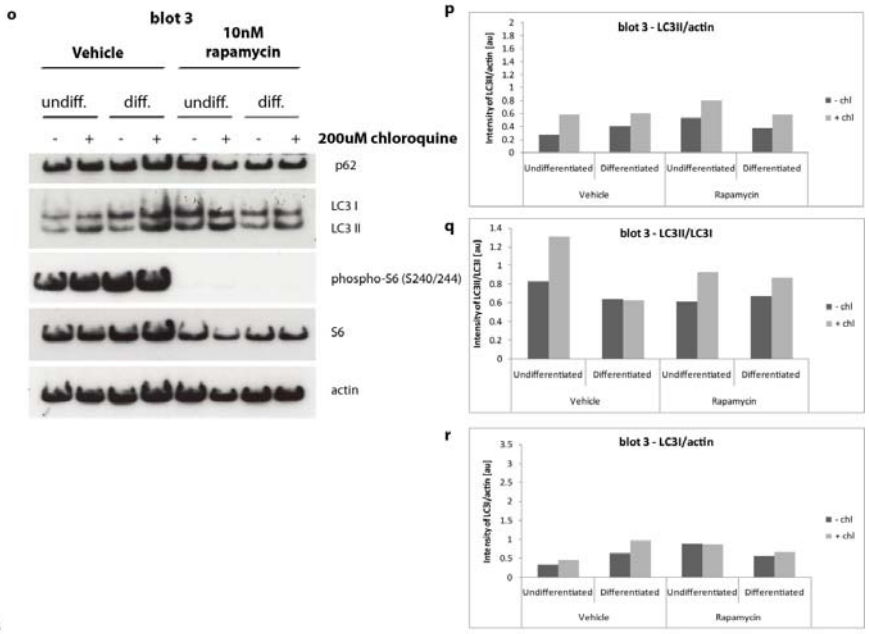

s

Blot 3

	LC3I	LC3II	LC3II/LC3I	actin	LC3I/actin	LC3II/actin
Undifferentiated Vehicle	3035.477	2509.113	***0.83***	8860.347	***0.34***	***0.28***
Undifferentiated Vehicle + chl.	3980.598	5221.355	***1.31***	8922.811	***0.45***	***0.59***
Differentiated Vehicle	5978.548	3819.82	***0.64***	9356.64	***0.64***	***0.41***
Differentiated Vehicle + chl.	11438.3	7248.355	***0.63***	11840.589	***0.97***	***0.61***
Undifferentiated Rapamycin	9961.811	6047.648	***0.61***	11231.296	***0.89***	***0.54***
Undifferentiated Rapamycin + chl	6827.79	6326.062	***0.93***	7837.225	***0.87***	***0.81***
Differentiated Rapamycin	5600.619	3793.113	***0.68***	9852.933	***0.57***	***0.38***
Differentiated Rapamycin + chl	6231.083	5446.355	***0.87***	9261.054	***0.67***	***0.59***

Appendix 14: Analysis of autophagic flux in rapamycin-treated primary keratinocyte cultures with and without chloroquine.

Appendix 14 continued.

(o) Western blot n=3 analysis of undifferentiated and differentiated monolayer primary keratinocytes treated with vehicle or rapamycin with or without of chloroquine.

(p) Graph of quantification for LC3II/LC3I for blot 3

(q) Graph of quantification for LC3II/actin for blot 3

(r) Graph of quantification for LC3I/actin for blot 3

(s) Quantification of LC3I, LC3II, actin and the LC3II/LC3I and LC3II/actin ratios for n=3 blots

Appendix 14 continued on the next page.

t

Average of n=3 blots

LC3II/LC3I

	Vehicle		Rapamycin	
	Undifferentiated	Differentiated	Undifferentiated	Differentiated
- chl	0.67	0.44	0.49	0.51
+ chl	1.40	0.78	0.77	0.73

u **Average of n=3 blots**

LC3II/actin

	Vehicle		Rapamycin	
	Undifferentiated	Differentiated	Undifferentiated	Differentiated
- chl	0.32	0.45	0.49	0.45
+ chl	0.89	1.10	0.91	0.72

v **Average of n=3 blots**

LC3I/actin

	Vehicle		Rapamycin	
	Undifferentiated	Differentiated	Undifferentiated	Differentiated
- chl	0.48	1.11	1.01	0.95
+ chl	0.63	1.57	1.22	1.00

Appendix 14: Analysis of autophagic flux in rapamycin-treated primary keratinocyte cultures with and without chloroquine.

Appendix 14 continued.

(t) Average band intensities of LC3II/LC3I for n=3 blots.

(u) Average band intensities of LC3II/actin for n=3 blots.

(v) Average band intensities of LC3I/actin for n=3 blots.

Appendix 14 continued on the next page.

w Standard error blots n=3

LC3II/LC3I

	Vehicle		Rapamycin	
	Undifferentiated	Differentiated	Undifferentiated	Differentiated
- chl blot 1	0.48	0.3	0.39	0.4
- chl blot 2	0.7	0.37	0.46	0.44
- chl blot 2	0.83	0.64	0.61	0.68
Std error	***0.10214369***	***0.103655412***	***0.064893074***	***0.087432514***

+ chl blot	1.47	1.08	0.68	0.59
+ chl blot	1.41	0.63	0.69	0.74
+ chl blot	1.31	0.63	0.93	0.87
Std error	***0.046666667***	***0.15***	***0.081717671***	***0.080897741***

x Standard error blots n=3

LC3II/actin

	Vehicle		Rapamycin	
	Undifferentiated	Differentiated	Undifferentiated	Differentiated
- chl blot 1	0.19	0.2	0.25	0.42
- chl blot 2	0.5	0.74	0.68	0.55
- chl blot 2	0.28	0.41	0.54	0.38
Std error	***0.092074849***	***0.157162336***	***0.126622799***	***0.051316014***

+ chl blot	0.81	0.84	0.88	0.67
+ chl blot	1.26	1.86	1.03	0.9
+ chl blot	0.59	0.61	0.81	0.59
Std error	***0.197174486***	***0.384115145***	***0.064893074***	***0.092915732***

y

Standard error blots n=3

LC3I/actin

	Vehicle		Rapamycin	
	Undifferentiated	Differentiated	Undifferentiated	Differentiated
- chl blot 1	0.39	0.67	0.65	1.06
- chl blot 2	0.72	2.03	1.48	1.23
- chl blot 2	0.34	0.64	0.89	0.57
Std error	***0.119210365***	***0.458415144***	***0.24659909***	***0.19784955***

+ chl blot	0.55	0.78	1.3	1.13
+ chl blot	0.89	2.95	1.49	1.2
+ chl blot	0.45	0.97	0.87	0.67
Std error	***0.133166562***	***0.693837957***	***0.183393929***	***0.166232769***

Appendix 14: Analysis of autophagic flux in rapamycin-treated primary keratinocyte cultures with and without chloroquine.

Appendix 14 continued.

(w) Standard error values for LC3II/LC3I values of n=3 blots.

(x) Standard error values for LC3II/actin values of n=3 blots.

(y) Standard error values for LC3I/actin values of n=3 blots.

This figure is referenced in section 4.2.

Appendix 15: Immunofluorescence analysis of the effects of rapamycin on autophagy in primary keratinocyte monolayer cultures treated with and without chloroquine

Next, I wanted to verify these findings with immunofluoresence analysis of LC3 expression levels in monolayer keratinocyte cultures. Immunofluorescence analysis of LC3 levels in vehicle-treated and rapamycin-treated cells shows that with chloroquine treatment, in both undifferentiated and differentiated keratinocytes, there is an accumulation of LC3. Quantification of LC3 intensities (Appendix 15) shows increased LC3 levels with chloroquine treatment.

However, in undifferentiated keratinocytes with choroquine, rapamycin induces a slight increase in LC3 levels compared to vehicle-treated cells (Appendix 15). In the differentiated keratinocytes with and without chloroquine, rapamycin does not increase LC3 levels, but appears to reduce LC3 levels slightly (see Appendix 15). The number of LC3 aggregates in undifferentiated and differentiated cultures is not affected by rapamycin treatment (Appendix 15).

Therefore, using immunofluorescence analysis and chloroquine as a drug to measure autophagic flux, I observe that rapamycin does not affect LC3 intensities or LC3 aggregate formation in keratinocyte cultures. With Western blot analysis, I observe that chloroquine has other effects on autophagy and leads to increased LC3I levels (Appendix 14) suggesting that the effects of chloroquine alone mask any effect rapamycin may have on autophagy. Therefore, I used another drug BafA1, to measure autophagic flux and to determine the effects of rapamycin on primary human monolayer keratinocytes.

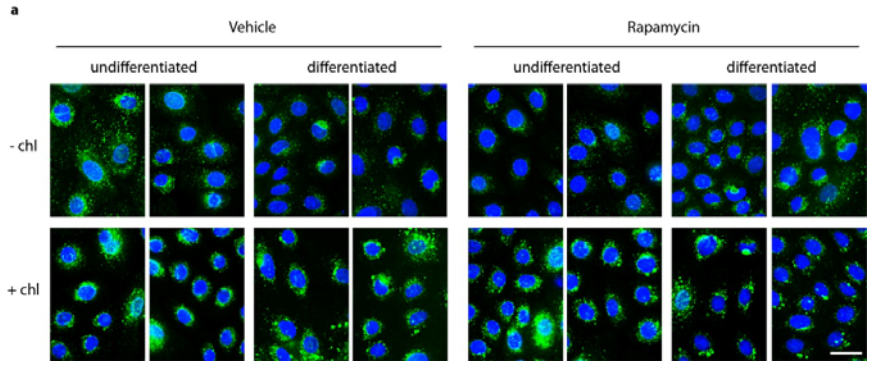

Appendix 15: The effects of rapamycin on the autophagosome marker, LC3 in primary keratinocyte cultures with and without chloroquine treatment.

(a) Primary monolayer keratinocyte cultures were treated with vehicle or with rapamycin, with and without chlororquine. Immunofluorescence analysis shows accumulation of LC3 in nucleophagic regions of differentiated keratinocytes, similar to observations made previously in chapter 3. In both undifferentiated and differentiated keratinocytes treated with vehicle and with rapamycin, chloroquine treatment leads to an increase in LC3 expression intensities and LC3 puncta formation compared to cells without chloroquine. ***Appendix 15 continued on the next page.***

Primary keratinocyte monolayers treated with 10nM rapamycin or vehicle for 4h before harvesting; 200uM chloroquine added 2h before harvesting. Bar = 20um.

b

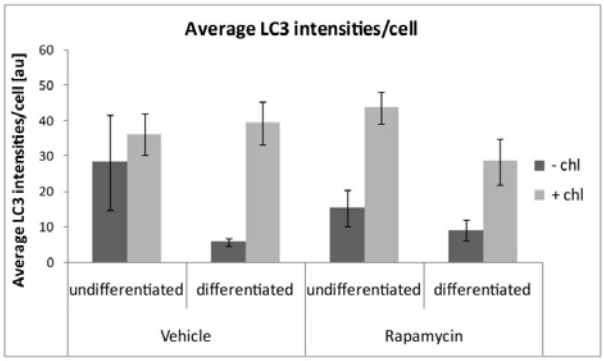

c

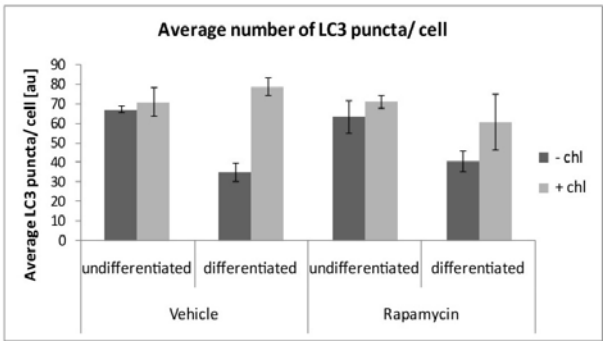

Appendix 15: The effects of rapamycin on the autophagosome marker, LC3 in primary keratinocyte cultures with and without chloroquine treatment.

Appendix 15 continued.

(b) Quantification of LC3 intensities per cell shows that chloroquine treatment increases LC3 intensities in undifferentiated and differentiated keratinocytes treated with vehicle and with rapamycin. However, in both undifferentiated and differentiated keratinocytes, rapamycin treatment in the presence and abscence of chloroquine has no significant effect on LC3 intensities compared to vehicle treated cells.

(c) Quantification of LC3 puncta per cell shows that chloroquine increases the number of LC3 puncta per cell in both undifferentiated and differentiated keratinocyte populations. However, rapamycin has no effects on the number of LC3 puncta per cell in both undifferentiated and differentiated keratinocytes with and without chloroquine.

Appendix 15 continued on the next page.

Average intensity per cell	**5.880417**		
Std error			**1.125108339**
high Ca nHEKs rap + 200uM chl LC3_g Lamp2_r 60x 19102012 image 1.tif (RGB) (green)	172.28	13	13.25230769
high Ca nHEKs rap + 200uM chl LC3_g Lamp2_r 60x 19102012 image 2.tif (RGB) (green)	283.24	8	35.405
high Ca nHEKs rap + 200uM chl LC3_g Lamp2_r 60x 19102012 image 3.tif (RGB) (green)	296.5	7	42.35714286
high Ca nHEKs rap + 200uM chl LC3_g Lamp2_r 60x 19102012 image 4.tif (RGB) (green)	187.38	5	37.476
Sum	939.4	33	
Average intensity per cell	**28.46667**		
Std error			**6.456694463**
Label	IntDen		
high Ca nHEKs rap LC3_g Lamp2_r 60x 19102012 image 1.tif (RGB) (green)	87.26	11	7.932727273
high Ca nHEKs rap LC3_g Lamp2_r 60x 19102012 image 3.tif (RGB) (green)	114.43	19	6.022631579
high Ca nHEKs rap LC3_g Lamp2_r 60x 19102012 image 4.tif (RGB) (green)	75.44	10	7.544
high Ca nHEKs rap LC3_g Lamp2_r 60x 19102012 image 5.tif (RGB) (green)	167.45	9	18.60555556
Sum	444.58	49	
Average intensity per cell	**9.073061**		
Std error			**2.889317202**
Label	IntDen		
low Ca nHEKs DMSO + 200uM chl LC3_g Lamp2_r 60x 19102012 image 1.tif (RGB) (green)	317.35	9	35.26111111
low Ca nHEKs DMSO + 200uM chl LC3_g Lamp2_r 60x 19102012 image 2.tif (RGB) (green)	404.85	11	36.80454545
low Ca nHEKs DMSO + 200uM chl LC3_g Lamp2_r 60x 19102012 image 3.tif (RGB) (green)	172.95	8	21.61875
low Ca nHEKs DMSO + 200uM chl LC3_g Lamp2_r 60x 19102012 image 4.tif (RGB) (green)	403.63	8	50.45375
Sum	1298.78	36	
Average intensity per cell	**36.07722**		
Std error			**5.894345588**
Label	IntDen		
low Ca nHEKs DMSO LC3_g Lamp2_r 60x 19102012 image 1.tif (RGB) (green)	77.35	7	11.05
low Ca nHEKs DMSO LC3_g Lamp2_r 60x 19102012 image 2.tif (RGB) (green)	353.01	5	70.602
low Ca nHEKs DMSO LC3_g Lamp2_r 60x 19102012 image 3.tif (RGB) (green)	126.24	6	21.04
low Ca nHEKs DMSO LC3_g Lamp2_r 60x 19102012 image 4.tif (RGB) (green)	148.67	7	21.23857143
Sum	705.27	25	
Average intensity per cell	**28.2108**		
Std error			**13.41891323**

Appendix 15 Table 1: The effects of rapamycin on the autophagosome marker, LC3 in primary keratinocyte cultures with and without chloroquine treatment.

Appendix 15 continued.

Quantification of LC3 intensities per cell for 4 fields of view.

Quantification of LC3 intensities per field of view was done with imageJ. However, number of cells per field of view was determined by eye.

Appendix 15 continued on the next page.

Label	IntDen		
low Ca nHEKs Rap + 200uM chl LC3_g Lamp2_r 60x 19102012 image 1.tif (RGB) (green)	628.54	12	52.37833333
low Ca nHEKs Rap + 200uM chl LC3_g Lamp2_r 60x 19102012 image 2.tif (RGB) (green)	241.69	7	34.52714286
low Ca nHEKs Rap + 200uM chl LC3_g Lamp2_r 60x 19102012 image 3.tif (RGB) (green)	379.9	8	47.4875
low Ca nHEKs Rap + 200uM chl LC3_g Lamp2_r 60x 19102012 image 4.tif (RGB) (green)	320.71	9	35.63444444
Sum	1570.84	36	
Average intensity per cell	**43.63444**		
Std error			**4.407935475**
Label	IntDen		
low Ca nHEKs Rap LC3_g Lamp2_r 60x 19102012 image 1.tif (RGB) (green)	263.79	9	29.31
low Ca nHEKs Rap LC3_g Lamp2_r 60x 19102012 image 2.tif (RGB) (green)	54.62	5	10.924
low Ca nHEKs Rap LC3_g Lamp2_r 60x 19102012 image 3.tif (RGB) (green)	55.61	8	6.95125
low Ca nHEKs Rap LC3_g Lamp2_r 60x 19102012 image 5.tif (RGB) (green)	85.99	8	10.74875
Sum	460.01	30	
Average intensity per cell	**15.33367**		
Std error			**5.026415971**

Appendix 15 Table 2: The effects of rapamycin on the autophagosome marker, LC3 in primary keratinocyte cultures with and without chloroquine treatment.

Appendix 15 continued.

Quantification of LC3 intensities per cell for 4 fields of view.

Quantification of LC3 intensities per field of view was done with imageJ. However, number of cells per field of view was determined by eye.

Appendix 15 continued on the next page.

e Average LC3 intensities per cell (102012)

	Vehicle		Rapamycin	
	undifferentiated	differentiated	undifferentiated	differentiated
- chl	28.21	5.88	15.33	9.07
+ chl	36.08	39.41	43.63	28.47

Std errors (102012)

	Vehicle		Rapamycin	
	undifferentiated	differentiated	undifferentiated	differentiated
- chl	13.42	1.13	5.03	2.89
+ chl	5.89	6.09	4.41	6.46

f

t-Test: Paired Two Sample for Means for LC3 intensities in undifferentated cells with chloroquine; vehicle vs rapamycin treatment

	Variable 1	*Variable 2*
Mean	36.03453914	42.50685516
Variance	138.9732397	77.71958061
Observations	4	4
Pearson Correlation	-0.59231621	
Hypothesized Mean Difference	0	
df	3	
t Stat	-0.70221871	
P(T<=t) one-tail	0.266561459	
t Critical one-tail	2.353363435	
P(T<=t) two-tail	0.533122918	
t Critical two-tail	3.182446305	

g

t-Test: Paired Two Sample for Means for LC3 intensities in differentated cells with chloroquine; vehicle vs rapamycin treatment

	Variable 1	*Variable 2*
Mean	41.60555952	32.1226126
Variance	148.5025171	166.755614
Observations	4	4
Pearson Correlation	-0.484924144	
Hypothesized Mean Difference	0	
df	3	
t Stat	0.876813087	
P(T<=t) one-tail	0.222567435	
t Critical one-tail	2.353363435	
P(T<=t) two-tail	0.44513487	
t Critical two-tail	3.182446305	

Appendix 15: The effects of rapamycin on the autophagosome marker, LC3 in primary keratinocyte cultures with and without chloroquine treatment.

Appendix 15 continued.

(e) Table showing average LC3 intensities per cell and the standard errors

(f) Results from the paired t-test for LC3 intensities per cell performed on undifferentiated keratinocytes with chloroquine treated with vehicle compared to rapamycin

(g) Results from the paired t-test for LC3 intensities per cell performed on differentiated keratinocytes with chloroquine treated with vehicle compared to rapamycin

Appendix 15 continued on the next page.

Quantification of LC3 puncta		
Summary number of LC3 puncta per cell - threshhold 165-255, 0.00-500 pixel size, circularilyt 0.3-1.00		
	puncta	No of cells
high Ca nHEKs DMSO + 200uM chl LC3_g Lamp2_r 60x 19102012 image 1.tif (RGE	640	7
high Ca nHEKs DMSO + 200uM chl LC3_g Lamp2_r 60x 19102012 image 3.tif (RGE	570	7
high Ca nHEKs DMSO + 200uM chl LC3_g Lamp2_r 60x 19102012 image 2.tif (RGE	934	12
high Ca nHEKs DMSO + 200uM chl LC3_g Lamp2_r 60x 19102012 image 5.tif (RGE	698	10
No of counts total	2842	36
No of counts/cell	78.94444	
Std error		
high Ca nHEKs DMSO chl LC3_g Lamp2_r 60x 19102012 image 1.tif (RGB) (green)	379	12
high Ca nHEKs DMSO chl LC3_g Lamp2_r 60x 19102012 image 2.tif (RGB) (green)	487	17
high Ca nHEKs DMSO chl LC3_g Lamp2_r 60x 19102012 image 4.tif (RGB) (green)	397	8
high Ca nHEKs DMSO chl LC3_g Lamp2_r 60x 19102012 image 5.tif (RGB) (green)	431	11
No of counts total	1694	48
No of counts/cell	35.29167	
Std error		
high Ca nHEKs rap + 200uM chl LC3_g Lamp2_r 60x 19102012 image 1.tif (RGB) (	471	13
high Ca nHEKs rap + 200uM chl LC3_g Lamp2_r 60x 19102012 image 2.tif (RGB) (	593	8
high Ca nHEKs rap + 200uM chl LC3_g Lamp2_r 60x 19102012 image 3.tif (RGB) (	423	7
high Ca nHEKs rap + 200uM chl LC3_g Lamp2_r 60x 19102012 image 4.tif (RGB) (	524	5
No of counts total	2011	33
No of counts/cell	60.93939	
Std error		
high Ca nHEKs rap LC3_g Lamp2_r 60x 19102012 image 1.tif (RGB) (green)	468	11
high Ca nHEKs rap LC3_g Lamp2_r 60x 19102012 image 3.tif (RGB) (green)	590	19
high Ca nHEKs rap LC3_g Lamp2_r 60x 19102012 image 4.tif (RGB) (green)	430	10
high Ca nHEKs rap LC3_g Lamp2_r 60x 19102012 image 5.tif (RGB) (green)	517	9
No of counts total	2005	49
No of counts/cell	40.91837	
Std error		
low Ca nHEKs DMSO + 200uM chl LC3_g Lamp2_r 60x 19102012 image 1.tif (RGB	732	9
low Ca nHEKs DMSO + 200uM chl LC3_g Lamp2_r 60x 19102012 image 2.tif (RGB	573	11
low Ca nHEKs DMSO + 200uM chl LC3_g Lamp2_r 60x 19102012 image 3.tif (RGB	684	8
low Ca nHEKs DMSO + 200uM chl LC3_g Lamp2_r 60x 19102012 image 4.tif (RGB	577	8
No of counts total	2566	36
No of counts/cell	71.27778	
Std error		
low Ca nHEKs DMSO LC3_g Lamp2_r 60x 19102012 image 1.tif (RGB) (green)	571	7
low Ca nHEKs DMSO LC3_g Lamp2_r 60x 19102012 image 2.tif (RGB) (green)		5
low Ca nHEKs DMSO LC3_g Lamp2_r 60x 19102012 image 3.tif (RGB) (green)	525	6
low Ca nHEKs DMSO LC3_g Lamp2_r 60x 19102012 image 4.tif (RGB) (green)	585	7
No of counts total	1681	25
No of counts/cell	67.24	
Std error		

Appendix 15 Table 3: The effects of rapamycin on the autophagosome marker, LC3 in primary keratinocyte cultures with and without chloroquine treatment.

Appendix 15 continued.

Quantification of LC3 puncta per cell for 4 fields of view.

Quantification of LC3 puncta per field of view was done with imageJ. However, number of cells per field of view was determined by eye.

Appendix 15 continued on the next page.

low Ca nHEKs Rap + 200uM chl LC3_g Lamp2_r 60x 19102012 image 1.tif (RGB) (g	807	12	67.25
low Ca nHEKs Rap + 200uM chl LC3_g Lamp2_r 60x 19102012 image 2.tif (RGB) (g	527	7	75.28571429
low Ca nHEKs Rap + 200uM chl LC3_g Lamp2_r 60x 19102012 image 3.tif (RGB) (g	640	8	80
low Ca nHEKs Rap + 200uM chl LC3_g Lamp2_r 60x 19102012 image 4.tif (RGB) (g	599	9	66.55555556
No of counts total	2573	36	
No of counts/cell	71.47222		
Std error			**3.249393228**
low Ca nHEKs Rap LC3_g Lamp2_r 60x 19102012 image 1.tif (RGB) (green)	723	9	80.33333333
low Ca nHEKs Rap LC3_g Lamp2_r 60x 19102012 image 2.tif (RGB) (green)	307	5	61.4
low Ca nHEKs Rap LC3_g Lamp2_r 60x 19102012 image 3.tif (RGB) (green)	321	8	40.125
low Ca nHEKs Rap LC3_g Lamp2_r 60x 19102012 image 5.tif (RGB) (green)	556	8	69.5
No of counts total	1907	30	
No of counts/cell	63.56667		
Std error			**8.506943906**

Appendix 15 Table 4: The effects of rapamycin on the autophagosome marker, LC3 in primary keratinocyte cultures with and without chloroquine treatment.

Appendix 15 continued.

Quantification of LC3 puncta per cell for 4 fields of view.

Quantification of LC3 puncta per field of view was done with imageJ. However, number of cells per field of view was determined by eye.

Appendix 15 continued on the next page.

i

Average no of LC3 puncta/ cell

	Vehicle		Rapamycin	
	undifferentiated	differentiated	undifferentiated	differentiated
- chl	67.24	35.29	63.57	40.92
+ chl	71.27	78.94	71.47	60.94

Std errors

	Vehicle		Rapamycin	
	undifferentiated	differentiated	undifferentiated	differentiated
- chl	1.74	4.68	8.51	5.41
+ chl	7.44	4.48	3.25	14.3

j

t-Test: Paired Two Sample for Means for LC3 puncta in undifferentiated keratinocytes with chloroquine; vehicle vs rapamycin treatment

	Variable 1	*Variable 2*
Mean	72.76231061	72.27281746
Variance	221.141389	42.2342254
Observations	4	4
Pearson Correlation	-0.0112489	
Hypothesized Mean Difference	0	
df	3	
t Stat	0.060076355	
P(T<=t) one-tail	0.47793647	
t Critical one-tail	2.353363435	
P(T<=t) two-tail	0.955872941	
t Critical two-tail	3.182446305	

k

t-Test: Paired Two Sample for Means for LC3 puncta in differentiated keratinocytes with chloroquine; vehicle vs rapamycin treatment

	Variable 1	*Variable 2*
Mean	80.12261905	68.89608516
Variance	80.44245465	818.3847683
Observations	4	4
Pearson Correlation	-0.92722728	
Hypothesized Mean Difference	0	
df	3	
t Stat	0.605593123	
P(T<=t) one-tail	0.293765036	
t Critical one-tail	2.353363435	
P(T<=t) two-tail	0.587530073	
t Critical two-tail	3.182446305	

Appendix 15: The effects of rapamycin on the autophagosome marker, LC3 in primary keratinocyte cultures with and without chloroquine treatment.

Appendix 15 continued.

(i) Table showing average LC3 puncta per cell and the standard errors

(j) Results from the paired t-test for LC3 puncta per cell performed on undifferentiated keratinocytes with chloroquine treated with vehicle compared to rapamycin

(k) Results from the paired t-test for LC3 puncta per cell performed on differentiated keratinocytes with chloroquine treated with vehicle compared to rapamycin.

This figure is referenced in section 4.2.

Appendix 16: Immunofluorescence analysis of the autophagosome marker, LC3 in primary keratinocyte cultures with and without BafA1 treatment

Immunofluorescence analysis with antibodies against LC3 and p62 in untreated and BafA1-treated undifferentiated and differentiated keratinocytes was performed to determine whether BafA1 is more suitable to determine autophagic flux in primary human keratinocytes. Also, the effects of rapamycin on keratinocyte autophagy in the presence and absence of BafA1 was analysed.

Quantification of LC3 and p62 expression was carried out by determining the intensities of protein expression per cell. Immunofluorescence analysis for LC3 shows increased LC3 intensity per cell in undifferentiated cells treated with BafA1 compared to untreated undifferentiated cells, suggesting accumulation of LC3 aggregates (Appendix 16). In the differentiated keratinocytes, BafA1 treatment also leads to increased LC3 intensity per cell, indicating accumulation of LC3 aggregates when autophagy is blocked at the late stages (Appendix 16). These data show more membrane-bound LC3 (LC3II) after BafA1 treatment in both keratinocyte cultures (Appendix 16). Therefore, it is concluded that the autophagic pathway is functional in monolayer keratinocytes.

Label	Area	Mean	Min	Max	IntDen	No of cells	LC3 intensity/cell
DMSO low Ca LC3_g Lamp2_r 23112012 image 3g.tif	0.7	147.64	140	150	102.73	9	11.41444444
DMSO low Ca LC3_g Lamp2_r 23112012 image 1g.tif	1.07	148.04	140	150	158.21	7	22.60142857
DMSO low Ca LC3_g Lamp2_r 23112012 image 4g.tif	2.47	147.65	139	150	365.06	9	40.56222222
DMSO low Ca LC3_g Lamp2_r 23112012 image 2g.tif	0.88	146.92	140	150	129.94	7	18.56285714
Sum					755.94	32	
Average intensity per cell					**23.62313**		
Std error							**6.206034696**
DMSO + Baf low Ca LC3_g Lamp2_r 23112012 image 4g.tif	0.67	147.36	140	150	98.48	17	5.792941176
DMSO + Baf low Ca LC3_g Lamp2_r 23112012 image 1g.tif	1.21	147.79	140	150	179.06	4	44.765
DMSO + Baf low Ca LC3_g Lamp2_r 23112012 image 3g.tif	2.63	148.68	140	150	391.52	6	65.25333333
DMSO + Baf low Ca LC3_g Lamp2_r 23112012 image 2g.tif	1.41	147.41	140	150	208.4	7	29.77142857
Sum					877.46	34	
Average intensity per cell					**25.80765**		
Std error							**12.5273634**
DMSO high Ca LC3_g Lamp2_r 23112012 image 4g.tif	0.52	147.72	141	150	76.35	10	7.635
DMSO high Ca LC3_g Lamp2_r 23112012 image 1g.tif	0.29	146.48	140	150	42.97	7	6.138571429
DMSO high Ca LC3_g Lamp2_r 23112012 image 2g.tif	1.44	148.29	140	150	214.15	8	26.76875
DMSO high Ca LC3_g Lamp2_r 23112012 image 3g.tif	1.12	147.1	140	150	164.66	15	10.97733333
Sum					498.13	40	
Average intensity per cell					**12.45325**		
Std error							**4.738797326**
DMSO + Baf high Ca LC3_g Lamp2_r 23112012 image 4g.tif	0.71	147.54	140	150	104.26	5	20.852
DMSO + Baf high Ca LC3_g Lamp2_r 23112012 image 1g.tif	0.36	147.95	140	150	53.68	7	7.668571429
DMSO + Baf high Ca LC3_g Lamp2_r 23112012 image 3g.tif	2.7	147.59	140	150	398.63	14	28.47357143
DMSO + Baf high Ca LC3_g Lamp2_r 23112012 image 2g.tif	0.49	147.71	140	150	72.3	11	6.572727273
Sum					628.87	37	
Average intensity per cell					**16.99649**		
Std error							**5.302288507**
Rap low Ca LC3_g Lamp2_r 23112012 image 2g.tif	0.14	146.52	139	150	19.83	5	3.966
Rap low Ca LC3_g Lamp2_r 23112012 image 1g.tif	0.09	146.63	140	150	12.92	4	3.23
Rap low Ca LC3_g Lamp2_r 23112012 image 3g.tif	0.05	147.19	140	150	6.7	7	0.957142857
Rap low Ca LC3_g Lamp2_r 23112012 image 4g.tif	0.74	147.87	139	150	109.17	7	15.59571429
Sum					148.62	23	
Average intensity per cell					**6.461739**		
Std error							**3.28256034**
Rap +Baf low Ca LC3_g Lamp2_r 23112012 image 3g.tif	0.59	147.46	140	150	86.91	6	14.485
Rap +Baf low Ca LC3_g Lamp2_r 23112012 image 1g.tif	1.77	148.63	140	150	263.51	6	43.91833333
Rap +Baf low Ca LC3_g Lamp2_r 23112012 image 2g.tif	2.92	148.5	140	150	433.4	6	72.23333333
Rap +Baf low Ca LC3_g Lamp2_r 23112012 image 4g.tif	1.89	148.14	140	150	280.15	10	28.015
Sum					1063.97	28	
Average intensity per cell					**37.99893**		
Std error							**12.41149354**
Rap high Ca LC3_g Lamp2_r 23112012 image 2g.tif	0.66	147.88	140	150	98.07	10	9.807
Rap high Ca LC3_g Lamp2_r 23112012 image 1g.tif	1.38	147.79	140	150	203.96	6	33.99333333
Rap high Ca LC3_g Lamp2_r 23112012 image 4g.tif	0.47	147.6	140	150	69.97	11	6.360909091
Rap high Ca LC3_g Lamp2_r 23112012 image 3g.tif	0.91	148.11	140	150	135.33	8	16.91625
Sum					507.33	35	
Average intensity per cell					**14.49514**		
Std error							**6.147473337**
Rap +Baf high Ca LC3_g Lamp2_r 23112012 image 2g.tif	1.76	148.23	140	150	261.32	8	32.665
Rap +Baf high Ca LC3_g Lamp2_r 23112012 image 1g.tif	4.13	148.16	140	150	612.49	6	102.0816667
Rap +Baf high Ca LC3_g Lamp2_r 23112012 image 4g.tif	2.26	148.41	140	150	335.23	8	41.90375
Rap +Baf high Ca LC3_g Lamp2_r 23112012 image 3g.tif	1.08	147.95	140	150	159.09	7	22.72714286
Sum					1368.13	29	
Average intensity per cell					**47.1769**		
Std error							**17.84718318**

Appendix 16 Table 1: Analysis of the autophagosome marker, LC3 in primary keratinocyte cultures with and without BafA1 treatment.

Quantification of LC3 intensities in keratinocyte monolayer cultures treated with vehicle or rapamycin the presence or absence of BafA1.

Appendix 16 continued on the next page.

a LC3 intensities per cell (112012)

	Vehicle		Rapamycin	
	undifferentiated	differentiated	undifferentiated	differentiated
- BafA1	23.62	12.45	6.46	14.5
+ BafA1	25.81	17	38	47.18

b Std errors (112012)

	Vehicle		Rapamycin	
	undifferentiated	differentiated	undifferentiated	differentiated
- BafA1	3.57	4.74	3.28	6.15
+ BafA1	12.53	5.3	12.41	17.85

c

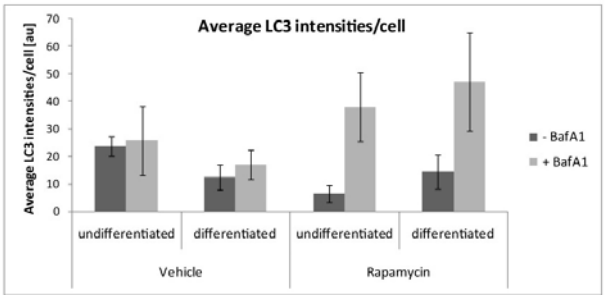

Appendix 16: Analysis of the autophagosome marker, LC3 in primary keratinocyte cultures with and without BafA1 treatment.

Appendix 16 continued.

(a) Average values of LC3 intensities per cell in keratinocyte monolayer cultures treated with vehicle or rapamycin the presence or absence of BafA1.

(b) Standard error for average LC3 intensities per cell in keratinocyte monolayer cultures treated with vehicle or rapamycin the presence or absence of BafA1.

(c) Graph shows the average values of LC3 intensities per cell in keratinocyte monolayer cultures. BafA1 treatment, increases of LC3 intensities in vehicle and rapamycin treated cells. Rapamycin treatment increases LC3 intensities per cell in the presence of BafA1 in both undifferentiated and differentiated keratinocytes.

Appendix 16 continued on the next page.

d

t-Test: Paired Two Sample for Means for means in LC3 intensities in undifferentiated cells with and without BafA1

	Variable 1	*Variable 2*
Mean	36.39567577	39.6629167
Variance	627.7393346	616.180688
Observations	4	4
Pearson Correlation	0.977164317	
Hypothesized Mean Difference	0	
df	3	
t Stat	-1.22491833	
P(T<=t) one-tail	0.154005672	
t Critical one-tail	2.353363435	
P(T<=t) two-tail	0.308011344	
t Critical two-tail	3.182446305	

e

t-Test: Paired Two Sample for Means for means in LC3 intensities in differentiated cells with and without BafA1

	Variable 1	*Variable 2*
Mean	15.8917175	49.8443899
Variance	112.457054	1274.08779
Observations	4	4
Pearson Correlation	-0.3187577	
Hypothesized Mean Difference	0	
df	3	
t Stat	-1.6830441	
P(T<=t) one-tail	0.09547803	
t Critical one-tail	2.35336343	
P(T<=t) two-tail	0.19095606	
t Critical two-tail	3.1824463	

Appendix 16: Analysis of the autophagosome marker, LC3 in primary keratinocyte cultures with and without chloroquine treatment.

Appendix 16 continued.

(d) Results from a paired t-test for LC3 intensities in BafA1-treated undifferentiated keratinocytes shows that the rapamycin-mediated increase in LC3 intensities is not statistically significant.

(e) Results from a paired t-test for LC3 intensities in BafA1-treated differentiated keratinocytes shows that the rapamycin-mediated increase in LC3 intensities is not statistically significant.

Appendix 16 continued on the next page.

Summary number of LC3 puncta per cell - threshhold 165-255, 0.00-500 pixel size, circularilyt 0.3-1.00

	Puncta		No of cells	puncta per cell
DMSO + Baf high Ca LC3_g Lamp2_r 23112012 image 2.tif (RGB) (green)	835	1.08	7	119.2857143
DMSO + Baf high Ca LC3_g Lamp2_r 23112012 image 3.tif (RGB) (green)	1026	0.94	14	73.28571429
DMSO + Baf high Ca LC3_g Lamp2_r 23112012 image 4.tif (RGB) (green)	723	0.97	11	65.72727273
DMSO + Baf high Ca LC3_g Lamp2_r 23112012 image 1.tif (RGB) (green)	651	0.72	5	130.2
No of counts total	3235		37	
No of counts/cell	87.43243			
Std error				**16.17400616**
DMSO high Ca LC3_g Lamp2_r 23112012 image 1.tif (RGB) (green)	448	1.09	7	64
DMSO high Ca LC3_g Lamp2_r 23112012 image 2.tif (RGB) (green)	599	2.09	8	74.875
DMSO high Ca LC3_g Lamp2_r 23112012 image 3.tif (RGB) (green)	1309	1.06	15	87.26666667
DMSO high Ca LC3_g Lamp2_r 23112012 image 4.tif (RGB) (green)	879	0.95	10	87.9
No of counts total	3235		40	
No of counts/cell	80.875			
Std error				**3.671995024**
DMSO + Baf low Ca LC3_g Lamp2_r 23112012 image 1.tif (RGB) (green)	262	0.28	4	65.5
DMSO + Baf low Ca LC3_g Lamp2_r 23112012 image 2.tif (RGB) (green)	356	0.42	7	50.85714286
DMSO + Baf low Ca LC3_g Lamp2_r 23112012 image 3.tif (RGB) (green)	320	1.66	6	53.33333333
DMSO + Baf low Ca LC3_g Lamp2_r 23112012 image 4.tif (RGB) (green)	446	0.6	17	26.23529412
No of counts total	1384		34	
No of counts/cell	40.70588			
Std error				**8.229556558**
DMSO low Ca LC3_g Lamp2_r 23112012 image 1.tif (RGB) (green)	397	1.02	7	56.71428571
DMSO low Ca LC3_g Lamp2_r 23112012 image 2.tif (RGB) (green)	427	0.92	7	61
DMSO low Ca LC3_g Lamp2_r 23112012 image 3.tif (RGB) (green)	817	0.69	9	90.77777778
DMSO low Ca LC3_g Lamp2_r 23112012 image 4.tif (RGB) (green)	361	2.28	9	40.11111111
No of counts total	2002		32	
No of counts/cell	62.5625			
Std error				**10.55198153**

Appendix 16 Table 2: Analysis of the autophagosome marker, LC3 in primary keratinocyte cultures with and without BafA1 treatment.

Appendix 16 continued.

Quantification of LC3 puncta in keratinocyte monolayer cultures treated with vehicle or rapamycin the presence or absence of BafA1.

Appendix 16 continued on the next page.

	Puncta		No of cells	puncta per cell
Rap +Baf high Ca LC3_g Lamp2_r 23112012 image 1.tif (RGB) (green)	665	0.71	6	110.8333333
Rap +Baf high Ca LC3_g Lamp2_r 23112012 image 2.tif (RGB) (green)	471	0.46	8	58.875
Rap +Baf high Ca LC3_g Lamp2_r 23112012 image 3.tif (RGB) (green)	499	0.83	7	71.28571429
Rap +Baf high Ca LC3_g Lamp2_r 23112012 image 4.tif (RGB) (green)	270	2.03	8	33.75
No of counts total	1905		29	
No of counts/cell	65.68966			
Std error				**16.07258545**
Rap high Ca LC3_g Lamp2_r 23112012 image 1.tif (RGB) (green)	553	1.63	6	92.16666667
Rap high Ca LC3_g Lamp2_r 23112012 image 2.tif (RGB) (green)	939	0.81	10	93.9
Rap high Ca LC3_g Lamp2_r 23112012 image 3.tif (RGB) (green)	531	1.86	8	66.375
Rap high Ca LC3_g Lamp2_r 23112012 image 4.tif (RGB) (green)	708	0.72	11	64.36363636
No of counts total	2731		35	
No of counts/cell	78.02857			
Std error				**8.004284001**
Rap +Baf low Ca LC3_g Lamp2_r 23112012 image 1.tif (RGB) (green)	184	0.22	6	30.66666667
Rap +Baf low Ca LC3_g Lamp2_r 23112012 image 2.tif (RGB) (green)	457	0.41	6	76.16666667
Rap +Baf low Ca LC3_g Lamp2_r 23112012 image 3.tif (RGB) (green)	619	0.65	6	103.1666667
Rap +Baf low Ca LC3_g Lamp2_r 23112012 image 4.tif (RGB) (green)	477	0.39	10	47.7
No of counts total	1737		28	
No of counts/cell	62.03571			
Std error				**15.96385022**
Rap low Ca LC3_g Lamp2_r 23112012 image 1.tif (RGB) (green)	351	0.28	4	87.75
Rap low Ca LC3_g Lamp2_r 23112012 image 2.tif (RGB) (green)	423	0.39	5	84.6
Rap low Ca LC3_g Lamp2_r 23112012 image 3.tif (RGB) (green)	277	0.19	7	39.57142857
Rap low Ca LC3_g Lamp2_r 23112012 image 4.tif (RGB) (green)	557	0.53	7	79.57142857
No of counts total	1608		23	
No of counts/cell	69.91304			
Std error				**11.22761203**

Appendix 16 Table 3: Analysis of the autophagosome marker, LC3 in primary keratinocyte cultures with and without BafA1 treatment.

Appendix 16 continued.

Quantification of LC3 puncta in keratinocyte monolayer cultures treated with vehicle or rapamycin the presence or absence of BafA1.

Appendix 16 continued on the next page.

g

Average no of LC3 puncta/ cell

	Vehicle		Rapamycin	
	undifferentiated	differentiated	undifferentiated	differentiated
- BafA1	62.56	80.88	69.91	78.03
+ BafA1	40.71	87.43	62.04	65.69

h Std errors

	Vehicle		Rapamycin	
	undifferentiated	differentiated	undifferentiated	differentiated
- BafA1	10.55	3.67	11.23	8
+ BafA1	8.23	16.17	15.96	16.07

i

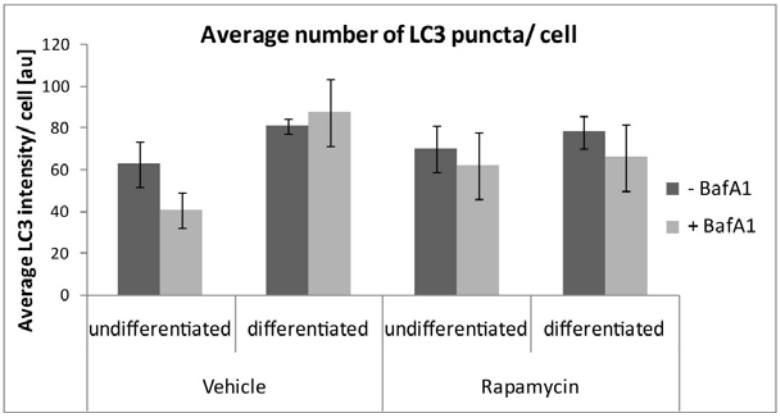

Appendix 16: Analysis of the autophagosome marker, LC3 in primary keratinocyte cultures with and without BafA1 treatment.

Appendix 16 continued.

(g) Average values of LC3 puncta per cell in keratinocyte monolayer cultures treated with vehicle or rapamycin the presence or absence of BafA1.

(h) Standard error for average LC3 puncta per cell in keratinocyte monolayer cultures treated with vehicle or rapamycin the presence or absence of BafA1.

(i) Graph shows the average values of LC3 puncta per cell in keratinocyte monolayer cultures. Compared to vehicle-treated keratinocytes, rapamycin has no effect on the number of LC3 puncta per cell in cells with and without BafA1. BafA1 treatment also does not affect the number of LC3 puncta per cell in all keratinocyte cultures.

This figure represents quantifications for Figure 4.6.

Appendix 17: Western blot analysis of the autophagosome marker, LC3 in primary keratinocyte cultures with and without BafA1 treatment

Western blotting shows that in both undifferentiated and differentiated keratinocytes, BafA1 treatment, which prevents degradation of autophagic vesicles, leads to accumulation of LC3II bands (Appendix 17a). This indicates that under normal culture conditions the autophagy process is completed in both keratinocyte populations. The LC3II/LC3I ratios and LC3II/actin ratios are higher in the BafA1 treated undifferentiated and differentiated keratinocytes when compared to the untreated cells under normal culture conditions (Appendix 17b, c). These values indicate an accumulation of LC3II with BafA1 treatment, which blocks the last steps of the autophagy pathway, in both undifferentiated and differentiated keratinocytes. With these experiments, I also observed that the when autophagy is impaired, the LC3II/LC3I and LC3II/actin values are much higher for undifferentiated keratinocytes compared to differentiated keratinocytes (Appendix 17b, c). This indicates that undifferentiated keratinocytes may have a higher rate of autophagic flux compared to differentiated cells (Appendix 17b, c) supporting initial observations (Appendix 16).

a

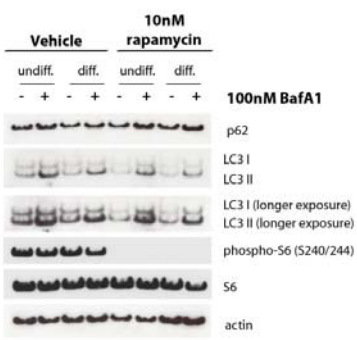

b

Blot 1

	LC3I	LC3II	LC3II/LC3I	actin	LC3II/actin
Undifferentiated Vehicle	3827.355	5298.77	***1.38***	6481.376	***0.82***
Undifferentiated Vehicle + BafA1	5868.79	8220.154	***1.40***	5492.305	***1.50***
Differentiated Vehicle	3805.426	3886.284	***1.02***	6071.962	***0.64***
Differentiated Vehicle + BafA1	3905.184	5393.82	***1.38***	6005.134	***0.90***
Undifferentiated Rapamycin	1267.991	2035.577	***1.61***	4661.891	***0.44***
Undifferentiated Rapamycin + BafA1	5196.841	5908.062	***1.14***	4383.82	***1.35***
Differentiated Rapamycin	1341.941	2517.234	***1.88***	7224.962	***0.35***
Differentiated Rapamycin + BafA1	2093.527	4905.648	***2.34***	7757.497	***0.63***

c

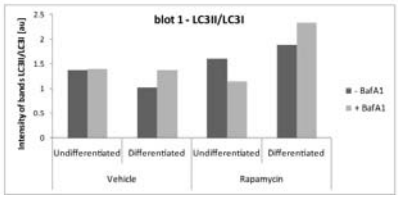

d

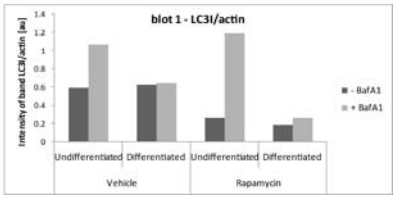

Appendix 17: Analysis of autophagic flux in rapamycin-treated primary keratinocyte cultures with and without BafA1.

(a) Western blot n=1 analysis of undifferentiated and differentiated monolayer primary keratinocytes treated with vehicle or rapamycin with or without BafA1.

(b) Quantification of LC3I, LC3II, actin and the LC3II/LC3I and LC3II/actin ratios for n=1 blots

(c) Graph of quantification for LC3II/LC3I for blot 1

(d) Graph of quantification for LC3II/actin for blot 1

Appendix 17 continued on the next page.

e

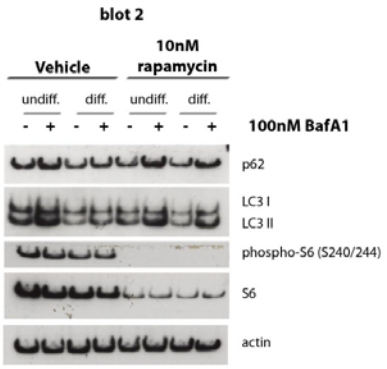

f

Blot 2

	LC3I	LC3II	LC3II/LC3I	actin	LC3II/actin
Undifferentiated Vehicle	7596.69	5397.77	***0.71***	8945.983	***0.60***
Undifferentiated Vehicle + BafA1	9643.104	8906.376	***0.92***	9112.761	***0.98***
Differentiated Vehicle	4556.79	3438.719	***0.75***	9874.054	***0.35***
Differentiated Vehicle + BafA1	5026.326	4986.962	***0.99***	9013.983	***0.55***
Undifferentiated Rapamycin	4755.376	4953.598	***1.04***	8445.104	***0.59***
Undifferentiated Rapamycin + BafA1	5284.376	7781.497	***1.47***	9474.933	***0.82***
Differentiated Rapamycin	2567.477	4017.426	***1.56***	8993.447	***0.45***
Differentiated Rapamycin + BafA1	3961.891	6765.962	***1.71***	8415.376	***0.80***

g

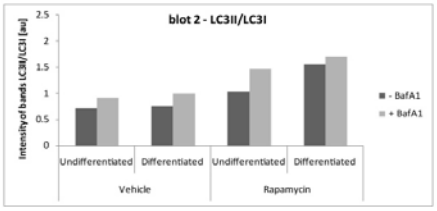

h

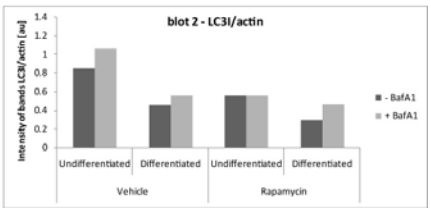

Appendix 17: Analysis of autophagic flux in rapamycin-treated primary keratinocyte cultures with and without BafA1.

Appendix 17 continued.

(e) Western blot n=2 analysis of undifferentiated and differentiated monolayer primary keratinocytes treated with vehicle or rapamycin with or without BafA1.

(f) Quantification of LC3I, LC3II, actin and the LC3II/LC3I and LC3II/actin ratios for n=2 blots

(g) Graph of quantification for LC3II/LC3I for blot 2

(h) Graph of quantification for LC3II/actin for blot 2

Appendix 17 continued on the next page.

i

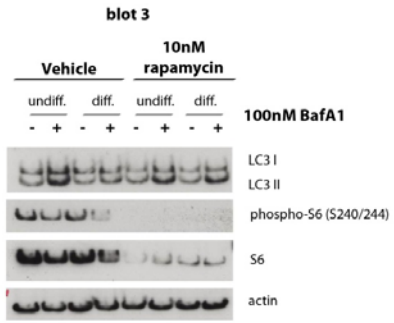

j

Blot 3

	LC3I	LC3II	LC3II/LC3I	actin	LC3I/actin	LC3II/actin
Undifferentiated Vehicle	6247.347	5383.326	***0.86***	7015.497	***0.89***	***0.77***
Undifferentiated Vehicle + BafA1	12235.9	12199.81	***1.00***	5884.497	***2.08***	***2.07***
Differentiated Vehicle	7612.832	5060.74	***0.66***	7403.74	***1.03***	***0.68***
Differentiated Vehicle + BafA1	7170.539	6731.74	***0.94***	6778.104	***1.06***	***0.99***
Undifferentiated Rapamycin	4834.347	5685.033	***1.18***	5981.912	***0.81***	***0.95***
Undifferentiated Rapamycin + BafA1	8211.539	10756.52	***1.31***	6319.74	***1.30***	***1.70***
Differentiated Rapamycin	4273.983	5608.397	***1.31***	6540.326	***0.65***	***0.86***
Differentiated Rapamycin + BafA1	6067.518	10524.81	***1.73***	6928.083	***0.88***	***1.52***

k

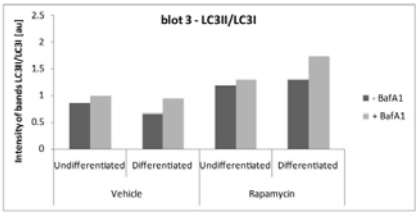

l

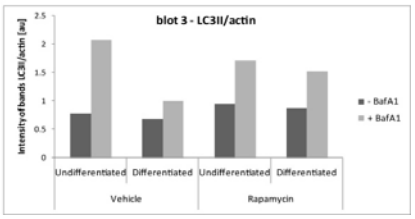

Appendix 17: Analysis of autophagic flux in rapamycin-treated primary keratinocyte cultures with and without BafA1.

Appendix 17 continued.

(i) Western blot n=3 analysis of undifferentiated and differentiated monolayer primary keratinocytes treated with vehicle or rapamycin with or without BafA1.

(j) Quantification of LC3I, LC3II, actin and the LC3II/LC3I and LC3II/actin ratios for n=3 blots

(k) Graph of quantification for LC3II/LC3I for blot 3

(l) Graph of quantification for LC3II/actin for blot 3

Appendix 17 continued on the next page.

m

Averages	*LC3II/LC3I*			
	Vehicle		**Rapamycin**	
	Undifferentiated	**Differentiated**	**Undifferentiated**	**Differentiated**
- BafA1 blot 1	1.38	1.02	1.61	1.88
- BafA1 blot 2	0.71	0.75	1.04	1.56
- BafA1 blot 3	0.86	0.66	1.18	1.31
Average	0.983333333	0.81	1.276666667	1.583333333
Std error	*0.2030052*	*0.108166538*	*0.17149668*	*0.164957907*
+ BafA1 blot 1	1.4	1.38	1.14	2.34
+ BafA1 blot 2	0.92	0.99	1.47	1.71
+ BafA1 blot 3	1	0.94	1.31	1.73
Average	1.106666667	1.103333333	1.306666667	1.926666667
Std error	*0.148473716*	*0.139084307*	*0.095277373*	*0.206747296*

n

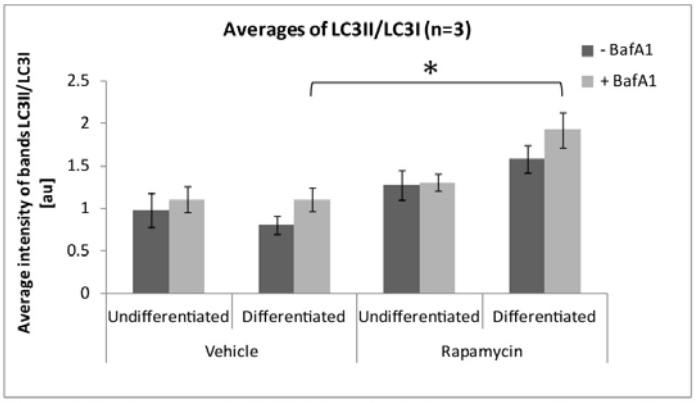

*Two tailed paired t-test for LC3II/LC3I ratios in between vehicle-treated and rapamycin-treated cells in the presence of BafA1, .P<0.05
n=3 individual experiments

Formatted: Font: Bold

m

Averages	*LC3II/LC3I*			
	Vehicle		**Rapamycin**	
	Undifferentiated	**Differentiated**	**Undifferentiated**	**Differentiated**
- BafA1 blot 1	1.38	1.02	1.61	1.88
- BafA1 blot 2	0.71	0.75	1.04	1.56
- BafA1 blot 3	0.86	0.66	1.18	1.31
Average	0.983333333	0.81	1.276666667	1.583333333
Std error	*0.2030052*	*0.108166538*	*0.17149668*	*0.164957907*
+ BafA1 blot 1	1.4	1.38	1.14	2.34
+ BafA1 blot 2	0.92	0.99	1.47	1.71
+ BafA1 blot 3	1	0.94	1.31	1.73
Average	1.106666667	1.103333333	1.306666667	1.926666667
Std error	*0.148473716*	*0.139084307*	*0.095277373*	*0.206747296*

n

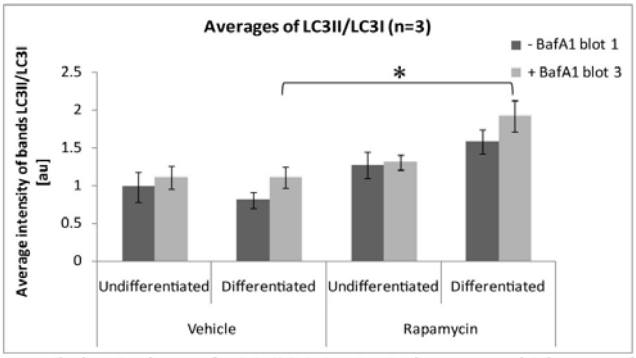

* Two tailed paired t-test for LC3II/LC3I ratios in between vehicle-treated and rapamycin-treated cells in the presence of BafA1, .P<0.05
n=3 individual experiments

Appendix 17: Analysis of autophagic flux in rapamycin-treated primary keratinocyte cultures with and without BafA1.

Appendix 17 continued.

(m) Average values and standard errors for LC3II/LC3I ratios for n=3 blots

(n) Graph shows average values for LC3II/LC3I for n=3 blots. In the presence of BafA1, the rapamycin mediates a statistically significant increase in LC3II/LC3I in differentiated keratinocytes, P<0.05.

Appendix 17 continued on the next page.

o t-Test: Paired Two Sample for Means for LC3II/LC3I in BafA1 treated undifferentiated cells, vehicle vs Rapamycin

	Variable 1	*Variable 2*
Mean	1.106666667	1.306666667
Variance	0.066133333	0.027233333
Observations	3	3
Pearson Correlation	-0.939397321	
Hypothesized Mean Difference	0	
df	2	
t Stat	-0.832610894	
P(T<=t) one-tail	0.246326855	
t Critical one-tail	2.91998558	
P(T<=t) two-tail	0.492653711	
t Critical two-tail	4.30265273	

p t-Test: Paired Two Sample for Means for LC3II/LC3I in BafA1 treated differentiated cells, vehicle vs Rapamycin

	Variable 1	*Variable 2*
Mean	1.10333333	1.9266667
Variance	0.05803333	0.1282333
Observations	3	3
Pearson Correlation	0.99131469	
Hypothesized Mean Difference	0	
df	2	
t Stat	-11.5541727	
P(T<=t) one-tail	0.00370378	
t Critical one-tail	2.91998558	
P(T<=t) two-tail	0.00740757	
t Critical two-tail	4.30265273	

Appendix 17: Analysis of autophagic flux in rapamycin-treated primary keratinocyte cultures with and without BafA1.

Appendix 17 continued.

(o) Results from a paired t-test for LC3II/LC3I in BafA1-treated undifferentiated keratinocytes shows that the rapamycin-mediated increase in LC3II/LC3I is not statistically significant.

(p) Results from a paired t-test for LC3II/LC3I in BafA1-treated differentiated keratinocytes shows that the rapamycin-mediated increase in LC3II/LC3I is statistically significant with $P<0.05$.

Appendix 17 continued on the next page.

q

Averages	*LC3II/actin*			
	Vehicle		**Rapamycin**	
	Undifferentiated	**Differentiated**	**Undifferentiated**	**Differentiated**
- BafA1	0.82	0.64	0.44	0.35
- BafA1 blot 2	0.6	0.35	0.59	0.45
- BafA1 blot 3	0.77	0.68	0.95	0.86
Average	0.73	0.556666667	0.66	0.553333333
Std error	*0.066583281*	*0.103976493*	*0.15132746*	*0.156027063*
+ BafA1 blot 1	1.5	0.9	1.35	0.63
+ BafA1 blot 2	0.98	0.55	0.82	0.8
+ BafA1	2.07	0.99	1.7	1.52
Average	1.516666667	0.813333333	1.29	0.983333333
Std error	*0.314766227*	*0.134205481*	*0.255799401*	*0.272784001*

r

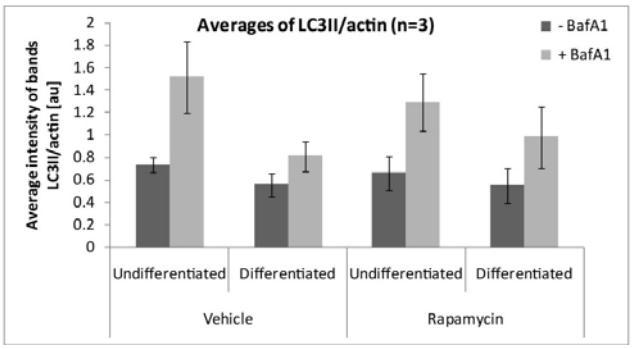

Appendix 17: Analysis of autophagic flux in rapamycin-treated primary keratinocyte cultures with and without BafA1.

Appendix 17 continued.

(q) Average values and standard errors for LC3II/actin ratios for n=3 blots

(r) Graph shows average values for LC3II/actin for n=3 blots.

Appendix 17 continued on the next page.

s

t-Test: Paired Two Sample for Means for LC3II/actin in BafA1 treated undifferentiated cells, vehicle vs Rapamycin

	Variable 1	*Variable 2*
Mean	1.51666667	1.29
Variance	0.29723333	0.1963
Observations	3	3
Pearson Correlation	0.98964593	
Hypothesized Mean Difference	0	
df	2	
t Stat	3.160228	
P(T<=t) one-tail	0.04361388	
t Critical one-tail	2.91998558	
P(T<=t) two-tail	0.08722776	
t Critical two-tail	4.30265273	

t

t-Test: Paired Two Sample for Means for LC3II/actin in BafA1 treated differentiated cells, vehicle vs Rapamycin

	Variable 1	*Variable 2*
Mean	0.81333333	0.983333333
Variance	0.05403333	0.223233333
Observations	3	3
Pearson Correlation	0.51201587	
Hypothesized Mean Difference	0	
df	2	
t Stat	-0.72532216	
P(T<=t) one-tail	0.27182065	
t Critical one-tail	2.91998558	
P(T<=t) two-tail	0.54364129	
t Critical two-tail	4.30265273	

Appendix 17: Analysis of autophagic flux in rapamycin-treated primary keratinocyte cultures with and without BafA1.

Appendix 17 continued.

(s) Results from a paired t-test for LC3II/actin in BafA1-treated undifferentiated keratinocytes shows that the rapamycin-mediated increase in LC3II/LC3I is not statistically significant.

(t) Results from a paired t-test for LC3II/actin in BafA1-treated differentiated keratinocytes shows that the rapamycin-mediated increase in LC3II/LC3I is statistically significant with $P<0.05$.

This figure represents quantifications for Figure 4.5.

Appendix 18: Vector cards of HA-AKT constructs used for transfection experiments of keratinocytes

a

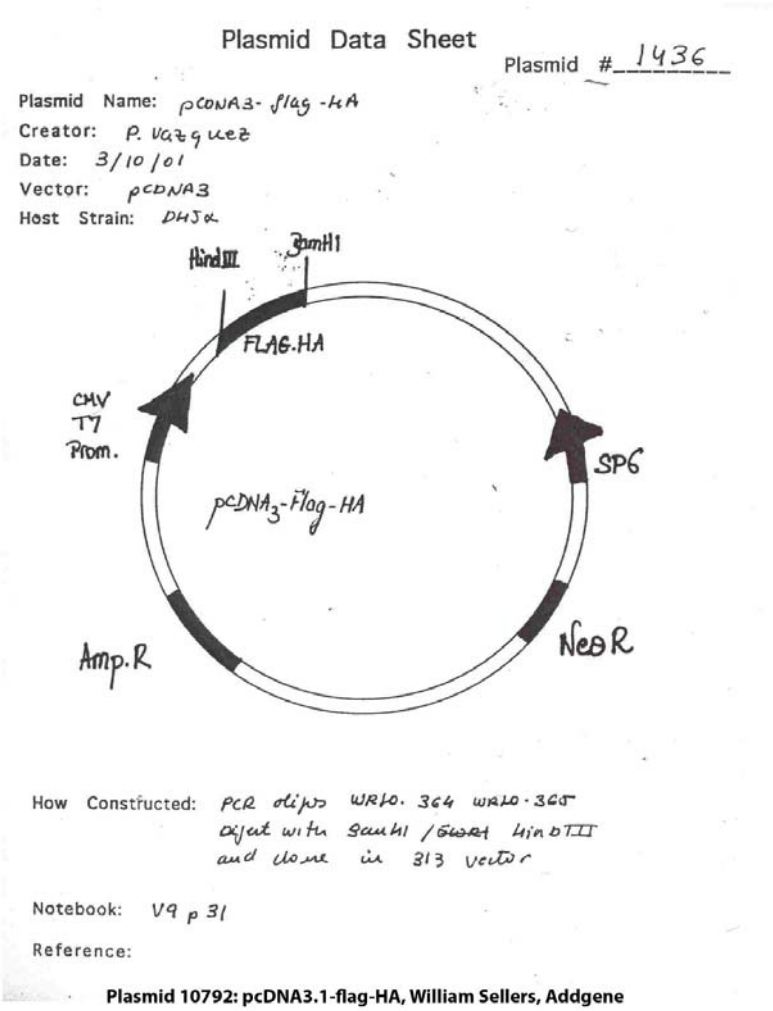

Plasmid 10792: pcDNA3.1-flag-HA, William Sellers, Addgene

Appendix 18: Vector cards of HA-AKT constructs used for transfection experiments in REKs

(a) The vector HA-flag pcDNA3.1 (plasmid 10792, Addgene) was made by W. Sellers and served as the vector backbone for the HA-flag-AKT1.

Appendix 18 continued on the next page.

b

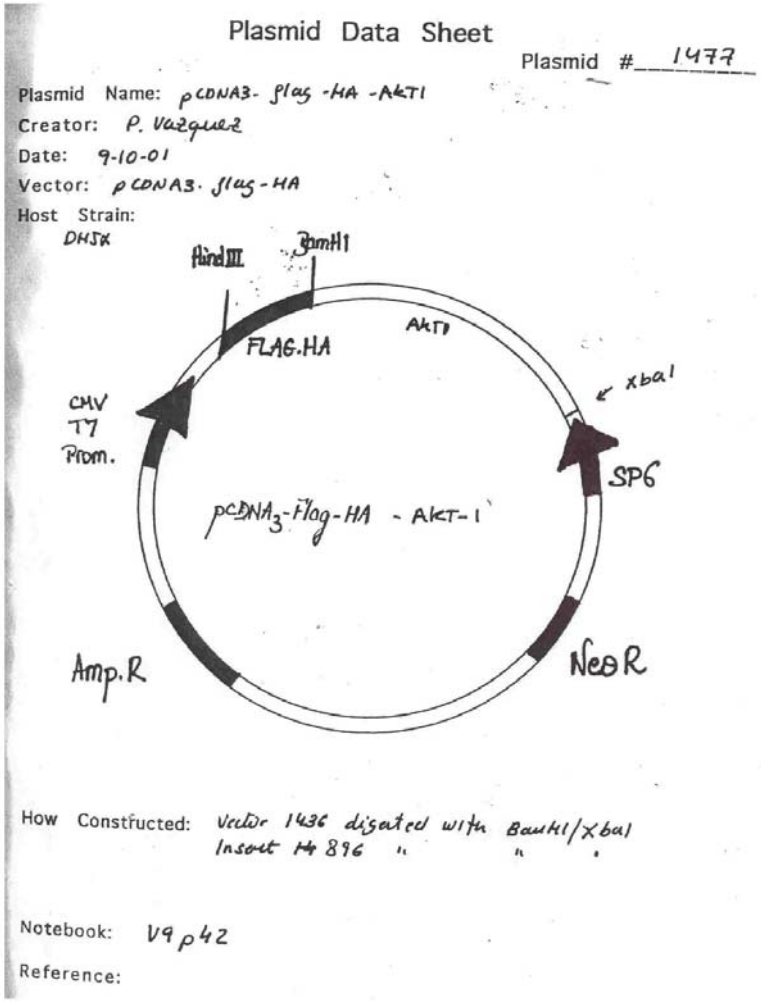

Plasmid 9021: pcDNA3.1-flag-HA-AKT1, William Sellers, Addgene

Appendix 18: Vector cards of HA-AKT constructs used for transfection experiments in REKs

Appendix 18 continued.

(b) The construct pcDNA3.1 HA-flag-AKT1 (plasmid 9021, Addgene) was made by W. Sellers. HA-flag-AKT1 was transfected into REKs and the phosphorylation status of HA-flag-AKT1 in response to rapamycin treatment was analysed.

Appendix 18 continued on the next page.

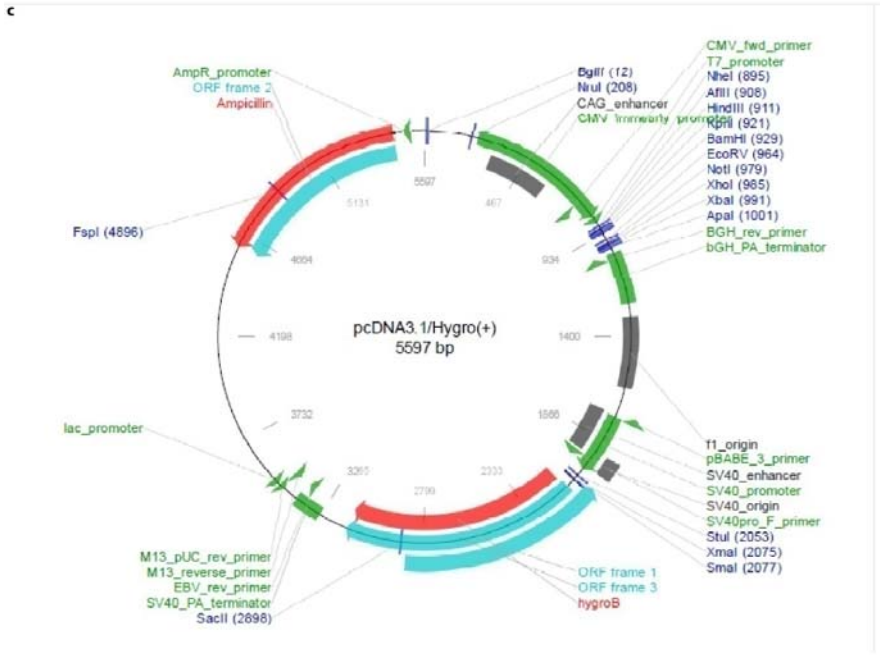

plasmid pcDNA3.1/ Hygo (+), from Invitrogen

Appendix 18: Vector cards of HA-AKT constructs used for transfection experiments in REKs

Appendix 18 continued.

(c) The vector backbone pcDNA3.1/Hygro (+) (Invitrogen) served as the vector backbone for the HA –AKT2.

Appendix 18 continued on the next page.

d

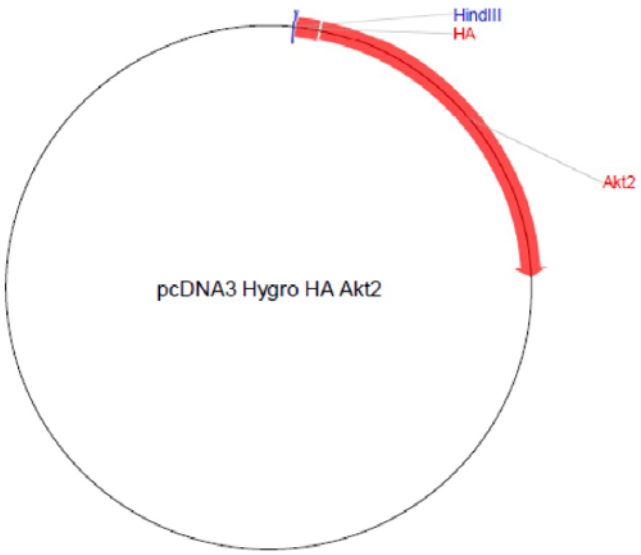

plasmid 16000: pcDNA3.1/ Hygo (+) HA-AKT2, Morris Birnbaum, Addgene

Appendix 18: Vector cards of HA-AKT constructs used for transfection experiments in REKs

Appendix 18 continued.

(d) The construct pcDNA3.1 Hygro HA-AKT2 (plasmid 16000, Addgene) was made by M Birnbaum. HA- AKT2 was transfected into REKs and the phosphorylation status of HA-AKT2 in response to rapamycin treatment was analysed.

Figure 4.2 shows the results from the over-expression experiments using these HA-AKT constructs.

Appendix 19: Immunofluorescence analysis of ABCA12 in rapamycin-treated mouse foetal explant cultures

Skin was isolated from mouse embryos at E15.5 and cultured with rapamycin for 3 days covering the period of barrier acquisition. This corresponds to new born skin. ABCA12 is a lipid transporter required for lamellar body formation (Akiyama *et al.* 2005) (Hovnanian 2005; Thomas *et al.* 2009).

In DMSO-treated epidermis (Appendix 19), ABCA12 is expressed in the supra-basal layers of epidermis. Rapamycin treatment appears to confine or concentrate ABCA12 expression to the granular layers only. This suggests that rapamycin changes properties of the epidermis which may also have implications for the epidermal barrier function.

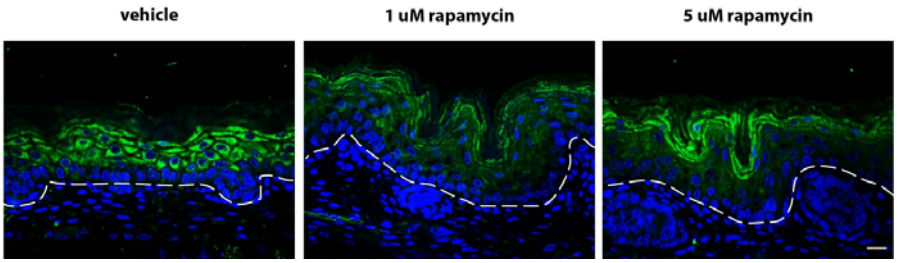

Appendix 19: Immunofluorescence analysis of ABCA12 in rapamycin-treated mouse foetal explant cultures

In vehicle treated explant cultures, ABCA12 is expressed in the supra-basal and granular layers. Rapamycin treatment changes the expression pattern of ABCA12 by restricting its expression to the granular layers.

Bar = 20um. Dotted line = basement membrane.

Appendix 20: Immunofluorescence analysis of phospho-mTORs (S2481 and S2448) in adult human epidermis

A number of mTOR phosphorylation sites have been discovered (S2448, S2481, T2446, S2159, T2164 and S1261), however there is still a lot of controversy on their regulation of the two mTOR complexes.

The mTOR phosphorylation site S2481 was initially discovered and shown to be an autophosphorylation site before the different mTOR complexes were known (Peterson *et al.* 2000). Recently, the S2448 site was associated with mTORC1 and S2481 with mTORC2 activity (Copp *et al.* 2009). However, the S2448 site was later said to be an autophosphorylation site (Rosner and Hengstschlager 2010). Based on these publications, the phosphorylation pattern of mTOR in adult human epidermis was analysed.

Since mTORC1 regulates autophagy, it was expected that if S2448 is specific for mTORC1 activity, it would be down regulated in the upper layers of epidermis where LC3 aggregates have been found. However, both phosphorylation sites S2481 and S2448 are present in the upper layers of epidermis. Interestingly, phospho-mTOR S2481 also appears to stain the cell membranes in the lower granular and upper spinous layers. Phospho-mTOR S2448 is not only present in the granular layer but also at low levels in the nuclei.

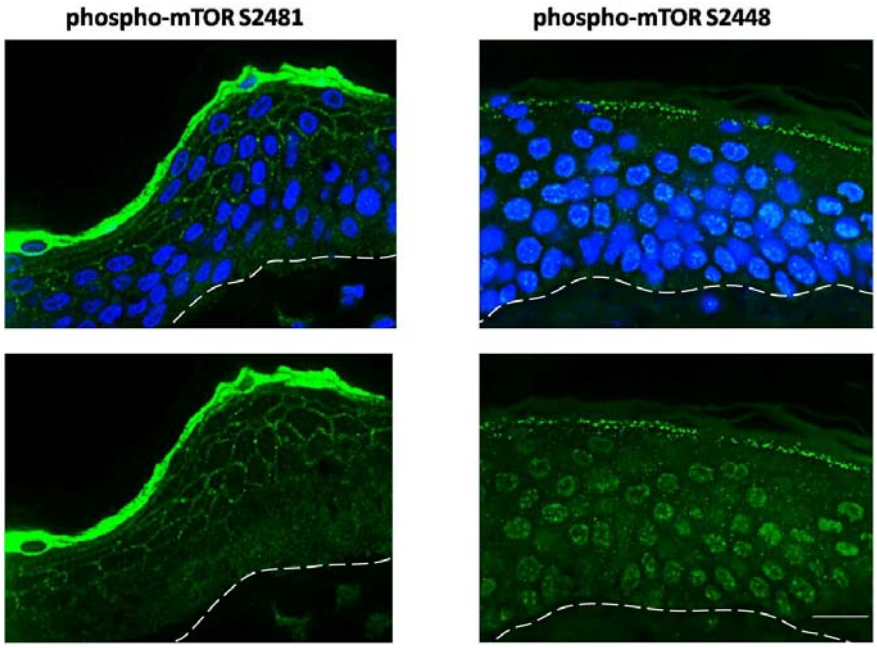

Appendix 20: Immunofluorescence analysis of phospho-mTOR (S2481 and S2448) in adult human epidermis

Phospho-mTOR (S2481) is strongly expressed in the granular layer. However, phospho-mTOR (S2481) is also expressed in the upper supra-basal layers where it is bound to the plasma-membrane. Phospho-mTOR (S2448) is present in the granular layer as well as at lower levels in the nuclei of keratinocytes.

Bar = 20um. Dotted line = basement membrane.

Appendix 21: Immunofluorescence analysis of K6 expression in foetal epidermal explant cultures

Cultured foetal epidermal explant cultures treated with vehicle or with the mTOR inhibitors rapamycin and Torin1, do not express the epidermal stress marker K6. Immunofluorescence analysis for cleaved Caspase-3, a marker for apoptosis, shows that the foetal epidermal explant cultures are also not apoptotic.

Therefore, in vitro culturing of foetal skin explants does not induce an epidermal stress response or cell death. Drug treatment with rapamycin and Torin1 also does not cause stress or apoptosis in the foetal explant cultures.

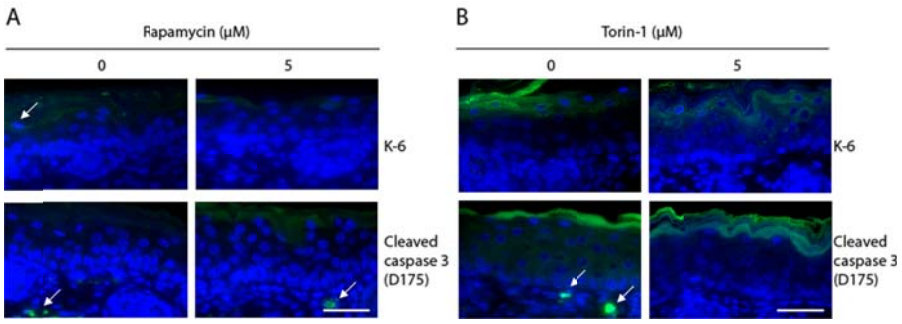

Appendix 21: Rapamycin and Torin-1 have no detectable effect on keratin-6 and cleaved caspase 3 in epidermis.

(K. Sully, unpublished data)

Mouse foetal explants were grown at the air-liquid interface for 72 hours. Immunofluorescence analysis for epidermal stress marker, keratin-6, and apoptosis marker cleaved caspase 3.

Bar=50μm. A) Skin cultured in the presence of vehicle or 5 μM rapamycin. B) Skin cultured in the presence of vehicle or 5 μM Torin-1.

(K. Sully, unpublished data)